Role of Wnt signaling pathway in adult mouse incisor growth

Akily, Basem Mohammed F

Awarding institution:
King's College London

Role of Wnt signaling pathway in adult mouse incisor growth

Basem M. Akily

A thesis submitted in fulfilment of the requirements of the degree of

Doctor of Philosophy

Centre for Craniofacial & Regenerative Biology

King's College London

Faculty of Dentistry, Oral & Craniofacial Sciences

University of London

June 2019

Supervised firstly by:

Prof. Paul T. Sharpe

Centre for Craniofacial & Regenerative Biology

King's College London, London, UK.

and secondly by:

Dr. Karen J. Liu

Centre for Craniofacial & Regenerative Biology

King's College London, London, UK.

Examined by:

Prof. Paul Cooper

and Prof. Rachel Weddington

Declaration

I declare that all the work presented in this thesis is my own, unless otherwise acknowledged.

Abstract

The continuously growing mouse incisor was used as a model in this project to study the role of Wnt signaling in adult mouse incisor growth *in vivo*. Mouse incisors grow continuously throughout life, which requires continuous cell renewal and compensation for the dental tissue loss due to mastication wear. This is achieved by the availability of the self-renewing MSCs at the proximal end of the mouse incisor. MSCs are slow-dividing cells which is not fast enough for the rapid turnover of the incisor, so they give rise to fast-dividing transit amplifying cells (TACs). However, TACs do not have the ability to self-renew and they terminally differentiate into either odontoblasts or pulp cells.

During development, many Wnt ligands are expressed in the developing incisor and have a crucial developmental role. Results obtained from adult mouse incisor RT-qPCR data has shown that their expression continues postnatally. The results obtained from Wnt reporter mouse line *Axin2-LacZ* and *Axin2* lineage tracing in the adult mouse incisor showed that only TACs and odontoblasts are Wnt-responsive cells.

To study Wnt signaling role in the adult mouse incisors, inhibition of Wnt ligands secretion by knocking out Wls, a transmembrane protein responsible for Wnt secretion, to deactivate Wnt pathway, and knocking-out *Axin2* to continuously activate Wnt/b-catenin pathway were done. Results from these experiments showed that depletion of Wnt signaling in adult mouse incisors leads to an abnormal incisor phenotype characterised by increased dentine thickness, disrupted cervical loop area and reduced growth rate, because of the reduced proliferation rate and increased apoptosis. Conversely, upregulation of Wnt/ β-catenin signaling by knocking out *Axin2* enhances adult mouse incisor growth rate with no apparent abnormal phenotype. Both models indicated that Wnt pathway regulates dentine secretion by controlling odontoblast *Dspp* expression.

Utilising different conditional knockout mouse lines to inhibit Wnt secretion from the different dental tissues was helpful to identify the source of Wnt ligands secretion that affect adult mouse incisor growth. Collectively, the obtained results of these knockouts indicated that Wnt ligands that activate Wnt pathway on TACs and odontoblasts are secreted from MSCs, TACs and odontoblasts and showed that epithelial-derived Wnt ligands have no role in the adult mouse incisor growth.

Acknowledgement

First of all, Praise is to ALLAH who gave me strength to go through this project.

I would like to express my sincere gratitude to my supervisor, *Professor Paul Sharpe*, for his patience, practical suggestions and expert guidance to help from the very beginning till the end of my project. I am also grateful to my second supervisor, *Dr Karen Liu* for her great support and kind assistance. I extend my thanks to my co-ordinator *Professor Tim Newton* for his time and academic support.

I am immensely grateful for Dr *Zhengwen An* for teaching and supporting me and her help with my experimental work. I am thankful to Mr. *Alex Huhn* and Mrs *Dhivya Chandrasekaran* for their help for animal procedures, Ms. *Fernanda* for her help in genotyping, Dr. *Christopher Healy* for his help in micro-CT scanning and Mrs. *Angela Gates* for her assistance.

My immense gratitude is extended to all former and current Sharpe lab members, *Longlong, Maja, Mushriq, Jing, Val, Willow, Vitor, Rebecca Babb, Abeer* and a very special thanks to *Araz Ahmed*.

I forever owe my wife, *Dwlah* and my lovely cute kid, *Mohammed* for their patience and support. Big thanks to them for sacrificing many of their rights to give me more time in the lab.

All love and go to my Parents, *Mohammed* and *Suad*, my brothers *Ahmed, Tariq and Fathuddin* and my sisters, *Amal* and *Anoud* for their encouragement and support. My father in law *Mansour* and My mother in law *Salma* for all the love and support. I love you all.

The financial support of the *Saudi Government* and *The Faculty of Dentistry, Taibah University* are also gratefully acknowledged.

Table of contents

List of figures

List of tables

List of abbreviations

μ-CT	micro-computed tomography
AER	apical ectodermal ridge
ALP	Alkaline phosphatase
AP	Anterior-posterior
APC	Adenomatous polyposis coli
Axin2	Axil inhibition protien 2
Bmp	Bone morphogenetic protein
BrDU	5-bromo-2'-deoxyuridine
BSA	Bovine serum antigen
CaMKII	calcium calmodulin-dependent protein kinase
Cbfa1	Core-Binding Factor, Runt Domain, Alpha Subunit 1
CD	Cluster of differentiation
cDNA	complementary DNA
CK1	Casein Kinase 1
Cn	calcineurin
CNS	Central Nervous System
CSF	Cerebrospinal fluid
Daam1	Dishevelled associated activator of morphogenesis 1
DAG	1,2 diacylglycerol
DEP	Dishevelled, Egl-10 and Pleckstrin domain
DFSCs	dental follicle stem cells
DKK	Dickkopf WNT Signaling Pathway Inhibitor
Dlx5	Distal-Less Homeobox 5

DMP-1	Dentine matrix acidic phosphoprotein 1
Dspp	Dentine sialophosphoprotein
Dvl	Dishevelled
E	Embryonic day
EDTA	Ethylenediaminetetraacetic acid disodium salt dihydrate
ER	Endoplasmic reticulum
ES	Embryonic stem cell
ESC	Epithelial stem cell
EtOH	Ethanol
Fgf	Fibroblast growth factor
Fgf10	Fibroblast growth factor 10
Fgf3	Fibroblast growth factor 3
Fgf9	Fibroblast growth factor 9
GAPDH	Glyceraldehyde-3-phosphate dehydrogenase
Germ1	Gremlin 1, DAN Family BMP Antagonist
GFP	Green fluorescent protein
Gli1	Glioma-Associated Oncogene Homolog 1
Gli2	Glioma-Associated Oncogene Homolog 2
Gli3	Glioma-Associated Oncogene Homolog 3
GSK3	Glycogen Synthase Kinase 3
H&E	Hematoxylin and eosin
Hoxa	Homeobox Protein
Hoxa-10	Homeobox Protein 10
Hoxa-11	Homeobox Protein 11
IHC	Immunohistochemistry

Ihh	Indian hedgehog protein
IMS	Industrial methylated spirit
IP	Intraperitoneal
IP3	inositol 1,4,5-triphosphate
K14	Keratin 14
LaCL	Labial cervical loop
Lef	Lymphoid enhanced factor
Lef-1	Lymphoid enhancer-binding factor 1
Lefty1	Left-Right Determination Factor 1
Lefty2	Left-Right Determination Factor 2
Lepr	Leptin receptor
Lfng	Lunatic Fringe Homolog
LiCL	Lingual cervical loop
LR	Lateral
LRC	Label-retaining cells
LRP	Low density lipoprotein receptor-related protein 1
MSC	Mesenchymal stem cell
Msx1	Msh Homeobox 1
Msx2	Msh Homeobox 2
Myf5	Myogenic Factor 5
MyoD	Myoblast Determination Protein
NEAT	nuclear factor associated with T cells
Ngn1	Neurogenin 1
Nkx2-1	NK2 Homeobox 1
N-myc	Neuroblastoma MYC Oncogene

Nodal	Nodal Growth Differentiation Factor
NVB	neurovascular bundle
OCN	Osteocalcin
OCT	Optimal cutting temperature
OPG	Osteoprotegerin
Osx	Osterix
P	Pulp
P (number)	Postnatal day
Pax2	Paired Box Protein Pax-2
Pax3	Paired Box Protein Pax-3
PBS	Phosphate-buffered saline
PCP	Planner cell polarity pathway
P-D	Proximal-distal
PDL	Periodontal ligaments
PFA	Paraformaldehyde
Pitx	Paired Like Homeodomain
PKC	protein kinase C
PRC	Protein Regulator Of Cytokinesis
RNA	Ribonucleic acid
ROCK	Rho associated kinase
RT-qPCR	Quantitative reverse transcription Polymerase chain reaction
Runx2	Runt Related Transcription Factor 2
Ser45	Serine 45
Shh	Sonic hedgehog
Sox9	SRY (sex determining region Y)-box 9

TAC	Transit amplifying cell
TCF	T-cell factor
TGFβ	Transforming growth factor beta
TNF	Tumour necrosis factor
Wnt-1	Wingless-Type MMTV Integration Site Family, Member 1
Wnt-10a	Wingless-Type MMTV Integration Site Family, Member 10a
Wnt-10b	Wingless-Type MMTV Integration Site Family, Member 10b
Wnt-11	Wingless-Type MMTV Integration Site Family, Member 11
Wnt-16	Wingless-Type MMTV Integration Site Family, Member 16
Wnt-2a	Wingless-Type MMTV Integration Site Family, Member 2a
Wnt-2b	Wingless-Type MMTV Integration Site Family, Member 2b
Wnt-3	Wingless-Type MMTV Integration Site Family, Member 3
Wnt-3a	Wingless-Type MMTV Integration Site Family, Member 3a
Wnt-4	Wingless-Type MMTV Integration Site Family, Member 4
Wnt-5a	Wingless-Type MMTV Integration Site Family, Member 5a
Wnt-5b	Wingless-Type MMTV Integration Site Family, Member 5b
Wnt-6	Wingless-Type MMTV Integration Site Family, Member 6
Wnt-7a	Wingless-Type MMTV Integration Site Family, Member 7a
Wnt-7b	Wingless-Type MMTV Integration Site Family, Member 7b
Wnt-8a	Wingless-Type MMTV Integration Site Family, Member 8a
Wnt-8b	Wingless-Type MMTV Integration Site Family, Member 8b
Wnt-9a	Wingless-Type MMTV Integration Site Family, Member 9a
Wnt-9b	Wingless-Type MMTV Integration Site Family, Member 9b
X-gal	5-bromo-4-chloro-3-indolyl ß-D-galactopyranoside
β-TrCP	beta-transducin repeat containing E3 ubiquitin protein ligase

Chapter 1. General Introduction

1.1. Wnt signaling pathway

Wnt signaling pathway is an essential pathway for early embryonic development, homeostasis of adult tissues and stem cell reproduction (Anger and Moon, 2009). It controls stem cells functions to repair and regenerate injured tissues. Different studies have shown that the Wnt pathway is essential for the homeostasis of different tissues such as bone (Chen et al, 2007), muscles (Chen et al., 2004) and lungs (Pongracz and Stockley, 2009).

Wnt pathway activation is established when Wnt ligands attach to the receptor. Wnt ligand is a glycoprotein that becomes lipid modified in the golgi apparatus in the producing cell. The modified Wnt ligand then binds to Wntless/evi protein to be secreted. Wntless/evi is a transmembrane protein which controls the secretion of the palmitoylated Wnt ligand (Ching and Nusse, 2006). Wntless/evi protein was first described by Banziger et al. in 2006, where it was identified as two alleles in the genetic screen of the Wnt gain of function phenotype. The Wntless/evi complex is controlled by retromer where the absence of the retromer components Dvps35 or Dvps26 in the cell leads to the degradation of Wntless (Port et al., 2008).

The secreted Wnt ligands are lipid modified which make them hydrophobic proteins (Willert et al., 2003). Therefore, Wnt ligand act as a short-range protein. Wnt ligands bind to the receptors to activate canonical β-catenin dependent and non-canonical signaling pathways (Clevers, 2006). Non-canonical Wnt pathway has two pathways; calcium pathway and planer cell polarity pathway (Nusse and van Amerongen, 2014; Sugimura and Li, 2010).

1.1.1. Wnt ligands

Wnt genes encode a large family of secreted glycoproteins. The first Wnt gene identified was *Wnt-1* (Nusse and Varmus, 1982). Following that, 19 members have been identified including *Wnt-1* in both human and mice. Wnt proteins share 27% to 83% amino acid sequence and a conserved pattern of 22 to 24 cysteine residues (Miller, 2002). Most Wnt genes are co-expressed in many organs, suggesting their functional redundancy (McMahon and Bradley, 1990; McMahon et al., 1992)

1.1.1.1. Wnt-1

Wnt-1 (was known as int-1 (McMahon and Bradley, 1990)) was identified in several mouse mammary cancers induced by mouse mammary tumour virus (MMTV) (Nusse and Varmus, 1982; Ooyen and Nusse, 1984). *Wnt-1* has 54% amino acid similar to its homologue *Drosophila wingless (Wg)* (Thomas and Capecchi, 1990). Wnt-1 is a canonical Wnt activator, and its signaling is required for midbrain patterning (McMahon et al., 1992; Makoto et al., 1997).

Wnt-1 expression is limited to the haploid round spermatids in the adult mouse testis and the developing central nervous system (CNS). Shortly after the induction of neural plate, *Wnt-1* is expressed in the open neural plate of the early somite-stage (E8.5) (Wilkinson et al., 1987). At this time, the expression covers the region of the future midbrain rostrally and hindbrain caudally. *Wnt-1* is expressed throughout the neural plate at the rostral region while it is restricted to the lateral margins of the neural plate at the caudal region, which is known to form the dorsal midline upon the closure of the neural tube (McMahon and Bradley, 1990).

By E9.5, *Wnt-1* expression extends from the midbrain to cover the length of the neural tube and it becomes limited to the midbrain dorsal midline, the spinal cord, and the myelencephalon

with no expression at the metencephalon caudally (McMahon and Bradley, 1990; McMahon et al., 1992).

Mutation of *Wnt-1* results in the loss of the posterior segmental pattern element, which is subsequently replaced by a duplication of the anterior segment (McMahon and Bradley, 1990). Furthermore, mice with mutation and loss of *Wnt-1* have an abnormal brain patterning with a deficiency of a vast region of the midbrain. The brain phenotype has shown that the caudal part of the midbrain, the midbrain-metencephalon and the rostral part of the metencephalon were missing due to development failure and retarded CNS development that caused death to the foetus 24h after birth (McMahon and Bradley, 1990; Thomas and Capecchi, 1990).

Deletion of *Wnt-1* also affects the number of thymocytes, which show a significant decrease in number. This mutation affects the number but does not affect thymocyte maturation (Mulroy et al., 2002).

1.1.1.2. Wnt-2

Wnt-2 is a canonical Wnt activator (Goss et al., 2009). Human *Wnt-2* was first identified during studying the gene mutations in cystic fibrosis (Wainwright et al., 1988) while mouse *Wnt-2* was cloned shortly after that (McMahon and McMahon, 1989). *Wnt-2* expression has been discovered in human and mouse (Monkley et al., 1996), rat (Levay-Young and Navre, 1992), sea urchin (Sidow, 1992) and leech (Kostriken and Weisblat, 1992).

Embryonic expression of *Wnt-2* starts after E7.5. At E7.5 *Wnt-2* is expressed in the mesodermal region of the heart primordium. At E7.75, the expression increases in the heart because of the differentiation of the precursor cells. Other sites of *Wnt-2* expression include tissues involved in the placenta; in particular, the chorioallantoic plate region and the blood vessels of the placenta. However, *Wnt-2* expression is only limited to the placenta tissues with no expression in the foetal trophoblast-derived placenta. At E8.0, *Wnt-2* is expressed in the allantois and when

the allantois fuses with chorion to form the chorioallantois plate at E8.5, the level of expression in this region increases and continues to be expressed in this region at E9.5 and E10.5 (Monkley et al., 1996). *Wnt-2* is also expressed in the developing lung mesenchyme which surrounds the ventral side of the anterior foregut from E9.0 and continues in the lung mesenchyme to adulthood, and the lateral plate mesoderm to regulate lung development and specification (Goss et al., 2009). However, *Wnt-2* is not expressed in the developing limbs nor CNS (Monkley et al., 1996).

The majority of *Wnt-2* null mice are cyanotic at birth and die neonatally with a lower birth bodyweight (Goss et al., 2009). Monkley et al. (1996) stated that *Wnt-2* null mice have no heart defect and their hearts look normal anatomically if compared to the wild-type mouse hearts. Mutant hearts have normal development and beat at the E8.0-8.5. However, *Wnt-2* null mice have shown abnormal placenta that is smaller in size and has severe oedema that causes an atypical maternal blood accumulation (Monkley et al., 1996). Poor placental development and function may lead to the low birth bodyweight because of the reduced nutritional supply to the foetus or by defective maternal hormonal functions on the placenta (Monkley et al., 1996).

Wnt-2 null mice have lung hypoplasia caused by the deficient development of the lung mesenchyme and sequentially leading to non-functional dilated vascular endothelial plexus. *Wnt-2* mutation has a negative impact and downregulates many important molecules that regulate lung growth, such as Fgf10, Nkx2.1, Bmp4, N-myc, and cyclin D1. Thus, cell proliferation is significantly impaired in both epithelial and mesenchymal cell progenies. Lung hypoplasia and poor development of *Wnt-2* null mice does not affect proximal-distal patterning and branching of the terminal airways (Goss et al., 2009).

1.1.1.3. Wnt-2b

Wnt-2b (formerly known as Wnt13 (Zakin et al., 1998)), is similar to Wnt-2 and it acts as a canonical Wnt activator (Goss et al., 2009). Although *Wnt-2b* is expressed in different regions during embryogenesis, it is not essential in most of them which suggests that other canonical Wnt ligands can compensate for Wnt-2b or that its main role is to provide support for the other Wnt ligands (Tsukiyama and Yamaguchi, 2012).

Wnt-2b is first expressed in the primitive streak mesoderm at E7. The expression of *Wnt-2b* is then detected in many different embryonic tissues such as retina, kidney, lung, limb bud, and the adult ovary. It is also expressed in the mouse brain; at E8.5–9.5, it is expressed in the dorsal midline of the telencephalon and the mesencephalon, at E11.5–17.5, it is expressed in the cortical hem, and at E15.5–17.5, it is expressed in the hippocampal fimbria and pineal body (Tsukiyama and Yamaguchi, 2012).

Between E9.0 to E10.5, *Wnt-2b* is expressed in the mesoderm lining the ventral side of the anterior foregut and later *Wnt-2b* is expressed in the mesenchymal tissue and lateral plate mesoderm (LPM) during lung development (Goss et al., 2009). In the retina, *Wnt-2b* is expressed in the marginal tip of the developing retina (Kubo et al., 2003). However, *Wnt-2b* is not expressed in the developing incisor (Suomalainen and Thesleff, 2010).

Wnt-2b null mice appeared normal and healthy. Depletion of *Wnt-2b* has no effects on body plane formation, despite *Wnt-2b* expression in the primitive streak (Zakin et al., 1998). Yamaguchi (2001) has found that *Wnt-3, 3a*, and *8a* are co-expressed in the primitive streak which could compensate for *Wnt-2b* loss of function. Moreover, no abnormal morphology has been detected in the other organs where *Wnt-2b* is expressed, such as limb, liver, kidney and adult ovary and cerebral cortex or hippocampus (Yamaguchi, 2001).

The only abnormal finding can be seen on the olfactory pulp where its length and width is significantly reduced. This is either because of the defect in the neuroblast cell migration to the olfactory pulp or by the defective neurogenesis in the subventricular zone (Tsukiyama and Yamaguchi, 2012).

Wnt-2b is responsible for the maintenance of progenitor cells in the peripheral retina. *Wnt-2b* overexpression supports retinal progenitor cells proliferation and inhibits neuronal differentiation as well as downregulating RNA transcription of some of the pro-neural genes such as *Notch1*. Thus, *Wnt-2b* maintains progenitor cells by preventing them from entering the differentiation cascade (Kubo et al., 2005).

1.1.1.4. Wnt-3

Wnt-3 is one of the canonical Wnt activators (Barrow et al., 2003), and was first detected as a proto-oncogene in mouse mammary tumours (Roelink et al., 1990). *Wnt-3* has been identified in different species such as *Xenopus laevis* (Christian et al., 1991), zebrafish (Krauss et al., 1992) and human (Roelink and Nusse, 1991).

Wnt-3 is expressed in the dorsal and lateral sides of the diencephalon and the spinal cord of the mouse embryos and adult brain. *Wnt-3* is expressed in the proximal epiblast between the embryonic and extra-embryonic ectoderm at E6.25. At late developmental stages, *Wnt-3* expression is localised to the primitive streak and the mesoderm (Liu et al., 1999).

Wnt-3 is also expressed all over the limb ectoderm (Roelink and Nusse, 1991). At E9.5, *Wnt-3* is expressed all over the forelimb bud ectoderm and at a lower level in the tail (Barrow et al., 2003). It is also expressed in the hair follicle after birth. Furthermore, *Wnt-3* is expressed at higher levels in the developing whisker follicles. By P9, *Wnt-3* expression is seen in the central cells that are differentiating to hair shaft medulla (Millar et al., 1999).

Sarkar and Sharpe (1999) showed that *Wnt-3* is expressed in the oral epithelium of the dental lamina at E11.5 but it is not expressed in the molar epithelium of E13.5 tooth bud. It becomes confined and limited to the primary enamel knots at the cap stage (E14.5) and becomes restricted to the internal enamel epithelium at the early bell stage at E15.5. Suomalainen and Thesleff (2010) stated that *Wnt-3* is not expressed in the mouse incisor at E16 and E18.

Wnt-3 signaling in the limb ectoderm is essential for apical ectodermal ridge (AER) formation, and it has a crucial role in distal growth and patterning of the limb (Barrow et al., 2003). *Wnt-3* mutants died during embryogenesis (Liu et al., 1999). There are no differences between the *Wnt-3* mutants, wild-type and heterozygous embryos before gastrulation. Unlike the wild-type mouse embryo, between E6.5 and 8.5, *Wnt-3* mutant embryos did not form any distinct embryonic structures and become restricted to grow as an egg cylinder. This malformation is lethal, and no foetus could survive after E10.5 (Liu et al., 1999).

Wnt-3 null malformed embryos consist of ectodermal and endodermal tissues while they lack mesodermal tissue. *Fgf8*, a posterior primitive streak marker, is not expressed in *Wnt-3* mutants, because of the lack of primitive streak and mesoderm formation. The mutants also lack anterior identity (Liu et al., 1999). Conditional deletion of *Wnt-3* from the limb ectoderm causes severe limb defects, and the mouse embryo fails to develop limbs (Barrow et al., 2003). Overexpression of *Wnt-3* in the skin leads to hair shaft abnormal structure and the formation of short hair (Millar et al., 1999).

1.1.1.5. Wnt-3a

Wnt-3a is a canonical Wnt activator (Nakaya et al., 2005; Nemoto et al., 2016). It is a major regulator of the trunk organiser (Nakaya et al., 2005) and the segmentation process (Aulehla et al., 2003).

Wnt-3a is expressed during all stages of both somitogenesis and axis extension, and it is expressed symmetrically in both primitive streak and dorsal posterior node (Takada et al., 1994). At E7.75 to E8.5, it is expressed in the ventral node and later in the tailbud (Nakaya et al., 2005; Lee et al., 2000). Yoshikawa et al., (1997) showed that *Wnt-3a* expression is confined to the primitive ectoderm. However, the expression was not seen in mesodermal lineages in both anterior and posterior positions. *Wnt-3a* is also expressed in the developing CNS, particularly in the diencephalon and spinal cord (McMahon et al., 1992; Parr et al., 1993).

Nemoto et al. (2016) stated that *Wnt-3a* is expressed in the dental structures and tooth developmental stages and its expression is detected in the epithelial root sheet, odontoblasts and dental follicle tissues. In five-week-old mice, *Wnt-3a* expression is also detected on apical cellular cementum with no expression in the acellular cementum. Suomalainen and Thesleff (2010) stated that *Wnt-3a* expression at E18 is limited to pre-ameloblasts and ameloblasts with no expression in dental mesenchyme.

Wnt-3a null mice die prenatally, and they cannot survive after E12.5 because of the lack of posterior organs and defective somite formation (Takada et al., 1994). This mutation has shown multiple defects in different organs. Mutant mice have multiple laterality (LR) defects including dextrocardia and/or cardiac situs ambiguous, as well as liver situs inversus and situs ambiguous (Nakaya et al., 2005). Moreover, *Nodal, Lefty1, Lefty2* and *Pitx2*, which are necessary for LR asymmetry, have abnormal expression in *Wnt-3a* mutant mice, indicating that *Wnt-3a* plays an early and crucial role in LR determination (Nakaya et al., 2005).

Mutant mice also have ectopic neural tube formation that exhibits a similar polarity to CNS tissues. This ectopic neural tissue has formed in a place known for paraxial mesoderm which can illustrate the importance of *Wnt-3a* to regulate mesodermal cell fate (Yoshikawa et al., 1997). Although absence of *Wnt-3a* mainly affects somite development, it has also affected

notochord and tailbud formation. The neural tube anterior to the forelimbs was normal for both wild-type and mutant mice. However, caudal to the forelimbs, CNS, spinal cord and the neural tube was abnormal (Lee et al., 2000).

1.1.1.6. Wnt-4

Wnt-4 is a canonical Wnt activator (Park, Valerius and McMahon, 2007). Wnt-4 plays significant roles during kidney development (Stark et al., 1994), sex determination (Kim et al., 2006), adrenal gland development (Heikkila et al., 2002), mammary gland development (Brisken et al., 2000), and thymus (Heinonen et al., 2011).

Stark et al. (1994) showed that *Wnt-4* is expressed in the vertebrate kidney mesenchyme and its derivatives. The expression is also detected in the ureter. It is also expressed in comma-shaped bodies and S-shaped bodies. At later stages, *Wnt-4* is expressed and confined to newly formed tubules at the peripheral region of the kidney. In early stages, *Wnt-4* is expressed in the dorsal spinal cord and induces tubules differentiation in both chick and mouse.

Vainio et al. (1999) showed that *Wnt-4* is expressed in the mesenchyme of the gonad in both sexes before sex determination. When sex is determined, *Wnt-4* expression is downregulated in the male gonad and becomes absent from the Wolfen duct while it is maintained in the female gonad and Mullerian duct in the developmental stages, as well as in the ovary throughout foetal life. *Wnt-4* gene is expressed in neural tube, anterior foregut, foregut endoderm dorsal to the heart and ventral to the paired dorsal aortae (Caprioli et al., 2015).

Sarkar and Sharpe (1999) showed that *Wnt-4* is expressed in the dental mesenchyme after the initiation of tooth development at E11.5. By E13.5 (bud stage) and E14.5 (cap stage), *Wnt-4* is expressed throughout the tooth bud epithelium with no expression in the enamel knot. By E15.5 (early bell stage), *Wnt-4* is weakly expressed in dental epithelium. Suomalainen and Thesleff

(2010) stated that *Wnt-4* is the only Wnt ligand detected in the lingual cervical loop epithelium of E16 and E18 mouse incisors. It is also expressed in the outer enamel epithelium, ameloblasts and dental papilla mesenchyme.

Wnt-4 has a crucial role in the development of the kidney, and it has an auto-inductive role within the already induced renal mesenchyme (Stark et al., 1994; Park, Valerius and McMahon, 2007). *Wnt-4* mutation is fatal, and pups die within 24 hours after birth due to kidney malfunction (Stark et al., 1994). Although *Wnt-4* is expressed in the developing kidney, deletion of *Wnt-4* does not interrupt kidney induction, and kidney development was similar to wild-type mouse kidney, at least until E15. However, later than E15, *Wnt-4* null mice have a retarded and smaller kidney with undifferentiated mesenchymal cells. The expression of the early tubular induction genes such as *N-myc* and a tubular regulator *Pax2* were altered and absent in the *Wnt-4* null mice which affect the mesenchymal cell fate that failed to convert into epithelial structure (Stark et al., 1994).

Wnt-4 is essential for the development of the female reproductive system and the suppression of the male one (Vainio et al., 1999). Kim et al. (2006) showed that Wnt-4 opposes the male pathway by repressing expression of *Sox9* and *Fgf9*. Loss of *Wnt-4* leads to failure of Mullerian duct development, and the ovaries have only a few oocytes. However, male reproductive system development is unaffected by the loss of *Wnt-4* (Vainio et al., 1999). *Wnt-4* null mouse embryos have severe lung hypoplasia and tracheal abnormalities because of the decreased cell differentiation in the tip domain of the lung bud that downregulated lung growth factors Fgf9, Fgf10, Sox9 and *Wnt-2* (Caprioli et al., 2015).

1.1.1.7. Wnt-5a

Wnt-5a can activate both canonical (Mikels and Nusse, 2006) and non-canonical Wnt pathway (Qian et al., 2007), yet its primary activation mechanism is the non-canonical one (Qian et al., 2007; Roarty and Serra, 2007). Wnt-5a plays an essential role in the regulation of growth and pattern in multiple tissues (Yamaguchi et al., 1999) and its expression is controlled by TGF-β (Roarty and Serra, 2007).

Wnt-5a is widely expressed during the embryonic stages. Its expression is detected along the anterior-posterior (A-P) axis with a graded fashion in the caudal end of the embryo during gastrulation stages (Takada et al., 1994). It is also expressed in the primitive streak, paraxial pre-somatic mesoderm, tailbud, hindgut endoderm, developing gut mesenchyme, facial primordia, tongue, AER, limb bud mesenchyme, perichondrium and genitals (Yamaguchi et al., 1999). In the developing lungs, *Wnt-5a* is expressed in mesenchymal and epithelial developing tissues with more strong expression in the branching epithelium, and surrounding both large and small airways at later developmental stages (Li et al., 2002). *Wnt-5a* is also expressed in developing long bone chondrocytes (Yang et al., 2003).

Sarkar and Sharpe (1999) showed that *Wnt-5a* is expressed in the mandibular mesenchymal cells beneath the epithelial thickening of the dental lamina at E11.5. Its expression becomes confined around the mesenchymal layer of the tooth bud at E13.5. At the cap stage (E14.5) the expression is around both the dental follicle and the dental papilla tip. At early bell stage (E15.5), the expression remains in the mesenchyme of the tooth bud with no expression in the epithelial tissue. Suomalainen and Thesleff (2010) stated that at E16 and E18, *Wnt-5a* has a strong expression in the cervical loop area around the lingual cervical loop, and a weaker expression around the labial cervical loop. *Wnt-5a* is also expressed in the alveolar bone, ameloblasts and odontoblasts. At post-natal day 1 (P1), *Wnt-5a* is expressed in the alveolar bone. By P3, *Wnt-5a* expression in the alveolar bone continues with lower expression in

ameloblasts, the dental papilla and odontoblasts, and the expression continues to P11 in both alveolar bone and ameloblasts, but it decreases in the dental pulp and odontoblasts (Xiang et al., 2014).

Wnt-5a loss of function causes perinatal lethality, and the mutant embryos have severe morphological abnormalities in the outgrowing tissues that are truncated caudally, loss of the tailbud and short embryonic anteroposterior axis. *Wnt-5a* null mouse also has an abnormal head shape that has truncated mandible and tongue, and defective outgrowth of the external ear (Yamaguchi et al., 1999).

Wnt-5a null mouse axial skeleton is abnormal, with fused ribs and vertebrae. Vertebrae are smaller in size, and tail vertebrae are fused. Forelimbs and hindlimbs are short and have no digits. *Wnt-5a* loss of function also causes lung hyper-cellularity while *Wnt-5a* mutant mouse lungs have the normal number of lobes and the trachea is shorter with fewer cartilage rings (Li et al., 2002).

Wnt-5a mutant embryos also have a cleft palate, short endocranial regions, irregular ossification centres in the vertebrae and abnormal ribs (Yang et al., 2003). Wnt-5a signaling is essential for chondrogenesis, and it regulates the expression of *Sox9*, the earliest marker for mesenchymal condensation, and *Ihh*. Wnt-5a signaling regulates ossification directly by controlling *Cbfa1* or indirectly by controlling *Ihh* (Yang et al., 2003).

Wnt-5a is crucial for the development of both male and female reproductive organs. It controls the posterior growth of the Mullerian duct, and *Wnt-5a* gain of function inhibits ductal extension and branching (Mericskay et al., 2004; Roarty and Serra, 2007). Loss of *Wnt-5a* function leads to mammary accelerated development (Roarty and Serra, 2007). It also controls the prostate development in the same fashion, inhibits the ductal branching, and it is essential in the prostate duct outgrowth and patterning along the (P-D) axis, so that *Wnt-5a* null embryo

exhibits a less developed prostate because it is required for prostate bud positioning, size and cells movement (Huang et al., 2009).

In vitro, Wnt-5a signaling plays crucial roles in the undergoing fate of dental follicle stem cells (DFSCs) to differentiate to either PDL cells, cementoblasts, or osteoblasts. It is known that Wnt-5a has a vital role in bone remodelling as both osteogenesis enhancer and osteoclastogenesis mediator. Thus, it is essential for maintaining both the unmineralised PDL and the mineralised cementum and alveolar bone (Xiang et al., 2014).

Wnt-5a mutant mice tooth growth is retarded. *Wnt-5a* null embryos have normal tooth development until the cap stage. Beyond the cap stage, delayed development of tooth leads to smaller tooth and abnormal morphology. The impaired tooth size is because of decreased cell proliferation and excessive apoptosis. The mutant molars have abnormal blunted cusps and missing lingual and distal cusps (Lin et al., 2011).

1.1.1.8. Wnt-5b

Wnt-5b is a non-canonical Wnt activator (Bradley and Drissi, 2011). *Wnt-5b* mRNA is about half the size of *Wnt-5a,* and it is 79% and 38% similar to its homologue *Wnt-5a* in both mouse and human, respectively (Yang et al., 2003). Wnt-5b acts with other Wnt ligands in many organs, but its main function has been seen in the chondrogenesis (Wu et al., 2015).

Wnt-5b is co-expressed with *Wnt-5a* in the developing long bone chondrocytes in mice, and its expression is localised to the area between pre-hypertrophic and hypertrophic chondrocyte (Yang et al., 2003). *Wnt-5b* is also co-expressed with *Wnt-3a* and *Wnt-5a* in the primitive streak and tail bud. *Wnt-5b* expression is detected in the medial epiblast and mesodermal layer of the primitive streak with posterior restriction (Takada et al., 1994). *Wnt-5b* is also expressed in the

mouse incisors (Suomalainen and Thesleff, 2010). At E16, *Wnt-5b* expression is localised to the dental papilla mesenchyme and continues to E18.

Wnt-5b signaling is crucial for chondrogenesis. As chondrocytes have two zones with different properties of cell proliferation before hypertrophy, *Wnt-5b* deletion in mice shows impaired chondrocyte differentiation before chondrocyte hypertrophy. However, overexpression of *Wnt-5b* enhances the entrance of chondrocytes to zone II, and it also prevents chondrocytes cell cycle withdrawal (Yang et al., 2003).

Over-expression of *Wnt-5b* in chondrocytes results in the formation of abnormalities related to bone ossification such as shorter long bones, smaller rib cages, and skull formation failure (Yang et al., 2003).

Wnt-5b controls osteo-chondroprogenitor cell migration through activation of JNK, a non-canonical Wnt pathway, during patterning. Furthermore, Wnt-5b signaling decreases mesenchymal progenitor's cellular adhesion by controlling cadherin receptor (Bradley and Drissi, 2011).

Different species also show the role of Wnt-5b in chondrogenesis and bone development. Wu et al. (2015) showed that Wnt-5b controls jaw development of zebrafish by controlling *fgf3* expression and *Wnt-5b* loss of function in zebrafish leads to dislocated and smaller Meckel's and ceratohyal cartilages.

1.1.1.9. Wnt-6

Wnt-6 is a non-canonical Wnt activator and signals through the JNK pathway (Li et al., 2014). Wnt-6 ectodermal signal induces somite-derived progenitor cells to form muscle cells during limb development (Geetha-Loganathan *et al.*, 2005).

Wnt-6 in mouse and chicken is expressed in the limb ectoderm both dorsally and ventrally, including the dorsoventral boundary which corresponds to the potential apical ectodermal ridge (AER) (Rodriguez-Niedenfuhr et al., 2003). In addition to the surface and limb ectodermal expression, *Wnt-6* is also expressed in the AER, and the expression pattern is restricted to the handplate ventral ectoderm and extended dorsally to the limb shaft (Summerhurst et al., 2008).

Sarkar and Sharpe (1999) showed that *Wnt-6* is expressed in the mouse tooth bud. When tooth development is initiated at E11 to E12, *Wnt-6* expression is detected in the oral epithelium and dental epithelium thickening. When the tooth bud forms at E13.5, *Wnt-6* expression can be seen throughout the bud epithelium with stronger expression in the buccal side of the molar tooth bud. At cap stage (E14.5), *Wnt-6* is expressed in the enamel knots, and internal and external enamel epithelium, and continues to early bell stage (E15.5). Mouse incisor dental pulp at E16 and E18 expresses *Wnt-6*. At E16, *Wnt-6* expression is detected in dental papilla mesenchyme. At E18, *Wnt-6* is expressed in the lingual epithelial cervical loop area odontoblasts, pre-ameloblasts and ameloblasts (Suomalainen and Thesleff, 2010).

Wnt-6 is essential for somite formation and limb development (Geetha-loganathan et al., 2005). During limb muscle development, ectopic *Wnt-6* expression in the limb bud leads to ectopic expression of different myogenic markers such as *Pax3, Paraxis, Myf5* and *Myogenin*. *Wnt-6* can compensate for the surgical removal of the ectoderm and rescues the expression of the myogenic genes *in vitro* (Geetha-loganathan et al., 2005).

Wnt-6 also shows a role in controlling the behaviour of human dental pulp cells by controlling odontoblast development and differentiation *in vitro*. It enhances the expression of different genes which are responsible for dentine mineralisation such as *Runx-2, Dspp* and *DMP-1*. Thus *Wnt-6* might have a role in the pulp repair (Li et al., 2014).

1.1.1.10. Wnt-7a

Wnt-7a is a canonical Wnt activator (Hirabayashi et al., 2004). *Wnt-7a* is expressed in different organs during development. *Wnt-7a* is also expressed in the cerebellar granule cells (Hall, Lucas and Salinas, 2000). It is also expressed in the dorsal ectoderm before limb bud formation, and then it becomes distributed throughout the limb ectoderm (Parr and McMahon, 1995).

Wnt-7a is expressed in the developing female reproductive system. Expression of *Wnt-7a* is detected in the prenatal Müllerian tract epithelium. After birth, the expression becomes restricted to both oviduct epithelium and uterine luminal epithelium (Miller and Sassoon, 1998).

Wnt-7a is expressed in the developing mouse incisors. At E16, *Wnt-7a* expression is detected in the labial side dental epithelium, lingual epithelium and lingual cervical loop area and the expression becomes weaker at E18 (Suomalainen and Thesleff, 2010).

Wnt-7a null mice are viable but also have limb abnormalities which affect the dorsal tissue that adopts ventral tissues. The dorsal surface mimics some of the ventral sides and has thickened and pigmented dermal tissues and truncated nail (Parr and McMahon, 1995).

Wnt-7a signaling guides the development of the anteroposterior axis, radial axis patterning and uterine smooth muscle patterning. In the female reproductive tract, *Wnt-7a* mutant mouse uteri are smaller and thinner in diameter and the oviducts are either smaller or absent with abnormal coiling. The appearance of the mutant uterus has an abnormal phenotype that combines uterus and vaginal structures. Loss of Wnt-7a function leads to loss of *Msx1* expression in the uterus, as well as loss of *hoxa-10* and *hoxa-11* expression that leads to the abnormal uterus phenotype (Miller and Sassoon, 1998).

Wnt-7a signaling has a crucial role in neurogenesis. In the late stages of neocortex development, Wnt-7a signaling can promote the neuronal differentiation of the neural

precursor cells (NPC) by regulating *Ngn1*, while the inhibition of Wnt-7a signaling leads to neuronal differentiation suppression (Hirabayashi et al., 2004).

Wnt-7a induces neuron axonal *in vitro* by inhibiting the activity of GSK-3β and via controlling the level of synapsin1. It also shows an important and crucial role in the regulation of mossy fibre morphology (Hall, Lucas and Salinas, 2000).

Wnt-7a is also an essential factor that regulates female reproductive system development. At the neonatal stage, *Wnt-7a* mutant mouse Mullerian ducts exhibit no coiled oviducts, and a thinner and less muscular uterine wall with the absence of uterine glands (Parr and McMahon, 1998).

1.1.1.11. Wnt-7b

Wnt-7b activates the canonical Wnt pathway (Lobov et al., 2005), non-canonical planar cell polarity pathway (Rosso et al., 2005), and G protein-linked PKC delta pathway (Tu et al., 2007). Wnt-7b signaling is crucial for several organs development such as placenta, lung, eye, dendrite, bone formation and kidney (Yu et al., 2009).

Wnt-7b is widely expressed during developmental stages for both embryonic and extra-embryonic tissues. It is expressed in the lung epithelium, the developing kidney, the spinal cord and the brain and is also observed in the developing skin and the developing bile duct (Shu et al., 2002). *Wnt-7b* is also expressed in the extra-embryonic membranes and its pattern is restricted to the chorionic plate well before chorion fuses with allantois (Parr et al., 2001). Its expression is also detected in macrophages (Lobov et al., 2005) and osteogenic cells (Tu et al., 2007).

Sarkar and Sharpe (1999) stated that *Wnt-7b* is expressed in the developing molars. At E11.5, *Wnt-7b* is expressed in the oral epithelium, but its expression is absent from the dental

epithelium. However, by E13.5, *Wnt-7b* expression covered the whole tooth bud epithelium. At the cap stage (E14.5) *Wnt-7b* expression is still throughout the tooth epithelium but it is detected in the enamel knot. At the early bell stage (E15.5), *Wnt-7b* expression becomes weak, yet, at the same area as the cap stage. Suomalainen and Thesleff (2010) showed that *Wnt-7b* expression in the developing incisor at E18 is limited to the follicle mesenchyme.

Wnt-7b null embryos do not survive beyond E11.5 (Parr et al., 2001). Shu et al. (2002) used different methods and found mice can survive prenatally, but they die after birth due to respiratory failure. The lung of these mutant mice is hypoplastic, due to epithelial cell affected differentiation which subsequently reduces lung mesenchymal cells differentiation and has pulmonary haemorrhage caused by vascular defects.

The chorion and allantois in *Wnt-7b* mutants are not able to fuse, which leads to embryo necrosis and the formation of a ball of allantois cells posterior to the embryo, and that causes malformation of the placenta, and later death of the embryo. The mutants also show altered and smaller chorion (Parr et al., 2001).

Yu et al. (2009) stated the importance of Wnt-7b in the developing kidney as it is an essential factor for loop of Henle elongation, and growth which is mandatory for nephron medullary organisation. Tu et al. (2007) also demonstrated the role of Wnt-7b signaling in bone osteoblastogenesis whereas loss of *Wnt-7b* function reduces the embryonic bone mineralisation. *Wnt-7b* is expressed in macrophages and it is required for the programmed cell death in the hyaloid vessels' endothelial cells in the developing eye (Lobov et al., 2005).

1.1.1.12. Wnt-8a

Wnt-8a role is highly conserved in vertebrates (Cunningham et al., 2015). *Wnt-8a* is co-expressed with *Wnt-1* to maintain the Wnt signaling pathway in the otic placode (Vendrell et

al., 2013). In addition, *Wnt-8a* and *Wnt-3a* cooperate to preserve axial stem cell homeostasis during the early somite stages which are required for normal body axis extension (Cunningham et al., 2015).

At E7.5–E7.75, *Wnt-8a* is expressed throughout the epiblast and primitive streak (Zhao and Duester, 2009) and hindbrain (Niederreither et al., 2000). At the five and seven somite pair stages, *Wnt-8a* has two areas of expression; hindbrain and anterior part of the epiblast. The expression then downregulates at the 10-somite pair stage and disappeared at the 12-somite pair stage (Cunningham et al., 2015).

Wnt-8a is also expressed throughout the embryo with no expression in the anterior headfold region. It is expressed in the hindbrain during otic placode induction. During placode formation, *Wnt-8a* expression is maintained in the developing hindbrain and the primitive streak region (Vendrell et al., 2013).

Wnt-8a null mice are viable (van Amerongen and Berns, 2006). In *Xenopus*, overexpression of *Wnt-8a* has two abnormal effects; impaired somite mesoderm specification and defective posterior development (Hoppler et al., 1996). Genetic knock-down zebrafish *Wnt-8a* leads to a loss of posterior mesoderm expansion as well as defects in neural ectoderm posteriorisation (Wylie et al., 2014).

Wnt-8a is expressed in the otic placode. However, loss of *Wnt-8a* function does not affect the inner ear placode formation. Genes expression that depends on Wnt signaling which has been detected in the placode, such as *Dlx5, Pax2* and *Sox9* have regular expression pattern as well as *Lfng*, a component of the Notch signaling pathway (Vendrell et al., 2013). *Wnt-8a* co-expression with *Wnt-3a* compensate for *Wnt-8a* loss of function (Cunningham et al., 2015).

1.1.1.13. Wnt-8b

Wnt-8b has been used as a marker of the dorsomedial telencephalon (Fotaki et al., 2010). *Wnt-8b* is mainly expressed in the developing hypothalamus (Lee et al., 2006) and forebrain (Richardson et al., 1999).

At E10.5, *Wnt-8b* is expressed between diencephalic and telencephalic boundaries. At E12.5, *Wnt-8b* expression becomes limited to the dorsomedial telencephalon. By E14.5, the relative extent of expression in the telencephalon was significantly reduced in the dorsomedial side with stronger expression in the cortical hem. At E18.5, expression was restricted to the lateral margin of the remnant of the cortical hem known as the hippocampal fimbria (Bulchand et al., 2001).

Wnt-8b is also expressed in the developing diencephalon. At E10.5, it is strongly expressed in the presumptive hypothalamus. At E12.5, *Wnt-8b* expression is detected in the eminentia thalami and the developing hypothalamus ventricular zone neuroepithelium (Fotaki et al., 2010).

Wnt-8b null mice are healthy, and the adult hippocampus is normal. The dorsomedial telencephalon develops normally, and it shows no genes alteration and the overall hippocampus morphology is no different from the wild-type one (Fotaki et al., 2010). However, morpholino treated zebrafish to block *Wnt-8b* function causes loss of pro-neural gene expression and inhibits neurogenesis in the posterior hypothalamus (Lee et al., 2006).

1.1.1.14. Wnt-9a

Wnt-9a is a canonical Wnt activator (Spater et al., 2006) and little has been published on the expression of *Wnt-9a* (Summerhurst et al., 2008). *Wnt-9a* is expressed in the limb mesenchyme in the position of the future joints (Guo et al., 2004).

Although *Wnt-9a* mutant mice have no severe joint defects, skeletal abnormalities still exist; long bones are shortened, and the mineralised region size has more reduction (Spater et al., 2006). This abnormal bone phenotype affects the proximal bones such as ileum, femur and scapula. The skull frontal bone mineralisation is reduced, and hyoid bone is hyperplastic. The posterior part of the occipital bone of the mutant mice has both abnormal shape and smaller size. Moreover, the midline suture has areas of ectopic cartilage because of the ectopic differentiation of the suture cells to chondrocytes (Spater et al., 2006).

1.1.1.15. Wnt-9b

Wnt-9b, (previously known as Wnt-14b (Qian et al., 2003) and Wnt-15 (Bergstein et al., 1997)), is a non-canonical Wnt activator (Karner et al., 2009). Wnt-9b signaling mainly controls urogenital development (Carroll et al., 2005) and cell proliferation (Liu et al., 2013).

Wnt-9b is expressed in the Wolffian duct epithelium from E9.5 to E14.5. *Wnt-9b* is expressed in the ureteric bud of the metanephric kidney at E10.5–E11.0. At E11.5, *Wnt-9b* expression is strongly expressed in the stalk and horizontal epithelium but is weaker in the proximal branching tips. *Wnt-9b* expression continues throughout nephrogenesis in the developing collecting duct system (Carroll et al., 2005) and into adult stages (Karner et al., 2009).

Wnt-9b null pups die within 24h after birth. The mutant pups have cleft lip and palate and lack reproductive ducts at birth. *Wnt-9b* null mice nasal and maxillary processes development is impaired because of the reduced mesenchymal cells proliferation which causes cleft lip and palate (Jin et al., 2012).

Wnt-9b mutant mice mesenchymal cell of the ureteric system undergo tubulogenesis because of a cellular aggregation failure. Carroll et al. (2005) stated that *Wnt-9b* is not mandatory for the early development of the ureteric structures of the metanephric kidney. However, *Wnt-9b*

is essential for posterior extension of the Müllerian duct and the development of the female reproductive tract. Wnt-9b signaling regulates the diameter of kidney tubules by regulating cellular orientation. However, ablation of *Wnt-9b* after P10 did not have discernible effects on kidney morphology or function (Carroll et al., 2005).

1.1.1.16. Wnt-10a

Mouse *Wnt-10a* was identified in 1996 where it is widely expressed in both adult mouse and embryos (Wang and Shackleford, 1996). Wnt-10a is signaling through the canonical Wnt pathway and it is essential for tooth development, that loss of Wnt-10a function can lead to tooth agenesis (Yang et al., 2015). *Wnt-10a* has shown an important role in controlling adipogenesis and osteogenesis (Liu et al., 2013). Human *WNT-10a* mutation is associated with several abnormalities such as ectodermal dysplasia (Adaimy et al., 2007), and oligodontia (Plaisancie et al., 2013).

Wnt-10a is expressed in adult brain and pituitary gland at E13.5 and E15.5, and it is also expressed in the face, limbs, skin and the liver (Wang and Shackleford, 1996). *Wnt-10a* also is expressed in the molar dental epithelial thickening at E11.5 and in the primary and secondary enamel knots (Dassule and McMahon, 1998). *Wnt-10a* is also expressed in the secretory odontoblasts and differentiating odontoblasts around the epithelial root sheet that control root formation (Yang et al., 2015; Yamashiro et al., 2007).

Wnt-10a expression is detected in dental epithelial thickening at E12. Then, expression becomes localised to tooth bud epithelium of the tooth bud at E13.5. At cap stage (E14.5) the expression can be detected in the enamel knot (Dassule and McMahon, 1998). Once the early bell stage is established, the expression shifts from the epithelial cells to the mesenchymal cell (Liu et al., 2013).

Suomalainen and Thesleff (2010) showed that at E16, *Wnt-10a* is intensively expressed in the dental papilla mesenchyme, ameloblasts and pre-ameloblasts, and odontoblasts. At E18, the expression becomes confined to odontoblasts with weak expression in ameloblasts. *Wnt-10a* RNA is detected at different levels of odontoblast maturation, including differentiating, pre-odontoblasts and active odontoblasts (Yamashiro et al., 2007).

Cawthorn et al. (2012) stated that Wnt-10a regulates osteogenesis and adipogenesis. Overexpression of *Wnt-10a* increases bone formation and inhibits lipid formation. On the contrary, downregulating *Wnt-10a* improves adipogenesis.

Wnt-10a is also crucial for mice teeth development and patterning where *Wnt-10a* null mice develop supernumerary small distal molars. The maxillary molars also exhibit abnormal phenotype where the crown is smaller and has fused labial cusps and deep groves. The mandibular molars have a less severe phenotype that includes smaller molars and cusps fusion only affects some of them. Both maxillary and mandibular molars have wider pulp space (taurodontism), pulp stones, and thinner dentine. *Wnt-10a* null mouse incisors are abnormal where the cervical area shows irregularly shaped dentine with V-shape defects in the lingual side of the tooth (Yang et al., 2015).

Liu et al. (2013) and Yamashiro et al. (2007) stated that Wnt-10a could control odontogenesis *in vitro* by regulating *Dspp* levels. Deletion of *Wnt-10a* in the re-associated teeth germ leads to the formation of cysts and bony structure and inhibits the dental mesenchymal stem cells proliferation.

1.1.1.17. Wnt-10b

Wnt-10b is a canonical Wnt activator (Ling, Nurcombe and Cool, 2009). Wnt-10b binds to FZD1, 2, and 5 to activate Wnt/β-catenin signaling (Ross et al., 2000).

Suomalainen and Thesleff (2010) showed that *Wnt-10b* is expressed in the ameloblasts of mouse incisors at E16 while its expression is weak and absent in the mouse incisor ameloblasts at E18. Sarkar and Sharpe (1999) stated that at E11.5 when the tooth development is induced, *Wnt-10b* is expressed in the molar mesial cells of the dental epithelial thickenings with no expression in the oral epithelium. At the bud stage at E13.5, *Wnt-10b* expression is localised to the tip of the tooth bud epithelium. At the cap stage at E14.5, *Wnt-10b* is expressed in the outer dental epithelium and the enamel knots while it remains but with weaker expression in the dental epithelium. At the early bell stage (E15.5), *Wnt10-b* expression becomes localised to the internal enamel epithelium with no expression in external enamel epithelium.

Wnt-10b null mice appear normal and have normal growth (Bennett et al., 2005). Yet, they develop early bone maturation that enhances bone density and volume. However, after bone maturation is completed, bone shows a decrease in both volume and trabecular number (Stevens et al., 2010).

Wnt-10b signaling antagonises adipocytes differentiation and agonises osteoblastogenesis. So, it can determine the mesenchymal precursor cells fate (Bennett et al., 2005). Wnt10b suppress the expression of adipocyte genes in the adipogenesis sites even before its induction (Cawthorn et al., 2012).

On the contrary, Wnt-10b stimulation of osteogenesis increased trabecular bone that increases bone density and strength of femur, tibia, hip, vertebrae and humerus. The increased bone mass affects both sexes, and it is caused by the increase in trabecular number and thickness. The researchers also showed that *Wnt-10b* null mice have decreased bone volume (Bennett et al., 2005). That can explain the importance of Wnt-10b signaling to enhance osteoblasts differentiation and maintain mesenchymal differentiation to the osteoprogenitor lineage (Stevens et al., 2010).

1.1.1.18. Wnt-11

Wnt-11 act as a non-canonical Wnt activator (Majumdar et al., 2003). Kispert et al. (1996) illustrated *Wnt-11* expression so that at E6.75, *Wnt-11* is expressed in the posterior half of the embryo. Then, at E7, the expression continues in the posterior end with another expression domains in the node, mesoderm of the extra-embryonic tissue and allantois. After that, the node expression disappeared and the tailbud expression remains until E11.5 with strong expression in the newly formed somites at the tip. *Wnt-11* can also be detected in the heart tube at E7.75 and E9.5 in the myocardium. It is also expressed in the rostral somites of the future dermatome. In addition, *Wnt-11* is expressed in the branchial arches, limb bud and perichondrium.

Wnt-11 in the urogenital system is first detected at E9 in the mesonephric duct following the posterior ductal elongation. At E10.5, the mesonephric duct has reached the position of the metanephric mesenchyme which is located at approximately the level of the hindlimb buds. At E11, *Wnt-11* expression becomes limited to the nephric duct epithelium adjacent to the metanephric mesenchyme where the ureter bud is going to form. Expression of *Wnt-11* then becomes confined to the tip of the ureter, which continues at the tip after branching (Kispert et al., 1996).

In the developing mouse incisors, *Wnt-11* is expressed mainly in the dental follicle at E16 with weak expression in the odontoblasts. At E18, *Wnt-11* is expressed in the lingual cervical loop epithelium, odontoblasts and dental follicle mesenchyme (Suomalainen and Thesleff, 2010).

Wnt-11 null pups died within 48 hours. *Wnt-11* null embryos have a smaller kidney with normal nephron orientation. The abnormal and defective morphogenesis leads to ureteric tip deformation, which consequently causes smaller kidneys (Majumdar et al., 2003).

1.1.1.19. Wnt-16

Wnt-16 can signal through a non-canonical Wnt pathway in both osteoblasts and osteoclasts, while it activates the canonical Wnt pathway in osteoblasts (Movérare-skrtic et al., 2014).

Guo et al. (2004) showed that *Wnt-16* is expressed in mouse joints during different developmental stages. At E12.5, it is expressed in the carpal condensation area and, at E13.5, its expression can be detected in the metacarpal-phalangeal joints. *Wnt-16* is also expressed in the skin at E15.5 in the basal layer with no expression in the area of hair bud formation and the expression is limited to the epidermis basal cell layer (Witte et al., 2009). In the developing skeleton, *Wnt-16* expression is also detected in both perichondrium and periosteum of the developing skeleton. *Wnt-16* is strongly expressed in developing limbs in the region of developing somites at E9.5 to E10 (Witte et al., 2009). *Wnt-16* is also expressed in the human peripheral lymphoid organs, such as the spleen and lymph nodes (McWhirter et al., 1999).

Wnt-16 mutant mice have bone fractures because of the abnormal bone formation that has a decreased cortical bone thickness with porosities throughout the cortical plate. Despite the abnormal cortical plate, trabecular bone has a normal volume (Zheng et al., 2012; Movérare-skrtic et al., 2014). *Wnt-16* is expressed by cortical bone osteoblasts, and it inhibits osteoclast differentiation *in vitro*. *Wnt-16* admission to osteoblastic cell line induces the expression of osteoprotegerin (*Opg*) that suppresses osteoclastogenesis through the inhibition of the osteoclasts in bone marrow-derived macrophage (Movérare-skrtic et al., 2014).

1.1.2. Canonical Wnt pathway

The canonical Wnt pathway manipulates a multifunctional protein known as β-catenin (Clevers, 2006). In the absence of Wnt ligand binding to the receptor, β-catenin is degraded and phosphorylated by a protein complex known as the destruction complex (Rao and Kuhl, 2010).

When Wnt ligand binds to co-receptors Frizzled, a second response activates Low-density receptor-related protein 5 and 6 (LRP-5/6) to attract Axin2 to the plasma membrane, and then phosphorylates Dishevelled (Dvl) to inhibits kinase activity which deactivates the β-catenin destruction complex and therefore free the stable β-catenin in the cytoplasm, allowing β-catenin translocation to the nucleus. The translocated β-catenin then binds to the N-terminus of the DNA-binding proteins of both T-cell factor and lymphoid enhanced factor (Tcf/Lef) family and establishes their transcription (Rao and Kuhl, 2010) (Figure 1.1).

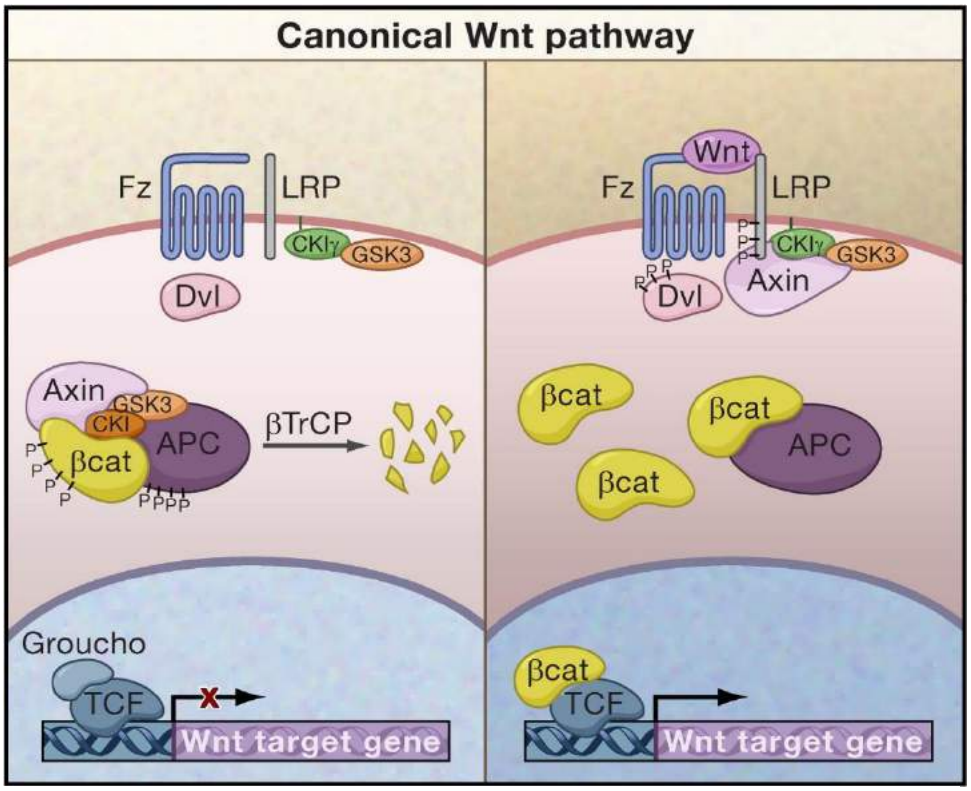

Figure 1.1. Canonical Wnt pathway

In the absence of Wnt ligand, β-catenin is phosphorylated and degraded by the destruction complex. When Wnt ligand binds to the receptor Frizzled, co-receptor LRP attracts and binds to Axin and Dishevelled to deactivates the destruction complex. Thus, β-catenin accumulates in the cytoplasm and then enter the nucleus to activate the target gene transcription. (Clevers, 2006).

1.1.2.1. β-catenin destruction complex

β-catenin destruction complex contains GSK-3, APC, Axin, CK1 and β-catenin itself. β-catenin phosphorylation is initiated by the CK1 phosphorylation of β-catenin serine (Ser45). This primes GSK-3 mediated phosphorylation of S37 and S33 to generates β-TrCP-binding site. Then, the proteasome interacts with β-TrCP and consequently proteolytically destroys β-catenin (Rao and Kuhl, 2010).

1.1.2.1.1. Casein kinase (CK1)

Casein kinase CK1, one of the destruction complex proteins, has several isoforms that are expressed in different cell structures. CK1γ is expressed in cell membrane while CK1α, CK1δ, and CK1ε are expressed in the cytoplasm. CK1δ and CK1ε can be auto-phosphorylated because they have a carboxy-terminal extension (Cegielska *et al.*, 1998). Moreover, the cytoplasmic isoforms can bind to Axin, another protein in the destruction complex, and phosphorylate β-catenin (Amit *et al.*, 2002).

1.1.2.1.2. Glycogen synthase kinase 3 (GSK-3)

Glycogen synthase kinase 3 (GSK-3) has multiple functions including glycogen synthesis, microtubule stability, cell-cycle control, and inflammation. It is also a part of the β-catenin destruction complex (Frame and Cohen, 2001). GSK-3 has two isoforms, GSK-3α and GSK-3β. The role of GSK-3 in Wnt signaling is to phosphorylate S37 and S33 to mediate β-catenin phosphorylation (Stamos and Weis, 2013).

1.1.2.1.3. Axin

Axin is a part of mouse *Fused* locus. Its mutation had shown a duplication of the body axis at the embryonic stage. There are two Axin isoforms, Axin1 and Axin2. *Axin1* is expressed in a wide range of locations while *Axin2* shows a more restricted expression. Both could substitute

each other because they are interchangeable (Zeng et al., 1997). *Axin2* expression is controlled by Wnt/β-catenin signaling as one of the target genes. It is also part of the degradation complex and thus, works as a Wnt/ β-catenin pathway negative feedback loop (Jho *et al.*, 2002). The binding of Axin to the other destruction complex proteins decreases the distance between them and enhances the effectiveness of the complex to stablise β-catenin phosphorylation (Komiya and Habas, 2008).

1.1.2.1.4. Adenomatous polyposis coli (APC)

Adenomatous polyposis coli (APC) is another protein in the destruction complex. APC has two isoforms, APC1 and APC2. It has different biological roles in the spindle formation and maintenance, and stability of the microtubules. APC exact role in the destruction complex is not fully understood. Day and Alber (2000) stated that APC has two binding regions to bind to Axin and β-catenin. Stamos and Weis (2013) suggested that it has a role in stabilising the complex for β-catenin phosphorylation. Xing et al. (2003) stated that APC becomes phosphorylated by CK1 and GSK-3 after β-catenin phosphorylation which free Axin to bind to another β-catenin molecule.

1.1.3. Non-canonical Wnt pathway

1.1.3.1. Planar cell polarity (PCP)

Planar cell polarity is a mechanism of cell orientation (Komiya and Habas, 2008). It has a fundamental role for the epithelial and mesenchymal cells to be well polarised along a plane perpendicular to the apical-basal axis of the basal cells (Seifert and Mlodzik, 2007). It is also important for neuronal cells orientation in the axonal-dendric plane (Mlodzik, 2002). In vertebrates, PCP have a crucial role in the organisation and orientation of the inner ear epithelium cilia, and hair follicles (Komiya and Habas, 2008).

When Wnt ligand binds to Frizzled, dishevelled (Dvl) becomes activated. PDZ and DEP domains of dishevelled activate two pathways through two domains; Rho and Rac. For the activation of Rho, Dvl recruits and activates (Dishevelled associated activator of morphogenesis 1) leading to Rho GTPase activation. Thus, Rho associated kinase (ROCK) becomes activated and consequently modifies Actin cytoskeleton. The second pathway is activated when DEP, the other domain of Dvl, triggers Rac GTPase which then stimulates JNK activity to control tissue polarity and movement (Komiya and Habas, 2008) (Figure 1.2).

1.1.3.2. Wnt/Ca^{2+} signaling pathway

Wnt/ Ca^{2+} pathway shares many molecules with the PCP signaling pathway (Slusarki and Pelegri, 2007). Wnt/ Ca^{2+} modulates both canonical Wnt and PCP pathways (Kohn and Moon, 2005).

When Wnt ligand binds to the cognate receptor Frizzled, which is bound to G-protein, this activates co-receptors Ror1/2 and results in the formation of inositol 1,4,5-triphosphate (IP3), and 1,2 diacylglycerol (DAG) from phospholipid phosphatidyl inositol 4,5-bisphosphate. DAG and IP3 release Ca^{+} ions and activate protein kinase C (PKC) and calcium calmodulin-dependent protein kinase II (CaMKII) which then translocate to the nucleus to antagonise β-catenin activity. IP3 can also activates phosphatase calcineurin (Cn) which activates nuclear factor associated with T cells (NFAT), a gene activator found in neurons and muscles, that enters the nucleus and activates lymphocytes pro-inflammatory genes to control cell fate and movement (Xiao *et al.*, 2017). NFAT also activates lymphocytes pro-inflammatory genes (Undi et al., 2016) (Figure 1.2).

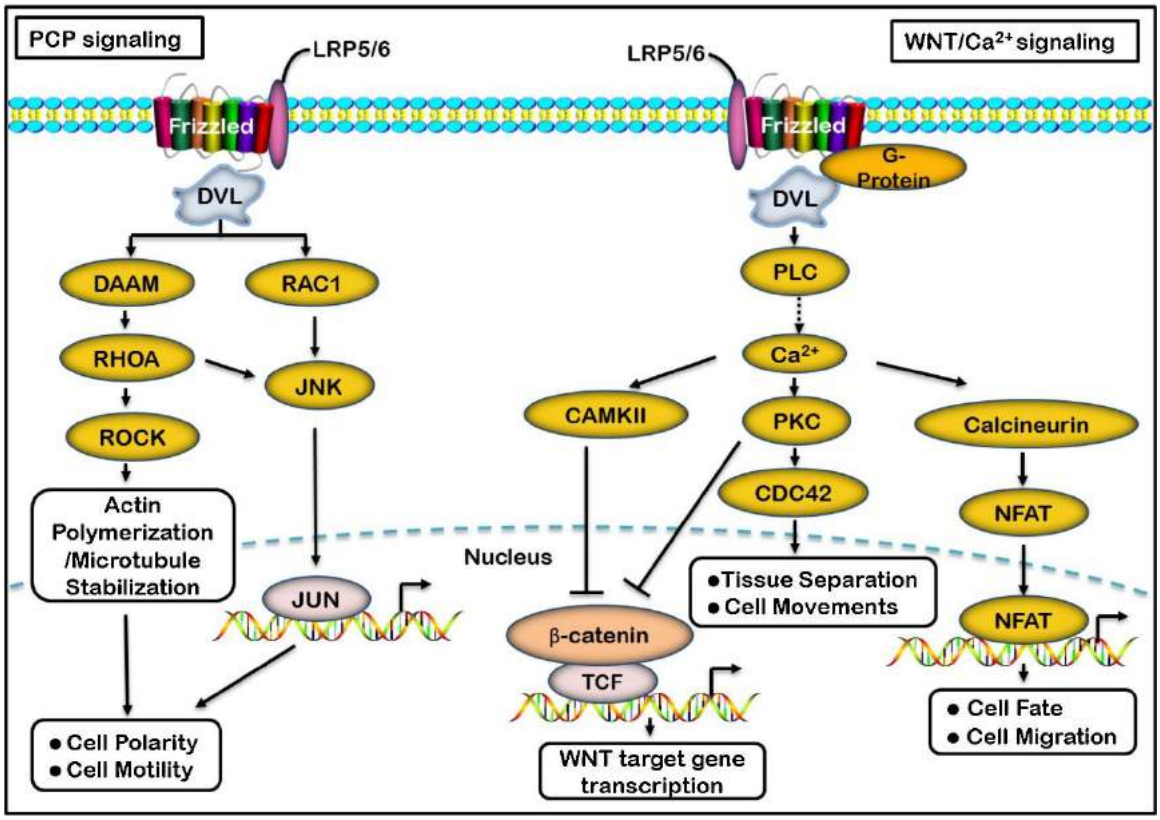

Figure 1.2. Non-canonical Wnt pathways

Planner cell polarity (PCP) pathway: when Wnt ligand binds to Frizzled, Dishevelled, activates the two domains Rho, which stimulate ROCK and modifies Actin cytoskeleton, and RAC, which stimulates JNK and controls cell mobility and polarity.

Wnt/Ca_2 pathway, when Wnt binds to Frizzled which is bound to G-protein, this activates co-receptors Ror1/2 and leads to IP3 and DAG formation. IP3 releases Ca_2 that antagonises canonical Wnt pathway via CAMKII and PKC. Ca_2 also stimulates Calcineurin to activate NFAT that enters the nucleus and activates lymphocytes pro-inflammatory genes to control cell fate and movement (Xiao et al., 2017).

1.1.4. Role of Wnt signaling in different stem cell populations

Wnt/β-catenin signaling regulate different stem cell population. It has a fundamental role in hair follicle stem cells regulation. The hair follicle consists of inner and outer bulge layers (Morris *et al.,* 2004). While in the rest stage, hair follicle stem cells remain quiescent (Cotsarelis *et al.,* 1990). After being activated, stem cells proliferate and produce new hair follicles and participate in the new hair cycle. Wnt/β-catenin signaling regulates active hair follicle stem cells while it is absent in the rest stage. Its role is to specify stem cell progenies in the follicle and to maintain stem cell label retention and markers. Lim *et al.* (2016) showed that hair follicle stem cells have an autocrine Wnt/β-catenin signaling activation system where the secreting cells are responding to their own secreted Wnt ligands.

Another example of Wnt/β-catenin signaling responsive stem cell populations is intestinal stem cells. This population resides in the crypt, where the niche is. Knocking out Wnt/β-catenin in the intestine shows complete loss of the stem cells from the crypt, and the mice died directly after birth (Korinek *et al.,* 1998). Postnatally, inactivation of Wnt/β-catenin pathway shows complete loss of epithelial stem cells from the crypt (Fevr *et al.,* 2007). Mutation of Wnt/β-catenin pathway down-streams could result in many kinds of tumours such as colorectal carcinoma which is caused by loss of function mutation of the *APC* gene (Korinek *et al*., 1997) as well as *Axin2* (Liu *et al*., 2000).

Skeletal stem cells are populations of mesenchymal stem cells that are responsible for bone development, repair and homeostasis. At least two populations of skeletal stem cells have been found and studied among their origin; stem cells with perivascular origin in long bones and stem cells of flat bones which originate from a different embryonic origin (Jiang *et al*., 2002). Skull bones are flat bones, and they are mainly formed by intramembranous ossification. The potential niche of skeletal stem cells in the skulls is in the mesenchyme in between the bone, in an area known as suture, and is responsible for the suture fusion and repair. Skeletal stem

cells at the suture are *Axin2*-expressing cells, and their abilities for proliferation and differentiation into osteoprogenitors and osteocyte are controlled by the Wnt/β-catenin pathway (Maruyama *et al.*, 2016).

Hematopoietic stem cells (HSCs) functions are controlled by Wnt signaling. both canonical and non-canonical Wnt pathways have been found to control HSC renewal (Rattis et al., 2004). Depletion of canonical Wnt signaling inhibits HSCs regeneration *in vivo* (Reya et al., 2003). Moreover, *In vitro*, up-regulation of canonical Wnt pathway promotes proliferation of hematopoietic progenitor cells (Austin et al., 1997). Famili et al, (2016) showed that canonical Wnt pathway regulation of HSCs by using different *Apc* mutations is dose dependent that high level of canonical Wnt pathway promotes HSCs differentiation. Non-canonical Wnt signaling members Flamingo and Frizzled8 is expressed in the HSCs and have shown to maintain the long-term quiescent HSCs (Sugimura et al., 2012). Thus, Wnt signaling is crucial for HSCs renewal and differentiation.

1.1.5. Wnt pathway interacts with other pathways in adult mouse incisor

Like incisor development, adult mouse incisor homeostasis is controlled by different signaling pathways, epigenetic programming and growth factors. Yu *et al.* (2015) (in Sharpe, 2016) reviewed the importance of many epithelial and mesenchymal signals that contribute to mouse incisor stem cells/progeny regulation such as Wnt, Fgf and Tgf-β (Figure 1.3). In this part of the introduction, a brief review of some of the signaling pathway affecting mouse incisor homeostasis was done to illustrate the signaling network on mouse incisors pulp.

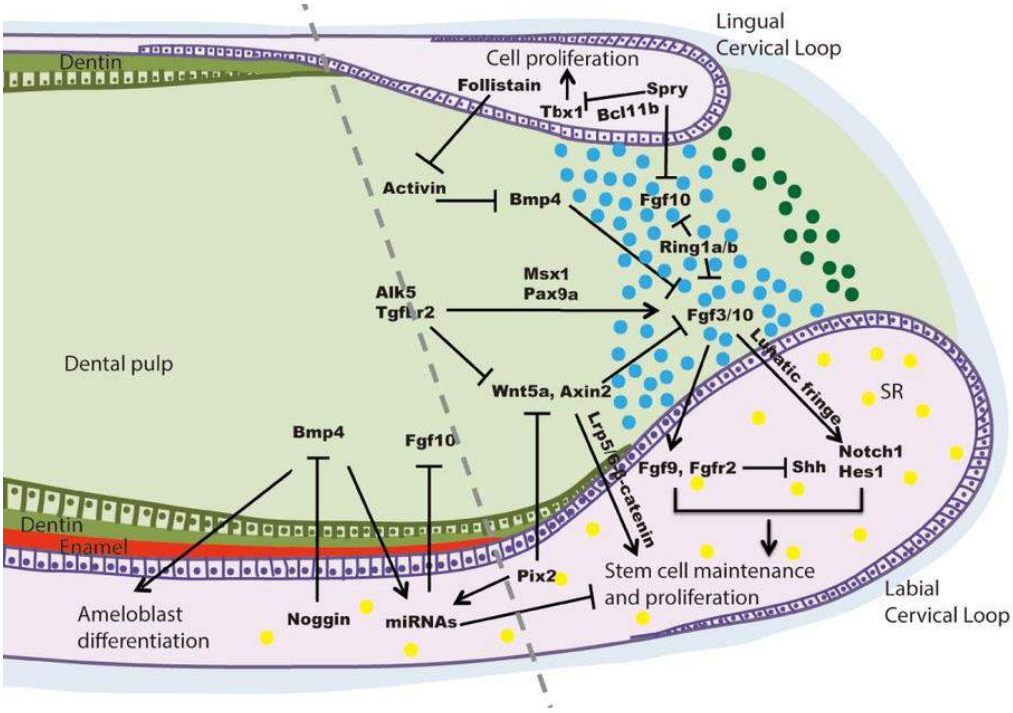

Figure 1.3. Mouse incisor stem cell population at the proximal end shows a variety of different regulators.
Mesenchymal stem cells (MSCs) (dark green dots) and transit amplifying cells (TACs) (blue dots) are at the proximal end of the tooth and located between the lingual and labial cervical loop. The regulatory network that controls mouse incisor MSCs is complex and a variety of signalling, transcriptional and epigenetic pathways is involved. The regulatory network controls both incisor mesenchymal (light green) and epithelial (purple) stem cells maintenance, proliferation and differentiation (Sharpe, 2016).

Wnt/β-catenin signaling interacts with N-cadherin to form cell–cell adhesion junctions which can also be regulated by TGFβ1 so that TGFβ1 controls the level of Wnt7a, which is essential for MSCs chondrogenic differentiation (Tuli *et al*., 2003). TGFβ1 also regulates β-catenin to control MSCs osteogenesis (Jian *et al.*, 2006). To suppress carcinogenesis, Wnt/β-catenin pathway can be switched to TGFβ pathway by the interaction between Runx3 and β-catenin/TCF4 (Ito *et al.*, 2008). Wang et al. (2004) showed that Follistatin, an inhibitor of TGF-β signals, is secreted by the epithelium to control dental mesenchyme Bmp4 downstream in the dental mesenchyme. Follistatin gain of function transgenic mice have an ameloblasts differentiation defect that consequently leads to the formation of enamel free areas that incisors

have a chalky white appearance with either broken or overgrown upper incisors while lower incisors are short. Newly born mice have no ameloblasts in the labial side of the incisors which give them the appearance of the enamel-free lingual side.

Loss of Follistatin function leads to ectopic enamel formation at the lingual side of the incisor, an area known to be an enamel-free area. Follistatin$^{-/-}$ newly born mice have well-polarised ameloblast-like cells at the lingual side capable to secrete enamel. These ameloblast-like cells are differentiated from the epithelial tissue at the lingual part of the tooth. However, the enamel layer at the lingual side is not as well-oriented as the labial one (Wang *et al*., 2004).

Bmp signaling, another signaling pathway that controls mouse incisor growth, interacts with Wnt/β-catenin signaling to control osteoblasts maturation through the interaction between Runx2 and Lef1/TCF (Westendorf, Kahler and Schroeder, 2004). Bmp signaling in the incisor pulp is also controlled by the epithelial-derived Follistatin (Sharpe 2016). *Bmp2* knockout mice have smaller and uneven incisors. Noticeably, incisors were asymmetrical as well as open forked, and the lower incisors have broken tips and dental pulp exposure due to over-worn teeth. Radiographic analysis showed that mouse incisors had a less opaque enamel layer due to lower enamel density and calcification (Feng, Yang, *et al.*, 2011).

BCL11B, a transcriptional factor, can interact with FGF, TGFβ and Shh pathways to control the incisor asymmetry in 2 different ways; epithelial stem cell niche development and maintenance in the labial cervical loop, and lingual cervical loop epithelial cell proliferation and differentiation suppression (Kyrylkova et al., 2012). Fgf10 is necessary for the epithelial cell fate in mouse incisor (Yang, Balic *et al.*, 2015). Fgf10 and Fgf3 can compensate for each other during tooth development and incisor. Both are co-expressed in the dental pulp around the incisor labial cervical loop and regulate the epithelial cell proliferation (Wang *et al.*, 2007).

Fgf pathway also regulate Tbx1, a transcriptional factor required for epithelial TACs proliferation and differentiation to ameloblasts (Catón et al., 2009)

Mesenchymal Wnt signaling also interacts with the epithelial Wnt pathway. Upregulation of Wnt/β-catenin signaling in the oral epithelium enhances the expression of Wnt antagonists and leads to Wnt/β-catenin signaling downregulation in the dental pulp mesenchyme (Järvinen *et al*., 2006) indicating an interaction between epithelial and mesenchymal dental tissues. During tooth development, Wnt ligands are expressed in the epithelial tissue of the tooth germ and shows a crucial role in enamel formation (Sarkar and Sharpe 1999). Inhibition of Wnt ligands secretion from either ameloblasts or odontoblasts leads to increased enamel production with no abnormal incisor phenotype formation (Jarvinen et al. 2006). Moreover, Fan et al., 2018 argued that Wnt/β-catenin pathway regulates ameloblasts functions during the late developmental stages, however, enamel initiation and secretion are not controlled by the Wnt/β-catenin pathway. *Lgr5,* a Wnt target gene, is expressed in the epithelial stem cells of the hair follicle, intestine and mouse incisors, however, no Wnt activity has been detected in *lrg5*-expressing epithelial stem cells of the mouse incisors which indicate that Wnt/ β-catenin pathway has no activity in the incisor epithelial stem cells (Suomalainen and Thesleff, 2010).

1.2. Mouse incisors

Mouse incisor is a model to study the activity of adult stem cell populations. The availability of mesenchymal and epithelial stem cells at mouse incisor proximal end facilitate incisor growth throughout the animal's life and compensate for the continuous attrition at the incisal tip (Harada *et al*., 1999). Unlike human, mice have only one set of teeth (Smith, 2003). Mouse molars are different to the incisors since they stop growing after their roots are fully formed, which makes them a model used to study injury response (Neves *et al.*, 2017). Both incisor and molar share most of the same histological structure known as enamel, dentine and dental pulp (Harada *et al.*, 2002).

Enamel, which is the hardest tissue in the body, covers the labial side of the incisor. Its proximal part is covered by epithelial tissue which differentiates into ameloblasts (enamel-secreting cells). Epithelial tissue forms a loop at the end of the proximal area known as the epithelial cervical loop and within the labial cervical loop is the epithelial stem cell niche (Harada *et al.*, 1999). Dentine is a calcified tissue that works as a defensive shield for the vital pulp tissues and it is lined by odontoblasts (dentine-secreting cells) that originate from mesenchymal stem cells at the cervical area and pericytes (Feng, Mantesso, *et al.*, 2011). Finally, dental pulp is the soft fibrous connective tissue occupying the centre of the incisor to provide sensation and nutrition to the dental tissues. Dental pulp consists of different connective tissue elements and cells; in particular, cellular and neural elements. It also contains fibrous components, namely, collagen type I and II as well as non-fibrous elements (Nanci, 2007).

Mouse incisors are asymmetrical and have no obvious crown or root. The labial side of the incisor is considered as the crown analogue while the lingual enamel-free side represents the roots (Wang *et al*., 2007). Due to the wide apical foramen between cervical loops in mouse incisors, vessels and nerves enter the pulp and provide the requirements for the continuously

growing teeth (Tummers and Thesleff, 2008). Mouse incisors grow continuously throughout life; a process requiring continuous dental cell renewal. This is achieved by stem cell populations at the cervical end of the tooth (Harada *et al.*, 1999). Mesenchymal stem cells (MCSs) are slow-dividing cells that reside in the area between the epithelial cervical loop (Seidel *et al*., 2010) and give rise to transit amplifying cells (TACs) which are mature and fast-dividing cells (Lapthanasupkul *et al.,* 2012*).* The epithelial stem cell niche is within the labial cervical loop (Harada *et al*., 1999). ESCs differentiate into ameloblasts which are responsible for the enamel secretion (Seidel *et al.*, 2010) (Figure 1.4).

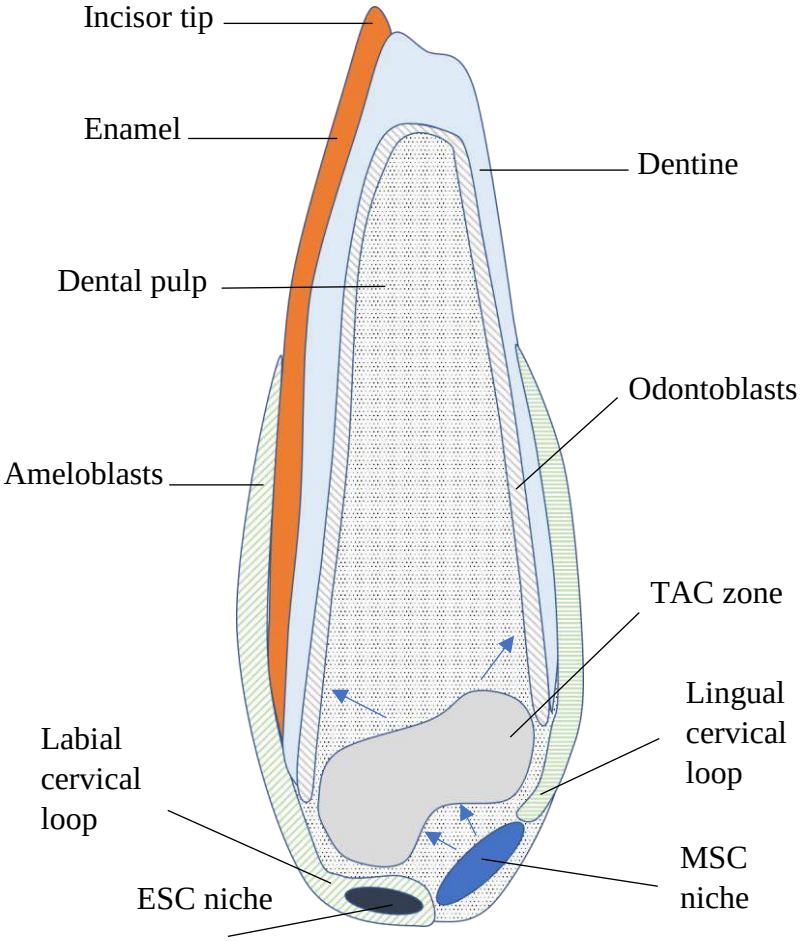

Figure 1.4. Mouse incisor histology

Mouse incisor is composed of enamel, dentine and dental pulp. The outside of the tooth is surrounded by epithelial tissue that makes a loop at the cervical end. At the cervical end, the epithelial stem cell niche is located within the labial cervical loop while the mesenchymal stem cell niche resides between the cervical loop. MSCs differentiate into another mesenchymal fast-dividing cell progeny known as TACs which reside in the TAC zone just distal to the MSC niche and differentiate into pulp cells and odontoblasts.

(ESC) epithelial stem cell, (MSC) mesenchymal stem cell, (TAC) transit amplifying cell.

1.2.1. Mouse incisors development

This project investigated Wnt signaling role in adult mouse incisors, however, understanding Wnt signaling role in incisor development is of a great help to understand how dental tissues respond to Wnt pathway. Therefore, this section briefly covers incisor development.

Jernvall and Thesleff (2000) showed that teeth development is controlled by epithelium-mesenchyme interactions and researchers illustrated that incisor development is initiated at E10.5 by ectodermal signaling, which leads to the thickening of the dental lamina. The epithelial bud at E12 invaginates into the underlying neural crest mesenchymal cells to form the tooth bud. Following that, the base of the epithelium buds fold into the mesenchymal dental papilla and form a cap-like structure at E13.5, where as a response to the mesenchymal signals, a non-proliferative structure forms at the tip of the epithelium known as the primary enamel knot (Vaahtokari *et al.*, 1996), which is a centre of signals and growth factors that control tooth development. By E14-15, the incisor tooth germ rotates anteroposteriorly to become parallel to the long axis (Harada *et al.*, 2002), and thus the cervical loop is formed. The mesenchymal cells lining the epithelial tissue react to epithelial signals and differentiate into odontoblasts and secrete dentine matrix to form the pre-dentine, and also signal back to the epithelial cells to differentiate into outer and inner enamel epithelium, stratum intermedium and stellate reticulum. Inner enamel epithelium then differentiates to pre-ameloblasts that start to secrete enamel. Inner enamel epithelium needs to be in contact with either active odontoblasts or dentine matrix to establish the ameloblasts differentiation (Jernvall and Thesleff, 2000; Harada *et al.*, 2002) (Figure 1.5).

As shown earlier, Wnt signaling has a vital role during tooth development. β-catenin, a downstream of canonical Wnt signaling, is required for incisor development to form the enamel knot (Chen *et al.*, 2009). Knocking out β-catenin arrests the bud at cap stage while the

continuous activation of β-catenin causes large tooth bud formation as well as the formation of supernumerary tooth (Liu and Millar, 2010).

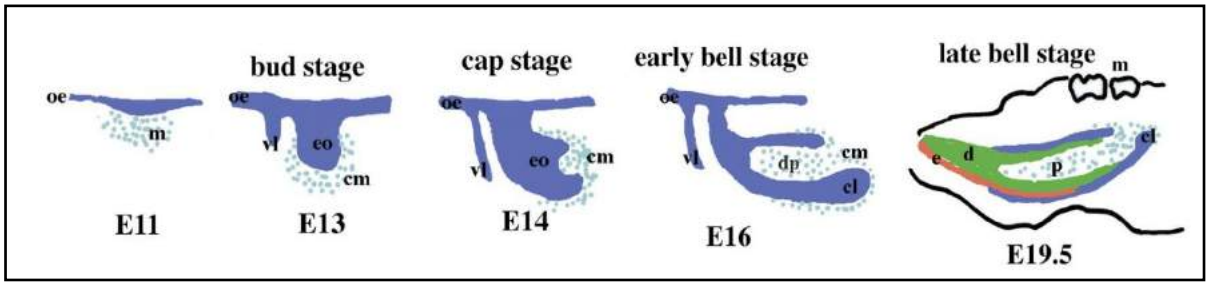

Figure 1.5. Incisor development stages

Incisor development starts at E10.5-11 with epithelial thickening and at E12-13, tooth bud forms. At E14, cap stage starts and tooth bud rotates horizontally. At E16, early bell stage forms followed by late bell stage at E19.5 where mineralisation of both enamel and dentine take over (Harada et al., 2002).

(oe) oral epithelium, (m) mesenchyme, (eo) enamel organ, (dp) dental papilla, (cl) cervical loop, (e) enamel, (p) pulp, (d) dentine, (cm) condensed mesenchyme, (vl) vestibular lamina, (m) molar.

1.3. Stem cells

Many tissues replenish and renew themselves (Logan and Nusse, 2004; Thesleff, Wang and Suomalainen, 2007; Bianco and Robey, 2015). This physiological process needs a special kind of cells known as stem cells. Stem cells are undifferentiated populations of cells characterised by two main abilities; they can renew themselves, and they can give rise to other cell types (Weissman, 2000). This group of cells reside in a specific location, known as a niche, that providing them with the proper environment and conditions to regulate their functions (McCulley et al., 2015; Clevers, Loh and Nusse, 2014).

Stem cell researches identify two main types of stem cells according to their level of maturity; embryonic stem cells (ES), which are extracted and harvested from the inner layer of the embryonic blastocyst, and adult stem cells, which are distributed in many developed tissues, facilitating their repair and regeneration (Leeb *et al.*, 2010). They can also be classified according to their capability for differentiation to different cell lineages into totipotent, pluripotent, multipotent and unipotent (Sell, 2004). Totipotent cells are cells that differentiate into all cell types including extraembryonic tissues. Pluripotent cells can differentiate into all three types of germ cells, namely ectoderm, mesoderm (muscles, bone and connective tissue) and endoderm (internal organ such as digestive tract). Multipotent stem cells can differentiate into one germ layer cell type such as hematopoietic stem cells, that can differentiate into many blood cells types. Finally, unipotent cells are a group of cells that can differentiate into only one cell type.

1.3.1. Embryonic stem cells

Embryonic stem cells were first described by Evans and Kaufman in 1981. This population of stem cells is extracted from the inner layer of the embryonic blastocyst, and it can differentiate into all other cell types. The procedure for extracting this population potentially leads to the death of the embryo, which makes them a controversial field of research. However, many

embryonic stem cell lines have been established and they are approved to have research conducted on them after being ethically approved (Yamanaka *et al.,* 2008).

Embryonic stem cells have tremendous ability to proliferate and differentiate *in vitro.* However, major issues have been considered, such as poor control which increases the risk of tumorigenicity, immunocompatibility for patients, moral and ethical concerns that affect and restrict their applications to conduct clinical trials (Wobus and Boheler, 2005; Salibian *et al.,* 2013).

1.3.2. Adult stem cells (ASCs)

Following organ development, embryonic stem cells disappear, and another type of stem cell becomes responsible for tissue repair, known as adult stem cells. Adult stem cells are multipotent stem cells that reside in adult tissues and organs and have the ability to renew themselves and to differentiate into different mature cells (Weissman, 2000). Unlike the difficulties in conducting research or treatment using embryonic stem cells, ASCs have no ethical issues, and have the potential for *in vitro* expansion as well as immunomodulatory properties, which make them of interest in research. Salibian et al. (2013) stated that ASCs are important factors for regenerative medicine because of their availability and as a source for autologous stem cells donation.

1.3.2.1. Mesenchymal stem cells

Mesenchymal stem cells (MSCs) are a sub-population of adult stem cells. They can differentiate *in vitro* into different mature mesenchymal cells such as osteocytes, chondrocytes, adipocytes and odontoblasts. In 1976, Friedenstein first identified MSCs as colonies of plastic adherent cells and found that they could be a source of osteoblasts, chondrocytes and adipocytes. Further research identified MSCs in different species including humans and rats as well as in various tissues such as cord blood (Erices *et al*., 1980), compact bone (Guo *et al.,* 2006), periosteum (Nakahara *et al.,*1991), and articular cartilage (Dowthewaite *et al.,* 2004).

According to International Society of Stem Cell and Gene Therapy (ISCT), any potential mesenchymal stem cells should have three main criteria to be considered as mesenchymal stem cells. The first criterion is the ability to differentiate *in vitro* into osteoblasts, chondroblasts and adipocytes. The second is to express the mesenchymal stem cell markers – CD73, CD105 and CD90 – while they lack expression of CD45, CD34, CD14 or CD11b, CD79a, or CD19 and HLA class II. The third criterion is to have the ability to be plastic adherent in the culture flask if maintained in standard culture condition.

Skeletal stem cells are known as multipotent stem cells where they differentiate into osteoblasts, chondrocytes and adipocytes. Many factors control skeletal stem cell functions such as Bmp and its antagonists Grem1 (Chan *et al.*, 2015). There are eight sub-populations of skeletal stem cells which have different abilities and, moreover, different factors control each of them (Chan *et al.*, 2015). Worthley *et al.* (2015) found that Grem1 has a vital role in controlling skeletal stem cell differentiation while Germ1 expression identifies the location of skeletal stem cells. Mendez-Ferrer *et al.* (2015) found that skeletal stem cells and hematopoietic stem cells affect each other in a complex scenario which decides the fate of each cell. This indicates the heterogenicity nature of skeletal stem cell niche.

Dental stem cells are another example of mesenchymal stem cell and they could be cultivated and obtained from a daily dental treatment of both permanent and exfoliated teeth, easily stored, and have the ability to produce neural cells, that make them of interest more than many other adult stem cell populations. Different stem cell populations of dental origin have been discovered; dental pulp stem cells (Gronthos *et al.*, 2000), exfoliated deciduous tooth stem cells (Miura *et al*., 2003), periodontal ligaments stem cells (Seo *et al.*, 2004), dental follicle stem cells (Morsczeck *et al.*, 2005), and apical papilla stem cells (Sonoyama *et al.*, 2006). Dental MSCs have been shown to exhibit many in vitro features of bone marrow-derived MSCs, including surface markers and differentiation abilities (Miura *et al.*, 2003).

1.3.2.1.1. Stem cell populations in the adult mouse incisor

The epithelial cervical loop is composed of inner and outer enamel epithelium and stellate reticulum. The basal epithelium of the loop give rise to the epithelial stem cells (Harada *et al.*, 1999; Tummers and Thesleff, 2003). It has been shown that the stem cells in the labial cervical loop give rise to two daughter cell types; the first remains in the cervical loop, and the second daughter cell enters the transit-amplifying zone and differentiates into ameloblast (Tummers and Thesleff, 2003). The epithelial stem cells reside in the niche within the labial cervical loop and their differentiation potential is crucial for the incisor continuous growth. The lingual cervical loop which is smaller in size has no epithelial stem cells and the remaining cell inside it act as epithelial rest of Malassez to regulate the signaling network in the cervical area of the incisor (Seidel *et al.*, 2010).

The mesenchymal stem cells are mainly found in a niche at the apical end of the tooth between the epithelial cervical loops (Zhao *et al.*, 2014). Another population of MSCs was identified as cells scattered in the dental pulp surrounding the blood vessels, known as pericytes, that can differentiate into odontoblast during tooth repair (Feng, Mantesso, *et al.*, 2011). Mesenchymal stem cells are usually identified by their *in vitro* features; the ability to give rise to different stromal mature cells such as osteoblast and chondrocytes, express mesenchymal stem cells markers, and finally differentiate into other cell types if the required media and *in vitro* conditions for each cell type are provided (Feng, Mantesso, *et al.*, 2011). However, mesenchymal stem cells do not necessarily meet these criteria *in vivo*.

Since *in vivo* mesenchymal stem cells behave differently, *in vitro* application and study are not informative. Genetic lineage tracing, a new golden standard for *in vivo* study, has been well established to understand how stem cells behave (Feng, Mantesso, *et al.*, 2011). This methodology is more reliable as it traces the fate of the cells in the tissues of interest. It shows

how the cells react and proliferate during the planned time and if those cells can renew themselves (Kretzschmar and Watt, 2012). Genetic lineage tracing of different MSC markers have shown a heterogenic niche at the proximal end of the tooth where MSCs were shown to have different origins such as trigeminal ganglia and neurovascular bundle (Zhao *et al.*, 2014; Kaukua *et al.*, 2014).

1.3.2.1.2. Mesenchymal stem cell niche in mouse incisors

Stem cells are found in a localised compartment within the tissues, known as a niche (Clevers, et al., 2014; Bianco and Robey, 2015). The niche must have three main properties: it provides an area for the stem cells to regulate their number, it provides a field in which stem cells control their ability to renew themselves and give rise to other cell lineages or remain quiescent, and it controls the motility of stem cells. To provide the favourable environment, the stem cells niche contains stem cells, supporting cells, an extracellular matrix and neurovascular tissues (Zhao *et al*., 2015). The MSC niche in the mouse incisor is believed to be in the proximal end where all the dental tissues are accessible to renew the incisor tissues. The niche in this area shows heterogeneity where different cell populations could be found, including slow-dividing mesenchymal stem cells and fast-cycling cells (TACs) (Zhao *et al*., 2014).

Two source of mesenchymal stem cells in mice incisors have been identified; glial origin (Zhao *et al*., 2014) and pericytes (Feng et al., 2011). Feng *et al.* (2011) stated that pericytes can differentiate into odontoblasts to respond for any injury. Lineage tracing of glial cell markers; in particular, PLP and Sox10, showed that 50% of the MSCs have originated from glial cells. Denervation of the nerve led to a decrease in the number of these cells, indicating that they are originated from the ganglion. However, genetic lineage tracing of glial origin cells showed $NG2^{+ve}$ pericytes are not of glial origin (Kaukua *et al.*2014). Zhao *et al.* (2014) found that

MSCs originate from the neurovascular bundle (NVB) at the incisor cervical area. Gli1^{+ve} mesenchymal stem cells contribute to incisor homeostasis and injury. The researchers found that 90% of MSCs are Gli1^{+ve}. However, Gli1^{+ve} cells do not express the mesenchymal stem cell markers *in vitro* while their progenies do. Zhao *et al.* (2014) also found that NG2^{+ve} cells are Gli1^{+ve} cells indicating the heterogenicity of the MSC niche.

1.4. Project hypothesis and aims

Mouse incisor development is controlled by Wnt signaling and many studies have shown that different Wnt ligands are expressed in almost every dental tissue during that. It is also well-known that Wnt signaling control many stem cell populations.

Based on these facts, this project aims to study the role of Wnt signaling on mouse incisor mesenchymal stem cells. To do that, the project was divided into three parts (Results chapters);

Part 1: Identify Wnt responsive cells in the dental pulp, where Wnt reporter mouse line (*Axin2-lacZ*) and *Axin2* genetic lineage tracing using (*Axin2-CreERT2*; $Rosa26R^{LacZ}$) were done. Wnt ligand expression was investigated by using immunofluorescent histochemistry and RT-qPCR.
Part 2: Study Wnt pathway functions in adult mouse incisors. Wnt gain of function by knocking-out *Axin2* by using ($Axin2^{lacZ/lacZ}$) and Wnt loss of function experiment by depleting Wnt signaling via inhibiting Wnt secretion ubiquitously from the producing cells by using ($pCagg^{CreERT2}$; $Wls^{fl/fl}$ mouse line) were done. The impact of those two models were investigated.
Part 3: Investigating the source of Wnt ligand secretion which controls the incisor growth. In this chapter, *Wntless*, a protein responsible for Wnt secretion, was knocked-out from different cell populations separately, namely MSCs, epithelial cells, TACs and odontoblasts by crossing $Wls^{fl/fl}$ mouse with $Gli1^{CreERT2}$, $K14^{CreERTM}$ or $Axin2^{CreERT2}$, respectively. The results of each mutation then were compared the ubiquitous deletion of *Wls.*

Chapter 2. Materials and methods

2.1. Mouse lines

Different mouse lines were used. To start with, *Axin2*$^{Lacz/+}$ Wnt reporter was used to identify Wnt-responsive cells (n=17) (Yu et al. 2005). Then, *Axin2* lineage tracing was done to trace *Axin2*$^{+}$ve cells within the dental pulp. To do that, the *Axin2*^{CreERT2} transgenic mouse line was crossed with *Rosa26R*^{lacZ} mouse reporter (n=15) (van Amerongen, Bowman, and Nusse 2012).

Axin2 knocout mouse line were used (*Axin2*$^{lacZ/lacZ}$) (n=15) to study upregulated Wnt/β-catenin pathway impact on mouse incisors (Yu *et al*., 2005). To study Wnt pathway loss of functions, *Wls*$^{fl/fl}$ mouse line (Carpenter et al. 2010) was crossed with *pCagg*^{CreERT2} (n=21) (Hayashi and McMahon, 2002), *Axin2*^{CreERT2} (n=15) (Van Amerongen et al., 2012), *K14*^{CreERTM} (n=9) (Vasiokhin *et al*., 1999) and *Gli1*^{CreERT2} mouse lines (n=3) (Ahn and Joyner 2004).

Finally, a triple transgenic mouse line was produced to trace *Wls* depleted *Axin2*-expressing cell lineages. *Axin2*^{CreERT2}*; Wls*$^{fl/fl}$ mouse line was crossed with *Rosa26R*$^{mT/mG}$ reporter (n=12) (Van Amerongen *et al.*, 2012).

Cre fusion with Tamoxifen-responsive Estrogen Receptor ligand binding domain (ERT) (Brocard, et al. 1997), ERT2 (Feil, et al. 1997) or ERTM (Hayashi and McMahon 2002) have been shown to be the most common method to regulate Cre activity. Tamoxifen administration releases CreER from Hsp90 to promote its translocation from the cytoplasm to the nucleus to induce Cre-loxP recombination.

2.1.1. *Axin2*^{LacZ} mice

Axin2 plays a role in the Wnt/β-catenin pathway, in particular in the β-catenin destruction complex. As such, it is a well-known read-out for active Wnt/β-catenin signaling (Yu et al., 2005). Axin2 is an isoform of Axin, which is a part of the degradation complex for β-catenin as well as a negative feedback loop (Jho et al. 2002).

Axin2^{lacZ} mouse line has a mutation that knocks out the *Axin2* and knock in *lacZ* to expresses β-galactosidase. Most of *Axin2 Exon2* was deleted and replaced by the insertion of β-galactosidase and then polyA and neo cassette were knocked in *Axin2* starting codon (Figure 2.1). Thus, a homozygous mouse would have an upregulated Wnt/β-catenin pathway while the heterozygous mouse will work as a reporter for this pathway (Lustig et al. 2002). Upon *Axin2* expression, β-galactosidase gene forms and makes it possible to detect *Axin2*-expressing cells by using X-gal staining. For this mouse line, adult mice were used (2-3 months old)

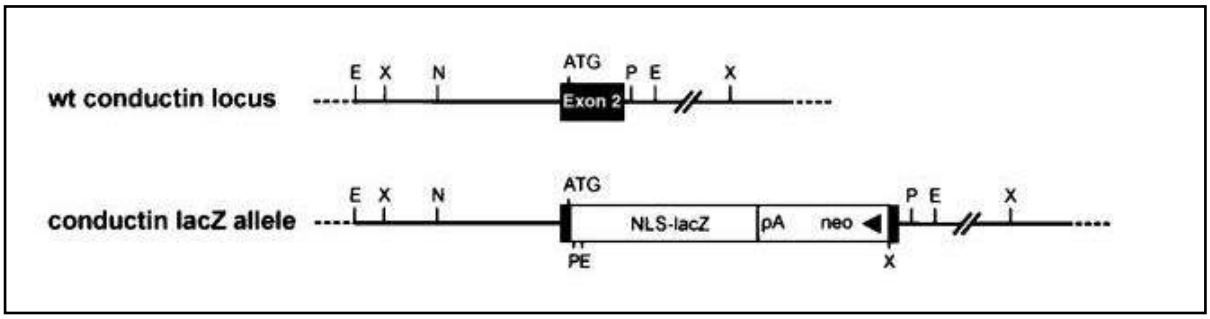

Figure 2. 3. *Axin2-LacZ* mouse line shows most of *Axin2 Exon2* is replaced by the *LacZ* gene (Lustig *et al*., 2002).

2.1.2. *Axin2*^{CreERT2}; *Rosa26R*^{lacz} mouse line:

Axin2^{CreERT2} mouse line is a tamoxifen-inducible Cre driver which is a helpful tool to lineage trace *Axin*$^{+ve}$ cells *in vivo* (Van Amerongen *et al*., 2012). In this tamoxifen inducible knock-out/knock-in strain, *CreERT2* was knocked into *Exon2* of *Axin2* gene.

Axin2^{CreERT2} mouse line was crossed with the *Rosa26R*^{lacZ} reporter mouse line. Upstream of the reporter gene is a stop codon flanked by two *loxp* sequences. Hence the reporter gene is only expressed in cells that express *Cre*. Once a recombination has occurred, it is passed to daughter cells without dilution; therefore, the progeny of cells of interest can be easily traced (Figure 2.2).

These mice are treated with three intraperitoneal injections of either tamoxifen (20 mg/ml) or corn oil in three consecutive days and then divided into groups in which each one was killed in a different time point (one day, one week, two weeks and four weeks).

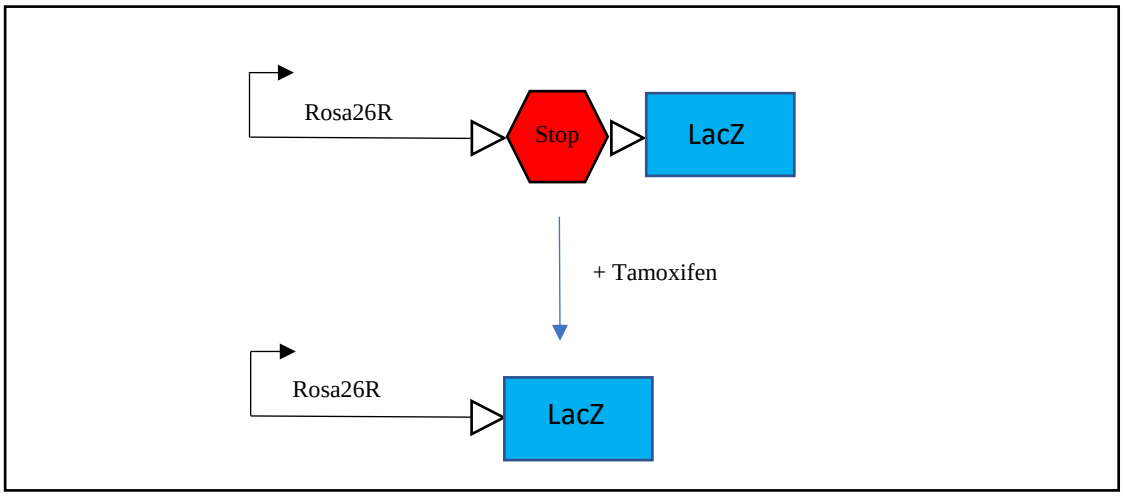

Figure 2. 4. *Rosa26R^{lacz}* mouse line

This mouse line has a Stop gene that is surrounded by two loxP sides to prevent the transcription of the LacZ gene. Upon Cre recombination, the Stop gene is removed and the LacZ gene can be produced. Edited from Van Amerongen et al. (2012).

2.1.3. *Wls$^{fl/fl}$* mouse lines

Wls$^{fl/fl}$ mouse line is a transgenic mouse that has two *loxP* sites; one before the ATG start site of *Wls* Exon1 and the other one located in the upstream of Exon2 (Carpenter *et al*., 2010) (Figure 2.3). *Wls fl/fl* mouse line was crossed with a different Cre driver so Wnt ligand secretion was inhibited in mouse incisors tissues.

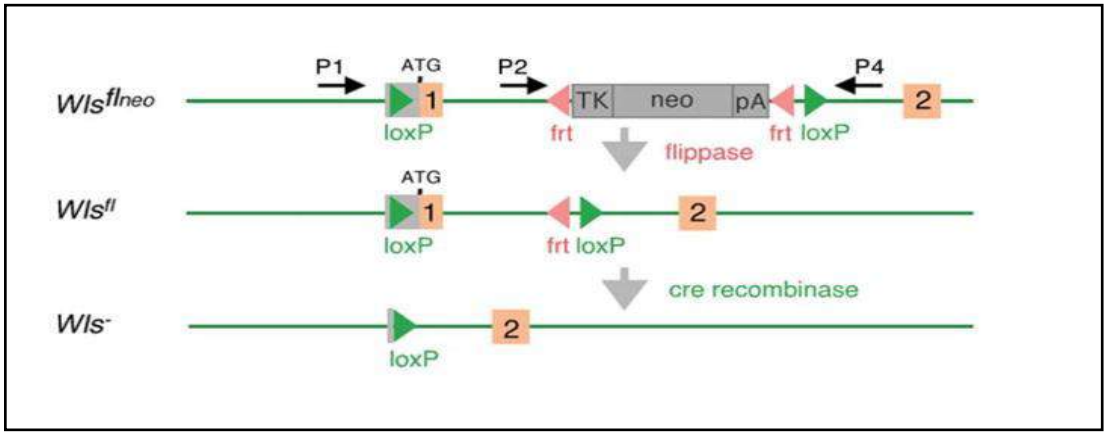

Figure 2.3. *Wls fl/fl* mouse line. Upon activation of Cre recombination, Wls gene becomes floxed and inactive (Carpenter *et al*., 2010).

2.1.3.1. *Pagg^{CreERT2}; Wls$^{fl/fl}$*

PCagg^{CreERT2} is a ubiquitous Cre driver (Hayashi and McMahon 2002). *pCagg* promoter consists of cytomegalovirus enhancer and chicken β-actin promoter. It provides the most consistent expression of reporter genes and has been shown to have a widespread expression (Lobe et al., 1999; Niwa et al., 1991, Hayashi and McMahon 2002).

PCagg^{CreERT2} was crossed with *Wls$^{fl/fl}$* mouse line so all Wnt ligand secretion from the producing cell is blocked in *PCagg^{ERT2Cre2}*; *Wls$^{fl/fl}$* mutant mice (Carpenter et al., 2010). *PCagg^{CreERT2}*; *Wls$^{fl/fl}$* is a tamoxifen-inducible transgenic mouse line to study the consequence of the Wnt signaling deactivation in all the tissues. Upon activation of the *Cre* recombination, *Wntless* will be knocked out, and the secretion of Wnt ligands will be blocked.

2.1.3.2. *Axin2^{CreERT2}; Wls fl/fl*

Axin2^{CreERT2} mouse line, a tamoxifen-inducible strain (Van Amerongen et al., 2012), was crossed with *Wls$^{fl/fl}$* mouse line to produce *Axin2^{CreERT2}; Wls$^{fl/fl}$* mouse line where Wnt secretion is inhibited in Wnt-responsive cells. Upon activation of the Cre-loxP system, Wnt secretion from *Axin2*-expressing cells will be inhibited.

2.1.3.3. *K14^{CreERTM}; Wls fl/fl*

K14^{CreERTM} is a tamoxifen inducible *Cre* mouse line driven by the expression of keratin 14 (*K14*) promoter, which is expressed in the ectodermal tissue and its derivatives (Vasiokhin *et al*., 1999). K14 CreERTm was produced by injecting Cre cDNA which is fused to an altered hormone binding domain of mouse estrogen receptor ERTam into the male pronucleus of a fertilised single cell mouse embryo and implemented into CD1 mouse oviduct. This estrogen receptor fails to bind to estrogen and only binds to tamoxifen (Vasiokhin *et al*., 1999).

K14^{CreERTM} mouse line was crossed with *Wls $^{fl/fl}$* mouse line to produce *K14^{CreERTM}*; *Wls$^{fl/fl}$* mouse line, where Wnt secretion is inhibited from *K14* expressing cells. When Cre recombination is activated, Wnt secretion from the epithelial cells will be blocked and this will show the role of epithelial Wnt protein in mouse incisor homeostasis.

2.1.3.4. *Gli1^{CreERT2}; Wls fl/fl*

CreERT2 insert was knocked into the ATG site of *Exon2* and first zinc finger domain in *Exon4* of *Gli1* (Ahn and Joyner 2004). *Gli1^{CreERT2}* transgenic mouse line was crossed with *Wls $^{fl/fl}$* mouse line to produce *Gli1^{CreERT2}*; *Wls $^{fl/fl}$* mouse line. Gli1 is a neurovascular cell marker and is expressed in the mouse incisor mesenchymal stem cells (Zhao *et al*., 2014). Thus, when Cre recombination is activated, Wnt secretion from mouse incisor MSCs will be blocked.

The above mouse lines were treated with three intraperitoneal injections of either tamoxifen (20 mg/ml) or corn oil in three consecutive days and then divided into groups in which each group was collected in a different planned time point following the injections.

2.1.3.5. *Axin2^{CreERT2}; Wls$^{fl/fl}$; R26R$^{mT/mG}$* mouse line

To study Wls deleted *Axin2*-expressing cells lineages, *Axin2^{CreERT2}; Wls$^{fl/fl}$* transgenic mouse line was crossed with *Rosa26R$^{mT/mG}$* mouse reporter. Upon injection of tamoxifen, a switch from membrane-bound tomato to membrane-bound green fluorescent protein (GFP) expression occurs (Figure 2.4) (van Amerongen, Bowman, and Nusse 2012) so, the mutated *Axin2*-expressing cell lineages can be traced.

Adult (4-6 weeks) mice were used (n=12). This mouse line were treated with three intraperitoneal injections of tamoxifen (20 mg/ml) in three consecutive days and then divided into groups in which each one was killed in a different time point (1 day, 3 days, 7 days and 14 days).

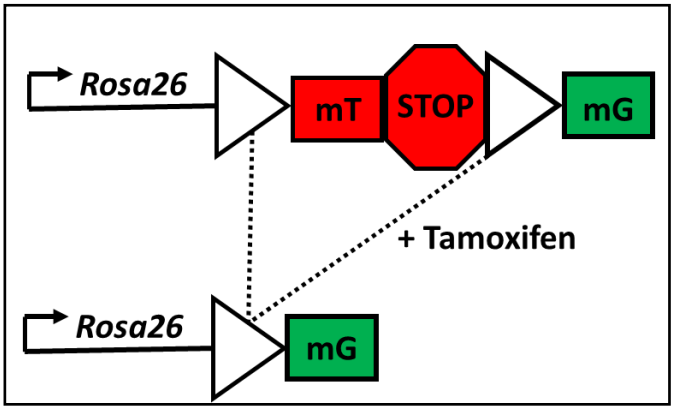

Figure 2. 4. *Rosa26R$^{mT/mG}$* mouse line

This mouse line has a membrane-bound tomato and Stop genes that is surrounded by two loxP sides. Upon Cre recombination, the membrane-bound tomato and stop gene are removed and the membrane-bound green gene can be produced. Edited from Van Amerongen et al. (2012).

2.2. Drugs administration

2.2.1. Reagents and materials

Tamoxifen	Sigma, T5648
Corn oil	Sigma, C8267
BrDU	Sigma, B5002

Table 2.1. Reagents and drugs used for mouse injections

Animal handling was carried out according to the Home Office guidelines in the UK under project license number PPL70/7866.

To activate Cre recombination, tamoxifen was given as intraperitoneal injections for three consecutive days. The dose given was 2µg of tamoxifen (20µg/ml). Mice were sacrificed by suffocation method in the CO_2 chamber and death was confirmed by nick dislocation according to the protocol. Control groups were handled similarly after the corn oil injection. To prepare tamoxifen solution, 20µg of tamoxifen powder was dissolved in 1ml of corn oil.

Labelling of fast dividing cells was performed by using thymidine analogue BrDU (5-bromo-2'-deoxyuridine) incorporated into DNA of dividing cells. BrDU injection was given intraperitoneally (220mg/kg body weight) 24 hours prior to collection. BrDU solution was made by dissolving 10mg of BrDU salt in 1ml of 0.9% saline solution.

2.3. Mouse incisor clipping

Mice were anaesthetised by IP injection (Hypnorm : water : hypnovel (1:2:1)). The injected dose was 100µl/10gm body weight. The lower left incisor then was clipped by using Chooling Nail Scissors (Made of Forged & Polished Stainless Steel). The notch was done by using high speed diamond bur. The incisor growth was measured daily by using a digital calliper.

2.4. Tissue processing:

2.4.1. Reagent and solution

Paraformaldehyde PFA (4%)	Sigma, P6148
Glutaraldehyde	Merck, 1042390250
Formic acid, 98%	Fisher, F/1850/PB17
Ethanol	VWR, 101077Y
Histoclear II	National Diagnostics, HS-202
ultraplast Polyisobutylene Histological Wax	Solmedia, WAX060
Erhlich's Haematoxylin	Solmedia, HST003
Eosin, aqueous solution (0.5%)	Riedel-de Haën, 32617
EDTA (Ethylenediaminetetraacetic acid)	VWR, 20302.293
EDTA (Ethylenediaminetetraacetic acid, tetrasodium salt)	ACROS, 446080010
DePex	BDH, 360294H
BrDU	Sigma, B5002
DEPC (Diethyl pyrocarbonate)	Sigma, D5758
O.C.T. compound	BDH (361306E)
Sucrose	Sigma (S0389)
Phosphate buffered saline (PBS)	Fisher, BP-665-1
$MgCl_2$	Fisher, BP214-500
Sucrose	Sigma, 57-50-1

Table 2.2. Reagents for tissue processing

2.4.2. Fixation, decalcification and dehydration:

Fixation of *Axin2*^{lacZ} and *Axin2*^{CreERT2}; *ROSA26R*^{lacZ} incisors was done by using 0.2% glutaraldehyde and 1% PFA in 1X PBS (Table 2.3) overnight.

Glutaraldehyde	400µl
4% PFA	12.5ml
1X PBS	37.1 ml

Table 2.3. 0.2% Glutaraldehyde fixative solution

The fixation of the other mouse line incisors was done in 4% PFA overnight. Then, both glutaraldehyde and PFA fixed incisors were washed thrice in PBS for five minutes each and decalcified by using 19% EDTA with pH 7.3 (Table 2.4) for 4-6 weeks at 4°C.

EDTA (Ethylenediaminetetraacetic acid)	90g
EDTA (Ethylenediaminetetraacetic acid, tetrasodium salt)	100g
H_2O	1L

Table 2.4. Recipe for 19% EDTA solution.

2.4.3. Dehydration and wax embedding:

Tissues were washed after they had become soft in PBS thrice for five minutes each. This was followed by a dehydration process, where ascending concentrations of [ethanol: water] were used (30%, 50%, 70%, 90%, and twice at 100%) for three hours or overnight for each step. Then tissues were embedded in histoclear-II six times for 30 minutes each. This was followed

by heating the samples at 65°C for 15 minutes and embedding them in 1:1 [histoclear: wax]. Finally, the samples were embedded in the wax five times for one hour each and finally the samples were placed in a metal mould where wax then added and were cooled down on the cold plate.

2.4.4. Tissue embedding of samples for frozen sectioning:

Optimal cutting temperature compound (OCT) embedding matrix was used for sample embedding for frozen sectioning. OCT is a water-soluble matrix that consists of glycol and resin and it prevents any background staining.

The softened incisors were washed four times in 1X PBS for five minutes each. Then samples were embedded in sucrose solution (Table 2.5) overnight at 4°C. This was followed by embedding the samples in the 1:1 (60% sucrose: OCT) overnight at 4°C and finally, the samples were snap frozen in OCT matrix using dry ice and absolute ethanol bath.

(To prepare 60% sucrose solution, 30g of sucrose powder was dissolved in RNase-free water with final volume of 50ml.)

60% Sucrose	12.5ml
1M $MgCl_2$	500µl
1X PBS	37ml

Table 2.5. Dehydration solution for pre-OCT embedding

2.5. Histology staining

2.5.1. Hematoxylin and eosin H&E staining

H&E staining is used to study general tissue histology and cell morphology. Haematoxylin is responsible to stain cell nuclei to blue. Eosin, which is the other staining solution in this

method, stains intra-cellular substance such as cytoplasm, connective tissue and extracellular substances to a pink or red colour.

To start with, wax was removed by washing the slides twice in histoclear. Then the sections were washed in gradually decreasing concentrations of industrial methylated spirit (IMS) followed by a deionised water wash to rehydrate the samples. Then the sections were stained by Ehrlich's haematoxylin solution and washed by running water, deionised water and acid alcohol. The sections were then stained by 0.5% eosin in 2mM acetic acid and washed with deionised water. This was followed by a dehydration process, where the gradually increasing concentrations of IMS were used. Finally, the sections were washed by histoclear three times and mounted in neo-mount and cover-slipped.

2.5.2. Masson's trichrome staining

Paraffin wax was dissolved using histoclear II twice for 10 minutes each. The sections then were rehydrated using decreasing concentrations of industrial methylated spirits (IMS), two minutes for each one, starting from 100% IMS and then 90%, 70%, and 50%, followed by deionised water. The sections were then stained by emerging the slides in Weigert's haematoxylin for 10 minutes and then washed with running water and deionised water. This is followed by Masson's stain, where the slides were emerged for 15 minutes and then washed with deionised water. Slides then were kept in 5% phosphomolybdic-phosphotungstic acid for 15 minutes. Then, the slides were emerged in 2.5% aniline blue staining solution in 1% acetic acid for 10 minutes and rinsed after that in deionised water. Slides then were incubated in 1% acetic acid until collagen became blue and then were rinsed in deionised water. Finally, sections were dehydrated using 90% and 100% IMS and neo-clear for five minutes each, and mounted and cover-slipped with neo-mount.

2.6. X-gal staining

X-gal staining is a useful technique to study gene expression *in vivo*. LacZ gene could be knocked in a codon of the targeted gene so gene transcription can produce β-galactosidase. Once β-galactosidase forms, X-gal can detect it and produce a blue colour, so any cell expressed gene of interest would be blue in colour under the light microscope.

2.6.1. Reagents and solutions

Sodium deoxycholate	Sigma, D6750
IGEPAL CA-630 (NP-40)	Sigma, I3021
Potassium ferricyanide (K4[Fe(CN)6])	BDH, 102054F
Potassium ferricyanide (K3[Fe(CN)6])	BDH, 102044D
Magnesium chloride (MgCl2)	Fisher, BP214-500
X-gal	Fermentas, R0404
0.2% Nuclear fast red	Sigma, 60700
36% Formaldehyde	VWR, 20910.363
Neo-mount	VWR, 1.09016.0500
Trizma® base (Tris base)	Sigma, T1503
Hydrochloric acid (HCl)	VWR, 20252.244
Distilled H_2O	

Table 2.6. Reagents for LacZ staining

2.6.2. Whole-mount LacZ staining:

Deminiralised mouse incisors were washed three times in 1X PBS for five minutes each. Then incisors were embedded in the staining solution (Table 2.8) overnight in a foil-wrapped dish at 37ºC.

10 mM TRIS-HCL pH. 7.3	1000µl
0.005% Na-Dexoxycholate	100µl
0.01% IGEPAL	10µl
5mM K4	200µl
5mM K3	200µl
2mM MgCl2	20µl
0.8 mg/ml X-gal	200µl
1X PBS	10ml

Table 2.8. Staining mix for LacZ staining (whole mount)

On the second day, staining reactions were stopped by removing the staining solution and rinsing the samples in 1X PBS followed by three PBS washes for five minutes each. The tissues then were fixed in 4% PFA for an hour and stored in 1% PFA at 4°C.

2.6.3. Frozen section LacZ staining:

The frozen tissues were cryo-sectioned with a thickness of 12um and placed on Superfrost+ slides. The sections were then kept at -20C overnight to dry. Then, the sections were fixed in 0.2% glutaraldehyde fixative solution for 30 minutes and washed with 1X PBS. Samples were then were embedded in the detergent solution for 30 minutes (Table 2.9).

1M $MgCl_2$	100µl
Na Deoxycholate 0.5%	1000µl
IGEPAL 20%	1250µl
1X PBS	Up to 50ml

Table 2.9. Detergent solution.

Then, 200 µl of the X-gal staining solution (Table 2.10) was added to the sections and the slides were covered by parafilm inside the humid chamber and incubated at 37^{o}C overnight.

$K_3Fe(CN)6$ 0.1M	0.5ml
$K_4Fe(CN)6$ 0.1M	0.5ml
$MgCl_2$ 1M	10µl
IGEPAL 20%	125µl
Na Deoxycholate 0.5%	100µl
X-gal (80mg/ml)	62.5µl
1x PBS	3.74ml

Table 2.10. LacZ staining solution (frozen section)

Once the colour was developed, slides were washed in 1X PBS thrice for five minutes each and fixed in 3.7% formaldehyde solution for 30 minutes (Table 2.11).

36% Formaldehyde	5ml
1X PBS	45ml

Table 2.11. Preparing 3.6% formaldehyde.

Finally, the sections were counterstained by using nuclear fast red staining solution (Table 2.12) and cover-slipped with neo-mount.

Nuclear fast red solution 0.2%	5 minutes
30% Ethanol	10 seconds
50% Ethanol	10 seconds
70% Ethanol	10 seconds
85% Ethanol	10 seconds
90% Ethanol	10 seconds
100% Ethanol	2 X 10 seconds
Histoclear-II	2 X 3 minutes

Table 2.12. Counterstaining protocol for LacZ stained tissues

2.7. Immunofluorescent histochemistry

2.7.1. Reagents and solutions

Triton X-100	Sigma, X100-500ML
Glycine	Sigma, G8898
Albumin from bovine serum, BSA (1%)	Sigma, A4919
Gelatin	Sigma, 9391
Trizma base	Sigma, T1503
Citifluor	EMS, 171024-AF1

Table 2.13. Reagents for immunofluorescent histochemistry staining

2.7.2. Primary antibodies

Antibody	Manufacture details	Concentration
Chicken polyclonal to GFP	Ab 13970	1:1000
Rabbit polyclonal to Wnt4	Ab 91226	1:100
Rabbit polyclonal to Wnt10a	Ab 106522	1:100
Mouse monoclonal to BrdU	Ab 8152	1:100

Table 2.14. Primary antibodies

2.7.3. Secondary antibodies

Antibody	Manufacture details	Concentration
Goat anti-Rabbit IgG H+L (Alexa Fluor® 488)	Invitrogen, A11008	1:250
Rabbit anti-Mouse IgG H+L (Alexa Fluor® 546)	Invitrogen	1:250
Goat anti-Chicken IgY H+L (Alexa Fluor® 488)	Invitrogen, A-11039	1:250

Table 2.15 Secondary antibodies

2.7.4. Immunohistochemistry staining for wax sections:

Wax embedded samples were sectioned (8-10um) then mounted in the slides and kept on the hot plates at 42°C overnight for dehydration.

2.7.4.1. De-waxing and rehydration

Xylene was used to remove the wax and followed by the rehydration process by using gradually descending concentrations of ethanol and finally washed with PBS (Table 2.16).

Xylene	2 X 10 minutes
100% Ethanol	2 X 5 minutes
95% Ethanol	5 minutes
90% Ethanol	5 minutes
70% Ethanol	5 minutes
PBS	2 X 5 minutes

Table 2.16. Dewaxing and rehydration for wax sections immunohistochemistry staining

2.7.4.2. Antigen retrieval

To retrieve the antigen and eliminate the heat side-effects, samples were washed and embedded in 0.1M Tris-HCL with pH. 9.5 (antigen retrieval buffer). Samples then placed in a box filled with antigen retrieval buffer and placed in the microwave for 15 minutes (3 X 5 minutes) followed by 20 minutes cooling down at room temperature. Sections were then washed thrice in 1X PBS for 5 minutes each.

2.7.4.3. Blocking step

The blocking step was done by placing the slides over plastic rods inside the humid chamber and 200µl of the blocking solution (10% goat serum and 0.2% gelatine in PBS + Tween-20(PBT)) was added to the slide and then covered by a parafilm and incubated for 1 hour at room temperature.

2.7.4.4. Antibodies incubation

Following the blocking step, sections were washed twice in 1X PBS for 10 minutes each. Diluted antibodies and blocking buffer were added to the slides which then covered by parafilm. Then, slides were incubated inside the humid chamber at 4°C overnight.

On the second day, sections were incubated with the diluted secondary antibodies in the blocking buffer with diluted Hoechst inside the humid chamber for one hour at room temperature and then followed by PBT washing. Finally, slides were mounted using citifluor and cover-slipped.

2.7.5. Immunofluorescence staining for frozen sections:

Frozen samples were sectioned using the cryostat with the thickness of 12um and mounted over Superfrost+ slides. Then the slides were allowed to dry for overnight at -20°C. The next day, the slides were washed in 1X PBS to remove the OCT. This is followed by the permeabilisation step where the slides were washed in PBS+Tween 20 (PBT).

The slides were then incubated with the blocking solution (Table 2.17).

10% Tween 20	7.5µl
Goat serum	15µl
BSA (20mg/ml)	15µl
Glycine (15%)	15µl
1X PBS	97.5µl

Table 2.17. Blocking solution

After that, slides were incubated with the primary antibody solution (Table 2.18) and covered by parafilm in the humid chamber at 4°C overnight, then washed with 0.5% tween20 in 1X PBS.

Primary antibody	According to the manufacture recommendation
Tween20 (10%)	5%
Goat serum	1%
Glycine (15%)	10%
BSA (20mg/ml)	10%
1X PBS	74%

Table 2.18. Primary antibody solution

The sections after that were incubated with the secondary antibody solution (Table 2.19) and covered by parafilm in the humid chamber for one hour, then washed with 0.5% tween20 in 1X PBS.

Finally, slides were mounted and cover-slipped using citifluor.

Hoechst (1:10 dilution)	1µl
Tween20 (10%)	5µl
Goat serum	1µl
BSA (20mg/ml)	10µl

Glycine (15%)	10µl
Secondary antibodies	0.5µl each
1X PBS	Up to 100µl

Table 2.19. Secondary antibodies solution.

2.8. Trap staining

2.8.1. Reagents and solutions

Naphthol-AS-TR-phosphate	Sigma, N-6125
N-N-Dimethylformamide	Sigma, 227056
Glacial acetic acid	Sigma, 64-19-7
Sodium acetate (anhydrous)	Sigma, S2889
Sodium tartrate	Sigma, S8640
Fast red TR salt	Sigma, F-2768
Aquamount	Thermo-Fisher, 14-390-5

Table 2.20. Reagents for TRAP staining

2.8.2. Trap staining protocol

Sections were de-waxed by using xylene and rehydrated by using gradually decreased concentrations of ethanol. To make the staining solution, 60mg naphthol-AS-TR-phosphate were dissolved in 300 ul N-N-dimethylformamide. Then 60ml of acetate buffer (pH 5.2) (Table 2.21) was

added to the mix. After that, 1.38g sodium tartrate and 60mg fast red TR salt was dissolved in the staining mixture. The final solution was then filtered.

0.2 M Glacial acetic acid	10.5ml
0.2M Sodium acetate (anhydrous)	39.5ml
H_2O	50ml

Table 2.21. Acetate buffer solution

The sections then were incubated in the staining solution for 10 minutes at 37ºC. This was followed by H_2O wash and then counterstained by hematoxylin for 30 seconds and washed in running water for two minutes. Finally, slides were mounted and cover-slipped by using aqua-mount.

2.9. TUNEL assay (apoptosis assay)

Skulls were fixed in 4% PFA for 48 hours at 4°C. Incisors were then dissected and decalcified in 19% EDTA for four weeks. For TUNEL assay In Situ Cell Death Detection Kit, Fluorescein, Roche were used following the manufacture protocols. Frozen incisor sections of 8-10 micrometre were post-fixed in 4% PFA then permeabilised in 0.1M sodium citrate buffer with pH 6.0 (11.5% 0.1M citric acid monohydrate + 88.5 0.1M trisodium citrate dihydrate) on ice. The sections were then incubated in tunnel reaction mixture for 60 minutes at 37°C. Sections were then counterstained with DAPI and detected in the range of 515-560nm wavelength under the confocal laser microscope.

2.10. In situ hybridisation

2.10.1. Reagents and solutions

Polymerase enzymes	Promega
DIG RNA labelling mix (10X)	Roche, 11277073910
SigmaSpin™ Post-Reaction Clean-Up Column	Sigma, 5059
DL-Dithiothreitol (DTT)	MP Biomedicals, 100597
Triton® X-100	BDH, 306324N
Tween-20	Sigma, P7949
IGEPAL CA-630	Sigma, I3021
Proteinase K	Sigma, P2308
Glycine	Sigma, G7403
Formamide	Merck, K36952408
Blocking reagent	Roche, 11096176001
SDS (sodium dodecyl sulphate)	Severn, 30-33-50
Anti-Digoxigenin-AP fab fragments	Roche, 11093274910
Acetic anhydride	BDH, 100022M
1% (w/v) Bovine serum albumin	Sigma, A9647
50% Dextran sulphate	Chemicon, 0702051849
QIAprep Spin miniprep kit	QIAGEN, 27104

Plasmid maxi kit	QIAGEN, 12163
QIAquick PCR purification kit	QIAGEN, 28104

Table 2.22. Reagents and kits for in situ hybridisation

2.10.2. Plasmids

Gene	Vector	Size of insert	Digestion enzyme	Polymerase enzyme
Dspp	pSport1	1Kb	Kpn1	T3

Table 2.23 Plasmid

2.10.3. Minipreparation of plasmid DNA

Plasmids were ordered from Source Bioscience. A swap of the plasmid contains bacteria was spread on a LB-agar plate containing 100 μg/ml Ampicillin. The plates were then incubated overnight at 37ºC. A single isolated clone was added to 5ml Luria-Bertani-medium (LB-medium) and incubated on the shaker overnight at 37ºC overnight.

Qiagen QIAprep Miniprep was used. The plasmid which was incubated in LB medium was centrifuged, and the supernatant was discarded. Following the provided manual, pelleted bacterial cells were re-suspended in buffer P1. Buffer P2 then was added and the solution was mixed by inverting the tube. After that, buffer N3 was added to and the tube was centrifuged for 10 minutes. The supernatants were added to the QIAprep spin column and centrifuged for one minute to attach DNA to the filter. Following that, the filter was washed by adding 0.75ml buffer PE and centrifuged for one minute twice. Finally, buffer EB was added to the filter to elute the clean DNA.

2.10.4. Maxipreparation of plasmid DNA

Qiagen Plasmid Maxi kit was used. a colony of the bacteria was incubated in 200ml LB containing 100 µg/ml Ampicillin on the shaker at 37ºC overnight. The next day, this 200ml was centrifuged, and the pellet was resuspended in 10ml buffer P1and followed by 10ml of buffer P2. Then, 10ml of buffer P3 was added to the mixture and left on ice for 20 minutes. To remove the bacterial lysate, the mixture then was centrifuged and the supernatant was then poured into the elluting tube to filter it. The filter then was cleaned adding buffer QC twice. DNA elution was done by using buffer QF. To clean the eluted DNA isopropanol and 70% ethanol washes was done and DNA then was resuspended in 200µl DNAse-free water.

2.10.5. Preparation of template DNA to make antisense riboprobes

2.10.5.1. Linearization of plasmid DNA

Maxi-prepared DNA was used and 20 µg of plasmid DNA were digested in the linearization reaction mixture listed below (Table2.24). The reaction was incubated at 37ºC for 2 hours. 0.2 µl of linearized DNA were then run o a gel to confirm the completion of the digestion. The linearised plasmid after that was purified by using a QIAquick PCR purification kit following manufacturer instructions.

DNA	10µl
Enzyme	2µl
10X buffer	5µl
BSA	0.5µl
ddH_2O	33.5µl

Table 2.24: Plasmid linearisation mixture

2.10.5.2. Synthesis of DIG-labelled RNA Probes

Antisense RNA probe was synthesised from the linearised plasmid by adding the linearised plasmid DNA to the transcription buffer mixture (Table 2.25) and incubated at 37ºC for two hours. Then, 1µl of the reaction mix was run on a gel to confirm the RNA size. To eliminate the DNA template, 2µl of RNase free DNase was added and the reaction was incubated at 37ºC for 10 minutes and then cleaned up by using SigmaSpin™Post-Reaction Clean-Up Column. The RNA probe was stored at -80ºC.

Linearised plasmid	2µl
5X transcription buffer	4µl
DIG labelling mix	2µl
0.1M DTT	2µl
RNase inhibitor	0.5µl
ddH_2O	10.5µl
Enzyme	1µl

Table 2.25. Probe synthesis mixture

2.10.6. In situ hybridisation protocol

2.10.6.1. Pre-hybridisation and hybridisation steps

All slide racks and instruments were sterilised by baking overnight at 180ºC. All the solutions used were DEPC treated for overnight and autoclaved.

The slides were firstly de-paraffinized thrice in Xylene for 15 minutes each. Then sections were later rehydrated in gradual decreasing ethanol concentration solutions: 100%, 95%, 70% (EtOH-RNAse free water) twice for 2 minutes each and finally the sections were embedded in RNase-free water twice for 10 minutes each. Following that, the tissue sections were fixed in 4% PFA for 10 minutes and washed thrice in 1XPBS for five minutes each. Section were permealised by embedding them in 10µg/ml Proteinase K at 37ºC for 10 minutes and then re-fixed in 4% PFA for 20 minutes at room temperature. To prevent the non-specific binding of the probe, tissues were incubated in a freshly made acetylation buffer (25µl acetic anhydride in 10ml 0.1 M Triethanolamine) for 10 minutes. Following that, tissues were dehydrated in 70% and 95% (EtOH- RNAse free water) and the left to dry inside box for 1 hour.

Following that, the sections were incubated in warm pre-hybridisation solution for 1 hour at room temperature. Then, the sections were horizontally placed on sterilised plastic rods in the humid chambers (with tissue towels soaked in 50% formamide and 50% RNAse free water). The DIG-labelled RNA probe diluted in 1 ml of hybridisation solution was denatured by heating at 95ºC for 3 minutes and immediately after that, 150µl of hybridisation solution was applied to each slide. Glass cover slips were placed on the slides to evenly spread the probe.

The chambers were sealed to prevent buffer evaporation and to maintain the humidity of the chamber and then the chamber was incubated at 68ºC for overnight.

2.10.6.2. Post-hybridisation steps

The cover slips were removed by dipping in pre-warmed 5X SSC solutions. To remove the unbound probe, the sections were washed in high stringency (HIS) buffer for 30 minutes at 65^{o}C followed by RNase buffer wash thrice for 10 minutes each at 37^{o}C. This was followed by HIS washes for 20 minutes twice. Sections then washed in 2XSSC and 0.2XSSC at 65^{o}C for 1 hour each. Then, the slides were imbedded in PBT at room temperature twice for 15 minutes each. The non-specific binding block was done using 10% heat-inactivated goat serum for one hour. To detect DIG-probe, the tissue sections were incubated with 1:2000 anti-dig probe in 10% heat inactivated goat serum and PBT solution at 4^{o}C overnight.

On the next day, to remove the unbound anti-DIG antibody, the sections were washed in PBT for 4 times 10 minutes each and incubated in fresh NTMT for 10 minutes at room temperature. For colour development, the slides were embedded in BM purple until the colour developed. After colour development, slides were embedded in PBT thrice for 15 minutes each. The tissues were then dehydrated using gradually increasing ethanol solutions 70%, 90%, 95% and 100% and then cover slipped and mounted with DePeX.

2.11. RT-qPCR

2.11.1. Reagents and kits

Sybergreen	Kappa Biosystem, K44602
Qiagen RNAeasy Minikit	Qiagen, 24104
Random primer	Promega, C1181
MMLV RT kit	Promega, M3682
RNA-lator	Sigma, R0901
β-Mercaptoethanol	Sigma, M6250

Table 2.26. Reagents and kits for RT-qPCR

2.11.2. Primers for RT-qPCR

Primer	Sequence
Wnt1 F	GTAAGATATGTGCCCAGCAGC
Wnt1 R	ACCTGTGCACACACTCCTATTG
Wnt2 F	CTCTGCTCTTGACCTGGCTC
Wnt2 R	CCTGGCACATTGTCACACATC
Wnt2b F	CACCCGGACTGATCTTGTCTAC
Wnt2b R	CTCGGCCACAACACATGATTTC
Wnt3 F	TCGGCGCTGCTTCTAATGG
Wnt3 R	AGATGTGTACTGCTGGCCC
Wnt3a F	ATGAACCGTCACAACAATGAGG

Wnt3a R	CCAGCAGGTCTTCACTTCACAG
Wnt4 F	GCAGGAAGGCCATCTTGACA
Wnt4 R	CACGTCTTTACCTCGCAGGA
Wnt5a F	GACGCTTCGCTTGAATTCCTC
Wnt5a R	CGGGCTTAATATTCCAATGGGC
Wnt5b F	ATGCCCGAGAGCGTGAGAAG
Wnt5b R	ACATTTGCAGGCGACATCAGC
Wnt6 F	TGCGGTAGAGCTCTCAGGATG
Wnt6 R	CTGGTAGGATCCATGACCAAGGG
Wnt7a F	GATCAAGCAGAATGCCCGGA
Wnt7a R	TCTCCTCCAGGATCTTCCGA
Wnt7b F	GTCCTCTACGTGAAGCTCGG
Wnt7b R	CACAATGATGGCATCGGGTC
Wnt9b F	AGTTCCAGTTCAGGCAGGAG
Wnt9b R	GACACTGCATACAGGAAGGC
Wnt10a F	TGAGTGCCAGCATCAGTTCC
Wnt10a R	ACTCTCTCGAAAACCTCGGC
Wnt10b F	TTCTCTCGGGATTTCTTGGATTC
Wnt10b R	TGCACTTCCGCTTCAGGTTTTC
Wnt11 F	GTAGGGCCTTCGCTGACAT
Wnt11 R	ACTCCCGTGTACCTCTCTCC
Wnt16 F	TCTTCCCATCAGAAACACCACA
Wnt16 R	ATTAACTTGGCGACAGCCTGC

Wls F	TCTAATGGTGACCTGGGTGTC
Wls R	TTCCAGCTCAGTGCCATACC
Axin2 F	ACGCACTGACCGACGATT
Axin2 R	AAGGCAGCAGGTTCCACA
Lef1 F	AACGAGTCCGAAATCATCCCA
Lef1 R	GCCAGAGTAACTGGAGTAGGA
β-catenin F	CCGTTCGCCTTCATTATGGA
β-catenin R	GGCAAGGTTTCGAATCAATCC
GapdH F	CCATGGAGAAGGCCGGGG
GapdH R	CAAAGTTGTCATGGATGACC

Table 2.27. Primer list

2.11.3. Tissue dissection

Dental pulp tissue was dissected by cracking the incisor and dissecting the pulp tissue in cold 1X PBS. The tissue was then stored in RNA-lator at -80^{o}C for future use. At least 3 incisors were used unless otherwise mentioned.

2.11.4. RNA extraction

QIAGEN RNeasy mini kit was used to extract RNA. Tissue dissociation was done by using buffer RLT with β-mercaptoethanol. Then the tube was centrifuged to pellet the lysate and then one volume of 70% ethanol was added to the supernatant and then the mixture were transferred to the RNeasy spin column to bind the RNA to the filter. To clean the filter, buffer RW1 was added and centrifuged for two minutes. Another wash was applied with buffer RPE for two

minutes twice, and finally, RNA was eluted by adding 30µl RNase-free water. The RNA concentration was tested using a Nanodrop.

2.11.5. Reverse transcription of RNA to cDNA

To produce cDNA, two steps were done. The first step was to melt the secondary structure within the RNA template. This step was done by adding 1µg RNA to the random primer solution (Table 2.28) at 70ºC for five minutes. This was followed by cooling down on ice for another five minutes.

RNA	1µg
Random primer	2µl
Water	Up to 14µl

Table 2.28. Random primer solution

Then, the reverse transcription solution (Table 2.29) was added to the mixture and the mixture was incubated at 42ºC for one hour. The cDNA consternation was tested by using Nanodrop and stored at -20ºC.

dNTPs	1.25µl
5 X buffer	5µl
mmLVRT	1µl
Water	3.75µl

Table 2.29. Reverse transcription solution

2.11.6. RT-qPCR run

To design the qPCR experiment, primers were ordered from IDT (table 2.27). To prepare the RT-qPCR mixture, cDNA, forward and backward primers and sybergreen were added to the template (Table2.30) in a cold surface to prevent any degradation.

cDNA	4.8ml
Forward primer	0.1ml
Reverse Primer	0.1ml
Sybergreen mix	5ml

Table 2.30. RT-qPCR mixture

Three runs were performed, and each run was used 3 different cDNA for each primer. The run was done using Roche LightCycler 48011 (Table 2.31):

Pre-incubation	1 cycle
Amplification	45 seconds
Melting curve	1 cycle
Cooling	1 cycle
Target temperature	95^{o}C
Melting temperature	60^{o}C

Table 2.31. RT-qPCR run parameters

2.11.7. RT-qPCR analysis:

To analyse the RT-qPCR data, a double delta Ct analysis method was used. Three runs of triplicate were done for both housekeeping genes and genes of interest for both experimental tissue and control tissue. The outcome of this calculation gave four values; average Ct for gene of interest of experimental tissue (E^{GOI}) and control tissue (C^{GOI}), and average Ct for housekeeping gene for experimental tissue (E^{HKG}) and control tissue (C^{HKG}). This was followed by the calculation of the difference between ($E^{GOI} – E^{HKG}$) to give ΔE, and then finally calculating the expression level by (2^-ΔE). Secondly, the expression level for the control group was calculated similarly to the experimental group by using (C^{GOI}) and (C^{HKG}) to give ΔC. To optimise the level of expression, ΔE was divided by ΔC.

The data figures were produced by using GraphPad Prism 7 with the option of error bar and the mean of every gene. Significant different was calculated by doing unpaired t-test.

2.12. µCT-scan

2.12.1. Fixation:

Mouse skulls were fixed in 4% PFA for two days to make sure internal tissue was fixed, and that PFA can penetrate the dental pulp. The fixed skulls were washed thrice in PBS for 30 minutes each and stored at 4ºC. At least 3 skulls were used unless otherwise mentioned.

2.12.2. µCT-scanning:

µCT scanning was done by using SkyScan 1272, Bruker. The X-ray tube voltage was 80 kVp and the current was 125 µA.

pCagg ^{CreERT2}; Wls $^{fl/fl}$ mouse skull scans were taken by GE healthcare Locus SP scanner. The X-ray tube voltage was 80 kVp and the current was 80 µA

2.12.2.1. Data presentation and 3D reconstruction

The scan was visualised by Parallax innovations Microview software version 2.5.0. The upper incisors were levelled to the X-axis and the pictures were taken. Using the same software, 3D reconstruction was done by tracing teeth by advanced ROI option and then running the isosurface option.

2.13. Mouse incisor measurements and bone volume analysis

Mouse incisor length was measured by using Parallax innovations Microview software version 2.5.0. The labial incisor curvature was measured, and the results was given by the software. Dentine thickness was measured similarly. Dentine thickness was measured as the average of three areas; cervical area, the middle of the tooth, and the incisal end. Bone volume was measured by using BMD analysis option to produce bone volume analysis of either left or right mandible.

2.14. Data analysis and statistics

Data entry and Statistical analysis was done using GraphPad Prism 7. Unpaired t-test was used to calculate statistical significance. The Values of $p< 0.05$ were considered statistically significant. A minimum of 3 animals were used for each experiment.

2.15. Microscopy and Imaging

Confocal microscopy images were taken by Leica TCS SP5 and imaging analysis was done by Leica LAS AF imaging software. For GFP, WNT-4, Wnt-10a and TUNEL detection, argon laser 488 nm line were used. For BrdU, the argon laser 561 nm was used. DAPI was detected using violet (405 nm) laser line. Histology and LacZ staining images were obtained on Nikon ECLIPSE Ci microscope. Whole-mount LacZ staining were obtained on LEICA MZFLIII.

Results

Chapter 3. Wnt signaling activity in adult mouse incisors

3.1. Introduction

Losing the incisal edge structure of mouse incisors due to mastication wearing is compensated by forming new dental tissues at the incisor cervical end. This happens because of the availability of stem cell populations at the incisor apical end, which balances the tooth turn-over and keeps the tooth functional and sharp through life (Harada et al., 1999). Therefore, incisors are considered as a model to study stem cells functions. Different signaling pathways contribute to incisor development and homeostasis, such as Shh, Bmp and Fgf which also can regulate different adult stem cell populations (Wang et al., 2007; Seidel et al., 2010)

The Wnt signaling pathway has a fundamental role in controlling many stem cell populations in many organs. It is known that the Wnt/β-catenin pathway controls proliferation, differentiation and maintenance of hair follicle epithelial stem cells (Lim *et al.*, 2016) and intestine epithelial stem cells (Kretzschmar and Clevers 2017). Tooth development is also controlled by Wnt signaling where in the absence of Wnt/β-catenin pathway activity, tooth bud development stops at the cap stage while upregulation of Wnt/β-catenin pathway activity leads to supernumerary tooth formation and large tooth bud development (Fujimori et al., 2010).

Logan and Nusse (2004) showed that the canonical Wnt pathway requires free β-catenin in the cytoplasm that can enter the nucleus and activate the transcription of the target genes. The absence of Wnt protein binding to the receptor causes phosphorylation and degradation of β-catenin by the destruction complex. When Wnt ligand attaches to the receptor Frizzled, coreceptor LRP5/6 attracts the degradation complex and consequentially free β-catenin protein in the cytoplasm. Wnt target genes have been of great interest, particularly for oncology research (Nusse and Varmus, 1982; Brennan and Brown, 2004), as well as developmental

biology (Liu and Millar, 2010; Xiang *et al.* 2014). Yu *et al*. (2005) found that a newly born Axin2 mutant mouse has a normal skull. However, post-natal growth causes premature skull suture fusion, leading to a smaller skull.

The Wnt ligand, which activates the Wnt signaling pathway is a lipid-modified protein, and there have been at least 19 ligands discovered in both humans and mice (Miller 2002). Therefore, studying Wnt signaling activity could be a complicated subject because of the variety of Wnt ligands and the complicated nature of the pathway, as Wnt ligands could activate the Wnt/β-catenin pathway, non-canonical Wnt pathway or both (Miller, 2002). Nevertheless, many agonists and antagonists might contribute to the pathway. This chapter will focus on the Wnt/β-catenin pathway activity and Wnt ligands expression in the adult mouse incisors.

3.2. Results

3.2.1. Identification of Wnt-responsive cells in mouse incisor pulp

Since Wnt/β-catenin signaling controls the proliferation and differentiation of different stem cell populations such as hair follicle epithelial stem cells (Lim *et al.,* 2016) and intestine epithelial stem cells (Kretzschmar and Clevers, 2017), mouse incisor mesenchymal stem cells could be a candidate for Wnt/β-catenin pathway activity. Therefore, I used a Wnt-reporter (Axin2-lacZ) mouse line, where *LacZ* reporter gene is knocked into the codon region of Axin2 (Lustig *et al.,* 2002), to identify which cell population are responding to Wnt/β-catenin signaling. Axin2 is a well-known Wnt/β-catenin pathway readout for two reasons; it is part of the β-catenin degradation complex, and it is one of the direct transcriptional targets of Wnt/β-catenin signaling and works as a negative feedback loop (Yu *et al*., 2005). This transgenic mouse expresses β-galactosidase in response to Wnt/β-catenin activity, which can be detected by using the X-gal staining.

3.2.1.1. µ Ct scan analysis for *Axin2$^{LacZ/+}$* mouse incisors

Adult *Axin2$^{LacZ/+}$* mouse skulls (n=3) were scanned and then compared to the wild-type mouse incisor (n=3). Both *Axin2$^{LacZ/+}$* and wild-type mice share normal incisor shape and dimensions (Figure 3.1 A, B). Incisor length for *Axin2$^{LacZ/+}$* mouse was 11.2 (± 0.02080) mm (n=6) while it was 11.24 (± 0.02963) mm for the wild-type mouse incisor (control) (n=6). Unpaired t-test analysis showed that the incisor dimension of both mouse lines has no significant difference (P= 0.3276) (Figure 3.1 C).

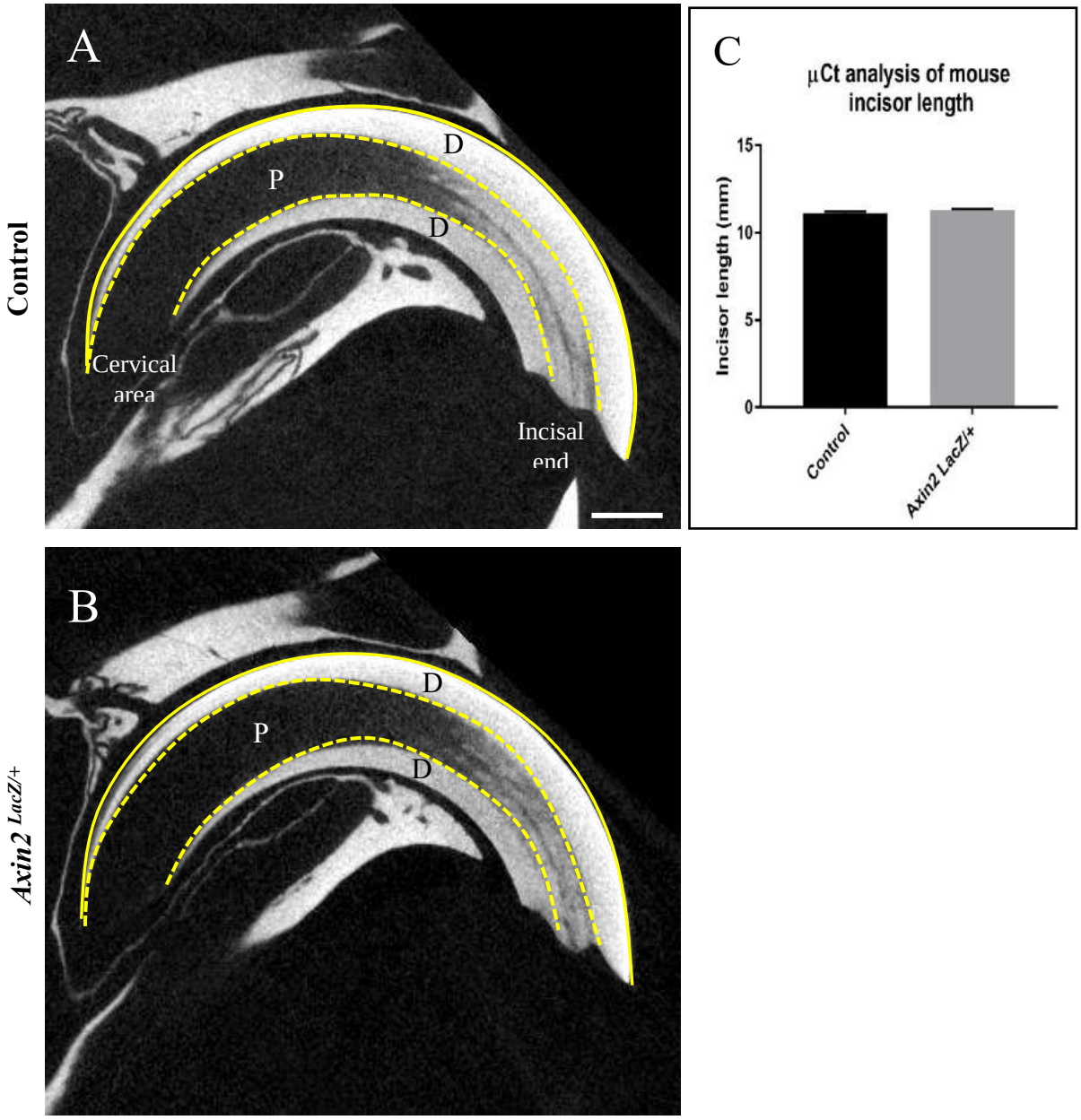

Figure 3.1. µ-Ct scan of *Axin2* $^{LacZ/+}$ mouse incisor

(A-B) Both wild type mouse incisor (n=6) and *Axin2*$^{lacZ/+}$ mouse incisor (n=6) share the same shape and no abnormalities can be detected.

(C) Unpaired t-test analysis of incisor length (Yellow line at the labial curvature) shows no significant difference between wild type mouse (n=6) and *Axin2*$^{lacZ/+}$ mouse (n=6).

(D) dentine, (P) pulp. Scale bar= 1000 µm

3.2.1.2. X-gal staining for *Axin2*$^{LacZ/+}$ mouse incisors

3.2.1.2.1. Whole-mount incisor staining

Axin2$^{LacZ/+}$ mouse produces β-galactosidase in the Axin2 expressing cells. When β-galactosidase forms, X-gal can detect it and label *Axin2* expressing cells with a blue colour.

Adult *Axin*$^{LacZ/+}$ (n=3) and wild type mice (n=3) were used. X-gal staining for the wild-type adult mouse incisors was negative to the staining, which eliminates the possibility of the endogenous β-galactosidase activity (Figure 3.2 A).

Whole-mount X-gal staining for adult *Axin*$^{LacZ/+}$ mouse incisors showed that most of the positive staining was located at the apical end. The staining was stronger around the cervical end and then faded away toward the tip where no visible staining was detected at the incisal tip (Figure 3.2).

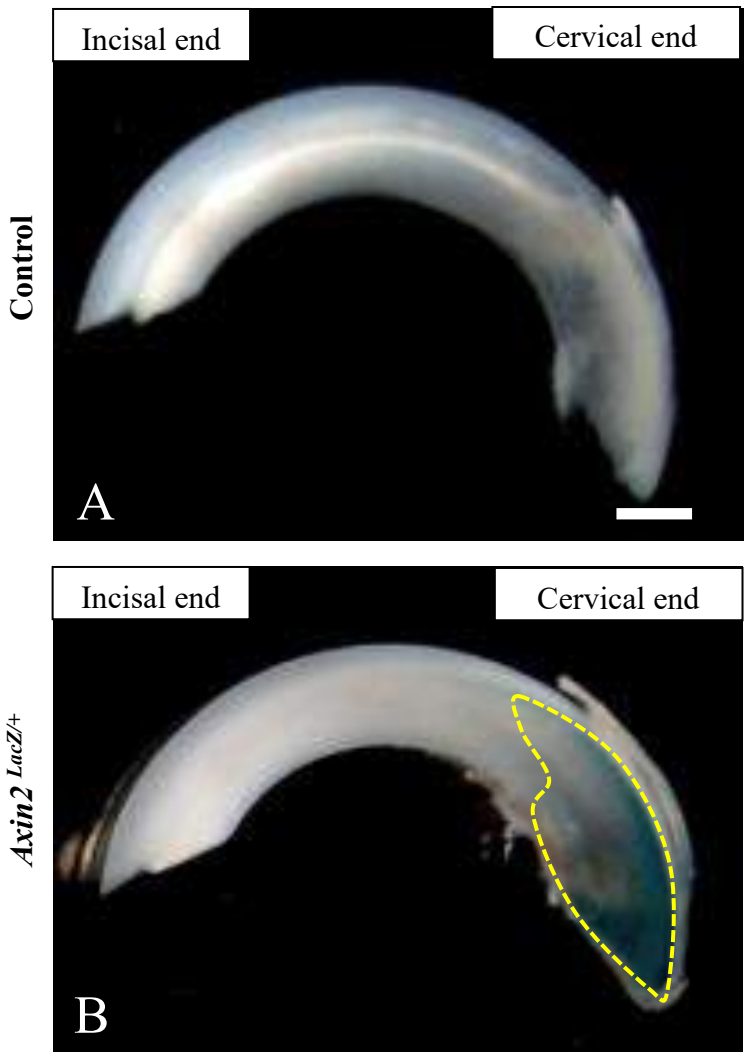

Figure 3.2. *Axin2* is expressed in the cervical area of the mouse incisor

X-gal staining for (A) Wild type mouse incisor (Control) (n=3) shows no positive staining. (B) *Axin2*$^{LacZ/+}$ mouse incisor (n=3) has positive staining at the cervical area of the tooth (dotted area) while the incisal end shows no staining.

Scale bar= 1000 µm.

3.2.1.2.2. X-gal staining for frozen sections

The whole-mount incisor staining outcome showed that the Wnt/β-catenin pathway is active at the incisor cervical end. To identify which cell population responds to Wnt/β-catenin signaling, X-gal staining for *Axin2*$^{LacZ/+}$mouse incisor frozen section was done. Adult *Axin*$^{LacZ/+}$ mouse incisors (n=3) and wild type mouse incisors (n=3) were used. Similar to the whole-mount staining, sections staining of wild-type mouse incisors (control) result was negative, and no staining was detected, which confirm that there is no endogenous activity of β-galactosidase in the mouse incisors. However, *Axin2*$^{LacZ/+}$ mouse incisor sections showed that the positively stained cells appear as colonies and mainly located distal to the MSC niche, an area known for the transit amplifying cells niche (TAC zone). Another positive stained cell population is odontoblasts. Moreover, X-gal staining was negative at the area between the cervical loops where the MSC niche is located (Figure 3.3).

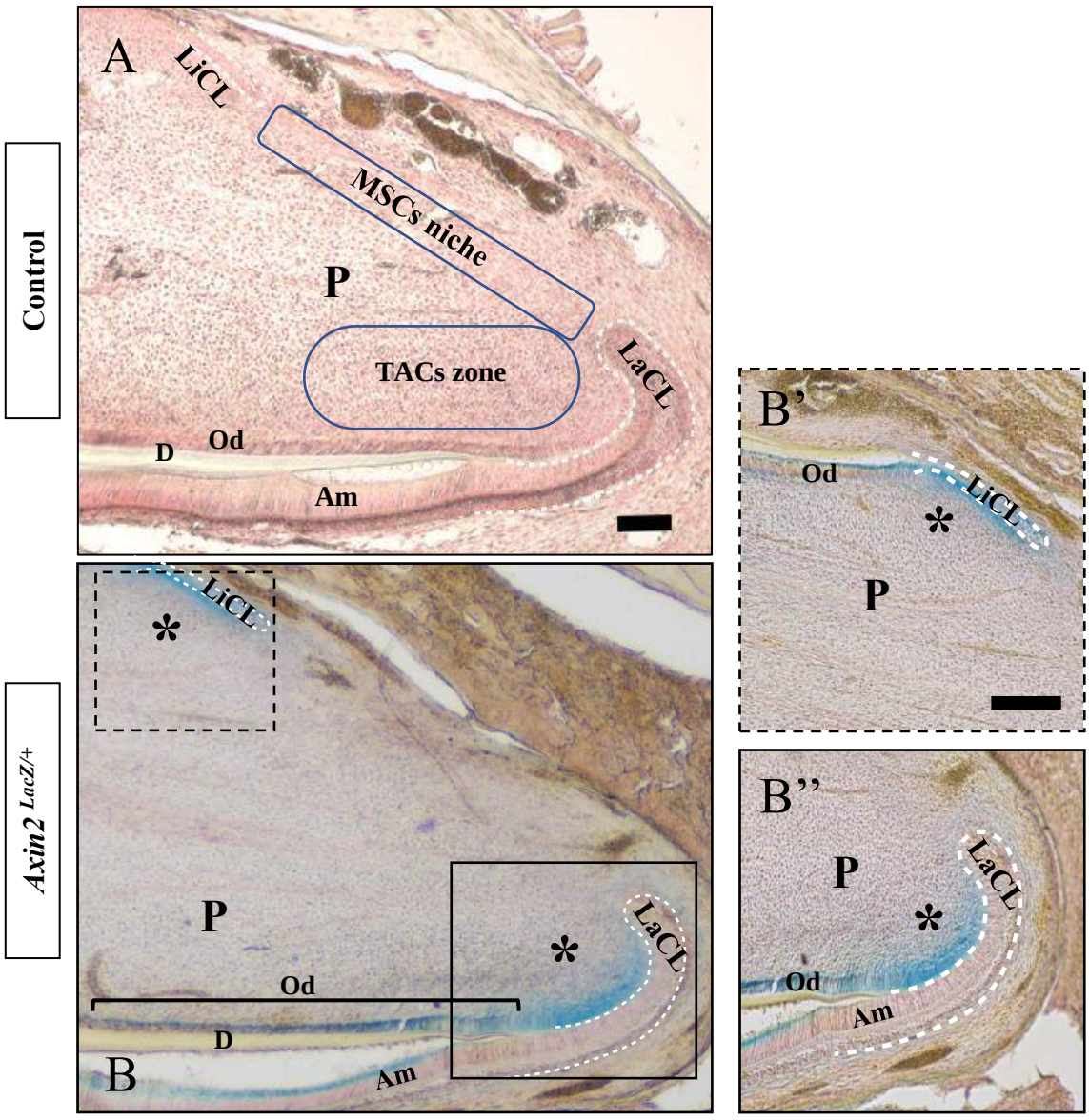

Figure 3.3. *Axin2* is expressed in the cervical loop area

(A-B) Incisor frozen sections X-gal staining. (A)Wild type mouse incisor (Control) (n=3) shows no positive staining. (B) *Axin2*$^{LacZ/+}$ mouse incisor (n=3) has positive staining at the TACs zone distal to the cervical loop (B') labially, and (B'') lingually (*). *Axin2* is also expressed in the odontoblasts, however, no staining is detected within the cervical loop (epithelial stem cell niche location) or at the MSC niche.

(LaCL) Labial cervical loop, (LiCL) Lingual cervical loop, (E) enamel space, (D) Dentine, (P) Pulp, (Am) Ameloblasts, (Od) odontoblasts. Scale bar = 100 µm.

3.2.2. *Axin2* genetic lineage tracing

As shown above, Wnt/β-catenin is active in both TACs and odontoblasts where *Axin2*-expression was detected, while it is not in the MSCs. To verify that, genetic lineage tracing for *Axin2*-expressing cell was performed. In genetic lineage tracing, cells are labelled in such a way that the label is transmitted to the cell clones, which will result in a population of labelled lineages (Kretzschmar and Watt, 2012). This technique has become a gold standard to definitively identify cell nature *in vivo* (Haegebarth and Clevers, 2009; Joyner and Zervas, 2006).

Axin2^{CreERT2} transgenic mouse line, where *Cre* is driven by *Axin2* promoters, were mated with *Rosa26R*^{lacZ} mouse reporters. In this transgenic mouse, tamoxifen treatment induces *Cre* expression, and when Cre-loxp recombination happens, the loxP-flanked STOP sequence located upstream to *lacZ* will be deleted, so targeted cells and all their progenies would permanently express *lacZ* (Van Amerongen et al., 2012).

In this study, six-week-old mice were treated by three IP tamoxifen injections in 3 consecutive days and then divided into four groups according to the collection time point into one day (n=4), seven days (n=4), 14 days(n=4) and 28 days (n=3).

Frozen section X-gal staining of one day post-tamoxifen treated *Axin2*^{CreERT2}*; Rosa26R*^{LacZ} transgenic mouse line incisors (n=6) showed no positive staining within the labial cervical loop (epithelial stem cells niche location). The area between the cervical loops where the MSC niche is located was negative to the staining as well. However, the area distal to the MSC niche where the TAC zone is located was positive and showed a small number of labelled cells. The odontoblastic layer showed some positively stained odontoblasts in the cervical area adjacent to the TAC zone. Another population of labelled cells was associated with the blood vessels in the middle of the tooth, which is a known anatomical area for pericytes (Figure 3.4).

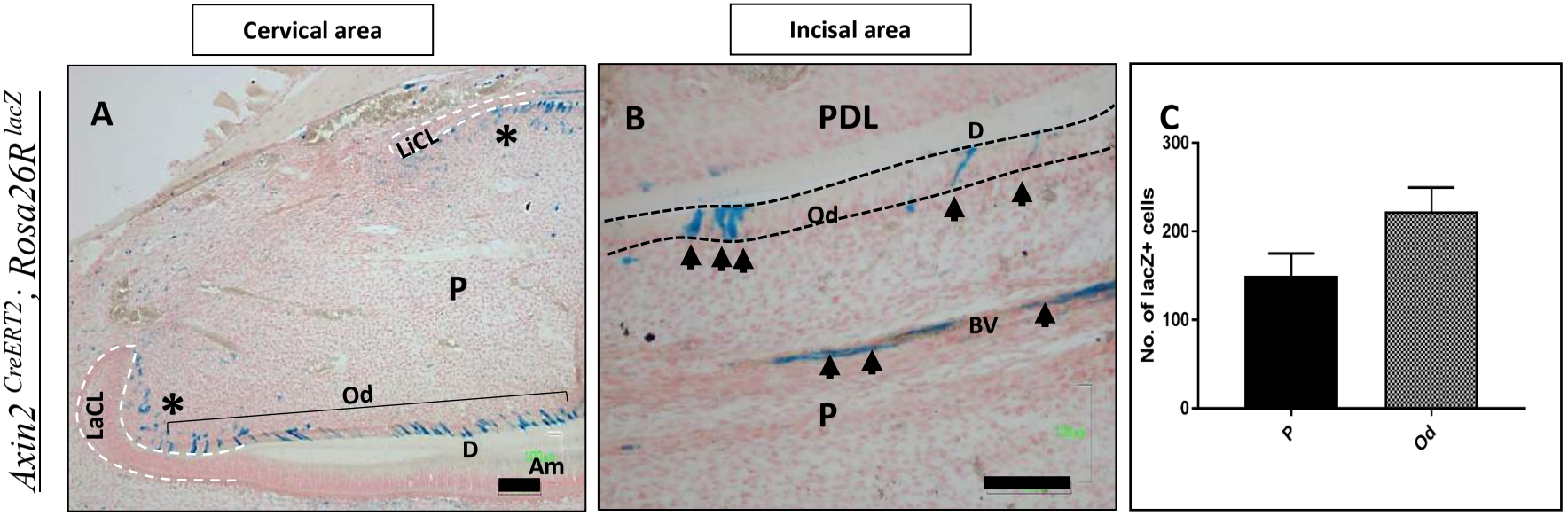

Figure 3.4. Incisor frozen section X-gal staining for 1-day post tamoxifen treated *Axin2 CreERT2; Rosa26R lacZ* mouse incisor

(A) At the cervical area, a small population of positively stained cells is located at TAC zone (*) distal to the cervical loop and few odontoblasts. (B) At the incisal area, cells lining blood vessel and some odontoblasts (arrows) are positively stained (n=6).

(C) Dental pulp cells and odontoblast positively stained cells count (n=6)

(LaCL) labial cervical loop, (LiCL) lingual cervical loop, (D) Dentin, (P) pulp, (BV) Blood vessel, (Od) Odontoblasts. Scale bar, 100um.

Seven days post-tamoxifen treatmet mouse incisors (n=6) generally showed more positive labelled cells. The epithelial stem cells niche within the labial cervical loop was negative to the staining. However, the area between the cervical loops, where the MSC niche is located, showed positive staining, which was negative in the first group (one-day post-tamoxifen). Distal to the MSC niche, more proliferating TACs and pulpal cell were labelled. The odontoblasts also showed more positively stained cells at the cervical end and in the middle of the tooth.

The population of labelled cells associated with the blood vessels showed more positive stained cells which need more investigation to study the role of pericytes on the incisor homeostasis (Figure 3.5).

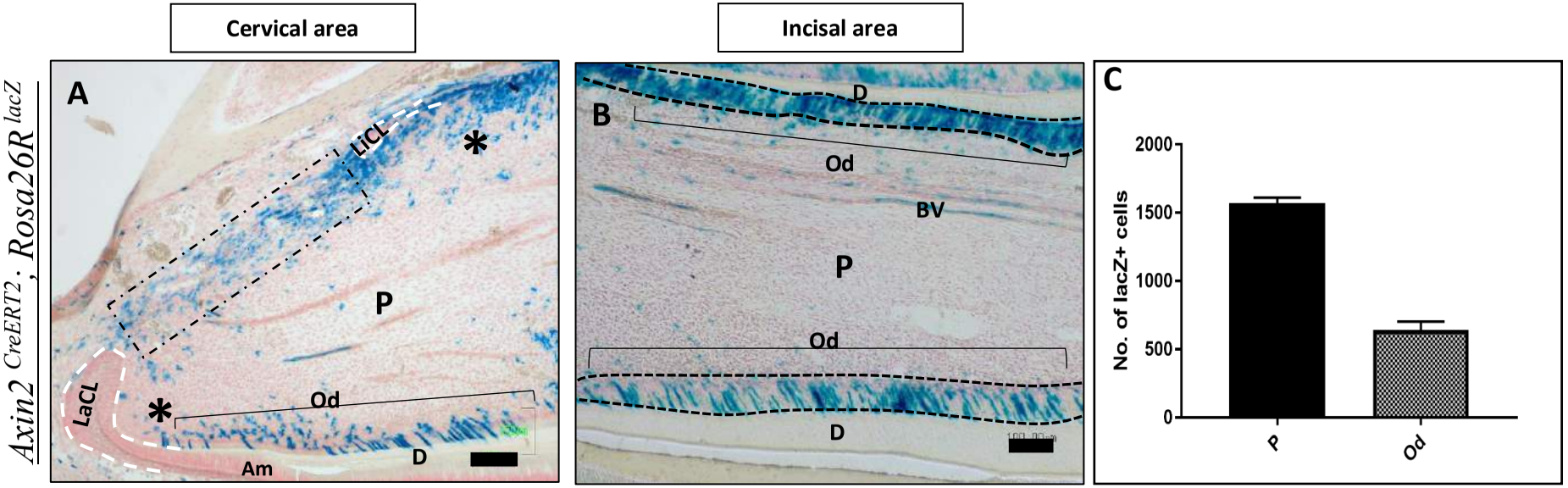

Figure 3.5. Incisor frozen section X-gal staining for 7-days post-tamoxifen treated *Axin2^{CreERT2}; Rosa26R ^{lacZ}* mouse incisor

(A) At the cervical area, more cells are labelled at MSC niche (black rectangles), TAC zone (*) and odontoblasts. (B) At the incisal area, cells surrounding blood vessel have positive staining with more positive stained odontoblasts (n=6).

(C) LacZ+ cell count at the cervical area shows more labelled pulp cells and odontoblasts (n=6)

(LaCL) labial cervical loop, (LiCL) lingual cervical loop, (D) Dentin, (P) pulp, (BV) Blood vessel, (Od) Odontoblasts. Scale bar, 100um.

X-gal staining for 14 days post-tamoxifen treated *Axin2^{CreERT2}; Rosa26R^{LacZ}* mouse incisor (n=6) sections can be divided into two findings; less labelled cells at the cervical end and more labelled cell at the middle of the tooth. The MSC niche which showed positive staining in the previous group (seven days post-tamoxifen) was negative to the staining at this time point. Distal to the MSC niche, fewer number of TACs, pulp cells and odontoblasts were labelled at the cervical end. However, more pulpal cells and odontoblasts were labelled in the middle of the tooth (Figure 3.6).

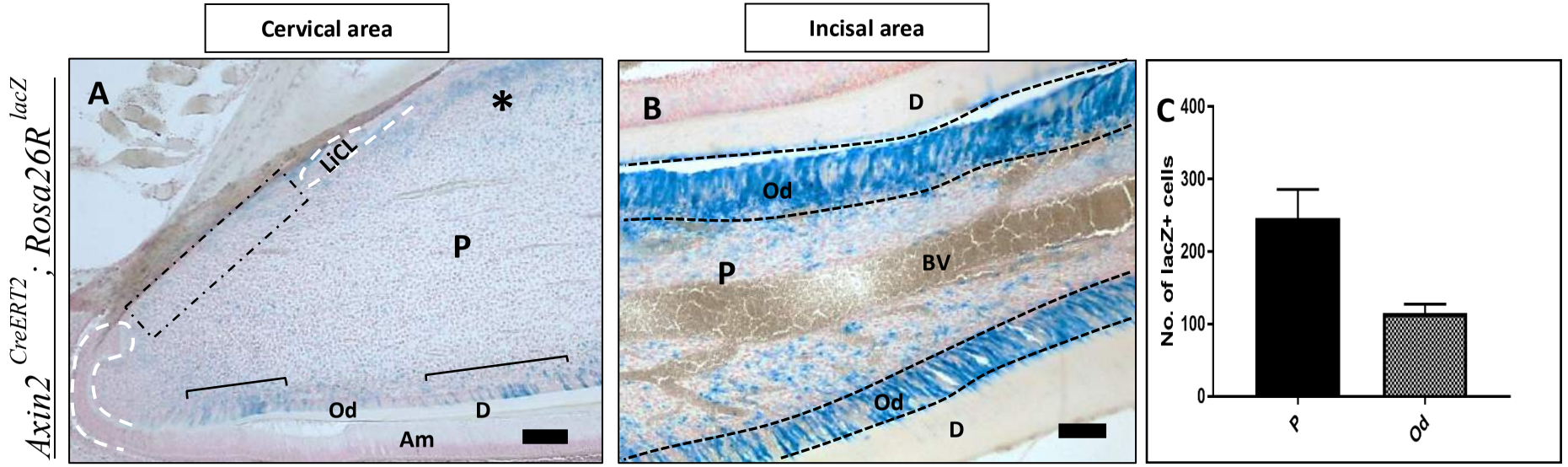

Figure 3.6. Incisor frozen section X-gal staining for 14-days post-tamoxifen treated *Axin2^{CreERT2}; Rosa26R ^{lacZ}* mouse incisor

(A) At the cervical area, TACs zone (*) have few labelled cells and few adjacent odontoblasts, however, no positive staining is detected in the MSC niche (dotted rectangle). (B) At the incisal area, more odontoblasts and their adjacent pulp cells are positively labelled than the previous time point (n=6).
(C) LacZ+ cell count shows fewer positive cells at the cervical area. (n=6)

(LaCL) labial cervical loop, (LiCL) lingual cervical loop, (D) Dentin, (P) pulp, (BV) Blood vessel, (Od) Odontoblasts. Scale bar, 100um.

Frozen section X-gal staining for the 28 days post-tamoxifen treated *Axin2^{CreERT2}; Rosa26R^{LacZ}* mouse incisor (n=6) was mainly showing no more labelled cells at the cervical end of the tooth. Epithelial and mesenchymal stem cell niches showed no positive staining as well as TACs and odontoblasts. However, a small population of labelled odontoblasts and pulp cells were detected at the incisal end (Figure 3.7). Nevertheless, another transgenic mouse line (*Axin2^{CreERT2}; Rosa26R$^{mT/mG}$*) was used that showed similar results in our recent publication (An et al. 2018).

To summarise this experiment, *Axin2* lineages were detected at the cervical end distal to the MSC niche (TAC zone) and odontoblasts at the beginning of the experiment. *Axin2* lineages proliferate through the first 14 days to include most of the cervical area mesenchymal cells. However, *Axin2* lineage cells cannot renew themselves, and they vanished from the cervical area after 28 days.

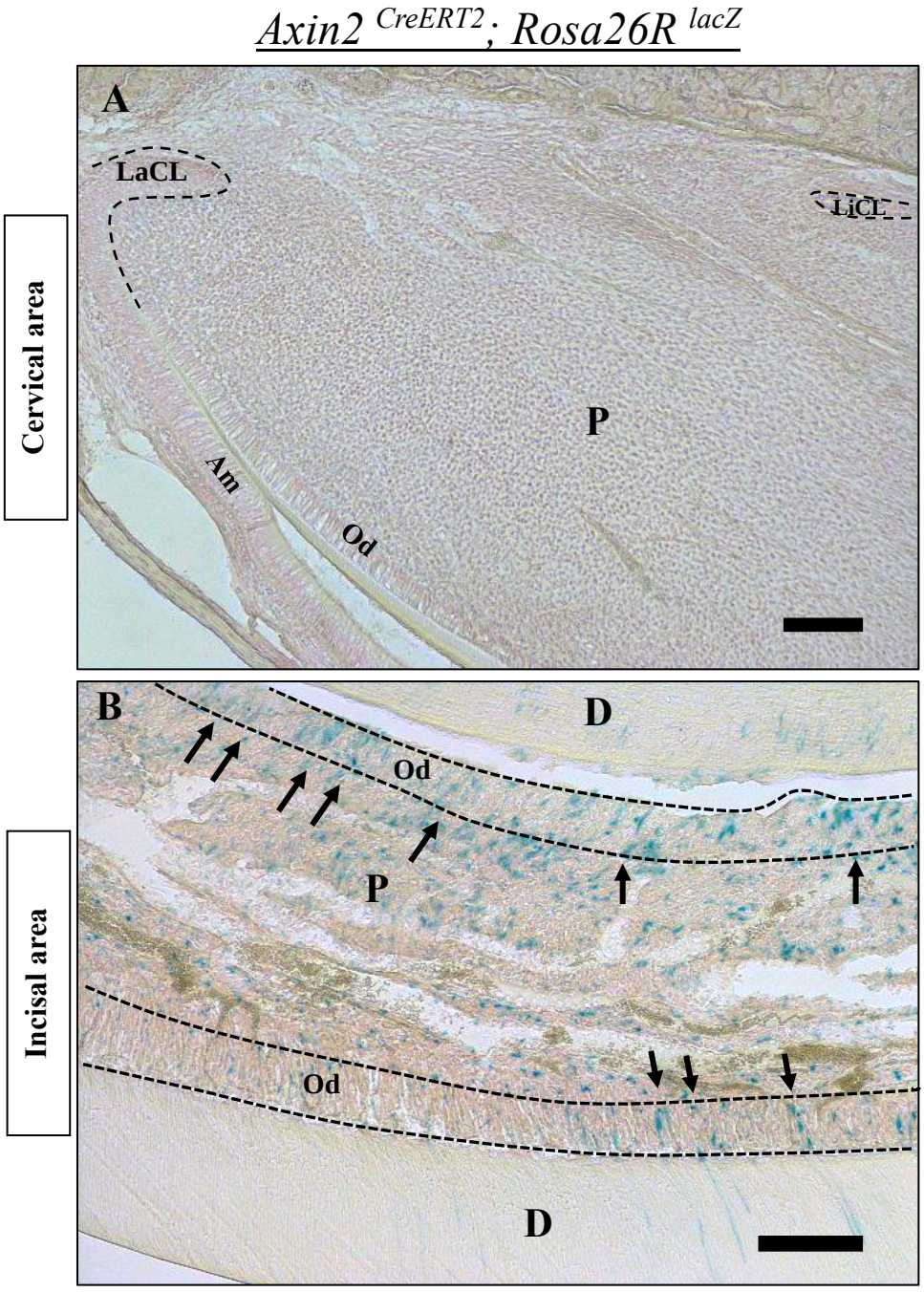

Figure 3.7 X-gal staining for 28-days post-tamoxifen treated *Axin2*^{CreERT2}*; Rosa26R* ^{lacZ} mouse incisor

(A) At the cervical area, no more positive staining can be seen in the pulp cells or odontoblasts
(B) At the incisal area, some odontoblasts and pulp cells are labelled (black arrows) (n=6).

(LaCL) Labial cervical loop, (LiCL) Lingual cervical loop, (D) Dentine, (P) Pulp, (Am) Ameloblasts, (Od) odontoblasts. Scale bar = 100 µm.

3.2.3. Wnt ligand expression

3.2.3.1. RT-qPCR data analysis

RT-qPCR was done for all Wnt ligands to investigate their expression by using adult wild type mouse incisor pulp and compared to wild type E13.5 full head. Adult wild type mouse incisors (n=6) were dissected and the pulp tissue was harvested in a cold PBS. Wild type E13.5 heads (n=3) were collected and then both tissues RNA was extracted as shown in the material and methods chapter. Three runs were done with triplicate cDNA for each primer in every run.

RT-qPCR data analysis showed that Wnt ligands are expressed in the dental pulp (Figure 3.9). They can be divided into two groups according to the significant difference in their expression level. The first group, which has no significant difference, includes *Wnt-1* which has 1.678-fold changes (P value = 0.079), *Wnt-2* which has 1.843-fold changes (P value = 0.206), *Wnt-2b* has 1.89-fold changes (P value = 0.028), *Wnt-3* has .07043-fold changes (P value = 0.303), *Wnt-7b* has 0.6391-fold changes (P value = 0.107), *Wnt-9a* has 1.105-fold changes (P value = 0.527), *Wnt-9b* has 1.1952-fold changes (P value = 0.101), *Wnt-11* has 1.708-fold changes (P value = 0.139) and *Wnt-16* has 0.7131-fold changes (P value = 0.315).

The second group which showed significant difference includes *Wnt-3a* which has 5.483-fold changes (P value = 0.009), *Wnt-4* which has 6.859-fold changes (P value = 0.002), *Wnt-5a* has 5.394-fold changes (P value = 0.009), *Wnt-5b* has 4.922-fold changes (P value = 0.0029), *Wnt-6* has 10.48-fold changes (P value = 0.0077), *Wnt-7a* has 2.806-fold changes (P value = 0.0001), *Wnt-10a* has 73.79-fold changes (P value = 0.000002), and *Wnt-10b* has 6.554-fold changes (P value = 0.0231).

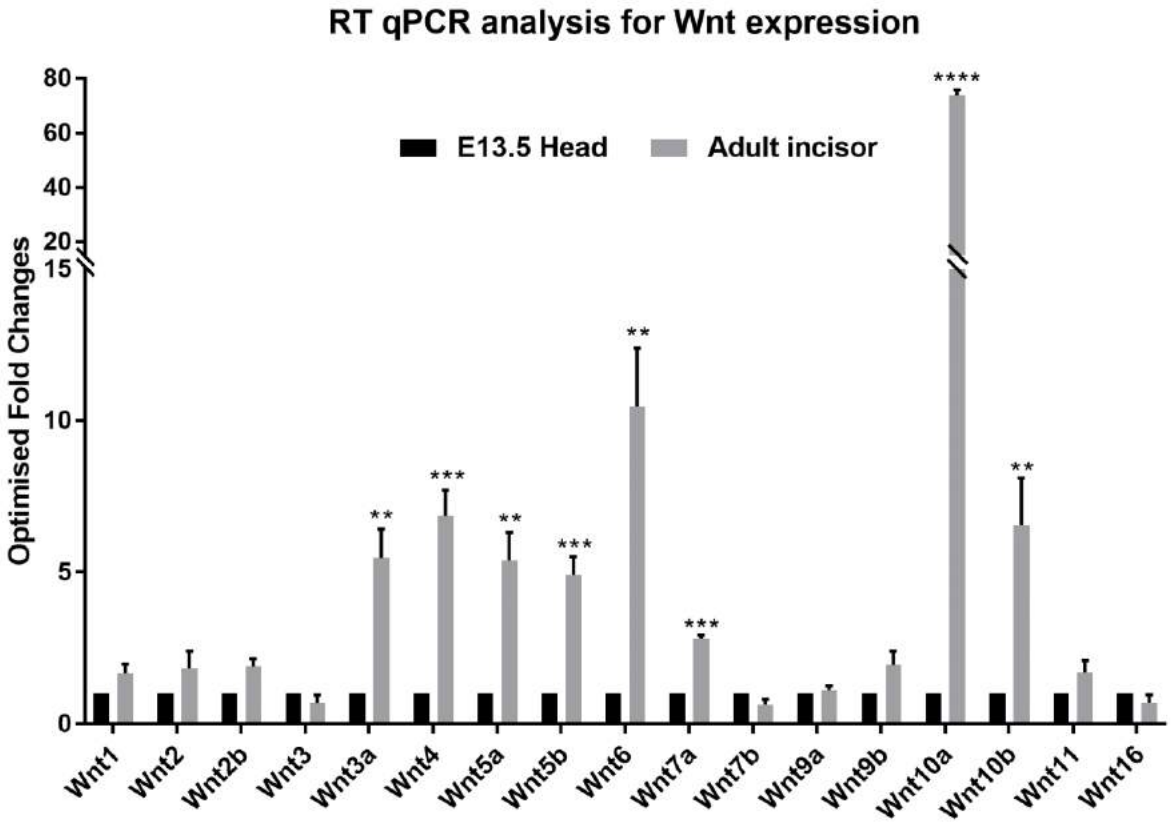

Figure 3.8. RT qPCR analysis for Wnt ligand expression in the dental pulp mesenchyme

Adult wild type mouse incisors (n=3) were used and compared to E13.5 full head (n=3). Among Wnt ligand expression, 8 ligands have significant high expression in the adult mouse incisor pulp, namely, Wnt-3a, 4, 5a, 5b, 6, 7a, 10a and Wnt-10b. the other Wnt ligand is also expressed but they have no significant different. (Unit, fold changes relative to E13.5 head). **p<0.01, ***p<0.001, ****p<0.0001.

3.2.3.2. Wnt-4 and Wnt-10a Immunofluorescent staining

To study Wnt expression on the dental tissue, a frozen section of adult wild-type mouse incisors was stained by using antibodies of Wnt-4 and Wnt-10a separately (n=3).

Wnt-4 is a non-canonical Wnt activator. It is one of the Wnt ligands that is expressed in the epithelial tissues during development (Sarkar and Sharpe, 1999; Suomalainen and Thesleff, 2010). Immunofluorescent staining for mouse incisors showed that Wnt-4 was not expressed in the epithelial stem cell niche within the labial cervical loop, nor the MSC niche in the cervical end. It was not expressed in the TACs either. However, Wnt-4 is expressed in the mature odontoblasts while it is not expressed in the pre-odontoblasts. Wnt-4 is expressed prenatally during incisor development in the ameloblasts and epithelial cells, which also continues postnatally (Figure 3.9 A-C).

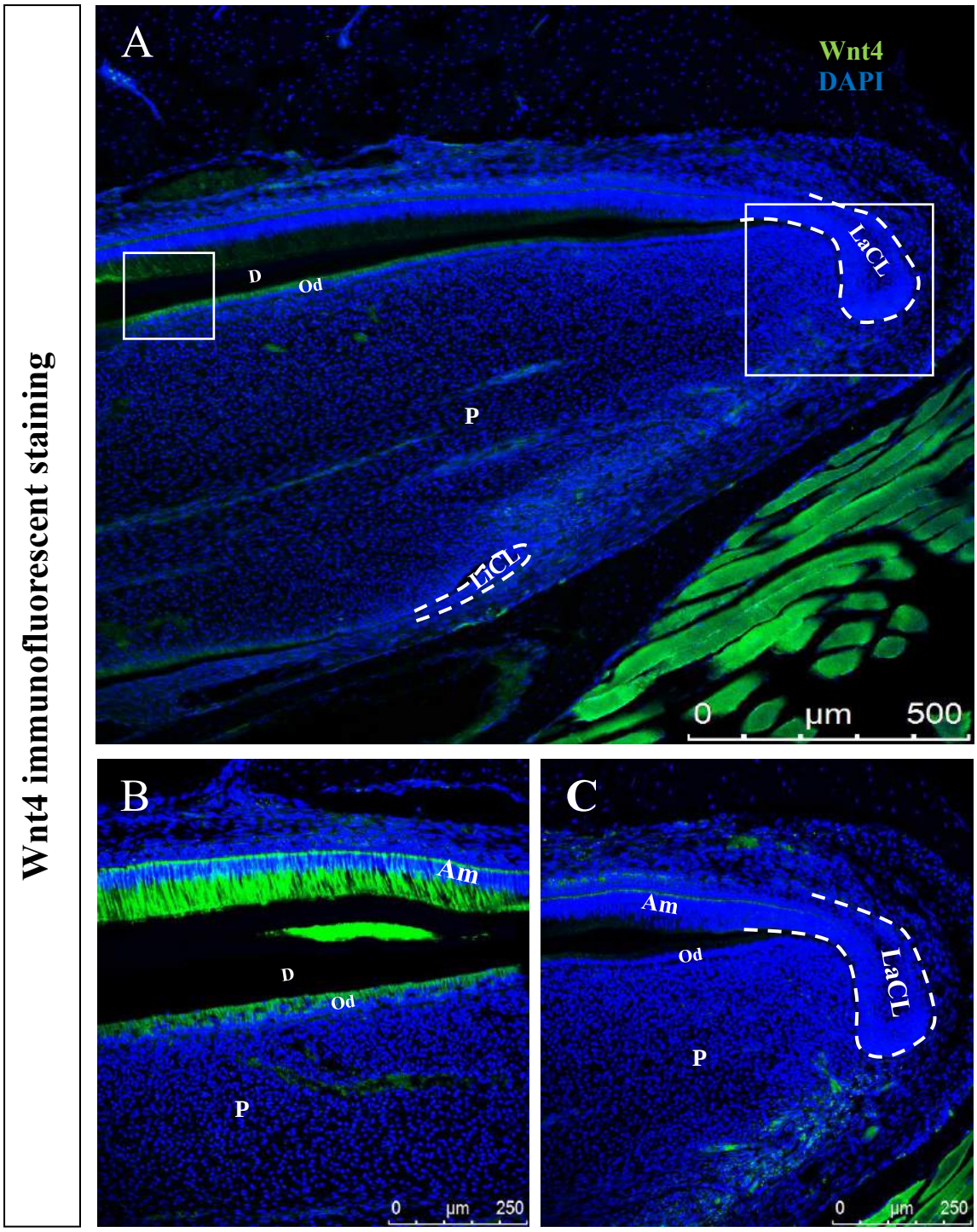

Figure 3.9. Wnt4 expression in the wild type mouse incisor

(A-C) Immunofluorescent staining for Wnt4 (Green) is limited to the mature odontoblasts and ameloblasts. However, no staining can be seen in the cervical area or within the cervical loop. (n=3)

(LaCL) Labial cervical loop, (LiCL) Lingual cervical loop, (D) Dentine, (P) Pulp, (Am) Ameloblasts, (Od) odontoblasts. Scale bar, (A)= 500 µm, (B-C)= 250 µm.

Wnt-10a is a canonical Wnt activator (Zhang et al. 2014). It is expressed in the enamel knot of the developing incisor and the odontoblasts of E16 and E18 incisors (Suomalainen & Thesleff, 2010). Immunofluorescent staining for Wnt-10a in the adult wild type mouse incisor (n=3) showed that Wnt-10a is not expressed in the epithelial stem cells, MSCs, TACs or pre-odontoblasts. However, Wnt-10a expression was limited to the mature odontoblasts distal to the cervical area (Figure 3.10 A-C).

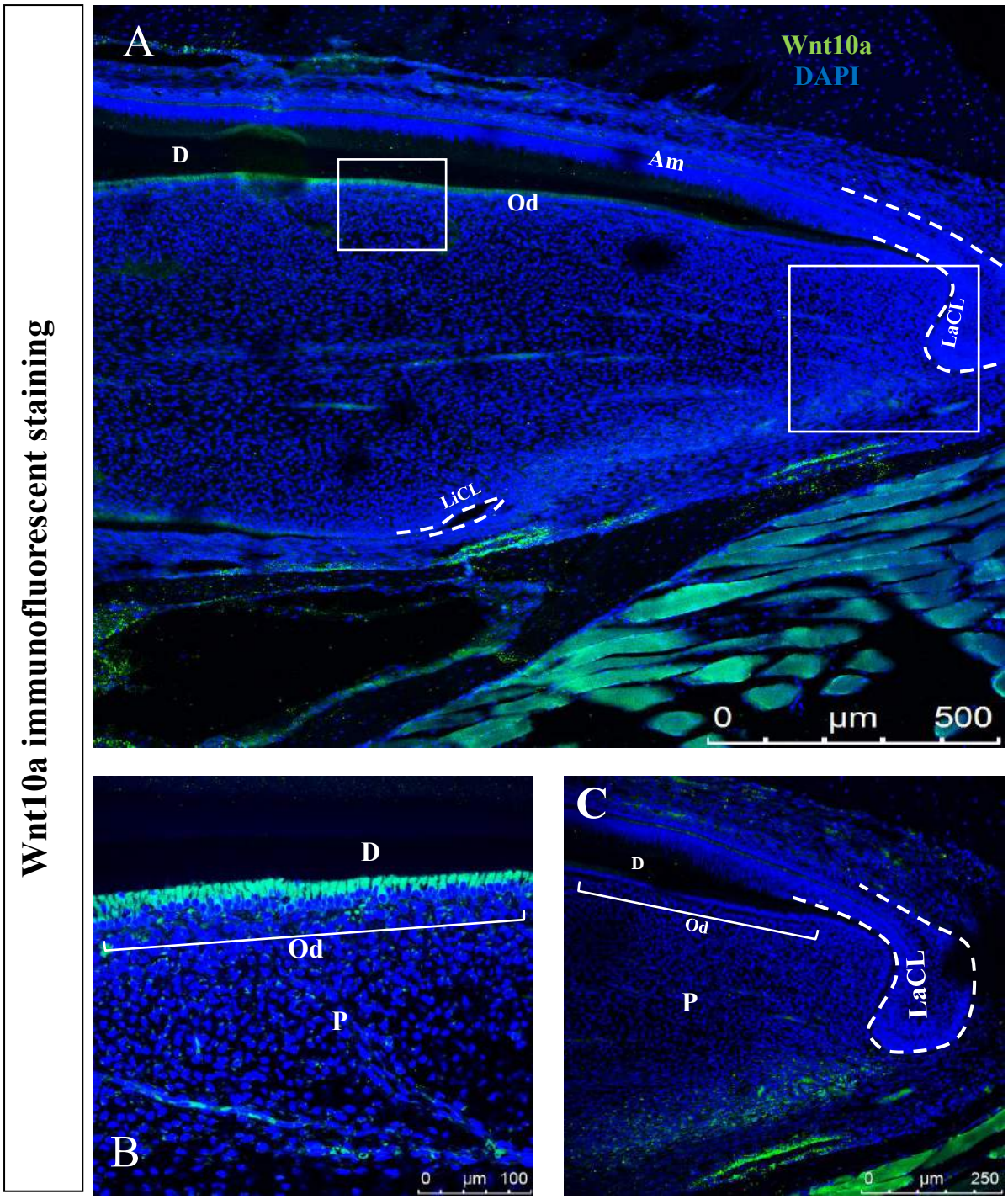

Figure 310. Wnt-10a expression in the wild type mouse incisor

(A-C) Immunofluorescent staining for Wnt-10a (Green) is limited to the odontoblasts distal to the cervical area (B). No staining can be seen in the cervical area, MSC niche, TACs zone or ameloblasts (C). (n=3)

(LaCL) Labial cervical loop, (LiCL) Lingual cervical loop, (D) Dentine, (P) Pulp, (Am) Ameloblasts, (Od) odontoblasts. Scale bar, (A)= 500 µm, (B)= 100 µm, (C)= 250 µm.

3.3. Discussion

3.3.1. Wnt-responsive cells in mouse incisors

Mouse incisors grow throughout the animal's life to compensate for mastication wear. This is because of the presence of the stem cells at the cervical area of the tooth (Harada *et al.*, 1999). Two populations of stem cells were identifed at the proximal end of the incisor; epithelial stem cells which mainly reside inside the labial cervical loop and mesenchymal stem cells that reside between the cervical loop (Lapthanasupkul *et al.*, 2012). Because of the continuous and rapid tooth wear, mesenchymal stem cells, which are slow-dividing cells give rise to the fast-dividing transit amplifying cells (TACs) which reside distal to the mesenchymal stem cell niche. Both MSCs and TACs are located in the cervical area of the incisor where their functions are regulated (Lapthanasupkul *et al.*, 2012).

The skeletal stem cells of the flat bones are Wnt-responsive cells, and Wnt/β-catenin signaling controls skeletal muscle stem cells proliferation and differentiation into osteoprogenitors and osteocytes (Bodine and Komm, 2006). The Wnt/β-catenin pathway also controls many epithelial stem cell populations such as hair follicle stem cells, where inactivation of Wnt/β-catenin pathways could lead to loss of these stem cell populations (Lim *et al.*, 2016). Wnt/β-catenin downstream, *Axin2*, is expressed in both developing incisors and early post-natal mouse incisors (Lohi *et al*., 2010). Wnt/β-catenin pathway is essential for incisor development where the loss of Wnt/β-catenin pathway function arrests tooth development at the bud stage while over-activation of Wnt/β-catenin pathway results in larger tooth buds and supernumerary tooth formation (Fujimori *et al*. 2010 ; Liu and Millar, 2010).

Since Wnt/β-catenin signaling contributes and regulates many different adult stem cell populations (Ling et al., 2009), and it has a crucial role in the mouse incisor development, it

can potentially control adult mouse incisor stem cells. Therefore, identifying Wnt-responsive cells in mouse incisors will help to initiate a full understating of its role.

Axin2, a Wnt target gene, is expressed in the odontoblasts and pulp cells at the incisor apex of the early post-natal mouse incisors (Lohi et al., 2010). Using the same Wnt-reporter mouse line showed that *Axin2* maintains its expression in the adult mouse incisor odontoblasts and TACs. However, MSCs and epithelial stem cells are not expressing *Axin2*, indicating that they do not have an active Wnt/β-catenin pathway. Another population of Wnt-responsive cells in the mouse incisor dental pulp was found proximal to the blood vessel in an anatomical area known for pericytes. Feng et al. (2011) showed that pericytes could act as MSCs and differentiate into odontoblasts in the injury scenario.

To study *Axin2*-expressing cell behaviour *in vivo*, genetic lineage tracing was done. In this study, the $Axin2^{CreERT2}$ transgenic mouse line was mated with $Rosa26R^{LacZ}$ reporter, where *Cre* is driven by *Axin2* expression. Labelled cells are not necessary to be *Axin2*-expressing cells because of the ability of the labelled cells to transcend the reporter gene to the daughter cells. Labelled cells start at the TAC zone and few odontoblasts. Then, labelled cells stream from the TAC zone to more pulp cell and odontoblasts along the tooth growth direction. Labelled cells showed no capability to renew themselves, and they vanished from the incisor apex as they moved distally toward the incisal end. Zhao *et al.* (2014) showed that because *Gli1* is expressed in the MSCs, 90% of the dental pulp was labelled after 28 days of *Gli1* lineage tracing. In this project, using the $Axin2^{CreERT2}$ $Rosa26R^{LacZ}$ mouse line showed the opposite outcome and all labelled cells vanished from the dental pulp cells after 28 days, which confirmed that MSCs are not Wnt-responsive cells.

3.3.2. Wnt ligands are expressed in adult mouse incisor pulp

Wnt ligands are lipid-modified secreted proteins, and 19 proteins have been identified. Among them, many activate either a canonical or non-canonical pathway, and some of them can activate both pathways (Miller, 2002). In the dental pulp, RT-qPCR data illustrated that several Wnt proteins are secreted and some of them have a high expression level such as Wnt-3a, Wnt-4, Wnt-5a, Wnt-5b, Wnt-6 and Wnt-10a.

3.3.2.1. Wnt-3a

Wnt-3a is a canonical Wnt activator (Nakaya et al., 2005; Nemoto et al., 2016). Wnt3a regulates many developmental processes, such as regulating the trunk organiser (Nakaya et al., 2005) and the segmentation process (Aulehla et al. 2003). It also has a role in the differentiation of the MSCs to both osteoblasts and cementoblasts (Nemeto et al., 2016). Nemoto et al. (2016) stated that *Wnt-3a* is expressed in the dental structures during tooth developmental stages and its expression is detected on the epithelial root sheet, odontoblasts and dental follicle tissues. In five-week-old mice, Wnt-3a expression is also detected on apical cellular cementum with no expression in the acellular cementum. Suomalainen and Thesleff (2010) showed that Wnt-3a expression in E18 developing incisor is in the pre-ameloblasts and ameloblasts with no expression in the dental mesenchyme. However, the results obtained from RT-qPCR data showed that it was highly expressed in the incisor pulp. Wnt-3a producing cell is not known due to the lack of *in situ* hybridisation results. However, since canonical Wnt signaling is active in the cervical area, that may suggest a location of *Wnt-3a* expression. Moreover, Wnt-3a function as being a regulator of differentiation would also recommend this location. So Wnt-3a could be a potential regulator of TACs differentiation to odontoblasts.

3.3.2.2. Wnt-4

Wnt-4 is a canonical and non-canonical Wnt activator (Park, Valerius and McMahon, 2007). Wnt-4 plays significant roles during different organ development, such as kidney (Stark et al., 1994), adrenal gland development (Heikkila et al., 2002), and thymus (Heinonen et al., 2011). Sarkar & Sharpe (1999) showed that *Wnt-4* is expressed in the dental mesenchyme during bud and cap stages with no expression at the enamel knot. Suomalainen and Thesleff (2010) stated that *Wnt-4* is the only Wnt ligand detected in the lingual cervical loop epithelium of the developing mouse incisor. It is also expressed in the outer enamel epithelium, ameloblasts and dental papilla mesenchyme. *Wnt-4* is expressed in the epithelial tissue during development, and its role is to stimulate the expression of the Msx1 in the mesenchymal tissue (Kettunen et al. 2005) which is one of the genes required for tooth development (Jernvall and Thesleff, 2000; Hardcastle et al., 1998). In the adult mouse dental mesenchyme, results obtained from RT qPCR data showed that it was highly expressed in the dental pulp. Results of immunohistochemistry staining for Wnt-4 showed that its expression is confined to the odontoblasts and the outer epithelium. Its role in the adult mouse incisor growth is not clear yet which needs further invisitgation.

3.3.2.3. Wnt-5a

Wnt-5a can activate both canonical, by binding to Frizzle4 and Lrp5 (Mikels and Nusse 2006) and non-canonical Wnt pathways by binding to the Ror receptor (Qian et al. 2007); yet, its primary activation mechanism is the non-canonical one (Qian et al., 2007; Roarty and Serra, 2007). *Wnt-5a* expression is controlled by Tgf-β (Roarty and Serra, 2007). Wnt-5a signaling regulates the expression of *Sox9*, the earliest marker for mesenchymal condensation, and *Ihh* (Yang *et al.*, 2003). Sarkar and Sharpe (1999) showed that *Wnt-5a* is expressed in the mandibular mesenchyme during the different tooth development stages. *Wnt-5a* expression then remains in the mesenchyme of the tooth with no expression in the epithelial tissue.

Suomalainen and Thesleff (2010) showed that *Wnt-5a* has a strong expression around the lingual cervical loop and a weaker expression around the labial cervical loop at E16-18. *Wnt-5a* is also expressed in the alveolar bone with little expression in ameloblasts, dental papilla and odontoblasts during the early post-natal tooth development (Xiang et al. 2014).

In vitro, Wnt-5a signaling is vital for maintaining both the unmineralised PDL, the mineralised cementum and alveolar bone (Xiang et al., 2014). It also inhibits and antagonises canonical Wnt pathway in the developing limbs (Yamaguchi et al., 1999; J Yang et al., 2015). Knocking out *Wnt-5a* has resulted in small and mispatterned tooth formation. *Wnt-5a* mutant mice tooth growth is retarded because of the defective odontoblast formation due to delayed differentiation and reduced TAC proliferation (Lin et al. 2011). *Wnt-5a* null embryos have healthy tooth development until the cap stage. Beyond the cap stage, the delayed development of tooth bud leads to smaller tooth and abnormal morphology. The impaired tooth size occurs because of decreased cell proliferation and excessive apoptosis. The mutant molars have abnormal blunted cusps and missing lingual and distal cusps (Lin et al. 2011). Results obtained from RT-qPCR data showed that *Wnt-5a* was expressed in the dental pulp. Based on its role during development and bone calcification, Wnt-5a could have an antagonising role for the Wnt/β-catenin pathway in the adult mouse incisors to regulate both TACs proliferation and odontoblast functions.

3.3.2.4. Wnt-6

Wnt-6 is a non-canonical Wnt activator and signals through the JNK pathway (Li et al. 2014). *Wnt-6* is expressed in the developing mouse tooth bud. *Wnt-6* expression can be seen throughout the bud epithelium with stronger expression in the buccal side of the molar tooth bud. At the cap stage, *Wnt-6* is expressed in the enamel knots, and internal and external enamel epithelium (Sarkar and Sharpe, 1999). At E18, *Wnt-6* is expressed in the lingual epithelial cervical loop, odontoblasts, and ameloblasts (Suomalainen and Thesleff, 2010).

The results obtained from RT-qPCR data showed that *Wnt-6* is expressed in the dental pulp. Li et al. (2014) showed that Wnt-6 has a role in controlling the behaviour of human dental pulp cells by controlling odontoblast development and differentiation *in vitro*. It enhances the expression of different genes which are responsible for dentine mineralisation such as *Runx-2, Dspp* and *DMP-1*. Thus Wnt-6 could potentially regulate dentine secretion during homeostasis and enhances incisor repair.

3.3.2.5. Wnt-10a

Wnt-10a signals through the canonical Wnt pathway. Wnt-10a signaling is essential for tooth development. It is expressed in the developing teeth primary and secondary enamel knots (Dassule and McMahon, 1998). *Wnt-10a* is also expressed in the secretory odontoblasts and differentiating odontoblasts around the epithelial root sheet (Yang et al., 2015; Yamashiro et al., 2007). Once odontoblasts form, *Wnt-10a* expresses in the differentiating odontoblasts and keeps its expression after that postnatally (Liu, Han, Wang, and Feng, 2013). *Wnt-10a* loss of function mutation leads to tooth agenesis (Jie Yang et al. 2015). Human *WNT-10A* mutation is associated with several abnormalities such as ectodermal dysplasia (Adaimy et al. 2007) and oligodontia (Plaisancie et al., 2013). Moreover, *Wnt-10a* null mice develop supernumerary small distal molars, and their incisors have an abnormal cervical area with irregularly shaped dentine that has V-shape defects in the lingual side (Yang et al., 2015).

Yamashiro et al. (2007) stated that *Wnt-10a* RNA is detected at many levels of odontoblast maturation, including differentiating, pre-odontoblasts and active odontoblasts. The results obtained from RT-qPCR data showed that *Wnt-10a* is highly expressed in the incisor dental pulp. However, the immunofluorescent histochemistry staining for Wnt-10a showed that Wnt-10a is only detected in the mature odontoblast. Liu et al. (2013) and Yamashiro et al. (2007) stated that Wnt-10a controls odontogenesis *in vitro* by regulating *Dspp* level and deletion of Wnt-10a in the re-associated teeth germ leads to the formation of cysts, bony structure and

inhibits the dental mesenchymal stem cell proliferation. Although this is *in vitro* data, Wnt-10a can potentially controls dentine secretion by regulating *Dspp* expression *in vivo*.

3.4. Conclusion

To identify Wnt-responsive cells in mouse incisors, the Axin2 reporter mouse line (*Axin2* $^{lacZ/+}$) and Axin2 lineage tracing (*Axin2*^{CreERT2}*; Rosa26R* ^{lacZ}) were used and showed that Wnt/β-catenin is active in only TACs and odontoblasts. Epithelial stem cells and mesenchymal stem cells at the cervical end of the tooth have not directly responded to Wnt/β-catenin signaling.

The results obtained from RT-qPCR data and immunofluorescent staining showed that Wnt ligands are expressed in the dental pulp, and some of them showed high expressions such as *Wnt-4, Wnt-6* and *Wnt-10a*. Based on the fact that canonical and non-canonical Wnt ligands were expressed in the dental pulp, both Wnt pathways are active in the mouse incisors pulp.

Results

Chapter 4. Role of Wnt signaling in adult mouse incisors

4.1. Introduction

Wnt ligands modification is essential for their secretion. After Wnt translation, it becomes modified in the endoplasmic reticulum (ER) by Porcupine, which facilitates lipid modification (Tanaka *et al.,* 2000; *Coombs et al.,* 2010). Lipid-modified Wnts are then modified by adding palmitate groups to their N-terminus (Takada *et al.,* 2006) and N- terminal glycosylation (Tanaka *et al.,* 2002). Loss of function mutation of Porcupine leads to the accumulation of Wnt protein in the producing cell, suggesting the importance of lipid modifications for Wnt secretion (van den Heuvel et al., 1993).

Wntless/Evenness/Gpr177 (Wls) which was discovered in 2006 as an evolutionarily conserved trans-membrane protein is responsible for Wnt ligand secretion (Banziger *et al*., 2006). Different studies demonstrated that deletion and mutation of *Wntless* give rise to Wnt loss-of-function phenotypes (Carpenter *et al.*, 2010; Yang et al., 2008), and illustrated the importance of Wntless for Wnt ligand secretion (MacDonald *et al.,* 2009).

Yu *et al.* (2010) showed that Wntless contains a long N-terminal region, either seven or eight transmembrane segments and an intracellular C-terminus, and the researcher proposed that it is a putative G-protein coupled receptor. Other studies have investigated the interaction between Wntless and retomers which controls Wntless movement inside the secreting cells from Golgi to the membrane and vice versa (Harterink *et al.*, 2011).

Wntless can be found in different locations within the cell, in particular, ER, Golgi, vesicles and cell plasma membrane (Banziger *et al.*, 2006; Fu *et al.*, 2009), which covers the Wnt secretion pathway. It binds to the modified Wnt palmitate end via its lipocalin-like structure (Fu *et al.*, 2009). All Wnt proteins need lipid modification to be secreted except for *Drosophila* WntD because it does not require lipid modification (Gasnereau *et al*., 201)1 (Figure 4.1)

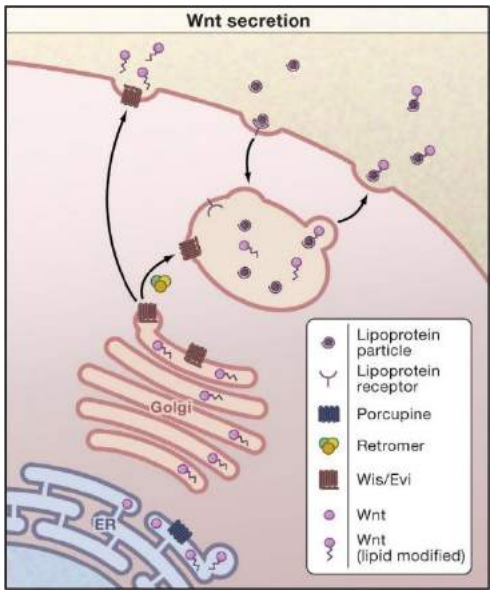

Figure 4.1. Wnt ligand synthesis and secretion

After Wnt ligand translation, it becomes modified in the endoplasmic reticulum by Porcupine. The modifed Wnt ligand then attached to Wls which facilitate its secretion (Clevers, 2006).

Wntless knockout consequences were shown in two different studies by using different gene target strategies. Carpenter et al. (2010) revealed that *Wntless* knockout is lethal for the foetus where they can live until E8.5 while Fu et al. (2009) knockout model showed the foetus dies at E10.5. Embryos of both models lack primitive streak and mesoderm. Despite the fact that *Wls* knockout inhibits Wnt ligand secretion, Wnt ligands synthesis is not affected and Western blot showed the presence of Wnt ligands in the producing cells (Fu et al., 2009). Loss of Wls affects canonical Wnt/β-catenin signaling pathway and *Wls* null mice have no active β-catenin in the

Wnt responsive cells (Fu et al., 2009). *Wls* depletion also affects the non-canonical Wnt pathway that controls epithelial cell polarity and epithelial to mesenchymal cell transition (Barrott *et al.*, 2011; Stefater *et al.*, 2011). Thus, Wnt signaling could not be activated without the secreted Wnt protein and any mutation in the secretion process inhibits Wnt secretion and leads to ablation of Wnt pathways.

Since it has been known that mouse incisor TACs and odontoblasts are Wnt responsive cells, deletion of *Wntless* might affect their functions. In this Chapter, the results of manipulating the Wnt/β-catenin pathway was investigated by studying two models, upregulation and downregulation of Wnt pathway models.

4.2. Results

4.2.1. Upregulation of Wnt/β-catenin pathway effect in mouse incisors

Axin2 knockout upregulates Wnt/β-catenin signaling due to the disruption of the destruction complex that leads to β-catenin saturation on the cytoplasm and therefore, continuous active transcription of target genes. This leads to the premature fusion of the skull suture and increases tumour formation (Yu et al., 2005). *Axin2* knocked out mice have the same skull shape as the wild-type mice after birth, but while they grow up, skull sutures prematurely fused, leading to a smaller skull. Therefore, $Axin2^{lacZ/LacZ}$ mouse lines were used to study the effect of the upregulated Wnt in the mouse incisors (Yu et al., 2005).

4.2.1.1. RT-qPCR analysis

To study the effect of Wnt/β-catenin pathway upregulation, *Axin2*$^{lacZ/LacZ}$ mouse line was used.

RT-qPCR was done by using adult *Axin2*$^{lacZ/LacZ}$ (n=3) and compared to *Axin2*$^{lacZ/+}$ (n=3) mouse incisor pulp. Incisor pulp tissue was dissected, and RNA was extracted as shown in the material and methods chapter. Three runs of triplicate cDNA were done.

The results obtained from RT-qPCR showed that knocking out *Axin2* upregulated the expression of Wnt/β-catenin pathway downstream. It showed that *β-catenin* has a significant high expression (P value <0.0001), and it has 272.2 (± 20.79) fold changes more than *Axin*$^{-lac/+Z}$. *Axin2*, a Wnt/β-catenin target and supressor, had no significant lower expression. *Dspp* expression was significantly increased (P value <0.0001). and showed 8.557 (± 0.67) more fold changes.

This experiment also investigated the upstream of the Wnt pathway, particularly *Wls*, which is responsible for Wnt ligand trafficking and secretion from the producing cells, and it showed that *Wls* expression was upregulated but with no significant difference.

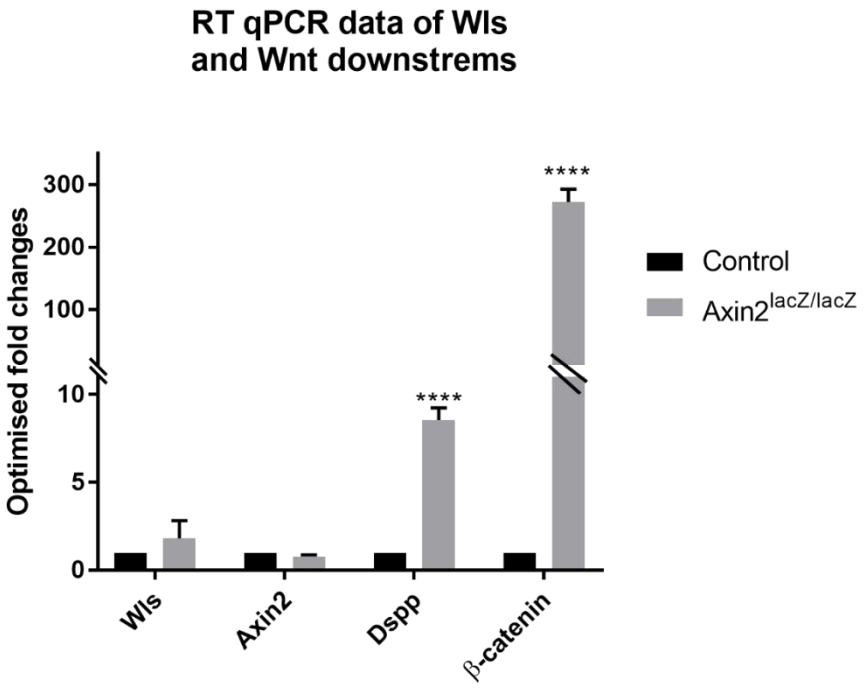

Figure 4.2. Wnt/β-catenin pathway up-regulation affect Wnt downstream expression level in mouse incisors.

RT-qPCR data analysis for *Axin2* $^{lacZ/lacZ}$ compared to wild type mouse incisor cDNA shows that Wnt downstream (β-catenin) has a significant high expression. Dspp which is a downstream of Wnt-10a signaling also has a significant high expression. Wnt upstream (Wls) has a higher expression with no significant different. However, Axin2, which is knocked-out, still exist, but it has a non-significant lower expression.
(Unit, fold changes relative to *Axin2* $^{lacZ/+}$ mouse incisor). ****$p<0.0001$.

4.2.1.2. µ CT scan analysis for *Axin2* $^{lacZ/lacZ}$ mouse incisors

To study *Axin2* knocked out mouse incisor phenotype, µ-CT scanning for the skulls was done on homozygous *Axin2-lacZ (Axin2* $^{lacZ/lacZ}$*)* (n=3) and compared to the heterozygous *(Axin2* $^{lacZ/+}$*)* (n=3) mouse skulls. Incisors of both mouse lines were normal without any tissue disruption. Enamel and dentine of both mouse line have normal appearance. (Figure 4.3 A-B). Incisor length was measured and showed that *Axin2*$^{lacZ/lacZ}$ incisor length was 11.1 mm (± 0.05774), while it was 11.2 mm (± 0.02028) for *Axin2* $^{lacZ/+}$ mouse incisors. Unpaired t-test analysis showed no significant different in the incisors length. (Figure 4.3 C)

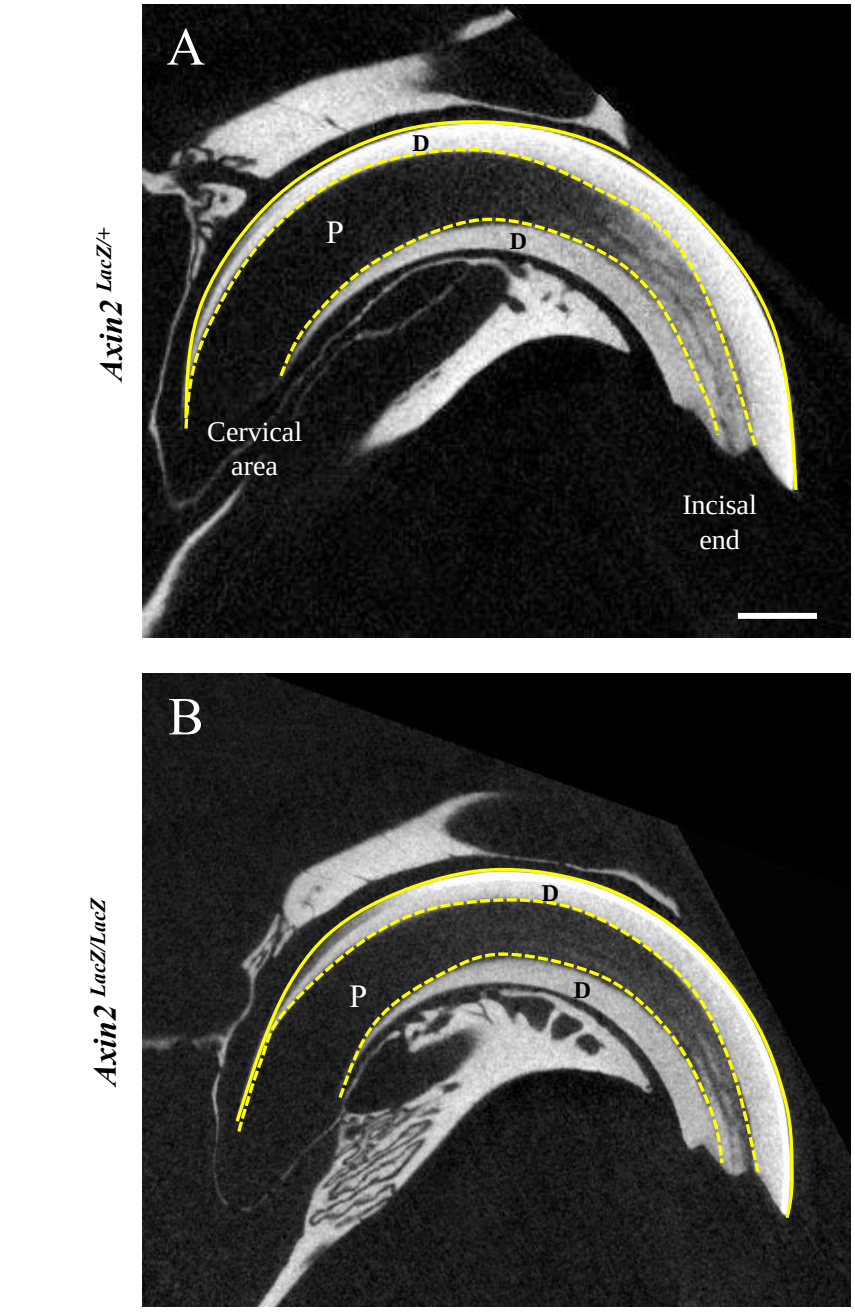

Figure 4.3. Wnt/β-catenin pathway upregulation has no impact in incisor shape and dimensions.

(A-B) µ-Ct scan of *Axin2* $^{LacZ/LacZ}$ mouse incisor (n=3) shows it is similar to *Axin2* $^{LacZ/+}$ mouse incisor (n=3). No apparent abnormalities can be detected in the scan.
(C) Unpaired t-test for incisor length measurement (yellow line covering the labial curvature of the tooth) for both *Axin2* $^{LacZ/+}$ and *Axin2* $^{LacZ/LacZ}$ shows no significant different (n=3)

(D) dentine, (P) pulp. Scale bar= 1000 µm.

4.2.1.3. X-gal staining for *Axin2*$^{lacZ/lacZ}$ mouse incisor

4.2.1.3.1. Whole mount X-gal staining

To study the effect of Wnt/β-catenin pathway upregulation on the mouse dental tissue, X-gal staining was done for both *Axin2* $^{LacZ/+}$ and *Axin2*$^{lacZ/lacZ}$ incisors. To describe the outcome of the whole-mount X-gal staining, incisor data can be divided into cervical and incisal halves. Both mouse lines had no staining in the incisal half. However, *Axin2*$^{lacZ/lacZ}$ showed deeper staining in the cervical half that extends more distally toward the incisal end than the control *(Axin2* $^{lacZ/+}$*)* (Figure 4.4).

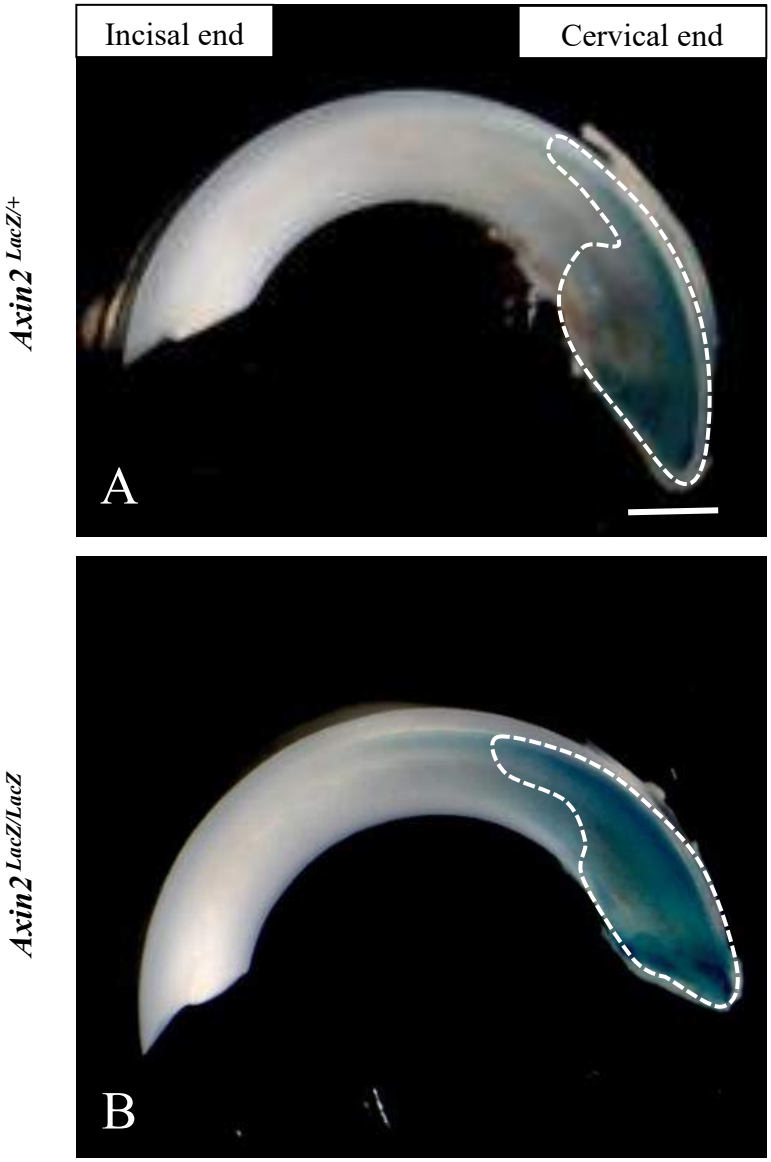

Figure 4.4. Wnt/β-catenin pathway upregulation does not affect Axin2 expression in mouse Incisor.

(A-B) Whole-mount X-gal staining for *Axin2*$^{LacZ/+}$ mouse incisor (Control) shows positive staining at the cervical end of the tooth (dotted area) which is similar to *Axin2*$^{LacZ/LacZ}$ mouse incisor. The expression is limited to the cervical area with no expression at the incisal end. Scale bar= 1000µm

4.2.1.3.2. Frozen section X-gal staining

Frozen section X-gal staining for adult *Axin2* $^{LacZ/LacZ}$ mouse incisors was done (n=4) to study *Axin2*-expression at the cellular level. X-gal staining showed no expression in the epithelial stem cells within the labial cervical loop. The area between the cervical loop, where the MSC niche is located, showed a small population of stained cells. Both mouse incisors showed positive staining distal to the cervical loop, namely the TAC zone, as well as odontoblasts and pulp cells at the cervical area. (Figure 4.5 A-B).

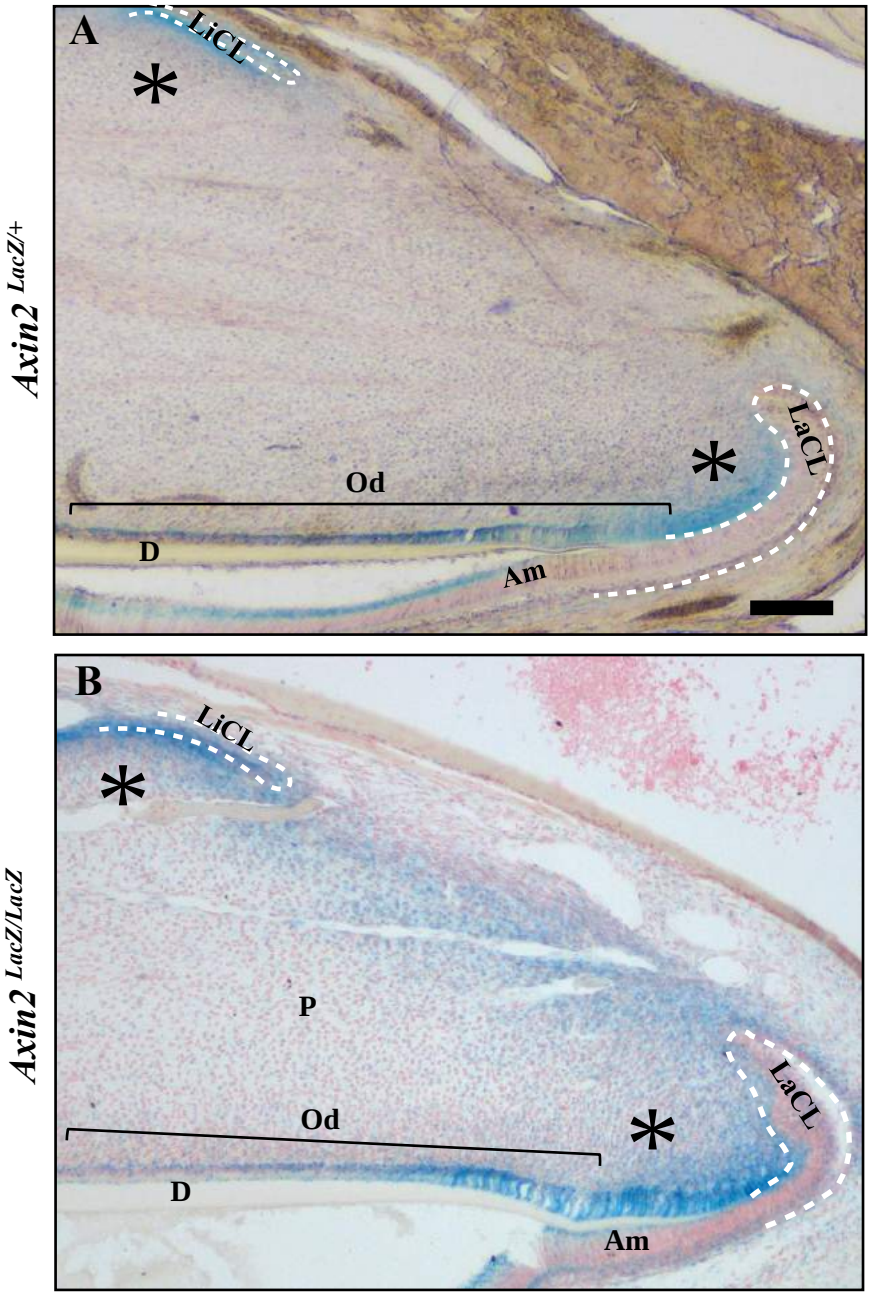

Figure 4.5. Axin2 knockout mouse incisor shows normal lacZ expression.
(A-B) Frozen sections X-gal staining (blue) for *Axin2* $^{LacZ/+}$ mouse incisor (Control) (n=3) shows positive staining at the TACs zone distal to the cervical loop (*) and odontoblasts. Upregulated Wnt/b-catenin activity in *Axin2* $^{LacZ/LacZ}$ mouse incisor (n=4) has no different expression and the staining is limited to the TACs zone (*) and odontoblasts.
(LaCL) Labial cervical loop, (LiCL) Lingual cervical loop, (D) Dentine, (P) Pulp, (Am) Ameloblasts, (Od) odontoblasts. Scale bar = 100 µm.

4.2.1.3.3. Growth rate of Wnt upregulated mouse incisors

This experiment was designed to study the effect of upregulated Wnt/β-catenin signaling on the incisor growth rate in two scenarios; homeostasis and injury.

Axin2 $^{LacZ/LacZ}$ mouse lower left incisor was clipped (n=3), an injury that enhances the incisor growth, and a notch was made in both lower incisors to compare the incisor growth rate. The control for this experiment was the *Axin2* $^{lacz/+}$ mouse incisor (n=3). In the homeostasis scenario where the incisor was not clipped, *Axin2*$^{lacZ/lacZ}$ mouse incisors grew 1.033 mm/day (± 0.04944), while t was 0.9 mm/day (± 0.05164) for *Axin2*$^{lacZ/+}$ incisors. Unpaired t-test analysis showed no significant difference (P value = 0.0918). Moreover, clipped incisors where growth is accelerated, *Axin2*$^{lacZ/lacZ}$ growth rate was 1.389 mm/day (± 0.03) and *Axin2*$^{lacZ/+}$ mouse incisor growth rate was 1.262 mm/day (± 0.03643). Unpaired t-test analysis showed a significant different (P value = 0.0336) (Figure 4.6).

A

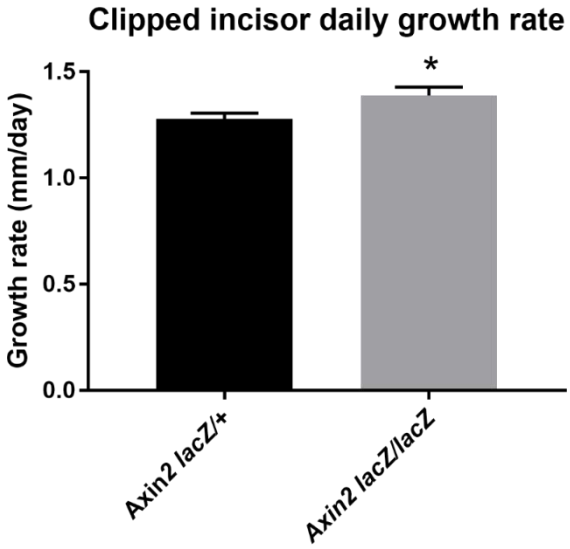

B

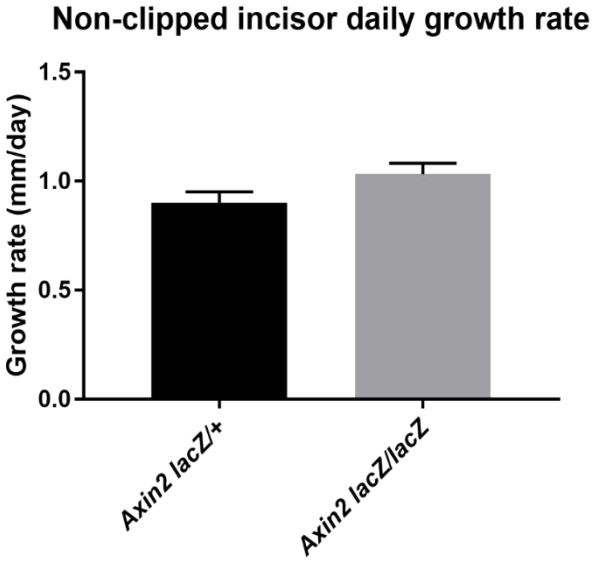

Figure 4.6. Incisor growth rate of *Axin2* $^{lacZ/lacZ}$ mouse line.

(A) *Axin2*$^{lacZ/+}$ mouse incisor (n=3) growth rate for the clipped incisor is 1.278 mm/day (± 0.03643), and for *Axin2*$^{lacZ/lacZ}$ *lacZ* incisor (n=3*)* is 1.389 /day mm (± 0.03). Unpaired t-test analysis showed a significant different.

(B) Incisor average daily growth for non-clipped mouse incisors shows that *Axin2* $^{LacZ/+}$ incisor (n=3) grows 0.9 mm/day (± 0.05164) while *Axin2*$^{lacZ/lacZ}$ incisor (n=3) grows 1.033 mm/day (± 0.04944). Unpaired t-test analysis shows no significant different. (Unit is mm/day), *p<0.05.

4.2.2. Downregulation of Wnt signaling pathway caused by ablation of *Wntless* leads to permanent and severe incisor phenotype

Utilising the ubiquitous tamoxifen *Cre* inducible *pCagg* ^{CreERT2} mouse line which was crossed with *Wls* $^{fl/fl}$ transgenic mouse line to inhibit Wnt ligands secretion and deactivate Wnt pathway provided a helpful tool to understand the role of Wnt signaling *in vivo* (Carpenter et al., 2010). We showed that *pCagg* has a ubiquitous expression in the mouse incisors (An et al., 2018, Figure S5).

This transgenic mouse line was given 3 intraperitoneal injection of either tamoxifen or corn oil in 3 consecutive days and then collected after 3, 6, 12 weeks. Since Cre-loxp recombination was not occurred in the corn oil treated mouse, it was considered as a negative control.

4.2.2.1. µ-CT scan analysis of *pCagg* ^{CreERT2}*; Wls* $^{fl/fl}$ mouse incisor

Mice were divided into three groups according to the collection time after the tamoxifen administration, into 3 (n=3), 6 (n=3) and 12 (n=3) weeks post-tamoxifen groups. The results were compared to corn oil-treated mice (n=3).

Incisors of the control group showed a thin layer of enamel on the labial side that covers the dentine, and the pulp space is in the middle of the incisor (Figure 4.7 A,A').

Three weeks post-tamoxifen treated *pCagg* ^{CreERT2}*; Wls* $^{fl/fl}$ mouse incisor (n=3) µ-CT scan analysis showed normal enamel and dentine with no abnormal or ectopic dentine formation at the labial side of the tooth. However, the lingual side showed defective dentine with irregular shape apex. Incisor pulp space is normal and as wide as the control group incisors (Figure 4.7 B). Incisor three-dimensional reconstruction shows the incisor abnormalities at the apico-lingual dentine with irregularities at the cervical end (Figure 4.7 B').

6 weeks post-tamoxifen treated mouse incisor (n=3) µ-CT scan data showed an accumulative disruption that more severe incisor phenotype formed. In the labial side, dentine was elongated cervically with bulky shape dentine at the cervical end. The lingual side showed more resorption and irregularities. The new finding at this time point is the formation of mineralised tissue islands inside the dental pulp space. Moreover, the pulp canal is thinner than the normal incisors because of the increased dentine thickness (Figure 4.7 C). Incisor three-dimensional reconstruction shows the abnormal phenotype of the incisor; disrupted lingual dentine, bulky labial dentine and the spherical-shape islands which are scattered in the middle of the incisor (Figure 4.7 C').

Abnormalities were increasing in severity wherein 12 weeks post-tamoxifen treated mouse incisors (n=3), µ-CT scan showed more disruption. The disrupted cervical end is full of hard tissue islands. The lingual side showed more defects affecting the half-length of the incisor. The labial side, which usually had no resorption, showed less dental structure due to dentine and enamel resorption and the pulp canal is very thin because of the thicker dentine (Figure 4.7 D). Incisor three-dimensional reconstruction showed the severe abnormal phenotype of the incisor. The labial and lingual cervical areas were disrupted with more lingual dentine resorption. The labial side also is disrupted with holes covering the enamel surface (Figure 4.7 D').

Furthermore, analysing the µ-CT scan images of *Wls* knockout mouse incisors showed significant shorter incisors. The disruption of the cervical area reduced the whole incisor length and as this disruption increases, incisor length decreases. The average incisor length of the control mouse (n=3) was 11.24 ± 0.02963 mm. 3 weeks post-treatment *pCagg* ^{CreERT2}*; Wls* $^{fl/fl}$ mouse incisor (n=3) length was 10.17 ± 0.06667 mm which is significantly shorter ($P < 0.001$). 6 weeks post-tamoxifen treated *pCagg* ^{CreERT2}*; Wls* $^{fl/fl}$ mouse incisor (n=3) length 8.867 ± 0.08819 mm which is significantly shorter ($P < 0.0001$). 12 weeks post-treatment *pCagg*

^{CreERT2}; Wls $^{fl/fl}$ mouse incisor (n=3) length was 8.3 ± 0.1mm which is significantly shorter (P <0.0001) (Figure 4.7 E).

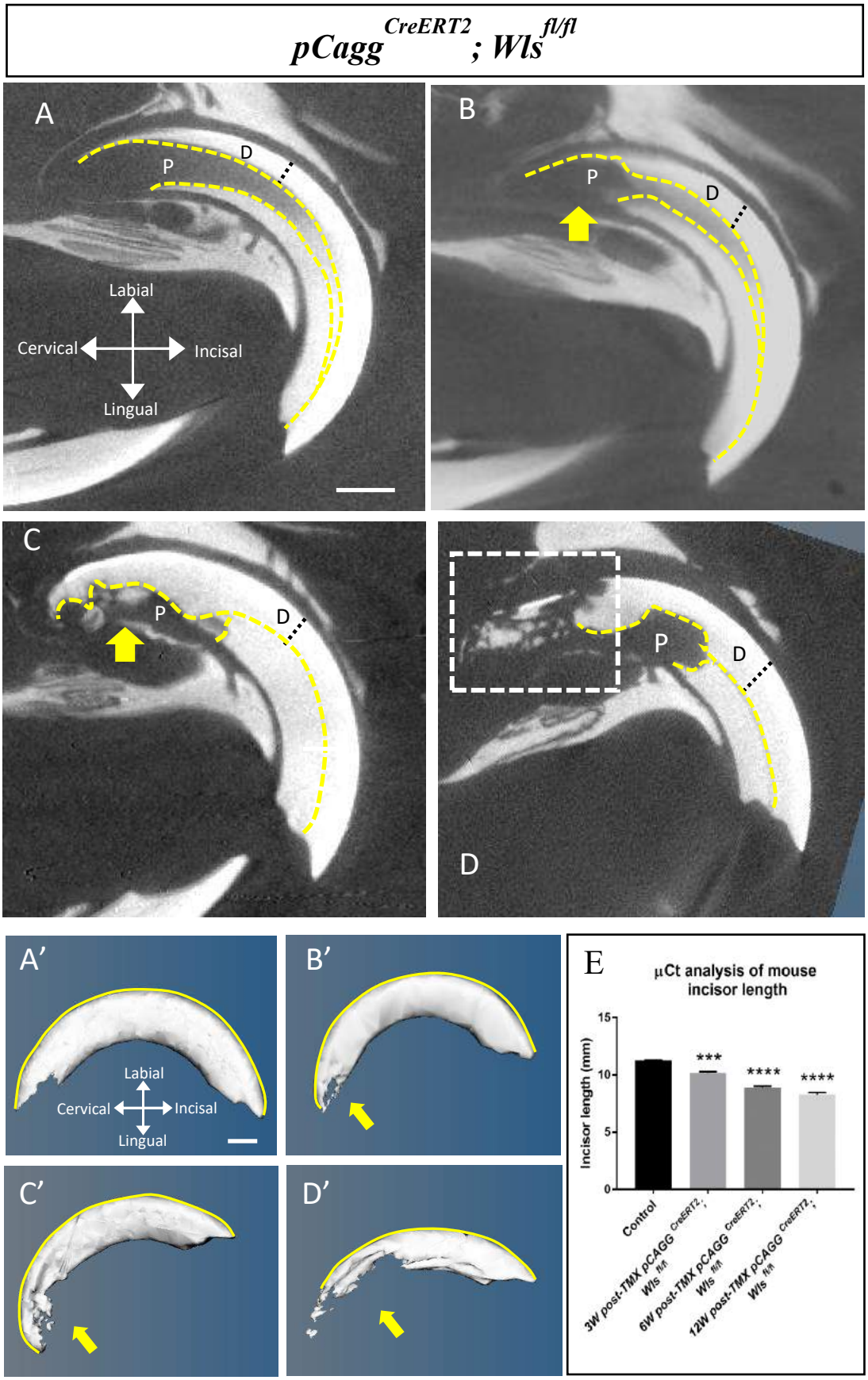
pCagg CreERT2 ; Wls fl/fl
A
P
D
Labial
Cervical
Incisal
Lingual
B
P
D
C
P
D
D
P
D
A'
Labial
Cervical
Incisal
Lingual
B'
C'
D'
E
µCt analysis of mouse incisor length
Incisor length (mm)
15
10
5
0
***
****
****
Control
3W post-TMX pCAGG CreERT2; Wls fl/fl
6W post-TMX pCAGG CreERT2; Wls fl/fl
12W post-TMX pCAGG CreERT2; Wls fl/fl

Figure 4.7. Depletion of Wnt signaling leads to abnormal incisor phenotype formation.

(A-D) µ-Ct scan analysis of *pCagg*$^{CreERT2/+}$; *Wls*$^{fl/fl}$ mouse incisors shows that, (A) corn oil treated mouse incisor (n=3) has a normal shape, dentin layer covers the dental pulp space with no irregularities or abnormalities. (B) 3 weeks post-tamoxifen treated mouse incisor (n=3) has abnormal phenotype where the lingual part of the dentine is lost (yellow arrow). (C) 6 weeks post-tamoxifin treated mouse incisor (n=3) has a severe phenotype that has cervical area disruption (yellow arrow), increased dentine thickness that block the pulp canal and also formation of spherical-shape hard tissue inside the pulp space. (D) 12 weeks post-tamoxifin treated mouse incisor (n=3) shows the severe abnormal incisor phenotype where the cervical area disruption affects most of the cervical half of the tooth (dotted rectangle).

(A'-D') 3-dimensional reconstruction of µ-Ct scan shows (A') Corn oil treated mouse incisor normal shape. (B') 3 weeks post-tamoxifen treated mouse incisor have irregular shape apex. (C') 6 weeks post-tamoxifen treated mouse incisor has severe disrupted cervical area and abnormal spherical-shape structures. (D') 12 weeks post-tamoxifen mouse incisor has lost most of the cervical area with severe cervical area disruption

(E) Statistical analysis of mouse incisor length was done by measuring the outside curvature of the tooth (yellow line) and shows that, mouse incisor length was affected because of the cervical area disruption. Depletion of Wnt signaling significantly reduces mouse incisor length (n=3).

(D) dentine, (P) pulp. Scale bar = 1000 µm. ***p<0.0001, ****p<0.00001

4.2.2.1.1. Wnt loss of function mouse skull bone shows area of defective bone

Mutant skull µ-CT scan three-dimensional reconstruction for the mandibles of the tamoxifen treated *pCagg* ^{CreERT2}; *Wls* $^{fl/fl}$ transgenic mouse line compared to corn oil treated ones showed significant bone loss. Looking at the lingual side of the mandible of the control group, a bone

plate covers the incisor with no irregularities. The first mutated group which was treated with 3 tamoxifen injections and collected three weeks after that (n=3), had almost normal mandibular bone; however, a small hole was formed next to the incisor. The second group which has been collected six weeks after tamoxifen treatment (n=3) shows more severe bone defect in two areas, alveolar bone defect exposing the molar roots, and large irregular holes at the lingual plate exposing the underneath incisor. With time, 12 weeks post-tamoxifen treated group (n=3) showed that severity was increased, and more bone loss was detected that affect the alveolar bone and exposed the molar roots (Figure 4.8).

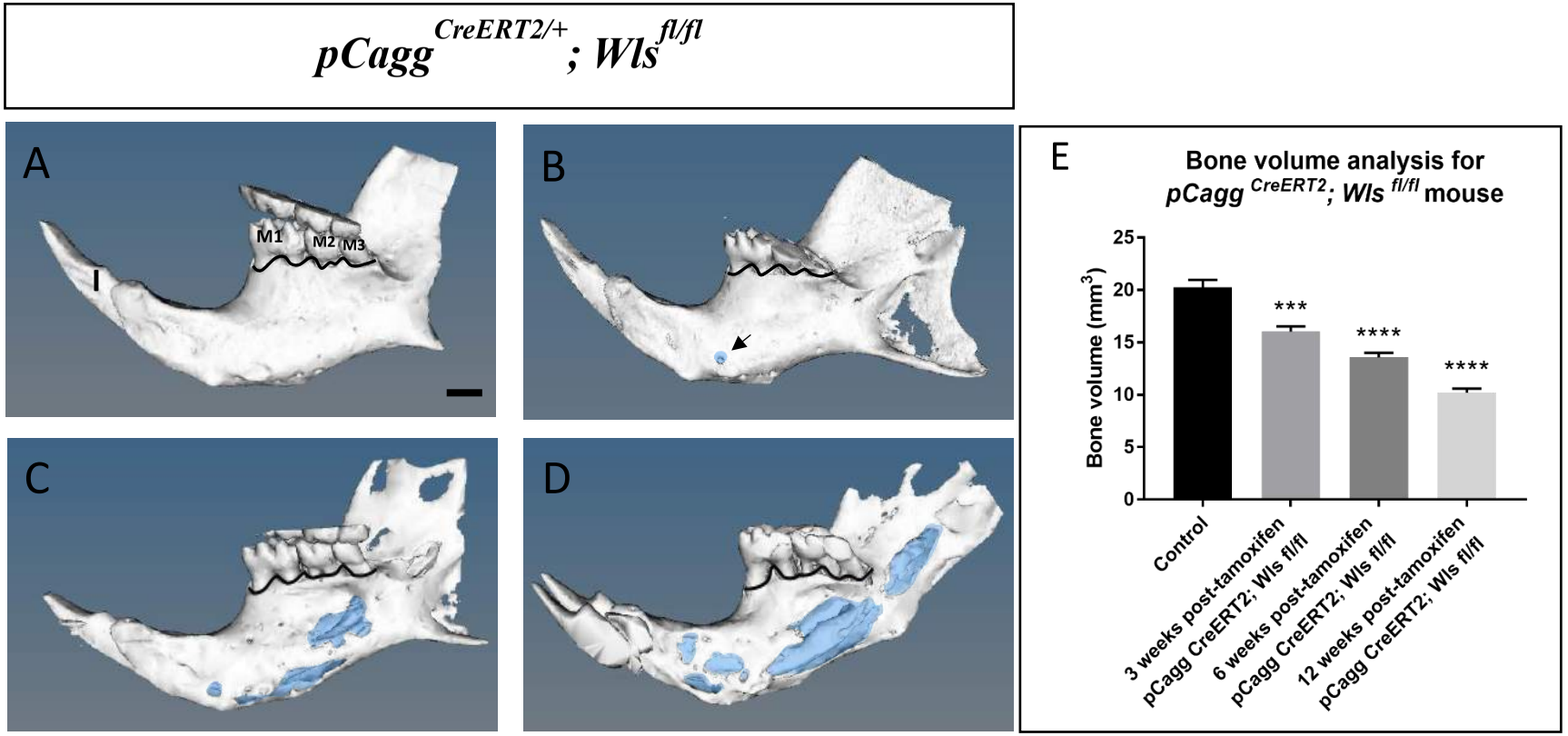

Figure 4.8. 3D reconstruction of Micro-Ct scan of *pCagg*$^{CreERT2/+}$; *Wls*$^{fl/fl}$ mouse mandible, (A) Corn oil treated mouse mandible shows the normal structure of the mandible. (B) 3 weeks post-tamoxifen treatment mouse mandible has a small area of bone loss (arrow). (C) 6 weeks post tamoxifen treated mouse mandible has a huge amount of bone loss (Blue area) and alveolar bone loss (black line) that exposes molar roots. (D) 12 weeks post tamoxifen treatment mouse mandible shows more bone loss (Blue area) which exposes the underneath incisor and alveolar bone at the posterior area has a defect (Black line) that exposes molar roots. (E) Bone volume analysis showed that depletion of Wnt signaling significantly reduced bone volume. This data represents bone volume of a hemi-sectioned mandible analysis. (Unit mm^3) (n=3 for each mouse line)

(M1) first moalr, (M2) second molar, (M3) third molar. (I) incisor. Scale bar = 1000 µm. ***p<0.001, ****p<0.0001

4.2.2.2. Histology analysis of *pCagg ^{CreERT2}; Wls $^{fl/fl}$* mouse incisor

Mouse incisors histology consists of epithelial tissue and ameloblast lining the enamel, odontoblasts lining the dentine and finally the dental pulp. The epithelial tissue formed a loop at the cervical area known as a cervical loop.

To investigate the role of Wnt signaling in the continuously growing mouse incisor, a histological analysis was done for *pCagg ^{CreERT2}; Wls $^{fl/fl}$* transgenic mouse incisors. The conditional deletion of *Wls* was carried out on adult mice by injecting 3 doses of tamoxifen or corn oil intra-peritoneally and mice were sacrificed after 3 (n=3), 6 (n=3), and 12 (n=3) weeks. Compared to the corn oil-treated mice incisors which have shown the normal incisor histology and dentine thickness of 86 ± 5.292 μm (Figure 4.9 A), the histology analysis of the *Wls* knockout mouse incisors have an abnormal phenotype that is mainly characterised by cervical area disruption and increased dentine thickness.

3 weeks post-tamoxifen treated *pCagg ^{CreERT2}; Wls $^{fl/fl}$* mouse incisors (n=6) showed that the labial cervical loop was smaller and squashed because of the ectopic elongated dentine while the lingual cervical loop was disappeared because of the resorption and disruption of the lingual dentine. Enamel which is only at the labial side of the tooth had normal shape with no irregularities or resorption. Dentine thickness at the labial side was 272 ± 17.04 μm which showed significant increase compared to the control group (P=0.0005). Odontoblasts vanished at the lingual disrupted cervical area, and pulp space looks wider in the cervical area because of the lingual dentine resorption that gives more room for the pulp tissue (Figure 4.9 B).

6 weeks post-tamoxifen-treated *pCagg ^{CreERT2}; Wls $^{fl/fl}$* mouse incisors (n=6) showed more disruption at the cervical area. The cervical loop area, compared with the previous group, showed an abnormal smaller labial cervical loop because of the thicker ectopic dentine formation at the distal side of the loop. The lingual cervical loop was disappeared. Dentine thickness at the labial side was 442.3 ± 39.73 μm which is significantly thicker than the control

(p=0.0009). The lingual side dentine showed more resorption that reaches the middle of the tooth. The dental pulp space showed abnormal odontoblast orientation. It also showed a formation of isolated dentine island in the middle of the tooth. The pulp space in the cervical area is wider due to the loss of the lingual dentine wall, but it is thinner and obstructed distal to the cervical area (Figure 4.9 C).

12 weeks post-tamoxifen-treated *pCagg* ^{CreERT2}*; Wls* $^{fl/fl}$ mouse incisors (n=6) have highly disrupted cervical area. Mouse incisor abnormal phenotypes at this time point exhibited more severe phenotypes compared to the previous groups. The cervical area showed no more epithelial cervical loop either labially or lingually. In the labial side, the epithelial layer as well as the ameloblasts were interrupted and the enamel layer was resorbed at the cervical area. Odontoblasts vanished both labially and lingually and remnants of dentine can be seen scattered randomly in the pulp space, and less dentine can be seen distal to this area, leading to a very severe cervical area disruption that changed the appearance of the tooth (Figure 4.9 D).

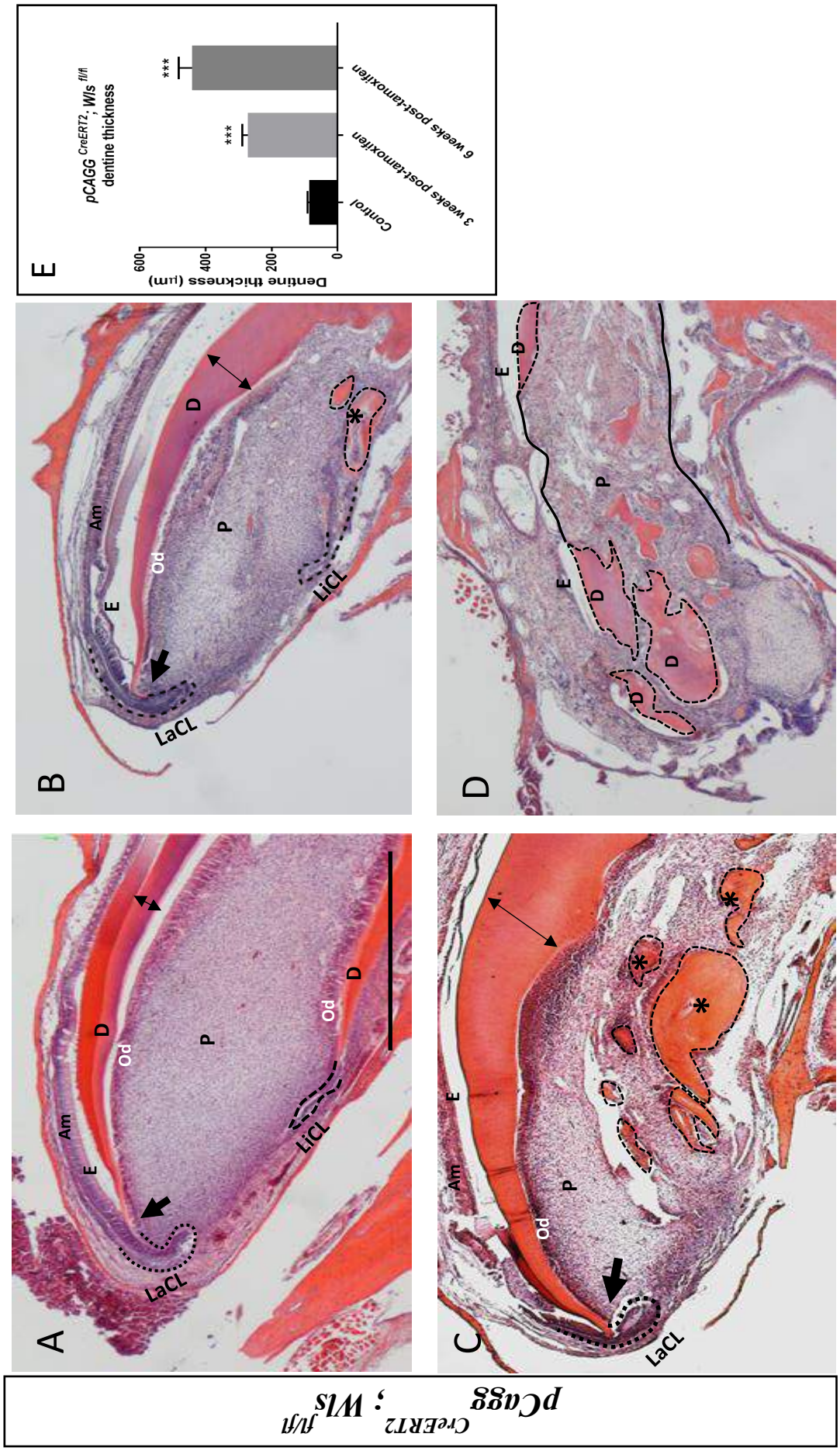
pCagg CreERT2 ; Wls fl/fl
A
B
C
D
E
LaCL
LiCL
Od
P
D
E
Am
pCAGG CreERT2; Wls fl/fl
dentine thickness
Dentine thickness (µm)
600
400
200
0
Control
3 weeks post-tamoxifen
6 weeks post-tamoxifen
***
***

Figure 4.9. Deletion of Wnt signaling causes cervical area disruption and increases dentine thickness

(A-D) H&E staining for *pCagg*$^{CreERT2/+}$; *Wls*$^{fl/fl}$ mouse incisors. (A) Corn-oil treated mouse incisor (n=6) shows no abnormalities at the cervical area. The cervical loop is intact and both enamel and dentin are not interrupted. (B) 3 weeks post-tamoxifen treated mouse incisor (n=6) has an abnormal phenotype with increased dentine thickness (black double heads arrow) and cervical area disruption with dentine resorption distal to the lingual cervical loop (black star). The labial cervical loop has abnormal shape because of the elongated dentine (black arrow). (C) 6 weeks post-tamoxifen treated mouse incisor (n=6) has a severe abnormal phenotype, dentine thickness is increased (black double headed arrow). The cervical area disruption and dentine resorption are both increased which leads to the formation of dentine island in the middle of the tooth (black stars). The labial cervical loop is smaller and mis-shaped because of the formation of dentine at the distal border of the cervical loop (black arrow). (D) 12 weeks post-tamoxifen treated mouse incisor (n=6) shows a highly disrupted cervical area that no cervical loop can be seen. The dentine island is scattered through the dental pulp.

(E) Quantification of dentine thickness shows dentine thickness is significantly increased for tamoxifen treated *pCAG*$^{CreERT2/+}$; *Wls*$^{fl/fl}$ mouse incisors

(LaCL) Labial cervical loop, (LiCL) Lingual cervical loop, (E) enamel space, (D) Dentine, (P) Pulp, (Am) Ameloblasts, (Od) odontoblasts. Scale bar = 1000 μm. ***p<0.0001

Furthermore, dentine was formed ectopically in 2 areas, dental pulp and distal to the labial cervical loop. 6 weeks post-tamoxifen treated *pCagg* ^{CreERT2}; *Wls* $^{fl/fl}$ mouse incisors (n=6) showed bulky dentine formation distal to the cervical loop which affect the labial cervical loop size and shape. The odontoblasts that occupy this area is mature and functional and they appear longer and disoriented. Distal to the cervical area, in particular in the dental pulp, dentine-like islands were formed (Figure 4.10).

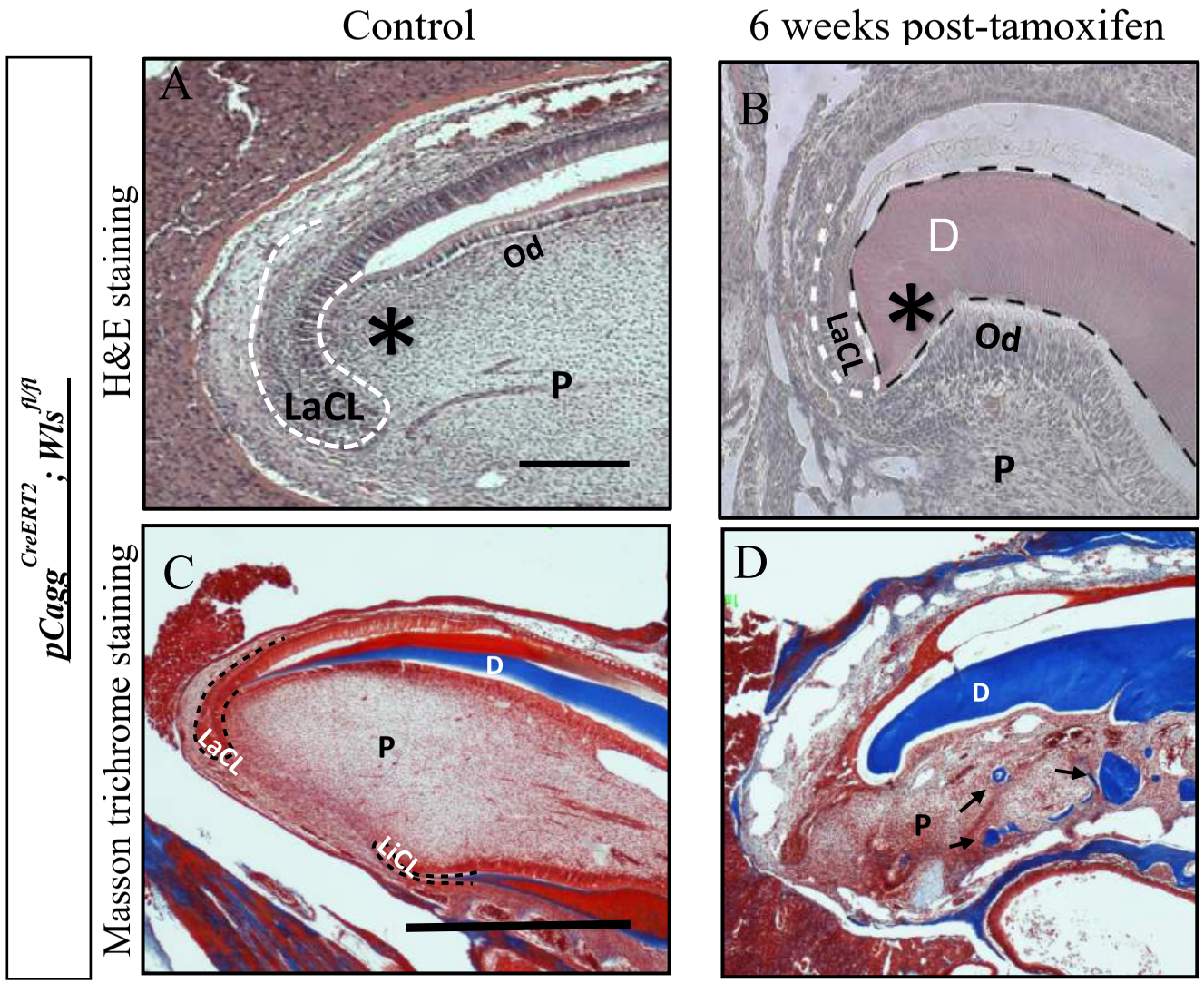

Figure 4.10. Deletion of Wnt signaling leads to ectopic dentine formation.

(A-B) H&E staining for 6 weeks post tamoxifen treated *pCagg*$^{CreERT2/+}$; *Wls*$^{fl/fl}$ mouse incisors (n=6) shows the formation of dentine at the distal border of the labial cervical loop. The odontoblasts at the area have an irregular shape and they are longer and condensed. This ectopic dentine affects the cervical loop shape and causes a smaller abnormal cervical loop.

(C-D) Masson trichrome staining for 6 weeks post tamoxifen treated *pCagg*$^{CreERT2/+}$; *Wls*$^{fl/fl}$ mouse incisors (n=6) shows the formation of the ectopic dentine at the middle of the dental pulp (arrows).

(LaCL) Labial cervical loop, (LiCL) Lingual cervical loop, (D) Dentine, (P) Pulp, , (Od) odontoblasts. Scale bar (A-B)= 100 µm, (C-D)= 1000 µm.

4.2.3. Analysis of gene expression in *Wls* knockout mouse incisor pulp

To study *Dspp* expression in the mouse incisors, in situ hybridisation for *pCagg* ^{CreERT2}*; Wls* $^{fl/fl}$ mouse incisors was performed. A total of 9 mice were used and divided equally to 2 mutants' groups (6 and 12 weeks post tamoxifen treated groups) and a control group (corn oil treated group). Three injections of either tamoxifen or corn oil were given intraperitoneally in 3 consecutive days and mice then were collected after 6 (n=3) and 12 (n=3) weeks.

Compared to the control corn oil-treated *pCagg* ^{CreERT2}*; Wls* $^{fl/fl}$ mouse incisors (n=3) where *Dspp* expression was limited to the odontoblasts and pre-ameloblasts (Figure 4.11 A), 6 weeks post-tamoxifen treated *pCagg* ^{CreERT2}*; Wls* $^{fl/fl}$ mouse incisor (n=3) showed upregulated and ectopic *Dspp* expression. Ectopic *Dspp* was expressed in the area surrounding the labial cervical loop, indicating active odontoblasts. The expression was also found surrounding the ectopic dentine islands in the dental pulp (Figure 4.11 B).

Surprisingly, 12 weeks post-tamoxifen treated *pCagg* ^{CreERT2}*; Wls* $^{fl/fl}$ mouse incisor (n=3) showed no *Dspp* expression in the dental pulp, indicating either odontoblasts were lost or odontoblast function was down-regulated (Figure 4.11 C).

To investigate gene expression changes upon *Wls* deletion, RT-qPCR analysis comparing corn oil and tamoxifen-treated adult *pCagg* ^{CreERT2}*; Wls* $^{fl/fl}$ mouse incisor dental pulp cells was performed. Adult *pCagg* ^{CreERT2}*; Wls* $^{fl/fl}$ mice were tamoxifen treated (n=3) and control mice were given corn oil (n=3) and collected after one week. 3 runs of triplicate cDNA were done.

Results obtained from RT-qPCR data analysis showed that *Wls* expression was 0.1462 (± 0.0786) fold changes which is significantly reduced (P value < 0.0001). Wnt/β-catenin pathway was significantly downregulated and *Axin2* expression was 0.7678 (± 0.06871) fold changes (p= 0.0038). However, *Dspp* expression was significantly increased (P value <0.0001) and showed 2.037 (± 0.1907) increased fold changes indicating upregulated odontoblast function (Figure 4.11 D).

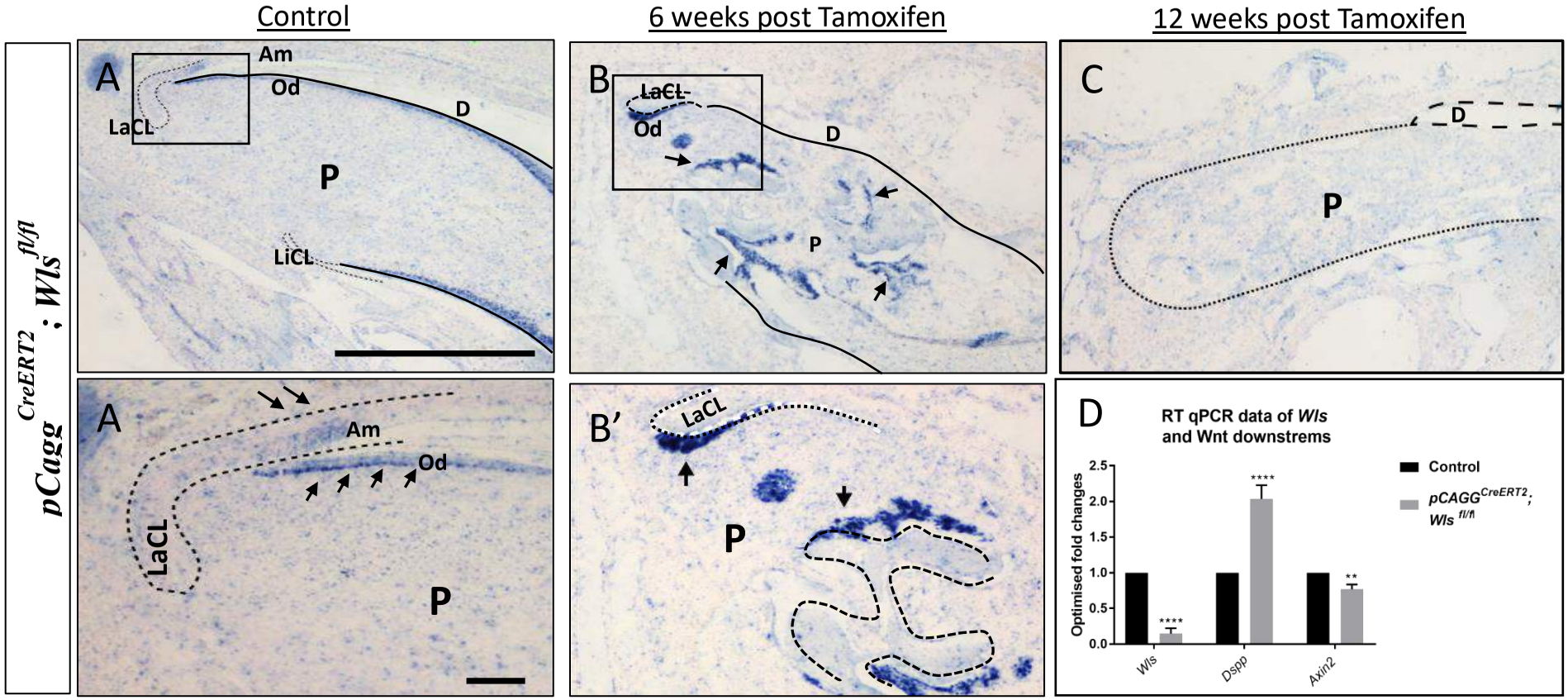

Figure 4.11. *Dspp* expression for *pCagg*$^{CreERT2/+}$; *Wls*$^{fl/fl}$ mouse incisor

(A-A') Corn oil treated adult mouse incisor (n=3) shows *Dspp* expression is limited to the odontoblasts and preameloblats (Black arrows). (B-B') 6 weeks post-tamoxifen mouse incisor (n=3) shows ectopic *Dspp* expression lining the distal border of the labial cervical loop and around the ectopic dentine islands in the dental pulp (Black arrows). (C) 12 weeks post-tamoxifen mouse incisors (n=3) show no *Dspp* expression. (D) RT-qPCR data analysis for1 week post-tamoxifen *pCagg*$^{CreERT2/+}$; *Wls*$^{fl/fl}$ mouse incisor (n=3) compared to corn oil treated mouse incisor cDNA (n=3) shows that Wnt downstream (*Axin2*) expression is significantly reduced. However, *Dspp*, which is a downstream of Wnt-10a signaling, has a significant high expression. *Wls*, which is knocked out, still exist, but its expression is significantly low. (LaCL) Labial cervical loop, (LiCL) Lingual cervical loop, (E) enamel space, (D) Dentine, (P) Pulp, (Am) Ameloblasts, (Od) odontoblasts. Scale bar (A-C) = 1000 µm. (A'-B')= 100 µm.

4.2.4. Wnt pathway deletion leads to dentine and enamel resorption.

4.2.4.1. Wnt pathway loss of function mutation leads to soft tissue invading enamel and dentine

To study mouse incisors dentine resorption of *pCagg ^{CreERT2}; Wls $^{fl/fl}$* mouse line, TRAP staining was performed. Tartrate-resistant acid phosphatase (TRAP) is expressed by osteoclasts, macrophages, dendritic cells (Hayman, 2008). Three injections of either tamoxifen or corn oil were given intraperitoneally in 3 consecutive days and mice then were collected after 3 (n=3), 6 (n=3) and 12 (n=3) weeks.

Compared to the corn oil-treated mice, which have no osteoclasts inside the dental pulp, results obtained from TRAP staining for *pCagg ^{CreERT2}; Wls $^{fl/fl}$* mice incisors showed that there were no osteoclasts in the dental pulp for the tamoxifen-treated mice incisor which was collected three and six weeks following tamoxifen treatment at the defective area in the cervical end of the tooth (Figure 4.12 A-B).

Soft tissue invasion was detected in the six weeks post-tamoxifen-treated *pCagg ^{CreERT2}; Wls$^{fl/fl}$* mouse incisors (n=6), starting from the outside to the inside of the incisor, and invading both enamel and dentine, yet, no osteoclasts were detected. However, the origin of the invading soft tissue is not clear yet. (Figure 4.12 C).

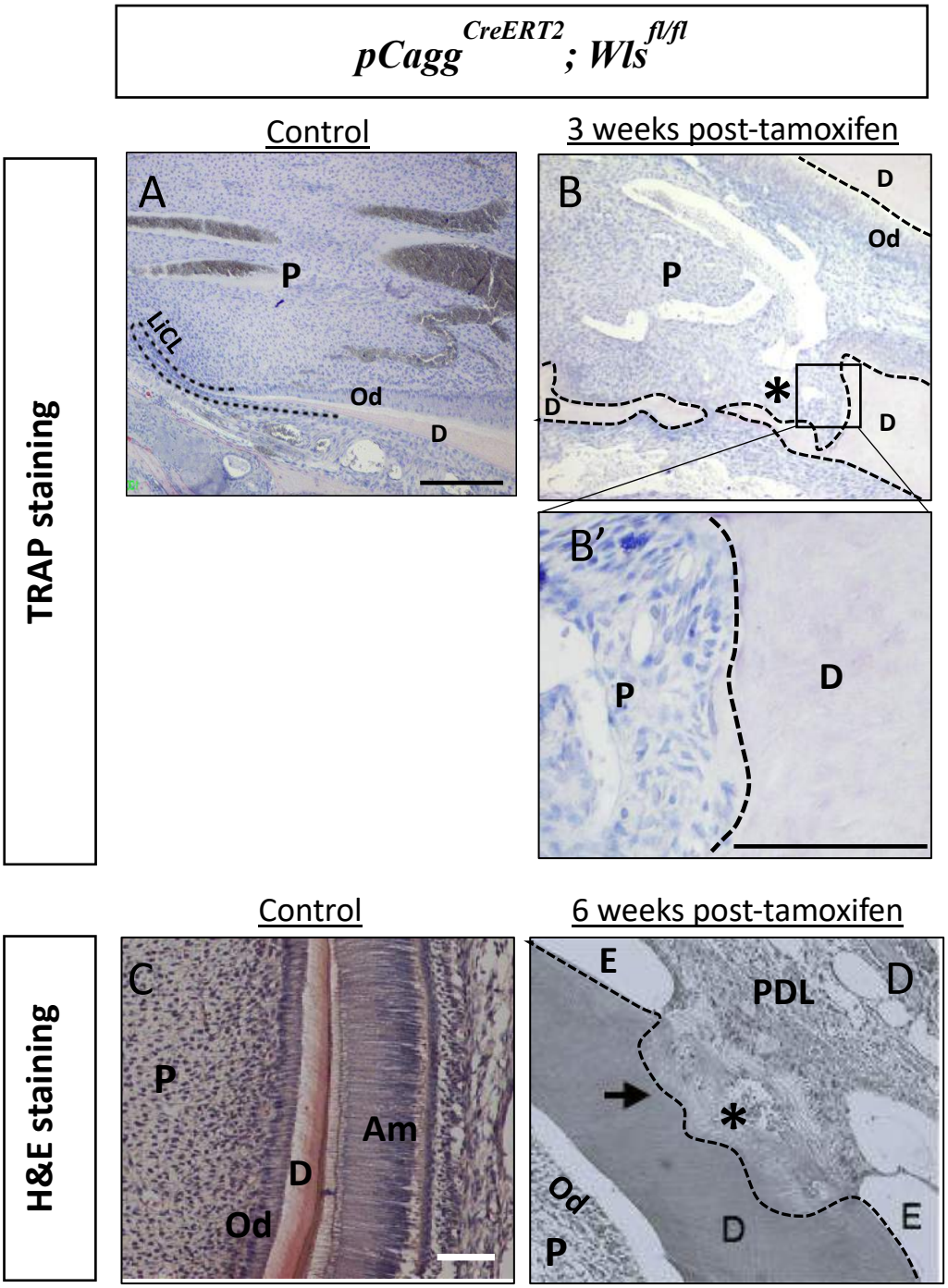

Figure 4.12. Loss of Wnt pathway function leads to dentine resorption and soft tissue invasion.

(A-B) TRAP staining for 3 weeks post-tamoxifen treatment *pCagg*$^{CreERT2/+}$; *Wls*$^{fl/fl}$ mouse incisor shows abnormal incisor phenotype with lingual area disruption and dentine thickening. However, no osteoclast could be seen in the dental pulp despite the dentine resorption. (B') No osteoclast can be seen to cause dentine resorption and the defective area is occupied by the dental pulp. (C-D) H&E staining for 6 weeks post-tamoxifen *pCagg*$^{CreERT2/+}$; *Wls*$^{fl/fl}$ mouse incisor shows soft tissue invasion from the labial side causing enamel and dentine resorption (arrow). The invasion is caused by PDL soft tissue (black star). (LiCL) Lingual cervical loop, (E) enamel space, (D) Dentine, (P) Pulp, (Od) odontoblasts, (PDL) periodontal ligaments. (n=6) Scale bar = 100 µm.

4.2.4.2. Wnt deletion leads to ectopic osteoclastic recruitment inside the dental pulp

Result obtained from 12 weeks tamoxifen-treated *pCagg CreERT2; Wls fl/fl* mouse incisors (n=6) TRAP staining showed that internal dentine resorption occurred because of the osteoclastic activity inside the dental pulp. In fact, osteoclasts were substituting the lost odontoblast and lined the residual dentine in the cervical area. Osteoclast count was 205.7 ± 15.3 and unpaired t-test showed that it has a significant different (P=0.0002) The source and the reason of this ectopic osteoclasts are not clear yet and need further investigation (Figure 4.13).

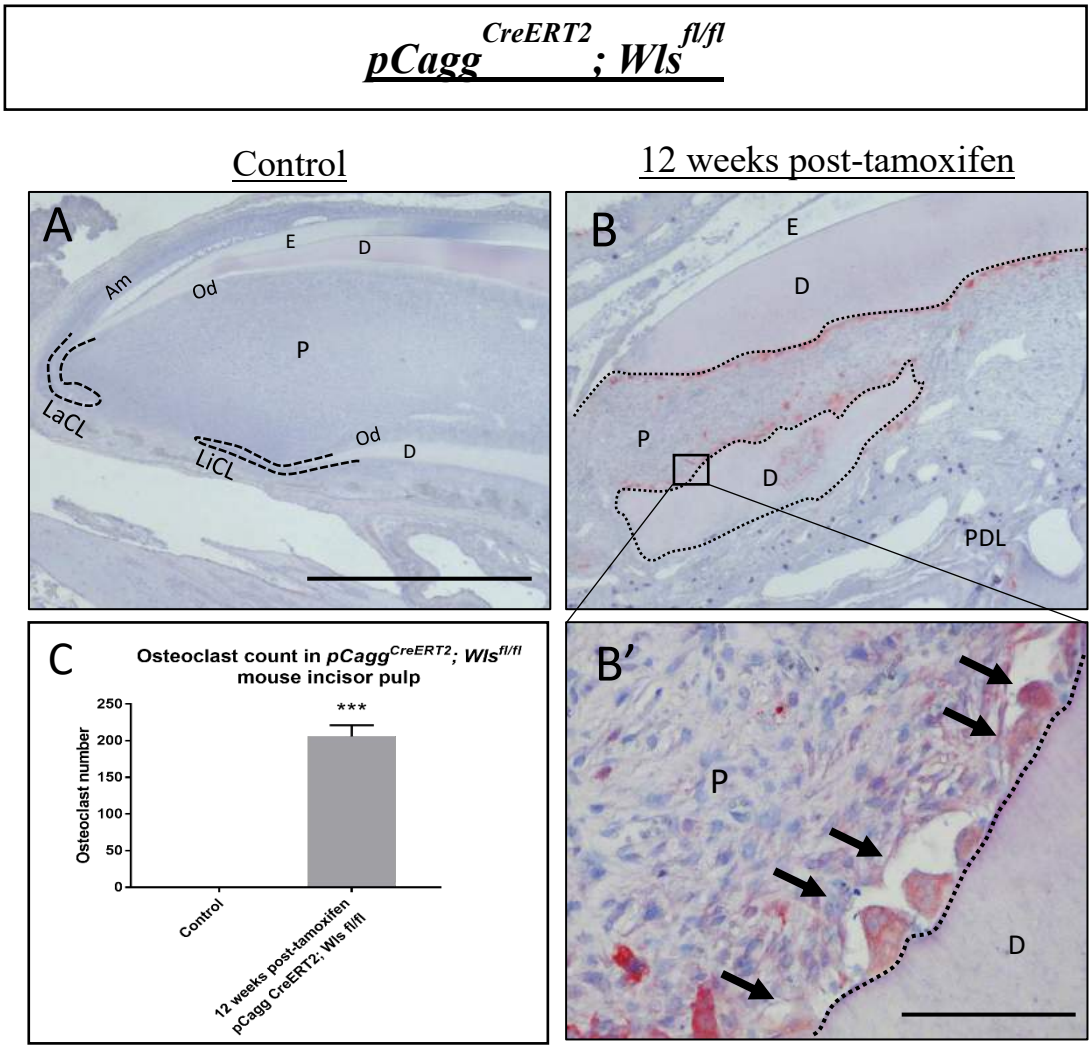

Figure 4.13. Loss of Wnt pathway function leads to osteoclast recruitment to the dental pulp. (A-B) TRAP staining for 12 weeks post-tamoxifen treatment *pCAG*$^{CreERT2/+}$*; Wls*$^{fl/fl}$ mouse incisor (n=6) shows dentine resorption by osteoclasts (multinucleated cells –black arrows in B') which occupy the odontoblasts region. (C) Osteoclast count showed a significant increase in osteoclast numbers inside the incisor pulp.

(LaCL) Labial cervical loop, (LiCL) Lingual cervical loop, (E) enamel space, (D) Dentine, (P) Pulp, (Am) Ameloblasts, (Od) odontoblasts, (PDL) periodontal ligaments. Scale bar, (A-B) = 1000 µm. (B') = 100 µm. ***p<0.001

4.2.5. Wnt is controlling TACs proliferation

Cells undergoing mitosis and divisions can be detected by many techniques, such as label retention assays by using nucleotide incorporation that confirms the presence of proliferative cells *in vivo*. BrdU (5-bromo-2'-deoxyuridine) is an analogue of thymidine which incorporates into the new DNA during the cell mitosis S phase and is subsequently diluted. The degree of dilution is dependent on the nature of cell divisions; slow cycling cells are label-retained cells that can retain their label after the assay is finished, while fast cycling cells dilute the label rapidly. Harada et al. (1999) demonstrated the presence of label-retaining cells in the labial cervical loop and identified the epithelial stem cells. Lapthanasupkul *et al.*, (2012) showed that there are two main populations of mesenchymal cells at the proximal end of the incisor: slow-dividing self-renwing MSCs and fast-dividing TACs.

In chapter 3, Wnt-responsive cells were identified as TACs and odontoblasts. Therefore, to investigate the role of Wnt signaling in Wnt responsive cell proliferation, a BrdU chase experiment was done on 1 weeks post-tamoxifen treated *pCagg* ^{CreERT2}*; Wls* $^{fl/fl}$ mouse incisors (n=3) and compared to corn oil treated *pCagg* ^{CreERT2}*; Wls* $^{fl/fl}$ mouse incisors (n=3). BrdU single injection was given 24 hours prior to collection to label fast dividing cells. Immunofluorescent staining results for BrDU showed that control group incisor-labelled cells were located in the area distal to the labial and lingual cervical loop area, known as the TACs zone and some of the odontoblasts. Epithelial cells and ameloblasts were also BrdU+ve cells and they were fast cycling cells (Figure 4.14). Tamoxifen-treated mouse incisors showed a significant reduction in BrdU+ve cells in both mesenchymal and epithelial cells (Figure 4.14).

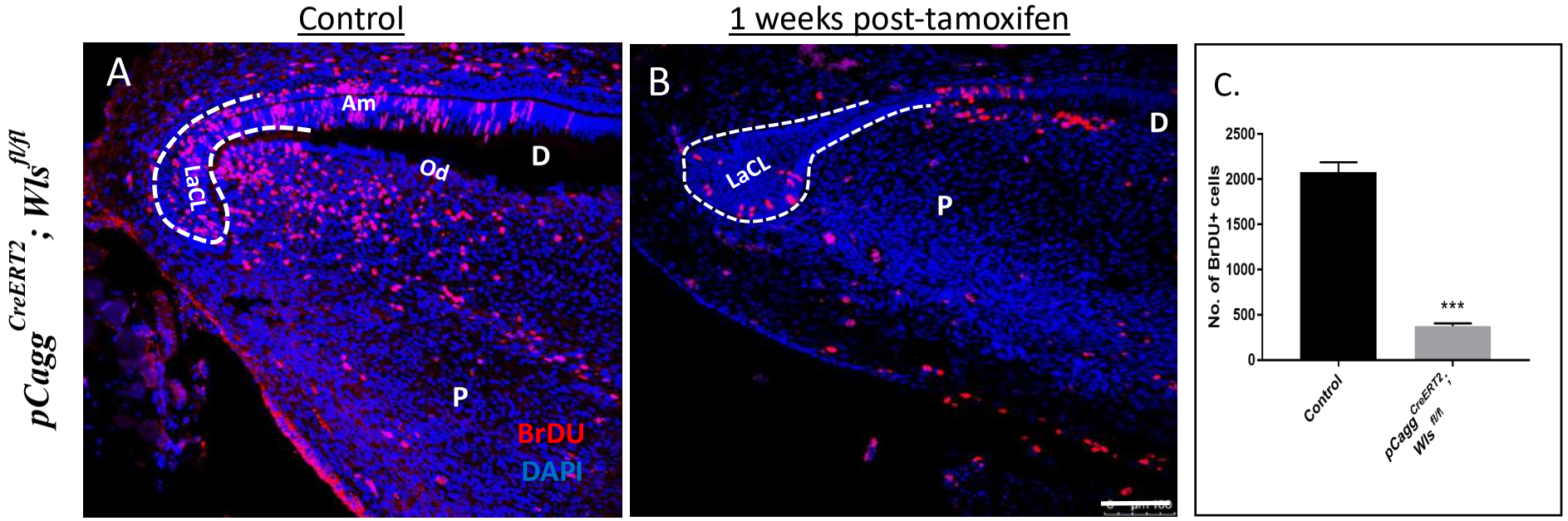

Figure 4.14. Wnt pathway deletion reduces TACs proliferation rate

(A-B) BrDU nucleotide incorporation for *pCagg*^{CreERT2}; *Wls*$^{fl/fl}$ mouse incisor fast dividing cells shows, (A) corn oil treated mouse incisor (n=3) have large population of BrDU+ cells (red) at the cervical area distal to the cervical loop (TACs zone) and some odontoblasts and ameloblasts. (B) 1 week post-tamoxifen treated mouse incisor (n=3) shows fewer BrDU+ cells at the same area. (C) Unpaired t-test analysis for BrDU+ cell count shows a significant decrease in fast cycling cell count in 1 week post-tamoxifen treated *pCagg*^{CreERT2}; *Wls*$^{fl/fl}$ mouse incisor

(LaCL) Labial cervical loop, (D) Dentine, (P) dental pulp, (Am) ameloblasts, (Od) odontoblasts. Scale bar 100um. ***p<0.001

4.2.6. Wnt is controlling TACs apoptosis

Knowing that TACs proliferation is downregulated in *Wls* knockout mice incisors, an apoptosis assay experiment was performed on 1 weeks post-tamoxifen treated *pCagg* ^{CreERT2}*; Wls* $^{fl/fl}$ mouse incisors (n=3) and compared to corn oil treated *pCagg* ^{CreERT2}*; Wls* $^{fl/fl}$ mouse incisors (n=3). Three injections of either tamoxifen or corn oil were given intraperitoneally in 3 consecutive days and mice then were collected after 1 week.

Compared to the control corn oil-treated *pCagg* ^{CreERT2}*; Wls* $^{fl/fl}$ mice incisors where there were no or few cells undergoing apoptosis, 1 week post-tamoxifen-treated *pCagg* ^{CreERT2}*; Wls* $^{fl/fl}$ mouse incisors (n=3) showed significant more cells undergoing apoptosis. TACs and odontoblasts which have been identified as Wnt-responsive cells were undergoing apoptosis, which could explain the few proliferative cell numbers. Surprisingly, MSCs which are not directly controlled by Wnt/β-catenin signaling were also undergoing apoptosis (Figure 4.15).

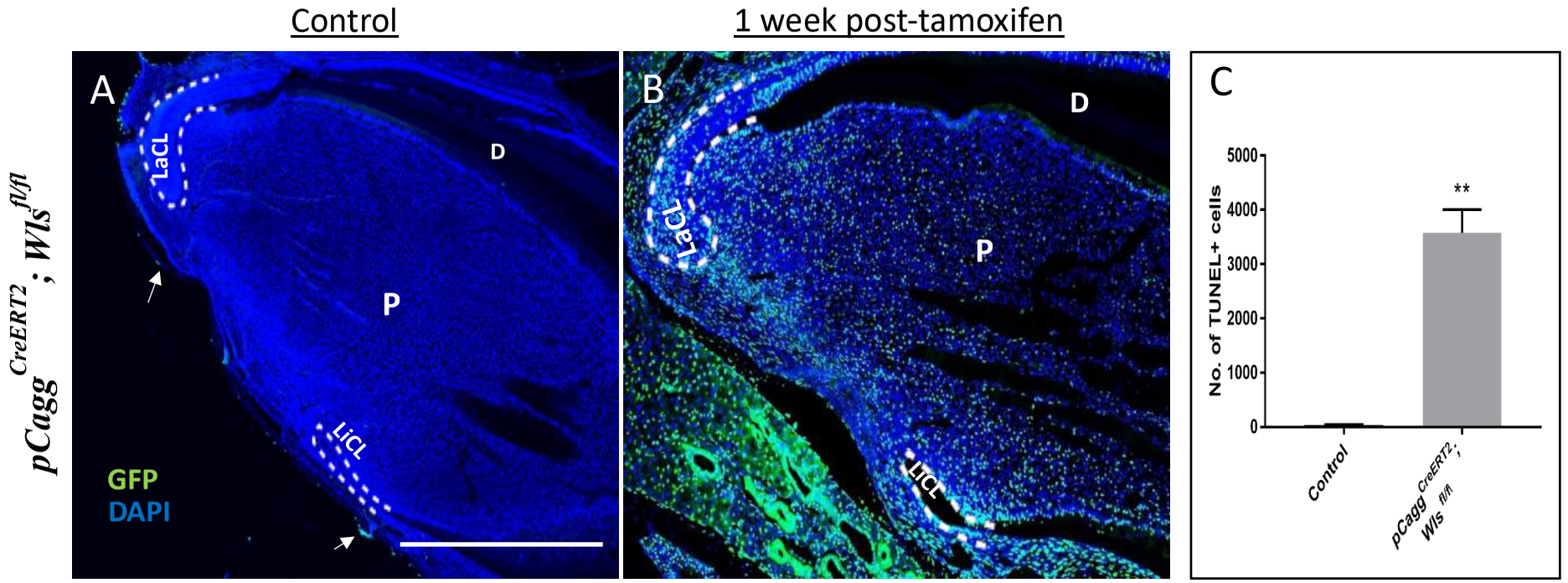

Figure 4.15. deletion of Wnt signaling pathway increases apoptosis rate.

Apoptosis assay (TUNEL) for *pCagg*^{CreERT2}; *Wls*$^{fl/fl}$ mouse incisor (A) corn oil treated mouse incisor (n=3) shows few positive cells undergoing apoptosis (white arrow). (B) 1 week post tamoxifen treated mouse incisor (n=3) shows cells undergoing apoptosis (Green) are spreading over TAC zone and MSC niche as well as dental pulp cell. (C) Unpaired t-test analysis for TUNEL+ cell count shows a significant increase of apoptotic cells in 1 week post-tamoxifen for *pCagg*^{CreERT2}; *Wls*$^{fl/fl}$ mouse incisor cervical area (n=3)

(LaCL) Labial cervical loop, (LiCL) Lingual cervical loop, (P) dental pulp, (D) Dentine. Scale bar 1000 um. **p<0.01

4.2.7. Loss of Wnt signaling reduces incisor growth rate

4.2.7.1. Incisor daily growth rate

Mouse incisors grow continuously throughout animal life to compensate for the attrition that happens at the incisor tip from the mastication wearing and to keep incisors sharp forever. Mouse incisors grow until they occlude to the opposing incisor and will keep growing if the mouse has malocclusion. 1 weeks post-tamoxifen treated *pCagg* ^{CreERT2}*; Wls* $^{fl/fl}$ mouse incisors (n=3) and corn oil treated *pCagg* ^{CreERT2}*; Wls* $^{fl/fl}$ mouse incisors (n=3) were used. Three injections of either tamoxifen or corn oil were given intraperitoneally on 3 consecutive days. 1 weeks after treatment, lower left mouse incisors were clipped to enhance incisor growth, and a notch were done on the enamel close to the gingiva. Growth rate was measured daily from the gingival line to the notch for 7 days and mice then were collected on the 7th day.

The results obtained from the daily measurement showed that the growth rate for 1 week post tamoxifen treated mouse incisors growth rate was significantly reduced ($P<0.0001$). The control non-clipped mouse incisor growth rate was 0.9 ± 0.05164mm/day while it was 0.07778 ± 0.01405 mm/day for the tamoxifen treated mouse incisor. Challenging the incisor by enhancing incisor growth showed that the corn oil treared incisor growth rate was increased to 1.3 ± 0.03651mm/day and the tamoxifen treated mouse incisor growth rate was 0.08333 ± 0.03073. Unpaired t-test showed that 1 week post tamoxifen treated clipped mouse incisors growth rate was significantly reduced ($P<0.0001$) (Figure 4.16)

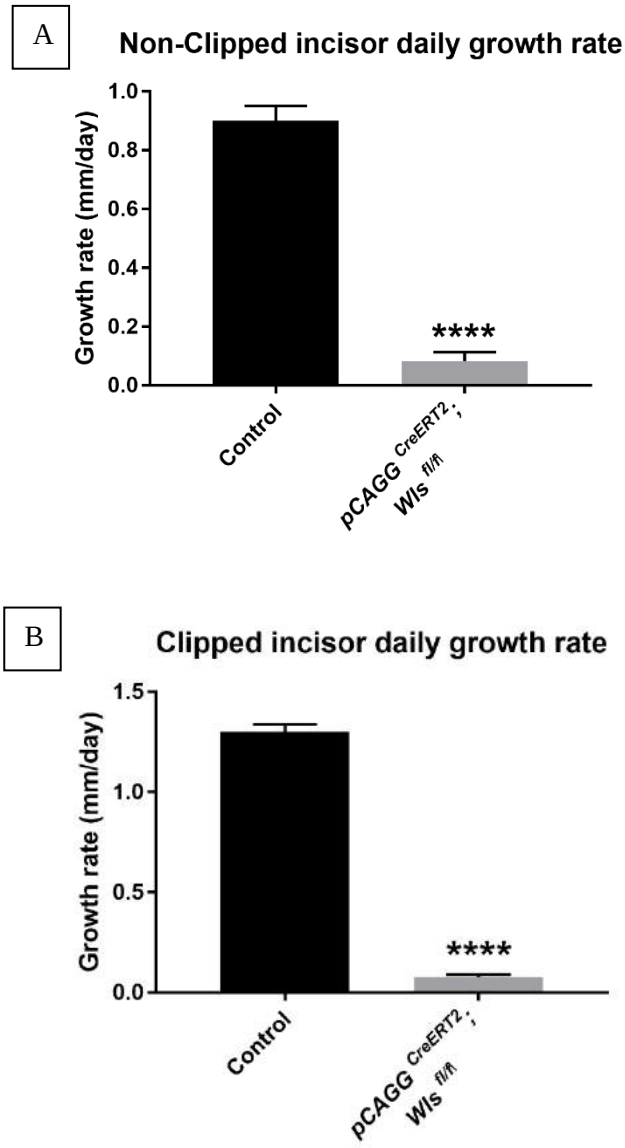

Figure 4.16. Deletion of Wnt signaling pathway reduces mouse incisor growth rate.

Analysis of daily growth rate of mouse incisor in 2 scenarios; (A) homeostatic status, where only a notch was made to the tooth, and (B) injury status, where incisor was clipped to enhance the growth, shows that Wnt signaling deletion greatly affect incisor growth rate. Both statuses have shown a highly significant reduction in daily growth rate. ****$p<0.0001$

4.3. Discussion

4.3.1. Wnt upregulation effect on mouse incisors

Axin2 acts as Wnt/β-catenin signaling supressor , and also is a downstream readout the Wnt pathway. Deletion of *Axin2* interrupts the destruction complex of the β-catenin and inhibits its phosphorylation. Thus, more β-catenin accumulates in the cytoplasm and enter the nucleus to activate the target genes transcription. Wnt/β-catenin upregulation is known to affect the development of different organs such as skull bone (Yu *et al*., 2005), and also increases the risk of tumour formation (Liu *et al*., 2000). Deletion of *Axin2* induces premature skull sutures fusion leads to smaller skull than wild-type mice (Yu et al., 2005). The results obtained from μ-CT scanning results showed that the incisor length was not affected, and it was similar to the wild-type incisors. This might be due to skull phenotype starts before incisors were entirely erupted.

Wnt downstream gene expression analysis showed that Wnt upregulation significantly increased the expression *of β-catenin,* and *Dspp*.Wnt-10a , a canonical Wnt activator, regulates Dspp function in the active odontoblasts (Yamashiro et al., 2007). However, no apparent dentine abnormalities were detected in the upregulated canonical Wnt pathway mouse incisor. This could be because of the other Wnt ligand activity which also was upregulated and might act as inhibitors for the increased Dspp activity.

Mouse incisors have high repair capacity that injured incisors show faster growth rate than normal incisors, and this maybe because of the increase of the stem cell activity at the incisor apex in response to the injury and tissue loss. Upregulated Wnt activity in mouse incisors showed a slightly faster growth rate than the control incisors without injury. However, mouse incisors growth rate showed significant increased growth rate after incisors were clipped. This

may suggest that Wnt/β-catenin pathway upregulate TACs and odontoblasts function upon stimulation.

4.3.2. Wnt signaling ablation affects bone remodelling

Bone remodelling is a process controlled by two bone cell populations; osteoblast forms bone on one side and osteoclast resorps bone from the other side. The balance between osteoblast and osteoclast activity is necessary where any defect can lead to bone disease. Bone remodelling are controlled by Wnt signaling which controls both osteoblast maturation and osteoclast differentiation (Lerner & Ohlsson, 2015).

Deletion of Wntless, a transmembrane protein responsible for Wnt protein secretion inhibits Wnt secretion. Thus, Wnt pathway will be depleted due to the absence of the Wnt ligand binding to the receptors. Lim *et al*. (2014) showed that inhibiting Wnt secretion from *osteocalcin*-expressing cells such as osteocytes affects mouse skull bone. Wnt signaling controls bone remodelling by controlling Runx2 function, and Runx2 down-regulation causes bone loss. It is known that Runx2 has a role in the maturation of the osteoblast and that loss of Runx2 leads to immature osteoblasts that cause bone deformity (Lerner and Ohlsson, 2015). Since Wnt signaling controls Runx2, loss of *Wls* eventually will reduce Runx2 expression and function which causes defective skull bone mineralisation. It is likely that the same scenario occurred in the ubiquitous deletion of *Wls* and My data also identified mandible lingual bone defects upon *Wls* deletion.

Wnt ligands secretion also affects bone formation and mineralisation. Movérare-skrtic et al. (2014) showed that *Wnt-16* mutant mice have bone fractures and abnormal bone formation that has decreased cortical bone thickness with porosities throughout the cortical plate. Tu *et al.*

(2007) also demonstrated the role of Wnt-7b signaling in bone osteoblastogenesis, whereas loss of Wnt-7b function reduces the embryonic bone mineralisation. Wnt-9a also controls bone mineralisation, where loss of Wnt-9a reduces the mineralised region size (Spater et al., 2006). Other Wnt ligands also control bone minerlisation, such as Wnt-10a and Wnt-10b (Cawthorn *et al.*, 2012) where they both inhibit adipogensis and enhance osteogenesis. Gain-of-function mutations of Lrp5 showed increased bone density and more active osteoblasts (Hartmann, 2006). However, mice lacking Lrp5 showed reduced bone density due to a defect in osteoblast proliferation and maturation (Kato *et al.*, 2002). Thus, many Wnt ligands are expressed in the osteoblast and have been shown a vital role in controlling bone formation. Therefore, blocking Wnt ligands secretion downregulated Wnt signaling and caused bony defect.

Wntless mutation on *OCN*-expressing cells has shown alveolar bone defect (Lim et al., 2014) similar to the ubiquitous deletion of *Wls* suggesting Wnt signaling role in alveolar bone maintenance. Periodontal ligament cells and osteoblasts are Wnt responsive cells that loss of Wnt signaling leads to widening of the PDL and thinning of the alveolar bone. These abnormalities are caused by *Osx, Runx2,* and *ALP* downregulation (Lim et al., 2014). Xiang et al. (2014) showed that Wnt-5a has a role in bone remodelling as both osteogenesis enhancer and osteoclastogenesis mediator, and it is essential for maintaining both the unmineralised PDL, the mineralised cementum and alveolar bone. Thus, inhibiting Wnt-5a secretion by knocking-out Wls could leads to Alveolar bone resorption and PDL widening.

The results obtained from the ubiquitous inhibition of Wnt ligand secretion showed that reduced osteogenesis is accompanied by increased osteoclastogeneis. Mature osteoclast forms when granulocyte and macrophage colony-forming unit cells bind to RANKL, CSF-1 or M-CSF and either IL-1 or TNF-α, which leads to the fusion of the unit cells to produce the multinucleated cell. Osteoblasts are required for the differentiation of the osteoclasts because they are the source of the cytokines (Matsuo & Irie, 2008). Indeed, osteoblasts play a role in

osteoclastogenicity; they also produce osteoclastogenic antagonists such as osteoprotegerin (OPG) which blocks RANKL and inhibits osteoclast differentiation (Moverare-Skrtic et al., 2014). Since osteoblast maturation is affected in the loss of the Wnt signaling model, osteoblast antagonising function was eliminated and osteoclastogenesis would be continually active (Zhong et al., 2012). TRAP staining data showed ectopic osteoclasts recruitment that accumulated in the incisor pulp and PDL and caused both PDL widening and incisor resorption. So, loss of Wnt signaling enhances osteoclast differentiation, however, the origin of the recruited osteoclasts inside the incisor pulp is not clear yet.

Activation of Wnt/β-catenin pathway via Wnt3a in osteoblasts induces *OPG* expression which antagonises osteoclast differentiation and increases bone mass, while downregulation of β-catenin in mature osteoblasts shows decreased bone mass as a result of increased bone resorption. Non-canonical Wnt signaling has also demonstrated the direct effect on osteoclasts precursors as Wnt5a-Ror2 signals regulate osteoclast differentiation. Osteoblasts secrete Wnt-5a which enhances RANKL-induced osteoclast formation by inducing RANKL production (Westendorf, Kahler, & Schroeder, 2004). Thus, the loss of Wnt function impairs osteoblast proliferation and maturation and enhances osteoclastogenesis, which imbalances the bone remodelling mechanism and reduces bone mineralisation in skull bones.

4.3.3. Loss of Wnt signaling leads to the formation of abnormal mouse incisor phenotype

The results obtained from *pCagg^{CreERT2}; Wls$^{fl/fl}$* mouse line showed the effect of the ubiquitous Wnt deletion in the incisor that an abnormal phenotype was formed. The abnormal incisor phenotype is characterised mainly by two features; disruption of the cervical area and increase dentine thickness. Loss of Wnt pathway function affects many cellular mechanisms which

leads to the formation of the abnormal incisor phenotype. Cell proliferation and differentiation at the cervical area were decreased, which was accompanied by increased cells apoptosis and ectopic osteoclast recruitment to the area that lead to the cervical area disruption. Moreover, the mature odontoblast function was enhanced, and dentine matrix secretion was increased, which led to the increased dentine thickness. Yang et al., (2015) showed that Wnt10a knockout affects incisors shape where the apical part of the incisor has a wedge-shaped defect at the lingual side.

4.3.3.1. Wnt signaling controls TACs proliferation and differentiation

Mouse incisor MSCs are slow dividing cells, and because of the fast incisor turnover, MSCs must give rise to TACs, a rapid cycling cell population to compensate for the tissue loss at the tip of incisors. TACs proliferation is a complex process requiring the interplay between several factors. Wnt signaling controls cell proliferation in many cell populations (Clevers, 2006) such as hematopoietic stem cells (HSCs) as overexpression of *Axin2* reduces stem cell proliferation (Reya *et al*., 2003) and intestine crypt epithelial stem cells (Clevers, 2006). Wnt signaling is also implicated in T lymphoid lineage determination as mice lacking either Tcf1 and/or Lef1 reduces thymocyte progenitor differentiation (Okamura *et al.*, 1998). Mouse intestine epithelium turns over within as little as three to five days and to maintain normal intestine physiology, the rapid production of transit amplifying cells (TACs) at the crypt is compensated by apoptosis at the villus (Clevers, 2006). Ablation of Wnt signaling by Dkk-1, one of the Wnt antagonists in adult mice intestine, promotes the entire loss of the crypts (Reya and Clevers, 2005) while upregulation of Wnt signaling by the overexpression of R-spondin-1, one of the Wnt agonist proteins, increases the proliferation rate of intestinal crypt cells (Kim *et al*., 2005). Van Es *et al.* (2005) stated that Wnt signals stimulate the proliferation of crypt progenitors and

regulate the terminal differentiation of another population at the crypt know as Paneth cells. Based on the well-established concepts that Wnt signaling controls the proliferation of different stem cell progenitors, the results obtained from the ubiquitous Wnt signaling ablation identified the role of Wnt signaling in the mouse incisor Wnt responsive cells proliferation (TACs and odontoblasts). Using nucleotide incorporation labelling of fast cycling cells showed a huge reduction in TACs number at the cervical end of the incisor as soon as one week after the inhibition of Wnt ligands secretion. Thus, Wnt signaling control mouse incisor TAC proliferation at the cervical area.

Lapthanasupkul et al. (2012) showed that Ring1a/b, the core Polycomb repressive complex1 (PRC1) component, is strongly expressed at the incisor cervical end in the TAC zone. Loss of Ring1a/b results in abnormal and defective epithelial cervical loops which are smaller than wild-type cervical loops, and down-regulates the formation of both enamel and dentine. Loss of Ring1a/b also reduces mesenchymal and epithelial cells proliferation and causes shorter incisors. Odontoblasts and ameloblasts differentiation of Ring1a/b mouse incisors was disrupted, resulting in disruption of enamel and dentine formation. Furthermore, *Dspp*, which is expressed in both odontoblasts and pre-ameloblasts (Begue-Kirn *et al*., 1998), was downregulated, and *Amelogenin*, a gene expressed in functional ameloblasts (Zeichner-David et al., 1995) was absent. Likely, the data obtained from the ubiquitous Wnt pathway deletion showed that TACs differentiation into odontoblasts was reduced, which leads to the disruption of the lingual dentine. However, more odontoblasts are differentiated at the labial side, leading to ectopic dentine formation near the labial cervical loop. Thus, Wnt signaling controls TACs differentiation to odontoblasts at the lingual side of the incisor, yet, the increased odontoblasts at the labial side needs more investigation.

4.3.3.2. Wnt controls odontoblast function

Odontoblasts, an ectomesenchymal cell population originating from neural crest, are tall columnar cells lining the dental pulp space. Odontoblasts secrete dentine, a collagen-based mineralised tissue, through secretion of organic and non-organic dentine matrix components. Wnt pathway target gene *Axin2* is expressed in differentiating odontoblasts, and also expressed in adult mouse incisor pre-odontoblasts and odontoblasts, but not in fully mature odontoblasts (Lohi et al., 2010). The role of the Wnt/β-catenin pathway in mouse teeth development is crucial, and manipulation of β-catenin expression at different pre-natal or post-natal stages leads to different abnormalities. Inactivation of Wnt/β-catenin before tooth development arrests the tooth bud to cap stage transition, while inactivation of Wnt/β-catenin during tooth development affects the differentiation of odontoblasts and root formation. Furthermore, the overexpression of β-catenin post-natally results in increased dentine formation in molars. The continuous Wnt/β-catenin activation causes large tooth formation and formation of supernumerary tooth (Liu and Millar, 2010).

Babb et al. (2017) showed the importance of Wnt/β-catenin signaling for molar odontoblasts in both normal physiology and in response to injury. Molar odontoblast-like cells are Wnt responsive cells and also have autocrine Wnt activation mechanisms. The role for Wnt/β-catenin signaling in mature primary odontoblasts is not clear. In the absence of damage, either overexpression or inhibition of Wnt/β-catenin signaling in primary odontoblasts did not trigger the production of excessive dentine or prevent dentine secretion, suggesting that Wnt/β-catenin signaling is not enhancing dentine secretion. Conversely, in the injury model, the ability of Wnt/β-catenin signaling selectively enhances dentine production in mouse molars, which could be as a result of Wnt/β-catenin signaling to promote dentine production. Neves et al. (2017) showed that enhancement of Wnt/β-catenin signaling activity by the delivery of Wnt agonists, in particular GSK-3 inhibitors, by using neurological disorder drug “Tideglusib” upregulate

the Wnt/β-catenin signaling pathway and promote odontoblast differentiation and dentine secretion in damaged mouse molars. Overall, Wnt/β-catenin play an important role in controlling odontoblast functions. Unlikely, the results obtained from the ubiquitous Wnt pathway ablation showed that downregulation of Wnt pathways increases dentine matrix secretion. Investigating the possible causes revealed that Wnt-10a/β-catenin pathway downstream *Dspp*, which is expressed in the active odontoblasts (Yamashiro et al., 2007), was upregulated in the mutant mouse odontoblasts. There are two possibilities to explain that. The first one is that other signaling pathways could be controlling *Dspp* expression while the other is that Wnt-10a could be secreted from the odontoblast in a different way.

4.3.3.3. Wnt signaling controls cell apoptosis

To date, two main apoptotic pathways have been identified and both involved in caspase activation. The first pathway is the death receptor pathway, which is initiated by extracellular ligands such as tumour necrosis factor alpha (TNF-a) binding to its corresponding cell membrane receptor (TNFR). The second pathway of apoptotic signaling is under the control of the Bcl-2 family (*B-cell lymphoma 2*) and its proteins, and is induced by the transmission of intrinsic signals via intracellular structures that lead to the activation of caspase (Pećina-šlaus, 2010).

Wnt signaling controls two stages of cell apoptosis, in particular; early and late stages (Pećina-šlaus, 2010). Wnt signaling pathway regulates apoptosis through a variety of mechanisms. APCs, part of the destruction complex of β-catenin, have a dual role in apoptosis; apoptosis activation and inhibition, depending on its condition as wild-type or mutation. Overexpression of wild-type APC induces apoptosis mechanism while overexpression of the mutated one inhibits the process (Brocardo and Henderson, 2008). Wnt-1, Wnt/β-catenin pathway activator,

has an anti-apoptotic function as it blocks cytochrome C release and inhibits the activity of caspase-9. Moreover, overexpression of dishevelled, positive mediator of β-catenin, has also been shown to initiate apoptosis (Strovel and Sussman, 1999) which could interfere with the fact that Wnt/β-catenin inhibits cell apoptosis. However, dishevelled is also a part of the non-canonical Wnt pathway and activates the JNK pathway which already has been shown to induce cell apoptosis (Tournier *et al*., 2000). GSK-3β has also been found to have dual effects as inhibition of GSK-3β prevents cell apoptosis and promotes cell survival, while overexpression of GSK-3β induces cell apoptosis (Hetman et al., 2000).

the data obtained from the ubiquitous Wnt signaling deletion showed that mouse incisor pulp cells has no or few cells undergoing apoptosis. However, ubiquitous ablation of Wnt signaling pathways showed extensive and diffused pattern of cells undergoing apoptosis. Thus, Wnt signaling is essential for TACs and odontoblasts maintenance as it controls apoptosis. Based on the fact that both Wnt pathways play a vital role in cell apoptosis, *Wls* deletion ablates both canonical and non-canonical Wnt pathways and initiates apoptosis via both pathways. It is not clear yet which Wnt ligand is responsible for cell apoptosis, but it has been addressed that Wnt-7b is required for the programmed cell death of the endothelial cells in the developing eye (Lobov et al., 2005). Wnt-1 is also an important factor to control apoptosis and it works as an apoptosis antagonist (Strovel and Sussman, 1999). So, loss of Wnt-1 secretion might lead to increased apoptosis rate.

4.3.3.4. Loss of Wnt signaling leads to ectopic osteoclasts activity within the dental pulp

As shown in section (4.1.2) Wnt signaling controls osteoclast differentiation and loss of Wnt signaling leads to increased osteoclastic activity in the bone (Zhong et al., 2012). Yet, no clues can explain the ectopic osteoclast recruitment inside the dental pulp. An explanation for the

ectopic osteoclasts recruitment is that osteoclast might be originating from PDL and migrating into the dental pulp. This is because osteoclasts appeared long time after apical dentine resorption. Dentine resorption in the incisor early abnormal phenotype happened without osteoclastic activity, which could support the suggestion of the osteoclast originating from outside the dental pulp. To exclude the idea of ectopic osteoclasts being originated from the macrophages in the dental pulp, further investigation should be made that after tamoxifen application, macrophages can be washed out and then the phenotype progression would be studied.

4.3.4. Manipulation of Wnt signaling affects incisor growth rate

It has been shown earlier that cells responsible for incisor growth, in particular TACs and odontoblasts, are Wnt responsive cells. The data obtained from the upregulated Wnt/β-catenin pathway mouse line showed that incisor growth rate was not enhanced during homeostasis. However, incisor injury which accelerates incisor growth, showed that upregulation of Wnt/β-catenin pathway enhances the mouse incisor growth rate. This can explain the role of the Wnt/β-catenin pathway on mouse incisors growth rate that Wnt/β-catenin pathway upregulates TAC and odontoblast functions to produce more dentine to regain normal teeth occlusion. A study in our laboratory showed that continuous upregulation of Wnt/β-catenin pathway in the molar injury site enhances the regeneration capacity of the dentine (Neves et al., 2017). Moreover, the data obtained from the ubiquitous Wnt signaling deletion showed that mutant incisors growth rate was reduced during both homeostasis and injury. This is because loss of Wnt pathway function leads to reduced TACs proliferation and increased apoptosis which subsequentially decreases the incisor growth rate. Collectively, the data obtained from the

upregulated and downregulated Wnt pathway mouse lines showed that Wnt signaling controls mouse incisor growth.

4.4. Conclusion

To study the role of Wnt signaling in adult mouse incisor growth, Wnt signaling was manipulated and two models were used; Wnt-gain and loss of function models. Wnt/β-catenin signaling up-regulation does not affect incisor morphology and mesenchymal cell fate. However, it enhances TACs and odontoblasts functions if injury happens. This suggested that Wnt-responsive cells can respond to Wnt selectively and due to the demands of more tissue formation. Loss of Wnt signaling function leads to abnormal incisor phenotype formation which is characterised by the cervical area disruption and the increased dentine thickness. These abnormalities happen because of the reduced TACs proliferation and differentiation into odontoblasts and increased TACs apoptosis. Loss of Wnt function affects bone remodelling so that osteoblastogenesis is increased and osteoclastogenesis is decreased leading to both bone and dentine resorption. Because of that, mutant incisors are short and have a significantly slow growth rate. Thus, Wnt signaling has a crucial role in adult mouse incisor growth and it regulates both TACs proliferation and differentiation and odontoblasts dentine secretion.

Chapter 5. Sources of Wnt ligands in adult mouse incisor

5.1. Introduction

Wnt ligand is a secreted glycoprotein which is required to activate the Wnt pathway by binding to co-receptors (Miller, 2002; Undi et al., 2016). Wnt protein was discovered in the *Drosophila* as wingless (Sharma and Chopra, 1976), and since then they have been well studied. Wnt signaling is a crucial pathway for the developing embryo and adult tissue homeostasis (Anger and Moon, 2009). At least 19 Wnt proteins have been discovered in humans and rodents, and among them, some can either activate canonical or non-canonical Wnt pathways while others can activate both pathways (Miller, 2002). After the transcription of Wnt ligand which is a soluble protein, Porcupine, a protein residing in the endoplasmic reticulum, lipid modifies Wnt and changes its nature from hydrophilic to hydrophobic (Tanaka et al., 2000; Coombs et al., 2010). Following that, modified Wnt ligand binds to Wntless/Evi protein to be able to go from golgi apparatus to the cell membrane. The secreted Wnt ligand acts as a short-range protein because of its hydrophobic nature (Willert et al., 2003).

Wntless/Evi is a transmembrane protein which controls the secretion of the palmitoylated Wnt protein through the cell membrane (Ching and Nusse, 2006). Wntless/Evi protein was first described by Banziger et al. (2006) where it was identified in the genetic screen in the Wnt gain of function phenotype. The Wntless/Evi complex is controlled by retromers, and the absence of either Dvps35 or Dvps26 will lead to its degradation and, therefore, prevent the secretion of Wnt protein (Port et al., 2008). The source providing and secreting Wnt ligands to activate Wnt pathways in mouse incisors is not clear yet.

Wnt activation mechanisms via binding of Wnt ligand to its receptor can be either an autocrine or paracrine mechanism. Some stem cell populations, such as hair follicle stem cells, have an autocrine Wnt/β-catenin signaling activation system where hair follicle stem cells in the outer

bulge are Wnt-responsive cells and Wnt secreting cells at the same time (Morris et al., 2004). Hair follicle stem cells are also controlled by a paracrine Wnt mechanism, where hair follicle stem cells in the outer bulge act as Wnt-responsive cells and Wnt pathway is activated by the secreted ligand from the inner bulge cells to control cells differentiation (Lim et al., 2016).

The mouse incisor, as described in Chapter 1, is a complicated organ that consists of epithelial, mesenchymal and endodermal tissues. Suomalainen and Thesleff (2010) concluded that many Wnt ligands are expressed in the dental tissue. *Wnt-4* is expressed in the lingual cervical loop, enamel epithelium and ameloblasts and *Wnt-6* is expressed intensely in the lingual cervical loop, however, none of the Wnt ligands are expressed in the labial cervical loop suggesting that epithelial stem cells are not Wnt secreting cells. Wnt ligands were expressed in both pre-ameloblasts and ameloblasts; in particular, *Wnt-3a*, *Wnt-6*, and *Wnt-10a*. Wnt ligands expression in the dental mesenchyme showed that *Wnt-5a* has a strong expression in the cervical loop area. At E16, *Wnt-5a*, *Wnt-4*, *Wnt-5b*, *Wnt-6*, and *Wnt-10a* were expressed in the dental papilla mesenchymal tissue. At E18, *Wnt-5a* expression continues in the dental papilla mesenchyme and the cervical loop area. *Wnt-6* and *Wnt-10a* expression were confined to the odontoblasts. Finally, *Wnt-11* expression is mainly detected at the dental follicle around incisors. Thus, different cell populations participate and secrete Wnt protein in the dental pulp.

In this chapter, identifying the source of Wnt ligand, that is responsible for adult mouse incisor growth, was explored. Different conditional knockout mouse lines were used to inhibit Wnt secretion from different dental tissue, and the outcome of each mouse line was compared to the ubiquitous deletion of the Wnt pathway (described in Chapter 4).

5.2. Results

5.2.1. Inhibition of Wnt ligand secretion from MSCs

Mesenchymal stem cells reside in the niche at the area between the cervical loop of the mouse incisors. MSCs are responsible for the incisor growth where their progeny TACs give rise to odontoblasts and pulp cells. Until now, there is no specific marker for MSC, meaning no specific knock-out mouse line could be used to eliminate Wnt secretion from MSCs (An et al., 2018a). Zhao et al. (2014) stated that Gli1 could be used as MSC marker, as it is expressed in around 90% of the dental pulp mesenchymal cells.

Gli1^{CreERT2} mouse line (Ahn and Joyner 2004) which was crossed with *Wls*$^{fl/fl}$ mouse line provided a tool to study the effect of MSC-derived Wnt ligand. Adult *Gli1*^{CreERT2}*; Wls*$^{fl/fl}$ mice (n=3) were treated with three IP tamoxifen injections (2mg/dose) in 3 consecutive days and then collected after 2 weeks and compared to the wild type mouse line.

5.2.1.1. µ Ct scan analysis of *Gli1*^{CreERT2}*; Wls*$^{fl/fl}$ mouse incisors

MSCs activity is not controlled by Wnt signaling, yet they could secrete Wnt ligand that affect mouse incisor physiology. 2 weeks post-tamoxifen treated *Gli* ^{CreERT2}*; Wls* $^{fl/fl}$ mouse skulls (n=3) were collected, fixed and scanned and compared to wild type mouse incisors. Inhibition of Wnt secretion from *Gli1*-expressing MSCs showed both labial and lingual dentine have been disrupted (Figure 5.1. A-B). Wild type mouse incisor (n=3) length was 11.24 mm ± 0.02963, while the 2 weeks post-tamoxifen treated mouse incisor (n=3) length was 9.633 mm ± 0.06667. Unpaired t-test analysis showed that *Gli1*^{CreERT2}*; Wls*$^{fl/fl}$ mice have a significantly shorter incisor ($P < 0.0001$) (Figure 5.1 C).

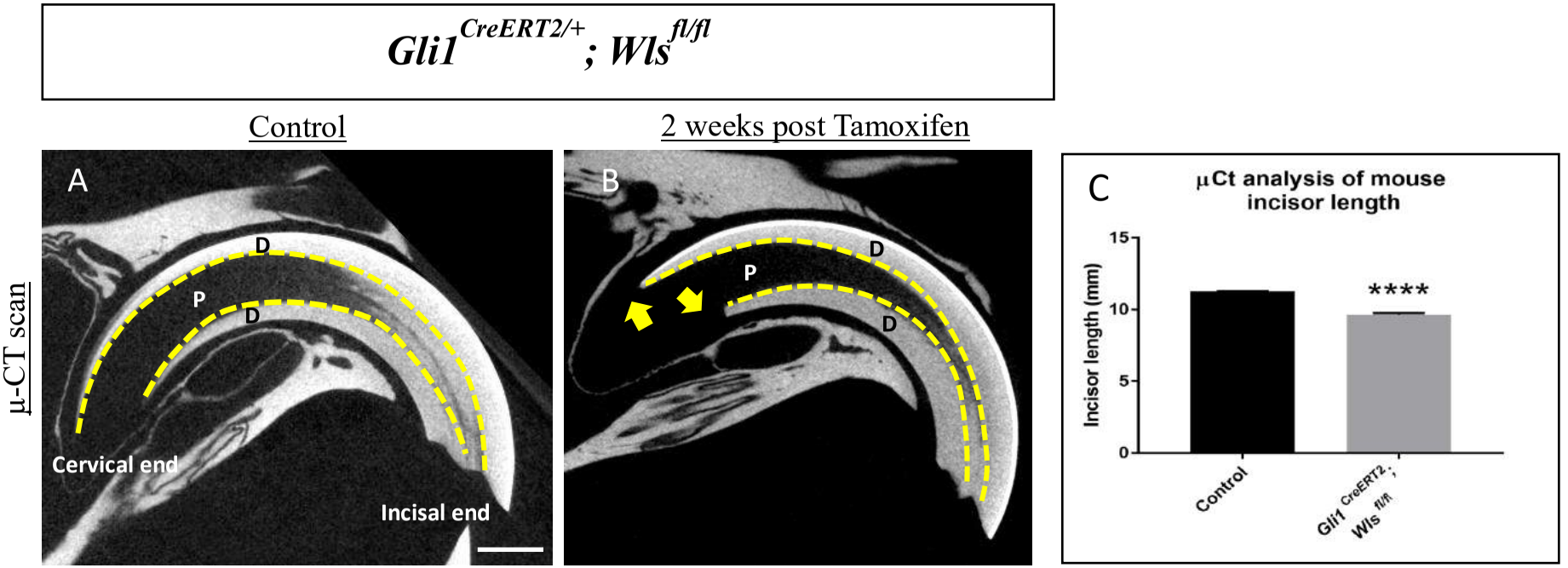

Figure 5.1. Inhibition of Wnt ligand secretion from MSCs causes cervical area disruption.

(A-B) µ-Ct scan of wild type mouse incisor (control) (n=3) shows the normal incisor structure. 2 weeks post-tamoxifen treated *Gli1*^{CreERT2}; *Wls*$^{fl/fl}$ mouse incisor (n=3) shows an abnormal resorption of labial and lingual dentine at the cervical region (arrows). The dentine resorption leads to shorter incisors that *Gli1*^{CreERT2}; *Wls*$^{fl/fl}$ mouse incisor was significantly shorter than wild type incisor (C). Unpaired t-test shows significant shorter *Gli1*^{CreERT2}; *Wls*$^{fl/fl}$ mouse incisor.

(P) pulp, (D) dentine. Scale bar = 1000 µm

5.2.2. Inhibition of Wnt ligand secretion from epithelial cells

The dental epithelial tissue – namely, ameloblasts and epithelial layer surrounding the incisor – secretes Wnts. Yet, its role on mouse incisor is not clear yet.

To study the effect of epithelial Wnt ligands secretion, Wnt secretion from epithelial tissue was inhibited by using $K14^{CreERTM}; Wls^{fl/fl}$ mouse line. K14 is expressed in the epithelial cells and it is a known epithelial cells marker (Turksen et al., 1992) and it is expressed in tooth ectoderm during development (Vasiokhin *et al*., 1999).

In this experiment, $K14^{CreERTM}; Wls^{fl/fl}$ mice were divided into 4 groups (1 control (n=3) + 2 tamoxifen treated groups (n=3 each)). Mice were treated with three IP injections of either corn oil or tamoxifen (2mg/dose) in 3 consecutive days. Mice were then collected at 6 and 12weeks following treatment. Then µ-CT scan for the skulls was done to study the incisors. Histological sections were done to study the effect of the epithelial Wnt ligand inhibition on the incisor growth and homeostasis.

5.2.2.1. µ Ct scan analysis of $K14^{CreERTM}; Wls^{fl/fl}$ mouse incisors

$K14^{CreERTM}; Wls^{fl/fl}$ mouse skulls were collected and scanned. The µ-CT data analysis for the mouse incisors (n=3) was compared to the corn oil-treated mice incisors (n=3) which have enamel at the labial side covering the dentine structure and the pulp space in the middle of the incisor. The overall finding of the tamoxifen-treated $K14^{CreERTM}; Wls^{fl/fl}$ mice incisor scanning showed normal-shaped incisors with no abnormalities in the cervical area and a normal cervical loop. Dentine at the lingual side end was normal with no signs of resorption (Figure 5.2).

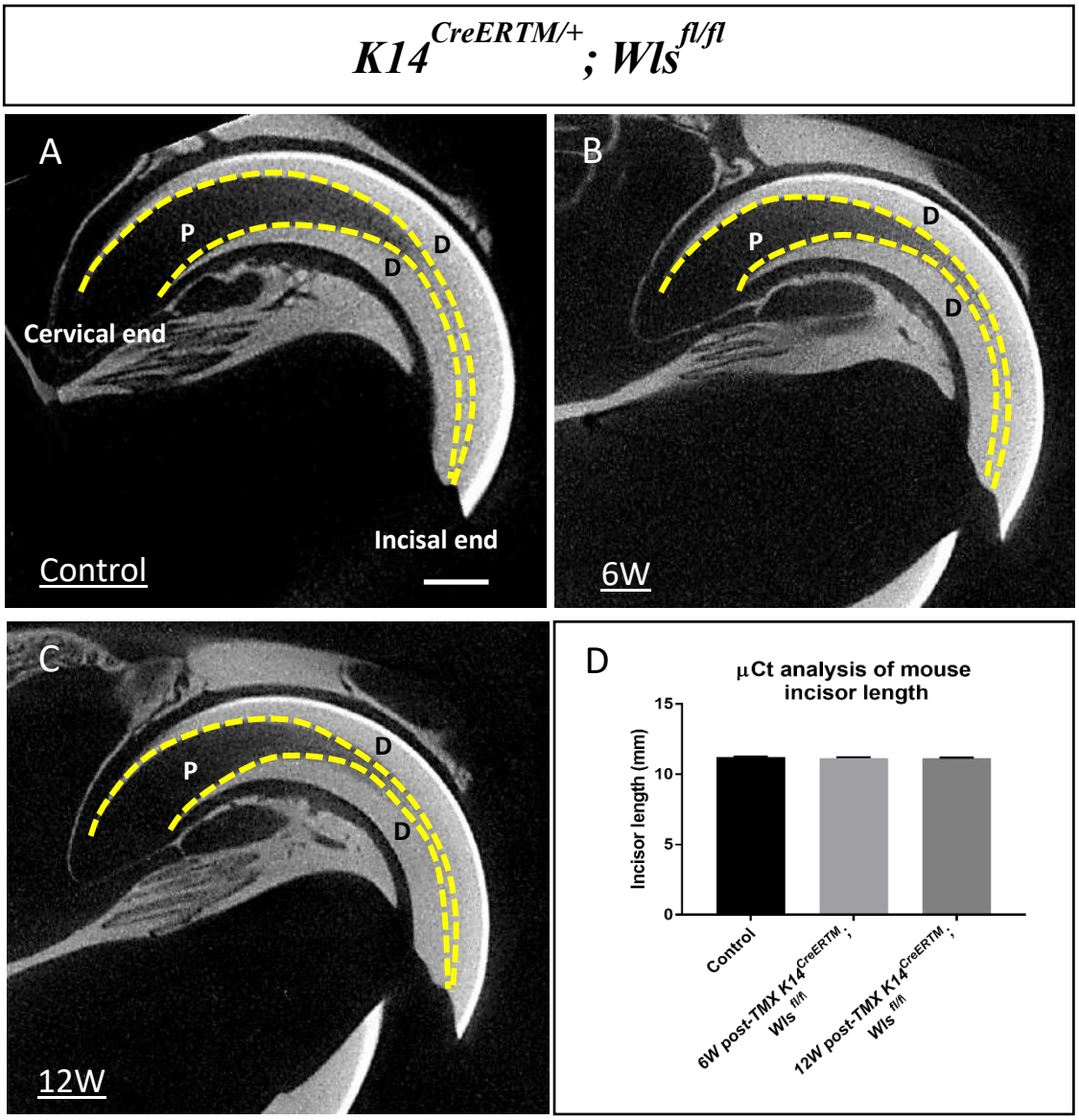

Figure 5.2. Inhibition of Wnt ligand secretion from the epithelial cells does not affect incisors. (A-C) µ-Ct scan of Corn oil treated *K14*^{CreERTm}*; Wls*$^{fl/fl}$ mouse incisor (control) (n=3) shows normal incisor shape. Moreover, 6 (n=3) and 12 weeks (n=3) post-tamoxifen treated *Gli1*^{CreERT2}*; Wls*$^{fl/fl}$ mouse incisor also show no abnormalities and incisors look normal. (D) Unpaired t-test for incisor length shows no significant different.

(P) pulp, (D) dentine. Scale bar = 1000 µm

5.2.2.2. H&E staining of *K14 ^{CreERTM}; Wls $^{fl/fl}$* mouse incisors

Previous of µ-CT scanning data showed a normal incisor shape for the tamoxifen-treated *K14^{CreERTM}; Wls$^{fl/fl}$* mouse incisors and that they are similar to the corn oil treated incisors. So, histological sections were stained to investigate the effect at the cellular level. For the group of mice collected six weeks after the tamoxifen treatment (n=3), H&E staining showed a normal shape and size cervical loop in both labial and lingual sides. The dentine layer was normal with no increased thickness or resorption. The dental pulp space was also normal (Figure 5.3 B).

To further investigate the effect of *Wls* deletion from epithelial tissues, another mouse group was collected 12 weeks after being treated with tamoxifen (n=3). Incisors were normal with no disrupted cervical area. The cervical loop has a normal size and shape. Hard tissue – namely enamel and dentine – was normal and showed no resorption or disruption (Figure 5.3 C).

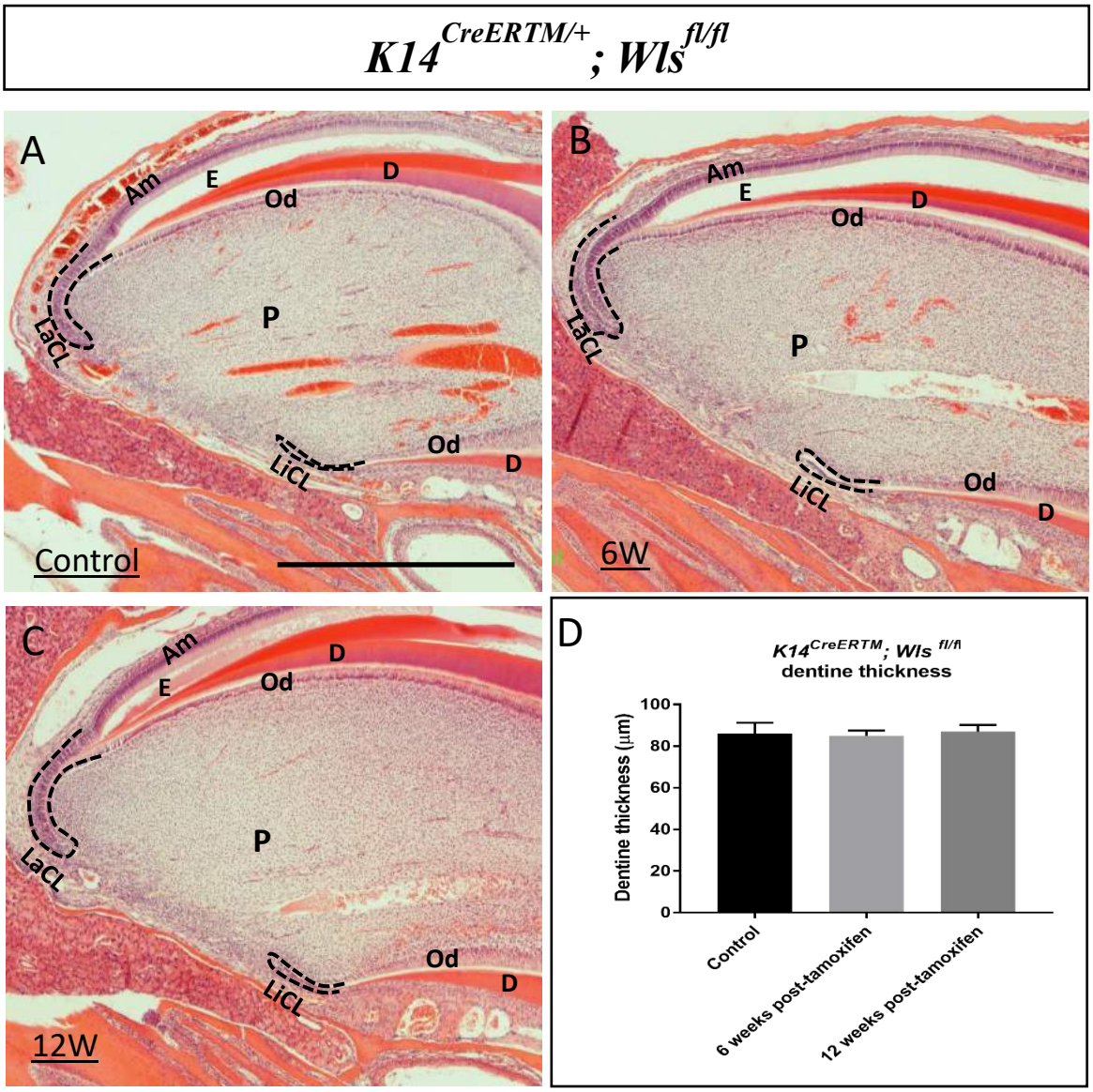

Figure 5.3. H&E staining for *K14*$^{CreERTM/+}$; *Wls*$^{fl/fl}$ mouse incisors. (A-C) Corn-oil treated mouse incisor (n=3) shows no abnormalities. The cervical loop is intact and both enamel and dentin are not interrupted. The tamoxifen treated ***K14***$^{CreERTM/+}$***; Wls***$^{fl/fl}$ mouse incisors (6 (n=3) and 12 (n=3) weeks post-tamoxifen) also show no abnormal histology. Enamel and dentine look normal with no resorption or increased thickness. Nevertheless, the epithelial cervical loop has normal size and shape and odontoblasts have columnar normal shape. (D) Unpaired t-test analysis for dentin thickness shows no significant different.

(LaCL) Labial cervical loop, (LiCL) Lingual cervical loop, (E) enamel space, (D) Dentine, (P) Pulp, (Am) Ameloblasts, (Od) odontoblasts. Scale bar = 1000 µm.

5.2.3. Inhibition of Wnt ligand secretion from TACs and odontoblasts

Axin2 has been identified as TACs and odontoblast markers as shown in Chapter 3. To further study the sources of Wnt ligands secretion which can control mouse incisor homeostasis and regulate TACs and odontoblasts functions, Wnt secretion was blocked from *Axin2*+ve cells by crossing *Axin2*^{CreERT2} mouse line with *Wls*$^{fl/fl}$ mouse line. *Axin2*^{CreERT2}*; Wls*$^{fl/fl}$ mice were treated with three IP injections of either corn oil or tamoxifen (2mg/dose) in 3 consecutive days. Mice were then collected after 3 (n=3), 6 (n=3), and 12 weeks (n=3).

5.2.3.1. µ-CT analysis of *Axin2*^{CreERT2}*; Wls*$^{fl/fl}$ mouse incisor

Axin2^{CreERT2}*; Wls*$^{fl/fl}$ mouse skulls were collected and scanned. µ-CT data analysis for the mouse incisors was compared to the corn oil-treated mouse incisors (n=3) which have enamel at the labial side covering the dentine structure and the pulp space in the middle of the incisor. (Figure 5.4 A) Tamoxifen-treated *Axin2*^{CreERT2}*; Wls*$^{fl/fl}$ mice incisors showed abnormal phenotype similar to the ubiquitous Wls deletion. The abnormal phenotype for both mouse lines was characterised by cervical area disruption and increased dentine thickness.

The µ-CT scan analysis of this group, which was collected three weeks after the tamoxifen treatment (n=3), showed abnormal incisor phenotype. The labial side of the incisor, which consists of enamel and dentine, was intact. Enamel was normal and covers the dentine layer. There was no resorption, yet dentine looks thicker than the control incisor. However, the incisor lingual side showed an abnormal finding where the cervical end has a defective dentine structure. The dentine layer covering the lingual wall of the cervical area has completely disappeared, leading to an irregular shaped apex. (Figure 5.4 B).

With time, an accumulative effect of the disruption can be seen, wherein the second group, which was collected six weeks after tamoxifen treatment (n=3), µ-CT scan analysis showed a

more severe incisor phenotype. The incisor labial-side dentine layer was elongated with a thicker dentine at the cervical end. The incisor lingual side showed more resorption and irregularities and the dentine layer resorption progressed to reach the middle of the incisor. Moreover, increased dentine thickness consequentially narrowed the pulp space (Figure 5.4 C).

12 weeks post-tamoxifen *Axin2^{CreERT2}; Wls$^{fl/fl}$* mouse incisor showed that the lingual side of the incisor has more dentine resorption, and dentine thickness was increased. The labial side of the incisor has no sign of resorption. (Figure 5.4 D).

The incisor length was affected, and tamoxifen treated mouse incisors length were significantly reduced. The control (corn oil treated mouse) has an incisor length of 11.24 ± 0.02963 mm. 3 weeks post-tamoxifen incisor length was 11.08 ± 0.04333 mm which was significantly shorter than the control incisor (P= 0.0337). 6 weeks post tamoxifen mouse incisor length was 10.96 ± 0.06839 mm which was significantly shorter than the control one (P=0.0198). Finally, 12 weeks post tamoxifin incisor length was 10.77 ± 0.1453 mm which also was significantly shorter (P=0.0324) (Figure 5.4 E)

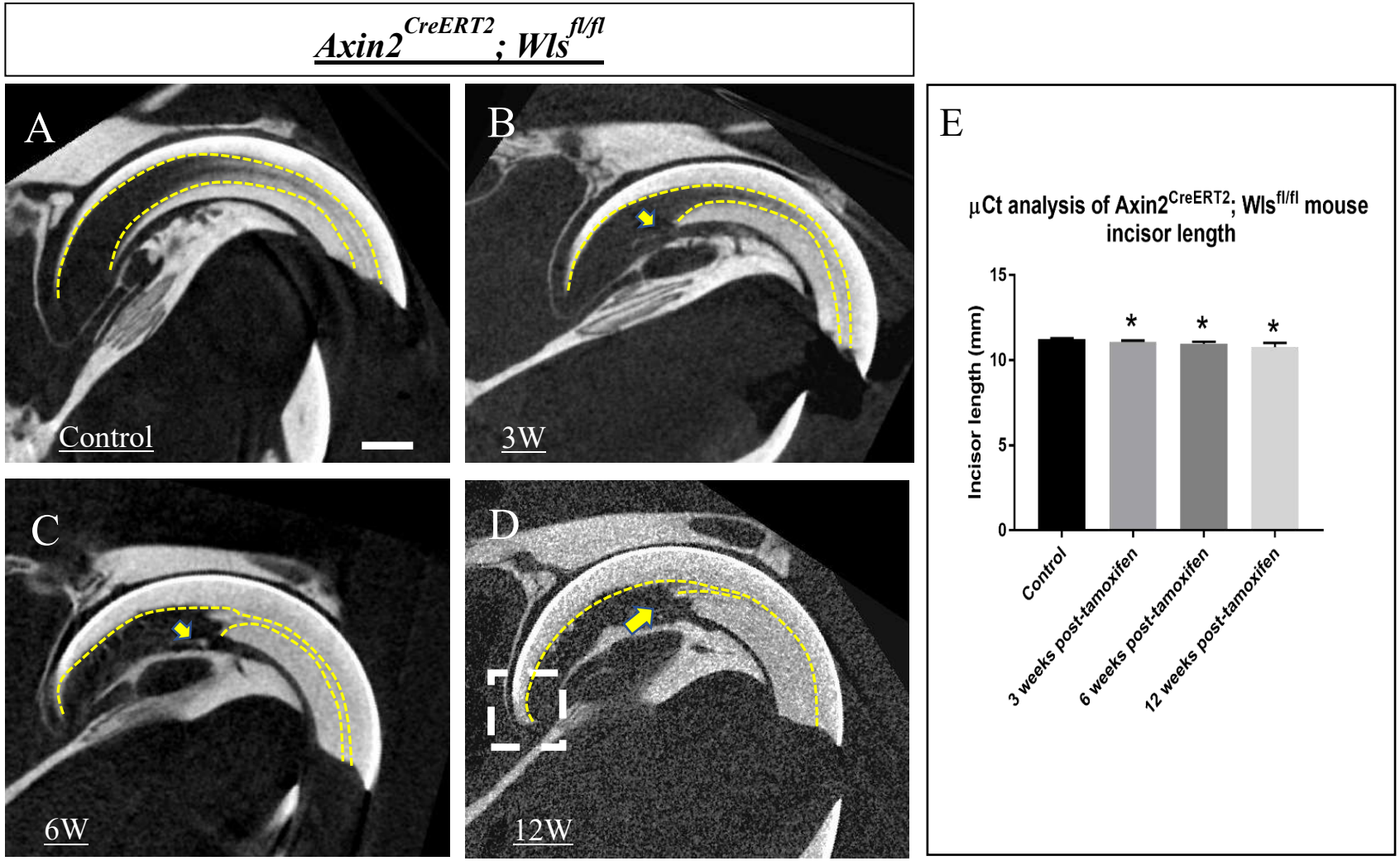
Axin2CreERT2; Wlsfl/fl
A
Control
B
3W
C
6W
D
12W
E
µCt analysis of Axin2CreERT2; Wlsfl/fl mouse incisor length
Incisor length (mm)
15
10
5
0
*
*
*
Control
3 weeks post-tamoxifen
6 weeks post-tamoxifen
12 weeks post-tamoxifen

Figure 5.4. Inhibition of Wnt ligand secretion from TACs and odontoblasts leads to abnormal incisor phenotype.

(A-D) µ-Ct scan of *Axin2*^{CreERT}; *Wls*$^{fl/fl}$ mouse incisor. (A) Corn oil treated mouse incisor (n=3) shows no abnormalities. (B) 3 weeks post-tamoxifen treated mouse incisor (n=3) have developed cervical area disruption and lingua dentin is lost. (C) 6 weeks post-tamoxifen treated mouse incisor (n=3) shows severe abnormalities at the cervical area with disruption(arrow) and thicker dentine. (D) 12 weeks post-tamoxifen treated mouse incisor (n=3) shows more dentine thickness and disruption at the cervical area.

(E) incisor length of tamoxifen treated *Axin2*^{CreERT}; *Wls*$^{fl/fl}$ mouse is reduced due to the cervical area disruption. 3, 6, and 12 weeks post-tamoxifen treated mice have significantly shorter incisors (n=3 each).

(P) pulp, (D) dentine. Scale bar = 1000 µm. *p<0.05

5.2.3.2. H&E staining analysis of *Axin2*^{CreERT2}; *Wls*$^{fl/fl}$ mouse incisor

Mouse incisors histology consists of three main parts; epithelial tissue surrounding the tooth, ameloblasts surrounding the enamel, odontoblasts lining the dentine, and the dental pulp in the middle of the tooth. The epithelial tissue forms a loop at the cervical area known as a cervical loop.

To study the role of Wnt ligand secreted by *Axin2*+ve TACs and odontoblasts on the mouse incisors, H&E histological analysis was performed for *Axin2*^{CreERT2}; *Wls*$^{fl/fl}$ mouse incisor. The outcomes were compared with the corn oil-treated mouse incisors (n=3), which have a normal incisor histology (Figure 5.5 A).

Three weeks post-tamoxifen *Axin2*^{CreERT2}; *Wls*$^{fl/fl}$ mouse (n=3) has an abnormal phenotype. The labial cervical loop was smaller and squashed because of the ectopic dentine formation at the distal border of the loop and the lingual cervical loop has disappeared because of the resorption and disruption of the lingual dentine. Dentine thickness was significantly increased, and its average thickness was 133 ± 4.583 µm (P= 0.0102). Odontoblasts were irregular with some of them longer than the others, which gave them a pseudostratified-like appearance. However, the

odontoblasts distal to the lingual cervical loop were vanished. The pulp space looks wider in the cervical area because of the loss of the lingual dentine (Figure 5.5 B).

Incisors of 6 weeks post-tamoxifen treated *Axin2^{CreERT2}; Wls$^{fl/fl}$* mouse (n=3) showed more disruption at the cervical area and more dentine formation. The labial cervical loop is smaller than the previous tamoxifen treated group and the lingual cervical loop disappeared. The lingual-side dentine showed more resorption that reaches the middle of the tooth. Dentine thickness was significantly increased, and the average thickness was 284.3 μm (± 13.45) (P= 0.0002) (Figure 5.5 C).

Incisor abnormal phenotype of 12 weeks post-tamoxifen treated *Axin2^{CreERT2}; Wls$^{fl/fl}$* mouse (n=3) has more dentine thickness where the average dentine thickness was 356.7 ± 16.33μm (p=.0001). The labial cervical loop was completely squashed by the ectopic dentine formation at the distal wall of the loop, while the lingual cervical loop disappeared because of the dentine resorption (Figure 5.5 D).

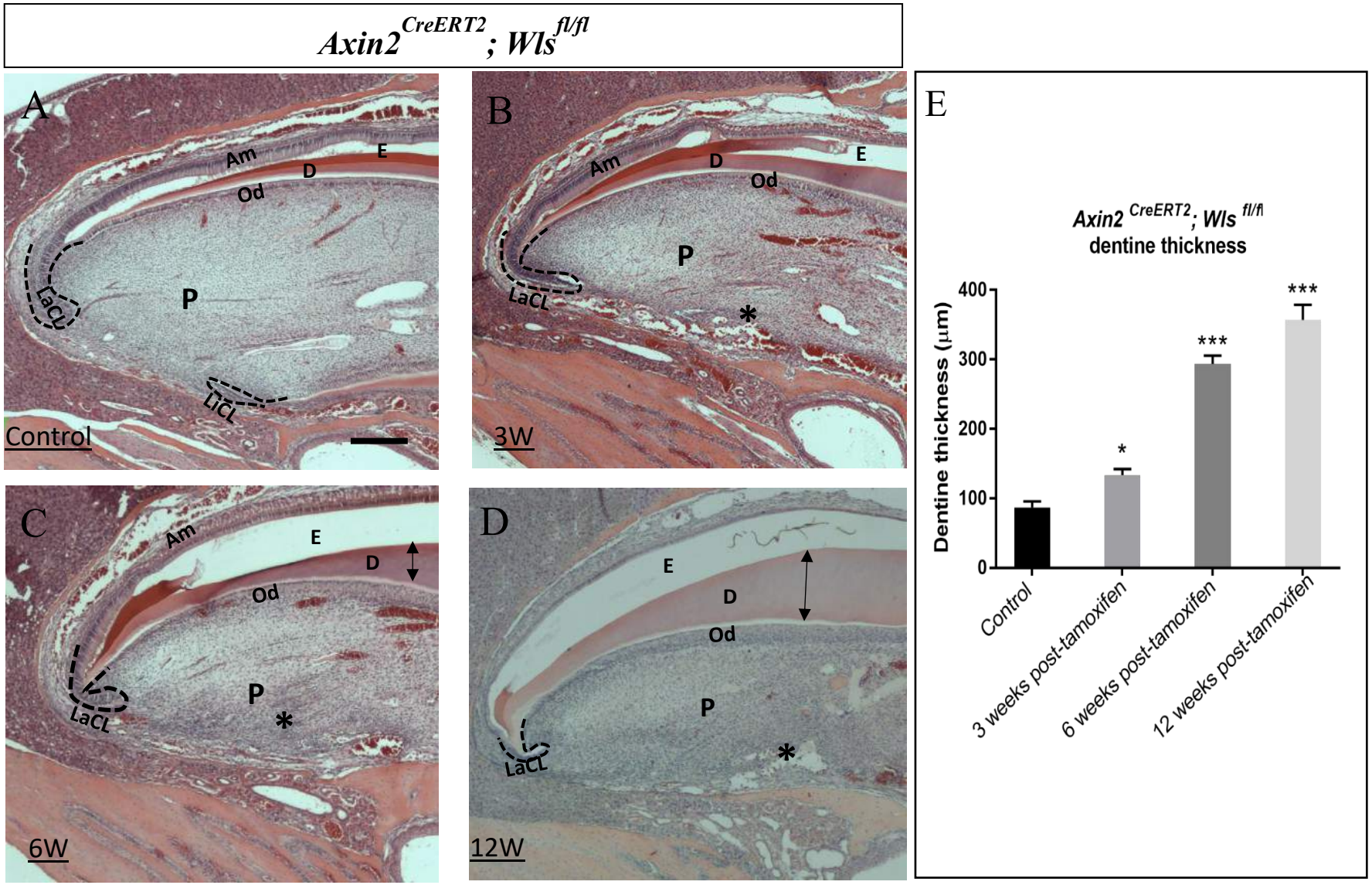
Axin2 CreERT2; Wls fl/fl
A
Am
E
D
Od
P
LaCL
LiCL
Control
B
3W
C
6W
D
12W
E
Axin2 CreERT2; Wls fl/fl
dentine thickness
Dentine thickness (μm)
400
300
200
100
0
*
***
***
Control
3 weeks post-tamoxifen
6 weeks post-tamoxifen
12 weeks post-tamoxifen

Figure 5.5. Inhibition of Wnt secretion from TACs and odontoblasts causes cervical area disruption and thicker dentine.

(A-D) H&E staining for *Axin2*$^{CreERT2/+}$*; Wls*$^{fl/fl}$ mouse incisors. (A) Corn-oil treated mouse incisor (n=3) shows no abnormalities at the cervical area. (B) 3 weeks post-tamoxifen treated mouse incisors (n=3) have an abnormal phenotype. The cervical area is disrupted and lingual cervical loop is lost (black star). (C) 6 weeks post-tamoxifen treated mouse incisor (n=3) exhibits an abnormal phenotype, dentine thickness is increased (black double headed arrow). The cervical area disruption and dentine resorption are both increased The labial cervical loop is smaller. (D) 12 weeks post-tamoxifen treated mouse incisor (n=3) shows a similar phenotype to the previous group but with a thicker dentine.

(E) Quantification of dentine thickness shows dentine thickness is significantly increasing for tamoxifen treated *Axin2*$^{CreERT2/+}$*; Wls*$^{fl/fl}$ mouse incisors (n=3 each)

(LaCL) Labial cervical loop, (LiCL) Lingual cervical loop, (E) enamel space, (D) Dentine, (P) Pulp, (Am) Ameloblasts, (Od) odontoblasts. Scale bar = 100 μm. ***p<0.05, ***p<0.0001

5.2.3.3. Gene expression in *Axin2*^{CreERT2}*; Wls*$^{fl/fl}$ mouse incisor pulp

To investigate gene expression changes upon *Wls* deletion, RT-qPCR analysis comparing corn oil and tamoxifen-treated *Axin2*^{CreERT2}*; Wls*$^{fl/fl}$ mouse incisor dental pulp cells was performed. *Axin2*^{CreERT2}*; Wls*$^{fl/fl}$ mice were tamoxifen treated (n=3) and control mice were given corn oil (n=3) and collected after one week. 3 runs of triplicate cDNA were done.

RT-qPCR data analysis showed that *Wls* expression was significantly reduced to 0.8468 ± 0.0238 fold changes (P<0.001). Wnt/β-catenin signaling target genes Axin2 and Lef-1 were significantly upregulated (P <0.0001) that *Axin2* expression was 2.423 ± 0.08954 and *Lef-1* was 2.446 ± 0.1093 increased fold changes. Moreover, *Dspp* gene expression was significantly increased to 1.263 ± 0.04681fold changes (P<0.001) (Figure 5.6)

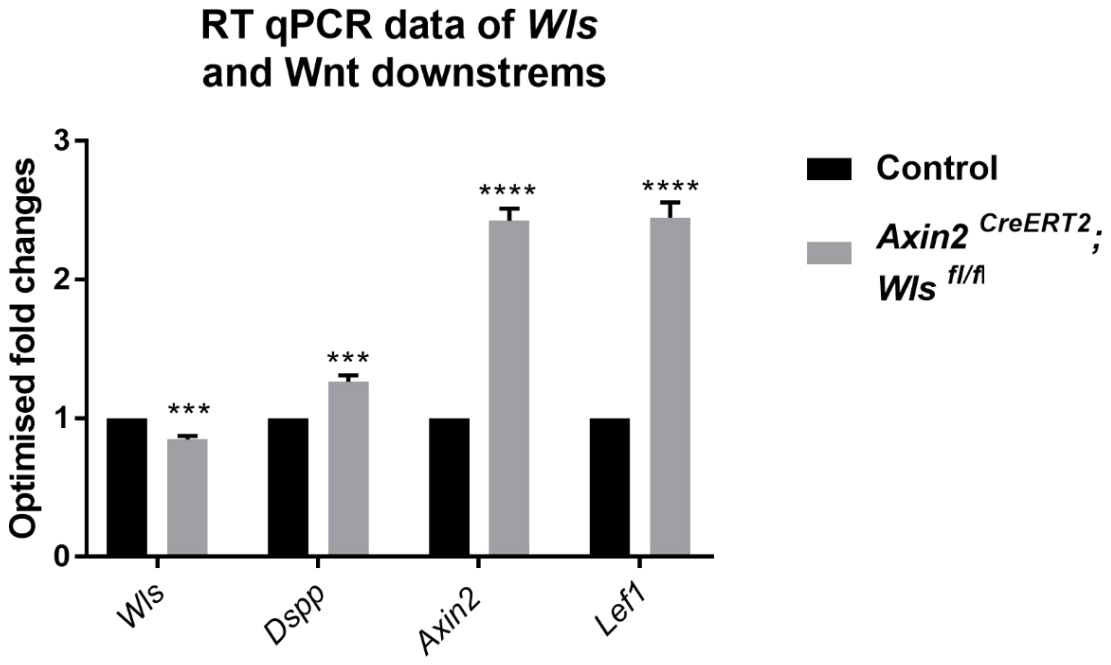

Figure 5.6. Wnt ligand secretion inhibition from TACs and odontoblasts affect Wnt downstream expression level in mouse incisors.

RT-qPCR data analysis for1 week post-tamoxifen *Axin2*^{CreERT2}; *Wls*$^{fl/fl}$ mouse incisor compared to corn oil treated mouse incisor cDNA shows that Wls expression is significantly downregulated. Wnt downstream (*Axin2* and *Lef-1*) expression are significantly reduced. However, *Dspp*, which is a downstream of Wnt-10a signaling, has a significant high expression.

4.2.6 Wnt ligand secretion from *Axin2*-expressing cells controls TACs proliferation

To investigate the role of Wnt ligand secretion from TACs and odontoblasts in the mesenchymal cell proliferation, BrdU nucleotide incorporation chase experiment was done on $Axin2^{CreERT2}$; $Wls^{fl/fl}$ mouse incisors. Mice were divided into two groups; the first was treated with corn oil (n=3), and the other was treated with tamoxifen (n=3). BrdU single injection was given 24 hours before the collection. Immunofluorescent histochemistry results showed that control group incisors labelled cells were in the area distal to the cervical loop and some of the odontoblasts. Tamoxifen-treated mouse incisors showed that BrdU labelled cells are reduced in the dental pulp mesenchyme, indicating a lower proliferation rate of the fast cycling TACs. (Figure 5.7)

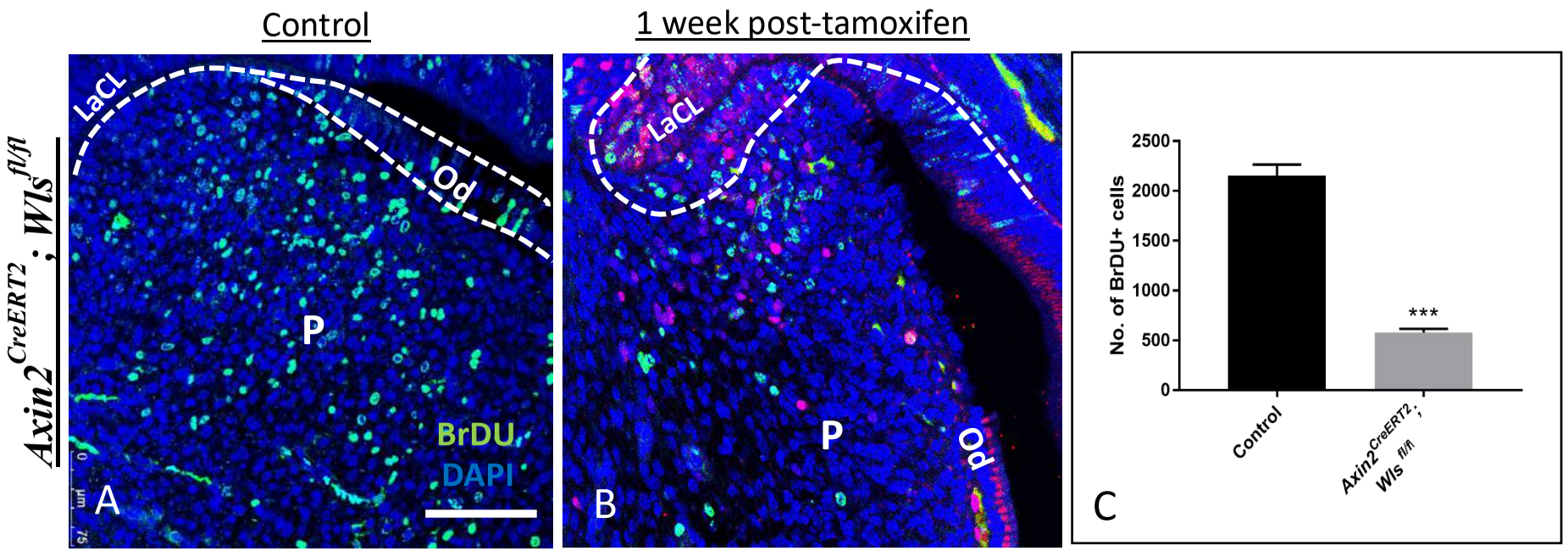

Figure 5.7. BrDU neuclease incorporation for 1 week post tamoxifen treated *Axin2^{CreERT2}; Wls$^{fl/fl}$* mouse incisor after 24 hours (fast dividing cells).

(A) Corn oil treated mouse incisor (n=3) shows number of TACs are BrDU+ cells at the area distal to the cervical loop (TACs zone) and some odontoblast as well. (B) 1 week post tamoxifen treated mouse incisor (n=3) shows less number of BrDU+ cells at the same area.

(C) Unpaired t-test analysis for BrDU+ cell count shows a significant decrease in proliferating TACs at the cervical area of 1 week post-tamoxifen for *Axin2^{CreERT2}; Wls$^{fl/fl}$* mouse incisor (n=3).

(LaCL) Labial cervical loop, (P) dental pulp, (D) Dentine. Scale bar 100 um. ***p<0.001

4.2.7 TACs and odontoblasts-derived Wnt ligands controls incisor growth rate

To study mouse incisor growth, 6 *Axin2* ^{CreERT2}*; Wls* $^{fl/fl}$ mice were divided into two groups; the first was treated with corn oil, and the other was treated with tamoxifen. Three injections of either tamoxifen or corn oil were given intraperitoneally on 3 consecutive days. 1 weeks after treatment, lower left incisor was clipped to enhance incisor growth, and a notch was done on the enamel close to the gingiva of both lower incisors to follow up incisor growth. Measurements were taken every day from the notch to gingival line. The mice then were sacrificed 1 week after that.

The growth rate for the control non-clipped mouse incisor was 0.9778 ± 0.0111mm/day while it was 0.242 ± 0.03972 mm/day for the tamoxifen treated mouse incisor. Compared to the control corn oil-treated mice, 1 week post tamoxifen treated mouse incisors growth rate was significantly reduced ($P<0.0001$). Enhancing incisor growth by clipping the incisor to acclerate the growth showed that the corn oil treared incisor growth rate was 1.2148 ± 0.1637mm/day and the tamoxifen treated mouse incisor growth rate was 0.317 ± 0.0462 mm/day. Unpaired t-test statistical analysis showed a significant reduced growth rate ($P<0.0001$) (Figure 5.8)

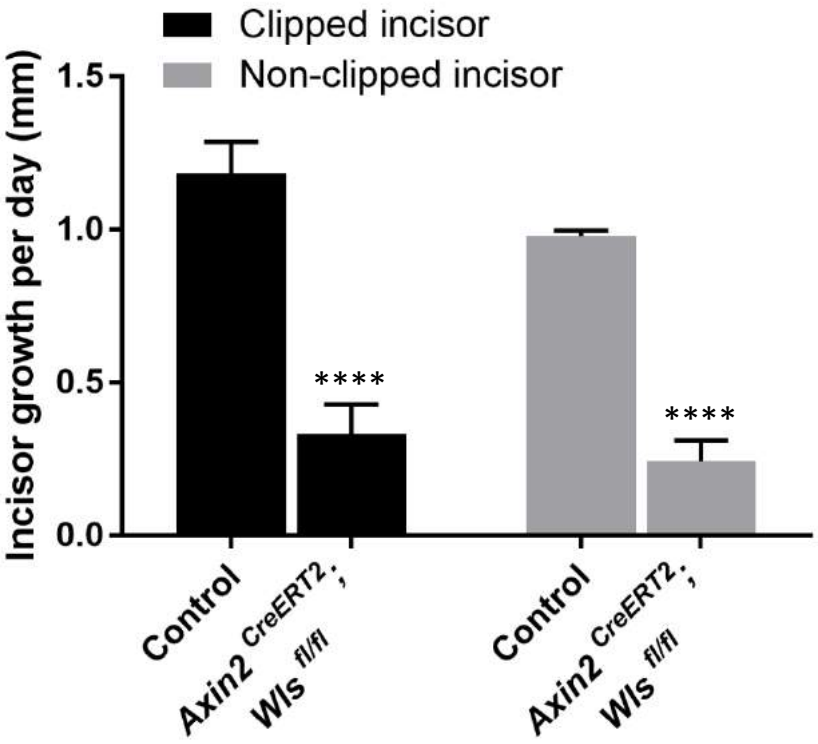

Figure 5.8. Inhibition of Wnt ligand secretion from TACs and odontoblasts reduces mouse incisor growth rate.

Analysis of daily growth rate of mouse incisor, (A) homeostatic status, where only a notch was made to the tooth, and (B) injury status, where incisor was clipped to enhance the growth, shows that inhibition of Wnt ligand secretion from both TACs and odontoblasts greatly affect incisor growth rate. Both scenarios have shown a highly significant reduction in daily growth rate. ****$p<0.0001$

5.2.3.4. Lineage tracing of *Wls* knocked-out *Axin2*-expressing cells

To study the behaviour ofWls deleted *Axin*- expressing cells *in vivo*, *Axin2^{CreERT2}; Wls$^{fl/fl}$* mouse line was crossed with *Rosa26R$^{mT/mG}$* mouse reporter. Adult (4-6 weeks old) *Axin2^{CreERT2}; Wls$^{fl/fl}$; Rosa26R$^{mT/mG}$* mice were treated with 3 tamoxifen injection in 3 consecutive days and then were divided into four groups and collected after 1 (n=3), 3 (n=3), 7 (n=3), and 14 (n=3) days. It was shown in Chapter 3 that *Axin2*-expressing cells reside at the cervical area distal to the MSC niche and then proliferate and differentiate into either odontoblasts or pulp cells.

5.2.3.4.1. 1-day post-tamoxifen treated *Axin2^{CreERT2}; Wls$^{fl/fl}$; Rosa26R$^{mT/mG}$* mouse incisor

Immunofluorescent staining for green fluorescent protein (GFP) has shown the behaviour of *Wls* depleted *Axin2*+ve cells. Recently after the administration of tamoxifen, GFP+ cells were seen in the dental pulp. Some cells in the MSC niche between the cervical loop were GFP+ and more cells were detected distal to the MSC niche, in particular TAC zone and some of the odontoblasts. However, no GFP+ cells were detected inside the labial cervical loop or the epithelial tissue lining the outer surface of the tooth. (Figure 5.9)

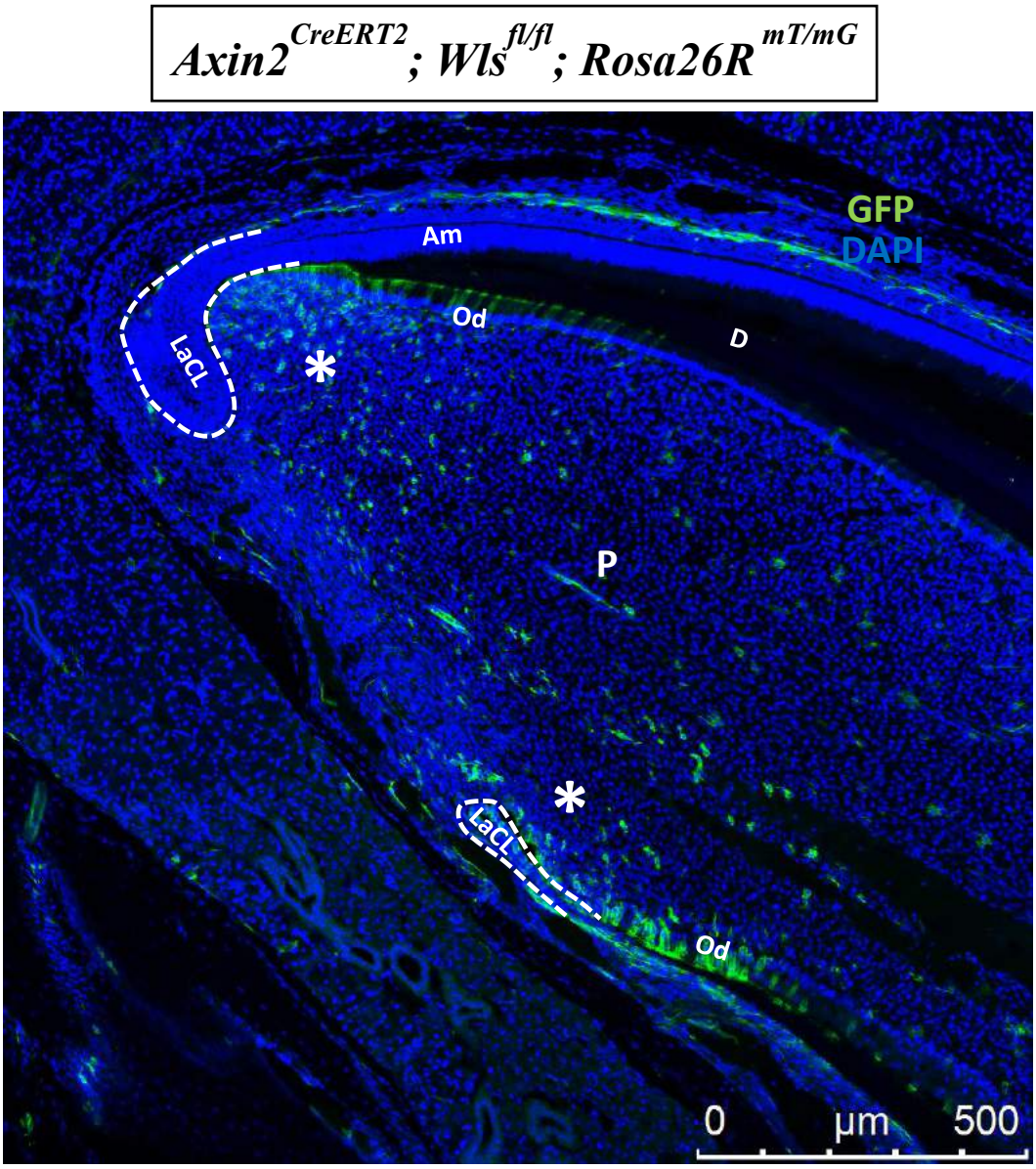

Figure 5.9. GFP immunofluorescent staining for 1 day post-tamoxifen *Axin2*^{CreERT2}; *Wls*$^{fl/fl}$; *Rosa26R*$^{mT/mG}$ mouse incisor 1 day post tamoxifen.

A small population of Wnt depleted Axin2+ve cells at the cervical area, positive staining is located at TACs zone distal to the cervical loop and few odontoblasts. (LaCL) Labial cervical loop, (LiCL) lingual cervical loop, (D) Dentine, (P) Pulp, (Am) ameloblasts, (Od) odontoblasts. Scale bar = 500 µm

5.2.3.4.2. 3-days post-tamoxifen treated *Axin2^{CreERT2}; Wls$^{fl/fl}$; Rosa26R$^{mT/mG}$* mouse incisor

Further investigation of the lineages of *Wls* depleted *Axin2*+ cells showed mainly more GFP+ cells. The MSC niche between the cervical loop showed more GFP+ cells as well as the TAC zone. More odontoblasts comparing to the first group were GFP+. However, no GFP+ cells were detected within the labial cervical loop. The lingual cervical loop has shown some GFP+ cells within the loop. The epithelial layer lining the outer surface and ameloblasts show a small population of GFP+ cells. Even though *Wls* have been depleted, *Axin2*+ cells were capable to proliferate and differentiate, and new unusual cells became GFP+ such as ameloblasts and epithelial cells within the lingual cervical loop (Figure 5.10)

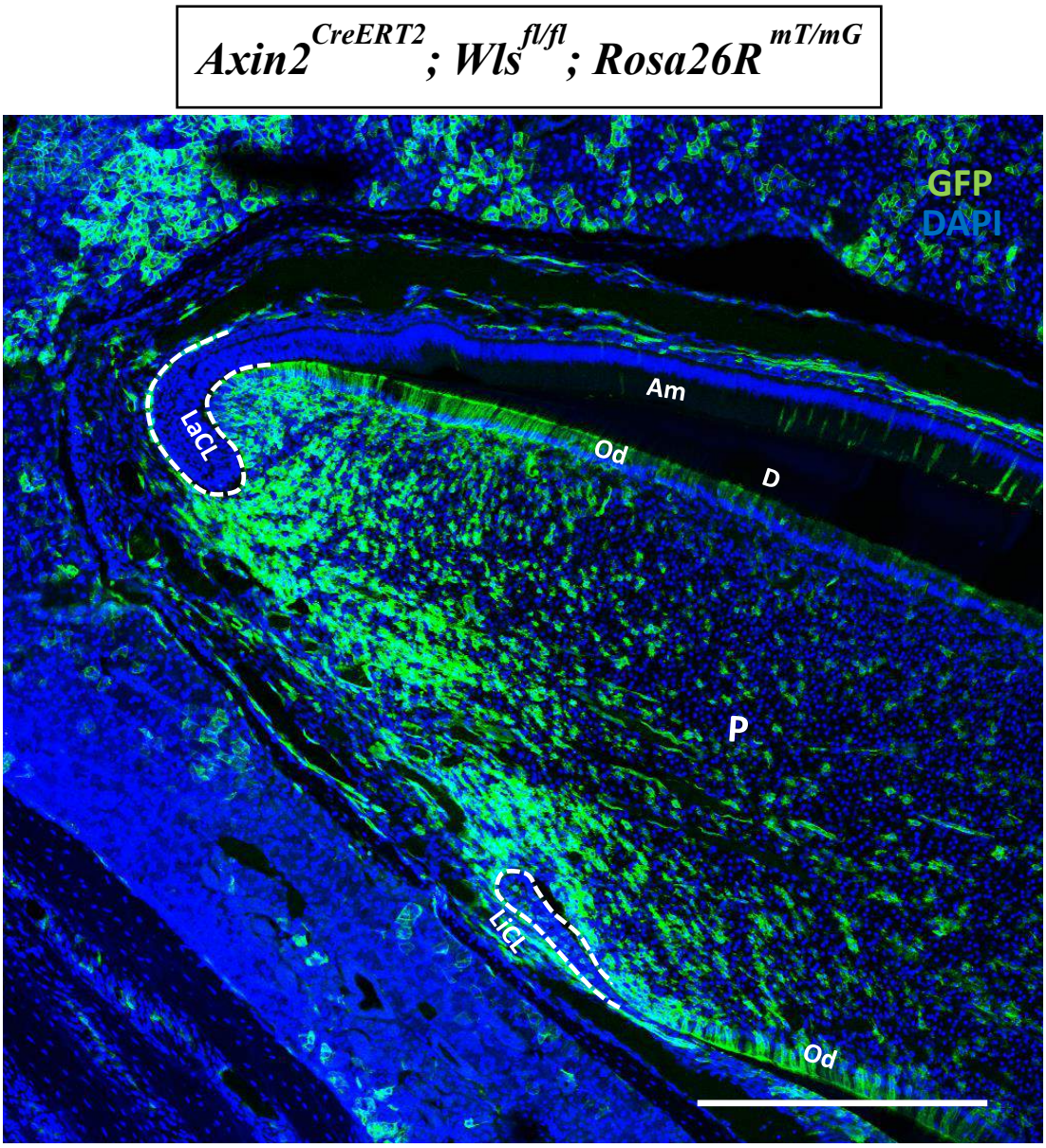

Figure 5.10 GFP immunofluorescent staining for 3 days post-tamoxifen *Axin2*^{CreERT2}; *Wls*$^{fl/fl}$; *Rosa26R*$^{mT/mG}$ mouse incisor.

Wnt depleted Axin2+ve cells at the cervical area are located at MSCs niche,TACs zone distal to the cervical loop and odontoblasts.

(LaCL) Labial cervical loop, (LiCL) lingual cervical loop, (D) Dentine, (P) Pulp, (Am) ameloblasts, (Od) odontoblasts. Scale bar = 500 µm

5.2.3.4.3. 7 days post-treatment

This group which was collected 7 days after the tamoxifen treatment showed an abnormal dentine resorption in the lingual side of the cervical area. Looking at GFP+ cells, the MSC niche still has a population of GFP+ cells but this population is smaller than the previous group. Distal to this population, TACs are still proliferating and differentiating into odontoblasts and pulp cells and more GFP+ cells could be seen at the cervical area. The epithelial cervical loop has no GFP+ cells but some ameloblasts are GFP+. Looking at the lingual side of the cervical area, particularly distal to the lingual cervical loop, an area of dentine disruption was formed. In this area, most GFP+ cells are pulp cells and no odontoblasts were in this area (Figure 5.11).

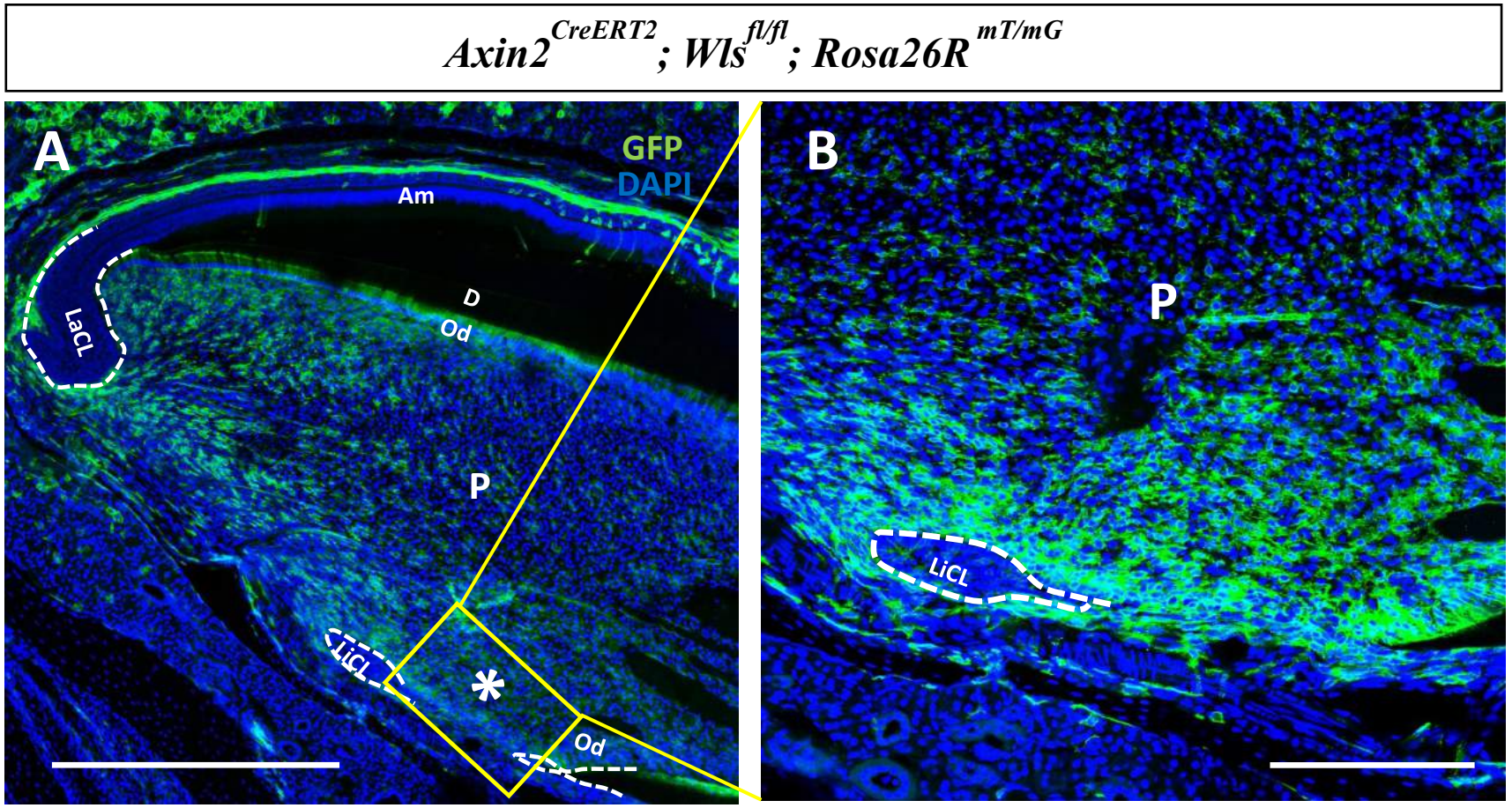

Figure 5.11. GFP immunofluorescent staining for 7 days post-tamoxifen *Axin2*^{CreERT2}; *Wls*$^{fl/fl}$; *Rosa26R*$^{mT/mG}$ mouse incisor.

(A) Wnt depleted Axin2+ve cells are proliferating and differentiating more at the labial side of the incisor. The disrupted area (star) was formed and separated the lingual cervical loop.

(B) More positive cells can be seen in TACs zone next to the disrupted area.

(LaCL) Labial cervical loop, (LiCL) lingual cervical loop, (D) Dentine, (P) Pulp, (Am) ameloblasts, (Od) odontoblasts. Scale bar, (A) 500 µm, (B) 100 µm.

5.2.3.4.4. 14-days post-treatment

14 days post-tamoxifen treated *Axin2^{CreERT2}; Wls$^{fl/fl}$; Rosa26R$^{mT/mG}$* mouse incisor showed GFP+ cells that was detected at the MSC niche were moving distally, a phenomenon similar to the lineage tracing of *Axin2+* cells (Chapter 3). The MSC zone has a small population of GFP+ cells and the TACs zone showed a lower number of GFP+ cells. However, some odontoblastic at the cervical area were still GFP+. The majority of the moved GFP+ cells were localised at the centre of the dental pulp with a cloudy green fluorescent appearance. Even though in the previous two groups, some mesenchymal stem cells were GFP+, in this group no cells in the MSC niche were GFP+. Looking at the lingual dentine resorption area, no GFP+ cells can be seen at the lingual cervical loop area (Figure 5.12).

***Axin2*^{CreERT2}; *Wls*$^{fl/fl}$; *Rosa26R*$^{mT/mG}$**

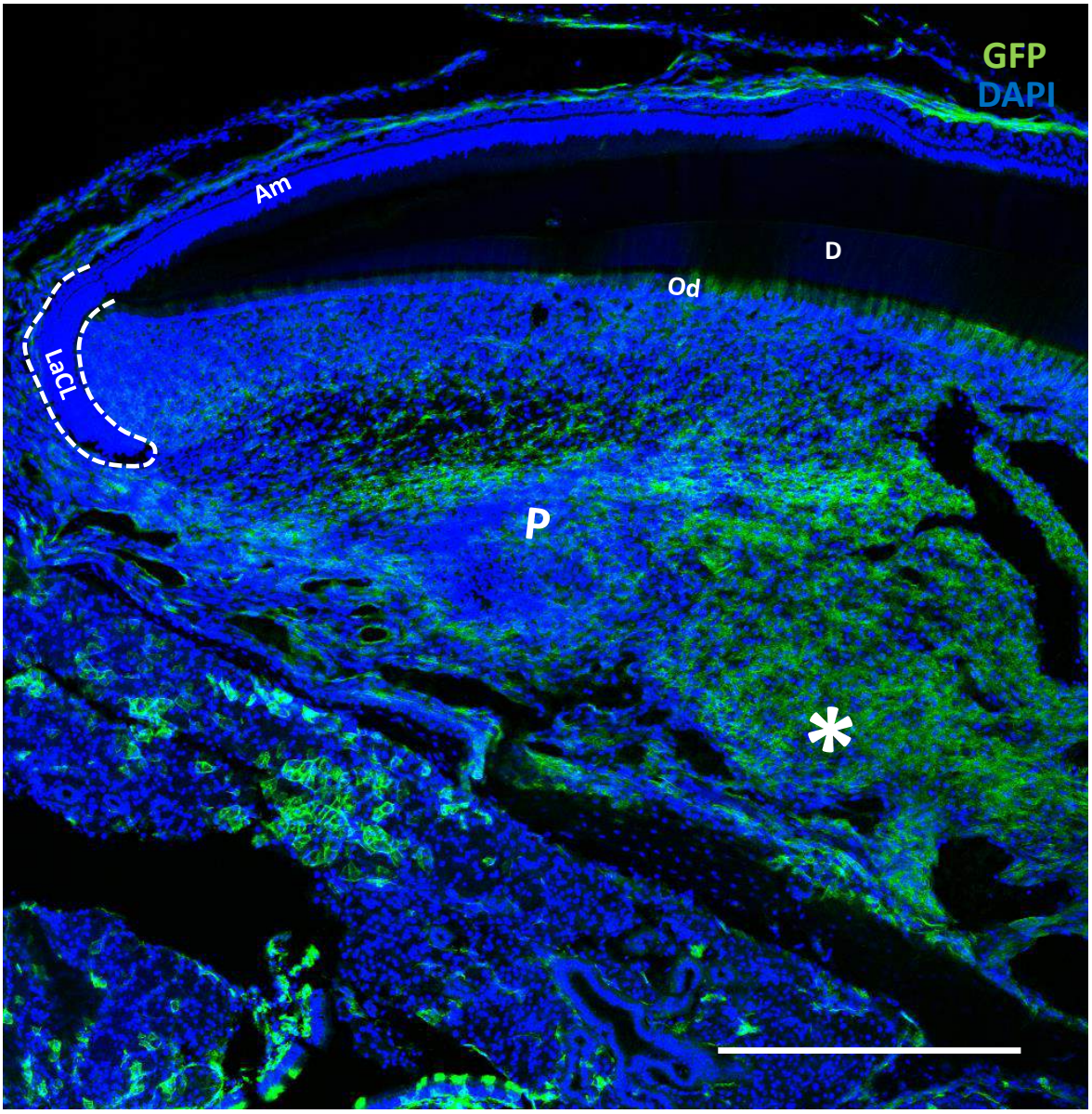

Figure 5.12 GFP immunofluorescent staining for 14 days post-tamoxifen *Axin2*^{CreERT2}; *Wls*$^{fl/fl}$; *Rosa26R*$^{mT/mG}$ mouse incisor.

Less Wnt depleted Axin2+ve cells can be detected at the cervical loop area. The positive moved distally (star) toward the incisal end. The disruption of the cervical area continues, and the lingual cervical loop disappeared.

(LaCL) Labial cervical loop, (D) Dentine, (P) Pulp, (Am) ameloblasts, (Od) odontoblasts. Scale bar = 500 µm

5.3. Discussion

5.3.1. Different sources of Wnt ligands in the mouse incisor pulp

Lim et al. (2014) showed the requirement for Wnt activation in the mouse incisors by knocking out *Wls* from the *OCN*-expressing cells, such as osteocytes and odontoblasts. Depletion of Wnt secretion affects bone remodelling and dentine secretion so that skull bone has lower mineralisation, while it is the opposite in the dentine mineralisation. However, inhibition of Wnt secretion from *OCN*-expressing cells does not have an incisor cervical area disruption and the abnormalities are restricted to odontoblasts functions.

In Chapter 4, inhibition of Wnt secretion ubiquitously illustrated the importance of the Wnt pathway in mouse incisors growth and homeostasis that an abnormal incisor phenotype chracterised by cervical area disruption, increased dentine thickness and reduced growth rate was formed. Suomalainen and Thesleff (2010) showed that Wnt ligands are secreted in many of the dental tissue, therefore, identifying the Wnt ligand secreting cells which contribute to the continuous incisor growth is crucial. Thus, utilising tamoxifen incucibe *Cre* lines to inhibits Wnt secretion from the MSCs by using $Gli1^{CreERT2}$; $Wls^{fl/fl}$ transigenic mouse line, Wnt secretion inhibition from the epithelial cells by using $K14^{CreERTM}$; $Wls^{fl/fl}$ transgenic mouse line and inhibition of Wnt secretion from TACs and odontoblasts by using $Axin2^{CreERT2}$; $Wls^{fl/fl}$ transigenic mouse line were helpful tools to identify the Wnt ligand secretory cells which are responsible for the incisor growth. To this end, inhibition of Wnt secretion from different Wnt secreting cells were investigated, and the results of the different conditional knock out were compared to the ubiquitous Wnt pathway inhibition data.

5.3.1.1. Epithelial Wnt secretion has no direct effect on mouse incisor growth

During development, Wnt ligand is expressed in the dental epithelium tissue such as outer epithelium, pre-ameloblasts and ameloblasts, while it is not expressed in the epithelial stem cells (Suomalainen and Thesleff, 2010). Epithelial Wnt secretion has shown a vital role in the incisor development participating in the epithelial-mesenchymal interaction during the different stages of tooth development (Thesleff, 2003). Epithelial Wnt signaling interacts with the mesenchymal one that upregulation of Wnt/β-catenin signaling in the oral epithelium downregulate Wnt/β-catenin signaling in the dental pulp mesenchyme (Järvinen *et al*., 2006). Ameloblasts, enamel-secreting cells, are not Wnt-responsive cells (Suomalainen and Thesleff, 2010; Yang et al., 2015). So, Wnt ligand secretion inhibition would not affect their function. However, Jarvinen et al. (2006) showed that inhibition of Wnt ligands secretion from either ameloblasts or odontoblasts during development leads to increased enamel production with no abnormal incisor phenotype formation.

However, the results obtained from inhibiting Wnt ligand secretion from the epithelial cells showed that no apparent shape or dimension abnormalities were developed in the adult mouse incisors. Wnt ligand secreted from epithelial cells in adult mouse incisors growth did not regulate mesenchymal and epithelial stem cells, TACs and odontoblasts, which suggests they do not have a role in mouse incisor growth. This is because mouse incisor dental pulp is enclosed between hard tissues, namely enamel and dentine, to protect it from oral pathogens, and the only tooth opening is the apical region of the tooth which has no epithelial tissues capable of secreting Wnt ligands (Suomalainen and Thesleff, 2010). Thus, epithelial Wnt ligand could not reach the adult mouse incisor pulp tissue and therefore has no role in incisor growth.

The epithelial cells are adjacent to the PDL and alveolar bone and they might have a role in their maintenance and PDL attachment to the tooth. The role of Wnt/β-catenin pathway in bone is well known, yet, the results obtained from inhibiting Wnt ligand secretion from the epithelial cells showed no abnormal resorption of alveolar bone. Moreover, the Wnt ligands responsible for activating Wnt pathways such as Wnt-3a and Wnt-5a, which regulate the canonical Wnt pathway for the production of OPG, and non-canonical pathway which controls the production of RANKL respectively (Westendorf et al., 2004; Krishnan et al., 2006), are not secreted by the epithelial cells. Therefore, inhibition of Wnt ligand secretion from epithelial cells have no role in alveolar bone remodelling.

5.3.1.2. Mesenchymal stem cell secretes Wnt ligands to control TACs

The mesenchymal stem cells were first identified within the bone marrow and then were found in many other locations such as blood, adipose tissue, bone and muscle (Caplan and Bruder, 2001). Wnt signaling has a crucial role in the regulation of proliferation and differentiation of MSCs *in vitro* (Ling et al., 2009). *In vitro* studies showed that canonical Wnt signaling maintains and enhances stem cells' self-renewal and keeps them in an undifferentiated state (Boland et al., 2004; Cho et al., 2006). Moreover, Wnt/β-catenin signaling regulates MSCs functions by controlling cyclin D1 and c-Myc (Baek et al., 2003) and it regulates MSCs proliferation ability where overexpression of LRP5 enhances MSCs proliferation (Baksh et al., 2007). However, non-canonical Wnt signaling antagonises the effect of Wnt/β-catenin signaling that overexpression of Wnt-5a downregulates the cyclin D1 level and reduces the MSC proliferation rate (Baksh and Tuan, 2007). In the mouse incisor, Wnt/β-catenin may not directly control MSC functions (as shown in Chapter 3), however, the results obtained from Wnt ligand inhibition from MSCs experiments showed that TAC abilities to proliferate and

differentiate to odontoblasts were downregulated, which leads to the incisor cervical area disruption. Thus, mouse incisor MSCs regulate TACs function and incisor growth by secreting Wnt ligands to activate the Wnt pathway on the TACs.

5.3.1.3. TACs secrete Wnt ligands and control TAC-odontoblast differentiation and odontoblast functions

Wnt signaling pathways control the stem cell lineage specification and differentiation of human MSCs *in vitro* (Boland et al., 2004; Etheridge et al., 2004). Over-activation of Wnt/β-catenin signaling can enhance osteogenesis in MSC and enhances osteoblast formation through upregulation of Runx2, Dlx5 or Osterix (Bennett et al., 2005). Odontoblasts, which are *OCN*-expressing cells (Lim et al., 2014; Bae et al., 2015), required Wnt signaling to regulate dentine secretion via regulating *Dspp* expression (Yamashiro et al., 2007). Wnt secretion inhibition from *OCN*-expressing cells affects hard tissue secreting cells differently, so named upregulation of odontoblast function while downregulation of osteoblast function (Lim et al., 2014). No cervical area disruption displayed when Wnt secretion was blocked from *OCN*-expressing cells. This is because TACs functions are not affected because TACs are not *OCN*-expressing cells and it also suggests that odontoblasts are not signaling back through Wnt pathways to TACs to control TACs-odontoblasts differentiation.

In the mouse dental pulp, the results obtained from the inhibition of Wnt ligand secretion from TACs and odontoblasts showed that an abnormal incisor phenotype similar to the the ubiqoutous Wnt ligand inhibition was formed. However, the severity and abnormalities were less when Wnt ligand secretion was inhibited from TACs and odontoblasts. This maybe because . Results obtained from RT-qPCR data showed *Wls* was not completely knocked out from the dental pulp When *Wls* was knocked out from *Axin2*-expressing cells suggesting that

MSCs were not affected upon *Wls* deletion and they could still generate new TACs capable of secreting Wnt ligands to replace the mutated TACs. Thus, inhibition of Wnt ligand secretion from *Axin2*-expressing cells has a temporary effect until mutated cells are replaced.

Furthermore, genetic lineage tracing of *Wls* mutated Axin2-expressing cells showed that mutated cells can still behave normally, in that they proliferate at the TAC zone and differentiate into odontoblasts. However, the odontoblasts differentiation distal to the lingual cervical loop was abnormal and led to the formation of more pulp cells instead of odontoblasts, which caused a dentine defect in that area, and together with the reduced TACs proliferation decreased incisor growth rate. Thus, TACs and odontoblasts secrete Wnt ligands to auto-activate Wnt pathway to regulate their functions.

5.4. Conclusion

To identify the source of Wnt ligand in the dental tissues, different transgenic mouse lines were used to block Wnt ligand secretion from epithelial cells, MSCs, TACS and odontoblasts and compared to the ubiquitous deletion of *Wls* data. It is known that different dental tissues are capable of secreting Wnt ligands, but the influence of these Wnt ligands in adult mouse incisor growth was not clear. The inhibition of Wnt ligand secretion from epithelial cells does not affect the incisor growth or the PDL maintenance. Thus, Wnt ligands secreted from epithelial cells are not contributed in the adult mouse incisor growth. However, Wnt secreted from the dental mesenchyme has shown a crucial effect in both mouse incisor growth and cell fate. Inhibition of Wnt ligand secretion from mesenchymal stem cells affects TACs and odontoblasts function and leads to cervical area disruption. Finally, inhibiting Wnt ligand secretion from TACs and odontoblasts has shown an abnormal incisor phenotype similar to the ubiquitous Wnt secretion inhibition. Thus, TACs and odontoblasts functions are controlled by Wnt/β-catenin signaling and they can both secrete and respond to their own Wnt ligands and respond to other Wnt ligands received from different sources, such as MSCs.

Chapter 6. General discussion and future consideration

6.1. Mouse incisor TACs and odontoblasts have dual Wnt signaling activation mechanisms

Wnt signaling is a short-range pathway, that means the producing cell is a neighbour cell to the responding cell (Clevers, 2006). However, sometimes stem cells auto-activate the Wnt pathway by producing their own Wnt ligands (Lim et al., 2016). Wnt/β-catenin signaling has a vital role in the maintenance of the active hair follicle stem cells, while it is absent in the rest stage. Its role is to specify stem cell progenies in the follicle and to maintains stem cells identity. Lim et al. (2016) showed that hair follicle stem cells have an autocrine Wnt/β-catenin signaling activation system where the secreting cells are responding to their own secreted Wnt ligands.

The data presented in this project collectively have shown that mouse incisor TACs and odontoblast have both ways of activation; autocrine and paracrine. Inhibiting Wnt secretion from TACs affects their functions and furthermore downregulates TAC differentiation to odontoblasts. Odontoblasts were also been affected that loss of Wnt signaling function enhances their ability to secrete dentine matrix indicating an autocrine activation mechanism of Wnt pathway. Both TACs and odontoblasts were affected when Wnt ligand secretion was inhibited from the adjacent MSCs which indicates the paracrine activation mechanism of Wnt pathway. Thus, TACs and odontoblasts respond to their own secreted Wnt ligands and also Wnt ligands from other sources, which can illustrate the Wnt pathway's highly conserved and complicated role in these populations.

The data obtained from $OCN^{Cre}; Wls^{fl/fl}$ and $Axin2^{CreERT2}; Wls^{fl/fl}$ transgenic mouse line showed that odontoblast-derived Wnt ligands only have a role in odontoblasts with no direct role in TACs. Both mouse lines have upregulated odontoblast functions that increases dentine thickness. However, mouse incisor cervical area disruption was only seen when the Wnt ligand

secretion was depleted from TACs (*Axin2*^{CreERT2}*; Wls*$^{fl/fl}$ transgenic mouse) while no cervical area disruption develops when Wnt ligand was inhibited from *OCN*-expressing odontoblasts. This indicates that odontoblasts could not signal back to TACs via Wnt signaling.

6.2. Mouse incisor TACs responsiveness to Wnt signaling is different according to their location

TACs at the cervical area differentiate to either odontoblast or pulp cells and their functions to proliferate and terminally differentiate to odontoblasts are controlled by the Wnt pathway. *Wls* knock-out from different cell populations have shown how TAC and odontoblast abilities have been mediated so that the lingual part of the incisor is lost, and the labial side has enhanced odontoblast ability to secrete more dentine matrix. However, a strange outcome was seen when Wnt ligands secretion was inhibited from MSCs so that both labial and lingual dentine were lost. Therefore, I hypothesised that there are at least two TACs populations at the cervical area of the tooth.

Analysing the data obtained from the different *Wls* knock-out mouse lines showed that TACs act differently to Wnt signaling according to where they reside. On the labial side, TACs can secrete Wnt ligands to auto-activate the pathway which supress TAC to odontoblast differentiation. This mechanism is antagonised by Wnt ligands secreted by MSCs. This can explain the dentine loss on the incisor labial side when Wnt ligands secretion was inhibited from MSCs that the antagonising effect of the MSC-derived Wnt ligand to supress Wnt ligand production in TACs will be deleted. Therefore, TAC-derived Wnt ligands will supress TAC to odontoblast differentiation and causes dentine defect. It also explains why odontoblast differentiation was increased in the labial side when Wnt secretion was inhibited from either TACs or ubiquitously. TAC-derived Wnt ligand role to inhibit odontoblast differentiation will be deleted which leads to increased odontoblast differentiation (Figure 6.1).

On the lingual side, MSCs secrete Wnt to activate TAC-derived Wnt ligands production in the lingual side, and TACs produce Wnt ligand to auto-activate the Wnt/β-catenin pathway to induce odontoblast differentiation. Thus, whenever Wnt secretion is inhibited from either MSCs, TACs or both, loss of odontoblast differentiation at the lingual side of the tooth occurred (Figure 6.1).

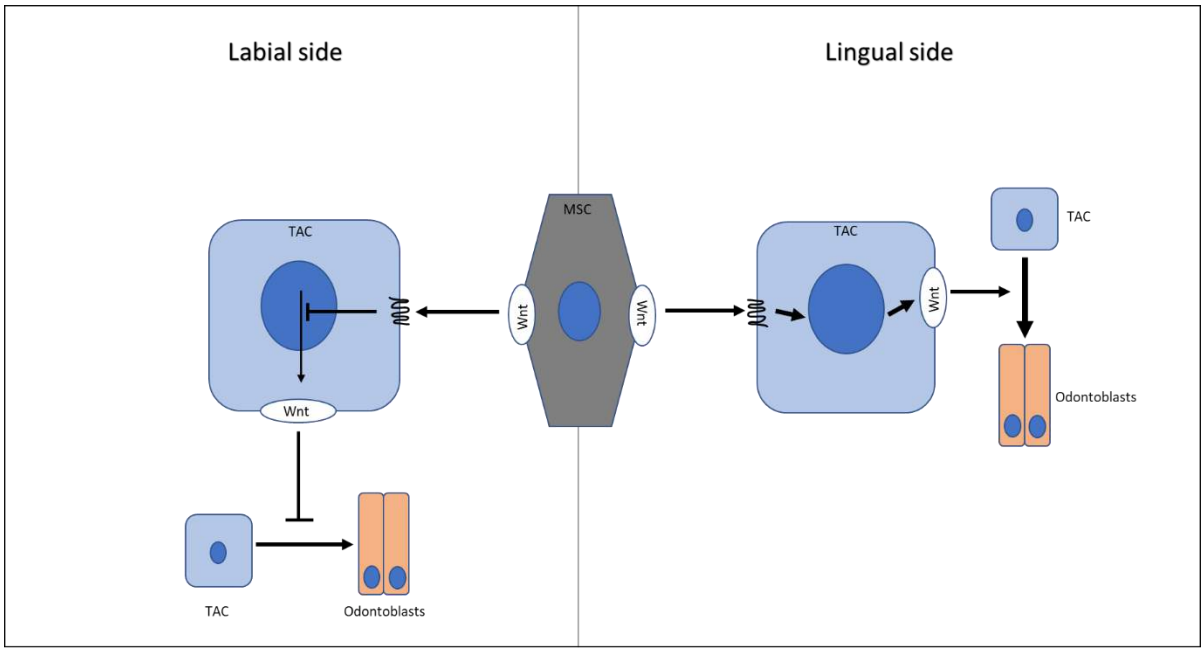

Figure 6.1. TACs in mouse incisor respond to Wnt signalling differently according to their location

The Wnt pathway inhibits TACs function in the labial side while it activates and enhances TACs and odontoblasts functions at the lingual side of the mouse incisor.

6.3. Other factors can control Wnt signaling to regulate MSC functions

The data presented in this project showed that Wnt signaling controls TACs function, and loss of Wnt pathway leads to the formation of an abnormal incisor phenotype. Moreover, MSCs which are Wnt-secreting cells, do not respond to Wnt signaling. However, MSC apoptosis occurs when the Wnt pathway is depleted. In our publication, we conclude that TACs, Wnt-responsive cells, might have a positive feedback mechanism to MSCs that loss of TACs caused MSCs apoptosis (An, Akily et al., 2018). Ring1 regulates the Wnt/β-catenin pathway which is involved in the control of cell proliferation, stem cell self-renewal, and cell fate, and is associated with several diseases (Clevers, 2006; Reya and Clevers, 2005). Loss of either the Ring1 or Wnt pathway leads to TACs and MSCs apoptosis. Through the inhibition of Zic transcription factors, PRC1 sustains Wnt/β-catenin activity and preserves adult stem cell identities (Chiacchiera et al., 2016) indicating that Wnt/β-catenin activity is required for the stem cell maintenance (An, Akily et al., 2018).

6.4. Future consideration and plans

This project has expanded my understanding on how the Wnt pathway can control teeth regeneration. To fulfil many of the aims of this project, different Wnt ligand null models are considered to understand the role of every single Wnt ligand in mouse incisor TACs and odontoblasts.

Mouse incisor MSCs are controlled by Shh signaling (Zhao et al., 2014) and it expresses *Gli1*, one of Shh signals downstream. It is known that Wnt and Shh pathways interfere with each other. To understand the role of Wnt pathway deletion on Shh pathway, an experiment is planned to study Wnt pathway activity in mouse incisors of the depleted Shh pathway. Another experiment, to study Shh activity on depleted Wnt pathway mouse incisors, is also planned.

Ubiquitous Wnt pathway deletion showed the vital role of the pathway. However, this model affects both canonical and non-canonical Wnt pathways. To study the non-canonical Wnt pathway role, a rescue model is planned by giving lithium chloride to activate the canonical pathway and therefore limit the effect of Wls deletion on non-canonical Wnt pathway.

Wnt pathway deletion demonstrated an abnormal phenotype similar to human teeth ageing that exhibits both pulp canal thinning and dentine stone in the dental pulp, suggesting that Wnt-based drugs could treat the side-effects of teeth ageing.

Bibliography

Adaimy, Lynn, Eliane Chouery, Hala Megarbane, Salman Mroueh, Valerie Delague, Elsa Nicolas, Hanen Belguith, Philippe de Mazancourt, and Andre Megarbane. 2007. "Mutation in WNT10A Is Associated with an Autosomal Recessive Ectodermal Dysplasia: The Odonto-Onycho-Dermal Dysplasia." *American Journal of Human Genetics* 81 (4): 821–28. https://doi.org/10.1086/520064.

Ahn, Sohyun, and Alexandra L Joyner. 2004. "Dynamic Changes in the Response of Cells to Positive Hedgehog Signaling during Mouse Limb Patterning That Shh Is Both Sufficient for and Necessary to Pattern the Distal Limb Skeletal Elements in a Concentration- Dependent Manner, with Digit 5 Requiring Th." *Cell* 118: 505–16.

Van Amerongen, R, A N Bowman, and R Nusse. 2012. "Developmental Stage and Time Dictate the Fate of Wnt/Beta-Catenin-Responsive Stem Cells in the Mammary Gland." *Cell Stem Cell* 11 (3): 387–400. https://doi.org/10.1016/j.stem.2012.05.023.

Amit S, Hatzubai A, Birman Y, Andersen JS, Ben-Shushan E, Mann M, Ben-Neriah Y, Alkalay I. 2002. Axin-mediated CKI phosphorylation ofβ-catenin at Ser 45: A molecular switch for the Wnt pathway. *Genes Dev* 16: 1066–1076.

An, Zhengwen, Basem Akily, Maja Sabalic, Guo Zong, Yang Chai, and Paul T. Sharpe. 2018. "Regulation of Mesenchymal Stem to Transit-Amplifying Cell Transition in the Continuously Growing Mouse Incisor." *Cell Reports* 23 (10): 3102–11. https://doi.org/10.1016/j.celrep.2018.05.001.

Aulehla, Alexander, Christian Wehrle, Beate Brand-Saberi, Rolf Kemler, Achim Gossler, Benoit Kanzler, and Bernhard G. Herrmann. 2003. "Wnt3a Plays a Major Role in the Segmentation Clock Controlling Somitogenesis." *Developmental Cell* 4 (3): 395–406. https://doi.org/10.1007/s10327-010-0221-x.

Austin TW, Solar GP, Ziegler FC, Liem L, Matthews W. A role for the Wnt gene family in haematopoiesis: expansion of multilineage progenitor cells. Blood. 1997;89:3624e3635.

Babb R, Chandrasekaran D, Carvalho Moreno Neves V, Sharpe PT. Axin2-expressing cells differentiate into reparative odontoblasts via autocrine Wnt/β-catenin signaling in response to tooth damage. *Sci Rep*. 2017 Jun 8;7(1):3102. doi: 10.1038/s41598-017-03145-6. PubMed PMID: 28596530; PubMed Central PMCID: PMC5465208.

Bae, C H, T H Kim, S O Ko, J C Lee, X Yang, and E S Cho. 2015. "Wntless Regulates Dentin Apposition and Root Elongation in the Mandibular Molar." *J Dent Res* 94 (3): 439–45. https://doi.org/10.1177/0022034514567198.

Baek, S.H., et al., 2003. Regulated subset of G1 growth-control genes in response to derepression by the Wnt pathway. *Proc. Natl. Acad. Sci*. U. S. A. 100, 3245–3250.

Baksh, D., Boland, G.M., Tuan, R.S., 2007. Cross-talk between Wnt signaling pathways in human mesenchymal stem cells leads to functional antagonism during osteogenic differentiation. *J. Cell. Biochem*. 101, 1109–1124.

Baksh, D., Tuan, R.S., 2007. Canonical and non-canonical Wnts differentially affect the development potential of primary isolate of human bone marrow mesenchymal stem cells. *J. Cell. Physiol*. 212, 817–826.

Banziger, C., Soldini, D., Schutt, C., Zipperlen, P., Hausmann, G., and Basler, K. (2006). Wntless, a conserved membrane protein dedicated to the secretion of Wnt proteins from signaling cells. *Cell* 125, 509-522

Barrott, J.J., Cash, G.M., Smith, A.P., Barrow, J.R., and Murtaugh, L.C. (2011). Deletion of mouse Porcn blocks Wnt ligand secretion and reveals an ectodermal etiology of human focal dermal hypoplasia/Goltz syndrome. *Proc Natl Acad Sci* U S A 108, 12752-12757.

Barrow, J R, K R Thomas, O Boussadia-Zahui, R Moore, R Kemler, M R Capecchi, and A P McMahon. 2003. "Ectodermal Wnt3/Beta-Catenin Signaling Is Required for the Establishment and Maintenance of the Apical Ectodermal Ridge." *Genes Dev* 17 (3): 394–409. https://doi.org/10.1101/gad.1044903.

Begue-Kirn, C., Ruch, J.V., Ridall, A.L., and Butler, W.T. (1998). Com- parative analysis of mouse DSP and DPP expression in odonto- blasts, preameloblasts, and experimentally induced odontoblast- like cells. *Eur. J. Oral Sci.* 106 (suppl 1), 254–259.

Bei, M., Maas, R., 1998. FGFs and BMP4 induce both Msx1-independentand Msx1-dependent signaling pathways in early tooth development.*Development* 125, 4325–4333

Bennett, Christina N, Kenneth A Longo, Wendy S Wright, Larry J Suva, Timothy F Lane, Kurt D Hankenson, and Ormond A MacDougald. 2005. "Regulation of Osteoblastogenesis and Bone Mass by Wnt10b." *Proceedings of the National Academy of Sciences of the United States of America* 102 (9): 3324–29. https://doi.org/10.1073/pnas.0408742102.

Bergstein, I., Eisenberg, L.M., Bhalerao, J., Jenkins, N.A., Cope- land, N.G., Osborne, M.P., Bowcock, A.M., and Brown, A.M. (1997). Isolation of two novel WNT genes, WNT14 and WNT15, one of which (WNT15) is closely linked to WNT3 on human chromosome 17q21. *Genomics* 46, 450–458.

Bianco, P, and P G Robey. 2015. "Skeletal Stem Cells." *Development* 142 (6): 1023–27. https://doi.org/10.1242/dev.102210.

Bodine PV, Komm BS. Wnt signaling and osteoblastogenesis. Rev Endocr Metab Disord. 2006 Jun;7(1-2):33-9. doi: 10.1007/s11154-006-9002-4. *Review. PubMed* PMID: 16960757.

Boland, G.M., Perkins, G., Hall, D.J., Tuan, R.S., 2004. Wnt 3a promotes proliferation and suppresses osteogenic differentiation of adult human mesenchymal stem cells. *J. Cell.* Biochem. 93, 1210–1230

Bradley, E W, and M H Drissi. 2011. "Wnt5b Regulates Mesenchymal Cell Aggregation and Chondrocyte Differentiation through the Planar Cell Polarity Pathway." *J Cell Physiol* 226 (6): 1683–93. https://doi.org/10.1002/jcp.22499.

Brack, A.S., Conboy, I.M., Conboy, M.J., Shen, J., Rando, T.A., 2008. A temporal switch from notch to Wnt signaling in muscle stem cells is necessary for normal adult myogenesis. Cell. Stem. Cell. 2, 50–59

Brennan KR, Brown AM. Wnt proteins in mammary development and cancer. J Mammary Gland Biol Neoplasia. 2004 Apr;9(2):119-31. doi: 10.1023/B:JOMG.0000037157.94207.33. Review. PubMed PMID: 15300008.

Brisken, C., Heineman, A., Chavarria, T., Elenbaas, B., Tan, J., Dey, S.K., McMahon, J.A., McMahon, A.P., Weinberg, R.A., 2000. Essential function of Wnt-4 in mammary gland development downstream of progesterone signaling. Genes Dev. 14, 650–654.

Brocardo M, Henderson BR: APC shuttling to the membrane, nucleus and beyond. Trends Cell Biol 2008, 18:587-596.

Brookes, E., de Santiago, I., Hebenstreit, D., Morris, K.J., Carroll, T., Xie, S.Q., Stock, J.K., Heidemann, M., Eick, D., Nozaki, N., et al. (2012). Polycomb asso- ciates genome-wide with a specific RNA polymerase II variant, and regulates metabolic genes in ESCs. Cell Stem Cell 10, 157–170.

Bulchand S, Grove EA, Porter FD, Tole S. 2001. LIM-homeodomain gene Lhx2 regulates the formation of the cortical hem. Mech Dev 100:165–175.

Caprioli, A, A Villasenor, L A Wylie, C Braitsch, L Marty-Santos, D Barry, C M Karner, et al. 2015. "Wnt4 Is Essential to Normal Mammalian Lung Development." Dev Biol 406 (2): 222–34. https://doi.org/10.1016/j.ydbio.2015.08.017.

Carpenter, A C, S Rao, J M Wells, K Campbell, and R A Lang. 2010. "Generation of Mice with a Conditional Null Allele for Wntless." Genesis 48 (9): 554–58. https://doi.org/10.1002/dvg.20651.

Carroll, T J, J S Park, S Hayashi, A Majumdar, and A P McMahon. 2005. "Wnt9b Plays a Central Role in the Regulation of Mesenchymal to Epithelial Transitions Underlying Organogenesis of the Mammalian Urogenital System." Dev Cell 9 (2): 283–92. https://doi.org/10.1016/j.devcel.2005.05.016.

Catón J, Luder H-U, Zoupa M, Bradman M, Bluteau G, Tucker AS, et al. Enamel-free teeth: Tbx1 deletion affects amelogenesis in rodent incisors. Dev Biol 2009;328(2):493–505.

Cawthorn, W P, A J Bree, Y Yao, B Du, N Hemati, G Martinez-Santibanez, and O A MacDougald. 2012. "Wnt6, Wnt10a and Wnt10b Inhibit Adipogenesis and Stimulate Osteoblastogenesis through a Beta-Catenin-Dependent Mechanism." Bone 50 (2): 477–89. https://doi.org/10.1016/j.bone.2011.08.010.

Cegielska A, Gietzen KF, Rivers A, Virshup DM. 1998. Auto- inhibition of Casein Kinase Ie (CKI1) is relieved by pro- tein phosphatases and limited proteolysis. J Biol Chem 273: 1357–1364.

Chan, C K, E Y Seo, J Y Chen, D Lo, A McArdle, R Sinha, R Tevlin, et al. 2015. "Identification and Specification of the Mouse Skeletal Stem Cell." Cell 160 (1–2): 285–98. https://doi.org/10.1016/j.cell.2014.12.002.

Chatzistavrou X, Papagerakis S, Ma PX, Papagerakis P. Innovative approaches to regenerate enamel and dentine. Int J Dent. 2012;2012:856470. doi: 10.1155/2012/856470. Epub 2012 May 14. PubMed PMID: 22666253; PubMed Central PMCID: PMC3359805.

Chen, J, Y Lan, J A Baek, Y Gao, and R Jiang. 2009. "Wnt/Beta-Catenin Signaling Plays an Essential Role in Activation of Odontogenic Mesenchyme during Early Tooth Development." Dev Biol 334 (1): 174–85. https://doi.org/10.1016/j.ydbio.2009.07.015.

Chiacchiera, F., Rossi, A., Jammula, S., Piunti, A., Scelfo, A., Ordo´ n˜ez-Mora´ n, P., Huelsken, J., Koseki, H., and Pasini, D. (2016). Polycomb compex PRC1 preserves intestinal stem cell identity by sustaining Wnt/β- catenin transcriptional activity. Cell Stem Cell 18, 91–103.

Cho, H.H., Kim, Y.J., Kim, S.J., Kim, J.H., Bae, Y.C., Ba, B., Jung, J.S., 2006. Endogenous Wnt signaling promotes proliferation and suppresses osteogenic differentiation in human adipose derived stromal cells. Tissue. Eng. 12, 111–121

Chrepa, V., Henry, M. A., Daniel, B. J., & Diogenes, A. (2015). Delivery of Apical Mesenchymal Stem Cells into Root Canals of Mature Teeth. Journal of Dental Research, 94(12), 1653–1659. https://doi.org/10.1177/0022034515596527

Christian, J.L., Gavin, B.J., McMahon, A.P. & Moon, R.T. Isolation of cDNAs partially encoding four Xenopus Wnt-1/int-1-related proteins and characterization of their

transient expression during embryonic development. Dev. Biol. 143, 230–234 (1991).

Clevers, H. 2006. "Wnt/Beta-Catenin Signaling in Development and Disease." Cell 127 (3): 469–80. https://doi.org/10.1016/j.cell.2006.10.018.

Clevers, H, K M Loh, and R Nusse. 2014. "Stem Cell Signaling. An Integral Program for Tissue Renewal and Regeneration: Wnt Signaling and Stem Cell Control." Science 346 (6205): 1248012. https://doi.org/10.1126/science.1248012.

Cotsarelis G, Sun T-T, Lavker RM (1990) Label-retaining cells reside in the bulge area of pilosebaceous unit: Implications for follicular stem cells, hair cycle, and skin carcino- genesis. Cell 61(7):1329–1337.

Coombs, G.S., Yu, J., Canning, C.A., Veltri, C.A., Covey, T.M., Cheong, J.K., Utomo, V., Banerjee, N., Zhang, Z.H., Jadulco, R.C., et al. (2010). WLS-dependent secretion of WNT3A requires Ser209 acylation and vacuolar acidification. J Cell Sci 123, 3357-3367.

Cunningham, Thomas J., Sandeep Kumar, Terry P. Yamaguchi, and Gregg Duester. 2015. "Wnt8a and Wnt3a Cooperate in the Axial Stem Cell Niche to Promote Mammalian Body Axis Extension." Developmental Dynamics 244 (6): 797–807. https://doi.org/10.1002/dvdy.24275.

Dassule, H. R., and A. P. McMahon. 1998. Analysis of epithelial-mesenchymal interactions in the initial morphogenesis of the mammalian tooth. Dev. Biol. 202:215–227

Day CL, Alber T. 2000. Crystal structure of the amino-ter- minal coiled-coil domain ofthe APC tumor suppressor. J Mol Biol 301: 147–156.

DOWTHWAITE, G. P., BISHOP, J. C., REDMAN, S. N., KHAN, I. M., ROONEY, P., EVANS, D. J. R., HAUGHTON, L., BAYRAM, Z., BOYER, S., THOMSON, B., WOLFE, M. S. & ARCHER, C. W. 2004. The surface of articular cartilage contains a progenitor cell population. Journal of Cell Science, 117, 889-97.

Etheridge, S L, G J Spencer, D J Heath, and P G Genever. 2004. "Expression Profiling and Functional Analysis of Wnt Signaling Mechanisms in Mesenchymal Stem Cells." Stem Cells 22 (5): 849–60. https://doi.org/10.1634/stemcells.22-5-849.

ERICES, A., CONGET, P. & MINGUELL, J. J. 2000. Mesenchymal progenitor cells in human umbilical cord blood. British Journal of Haematology, 109, 235-42.

EVANS, M. J. & KAUFMAN, M. H. 1981. Establishment in culture of pluripotential cells from mouse embryos. Nature, 292, 154-6.

Fan L, Deng S, Sui X, Liu M, Cheng S, Wang Y, Gao Y, Chu CH, Zhang Q. Constitutive activation of β-catenin in ameloblasts leads to incisor enamel hypomineralization. J Mol Histol. 2018 Oct;49(5):499-507. doi: 10.1007/s10735-018-9788-x. Epub 2018 Jul 31. PubMed PMID: 30066216.

Farbod Famili, Martijn H. Brugman, Erdogan Taskesen, Brigitta E.A. Naber, Riccardo Fodde, Frank J.T. Staal,High Levels of Canonical Wnt Signaling Lead to Loss of Stemness and Increased Differentiation in Hematopoietic Stem Cells,Stem Cell Reports,Volume 6, Issue 5, 2016, Pages 652-659, ISSN 2213-6711, https://doi.org/10.1016/j.stemcr.2016.04.009.

Feng, J, A Mantesso, C De Bari, A Nishiyama, and P T Sharpe. 2011. "Dual Origin of Mesenchymal Stem Cells Contributing to Organ Growth and Repair." Proc Natl Acad Sci U S A 108 (16): 6503–8. https://doi.org/10.1073/pnas.1015449108.

Feng, J, G Yang, G Yuan, J Gluhak-Heinrich, W Yang, L Wang, Z Chen, et al. 2011. "Abnormalities in the Enamel in Bmp2-Deficient Mice." Cells Tissues Organs 194 (2–4): 216–21. https://doi.org/10.1159/000324644.

Fevr, S. Robine, D. Louvard, J. Huelsken, Wnt/β-catenin is essential for intestinal homeostasis and maintenance of intestinal stem cells. Mol. Cell. Biol. 27, 7551–7559 (2007). doi: 10.1128/MCB.01034-07; pmid: 17785439

Fotaki, V, O Larralde, S Zeng, D McLaughlin, J Nichols, D J Price, T Theil, and J O Mason. 2010. "Loss of Wnt8b Has No Overt Effect on Hippocampus Development but Leads to Altered Wnt Gene Expression Levels in Dorsomedial Telencephalon." Dev Dyn 239 (1): 284–96. https://doi.org/10.1002/dvdy.22137.

Frame S, Cohen P. 2001. GSK3 takes centre stage more than 20 years after its discovery. Biochem J 359: 1–16.

FRIEDENSTEIN, A. J., GORSKAJA, J. F. & KULAGINA, N. N. 1976. Fibroblast precursors in normal and irradiated mouse hematopoietic organs. Experimental Hematology, 4, 267-74.

Fu, J., Jiang, M., Mirando, A.J., Yu, H.M., and Hsu, W. (2009). Reciprocal regulation of Wnt and Gpr177/mouse Wntless is required for embryonic axis formation. Proc Natl Acad Sci U S A 106, 18598-18603.

Fujimori, Sayumi, Hermann Novak, Martina Weissenböck, Maria Jussila, Alexandre Gonçalves, Rolf Zeller, Jenna Galloway, Irma Thesleff, and Christine Hartmann. 2010. "Wnt/β-Catenin Signaling in the Dental Mesenchyme Regulates Incisor Development by Regulating Bmp4." Developmental Biology 348 (1): 97–106. https://doi.org/10.1016/j.ydbio.2010.09.009.

Gasnereau, I., Herr, P., Chia, P.Z., Basler, K., and Gleeson, P.A. (2011). Identification of an endocytosis motif in an intracellular loop of Wntless protein, essential for its recycling and the control of Wnt protein signaling. J Biol Chem 286, 43324-43333.

Geetha-Loganathan, P, S Nimmagadda, F Prols, K Patel, M Scaal, R Huang, and B Christ. 2005. "Ectodermal Wnt-6 Promotes Myf5-Dependent Avian Limb Myogenesis." Dev Biol 288 (1): 221–33. https://doi.org/10.1016/j.ydbio.2005.09.035.

Goss, A M, Y Tian, T Tsukiyama, E D Cohen, D Zhou, M M Lu, T P Yamaguchi, and E E Morrisey. 2009. "Wnt2/2b and Beta-Catenin Signaling Are Necessary and Sufficient to Specify Lung Progenitors in the Foregut." Dev Cell 17 (2): 290–98. https://doi.org/10.1016/j.devcel.2009.06.005.

Green, J., Nusse, R., and van Amerongen, R. (2014) The role ofRyk and Ror receptor tyrosine kinases in Wnt signal transduction. Cold SpringHarb. Perspect. Biol. 6, a009175

GRONTHOS, S., BRAHIM, J., LI, W., FISHER, L. W., CHERMAN, N., BOYDE, A., DENBESTEN, P., ROBEY, P. G. & SHI, S. 2002. Stem Cell Properties of Human Dental Pulp Stem Cells. Journal of Dental Research, 81, 531-535.

Guo, X., Day, T.F., Jiang, X., Garrett-Beal, L., Topol, L., Yang, Y., 2004. Wnt/beta-catenin signaling is sufficient and necessary for synovial joint formation. Genes Dev. 18, 2404–2417.

Guo, Z., LI, H., LI, X., YU, X., WANG, H., TANG, P. & MAO, N. 2006. In vitro characteristics and in vivo immunosuppressive activity of compact bone derived murine mesenchymal progenitor cells. Stem Cells, 24, 992-1000.

Hall, Anita C, Fiona R Lucas, and Patricia C Salinas. 2000. "Axonal Remodeling and Synaptic Differentiation in the Cerebellum Is Regulated by WNT-7a Signaling Becomes Multilobulated as It Interdigitates with GC Den- Drites (Hamori and Somogyi, 1983). The Increase in Mossy Fiber Surface Area Permits the Formation Of." Cell 100: 525–35. https://doi.org/10.1016/S0092-8674(00)80689-3.

Harada, H, T Toyono, K Toyoshima, M Yamasaki, N Itoh, S Kato, K Sekine, and H Ohuchi. 2002. "FGF10 Maintains Stem Cell Compartment in Developing Mouse Incisors." Development 129 (6): 1533–41. http://dev.biologists.org/content/develop/129/6/1533.full.pdf.

Harada, Hidemitsu, Päivi Kettunen, Han-Sung Jung, Tuija Mustonen, Y Alan Wang, and Irma Thesleff. 1999. "Localization of Putative Stem Cells in Dental Epithelium and Their Association with Notch and Fgf Signaling." The Journal of Cell Biology 147 (1): 105–20. https://doi.org/10.1083/jcb.147.1.105.

Hardcastle, Z., Mo, R., Hui, C.C., Sharpe, P.T., 1998. The Shh signalingpathway in tooth development—defects in Gli2 and Gli3 mutants.Development 125, 2803–2811.

Harterink, M., Port, F., Lorenowicz, M.J., McGough, I.J., Silhankova, M., Betist, M.C., van Weering, J.R., van Heesbeen, R.G., Middelkoop, T.C., Basler, K., et al. (2011). A SNX3-dependent retromer pathway mediates retrograde transport of the Wnt sorting receptor Wntless and is required for Wnt secretion. Nat Cell Biol 13, 914-923.

Hayashi, S, and A P McMahon. 2002. "Efficient Recombination in Diverse Tissues by a Tamoxifen-Inducible Form of Cre: A Tool for Temporally Regulated Gene

Activation/Inactivation in the Mouse." Dev Biol 244 (2): 305–18. https://doi.org/10.1006/dbio.2002.0597.

Hayman AR. Tartrate-resistant acid phosphatase (TRAP) and the osteoclast/immune cell dichotomy. Autoimmunity. 2008 Apr;41(3):218-23. doi: 10.1080/08916930701694667. Review. PubMed PMID: 18365835.

Heikkila, M., Peltoketo, H., Leppaluoto, J., Ilves, M., Vuolteenaho, O., Vainio, S., 2002. Wnt-4 deficiency alters mouse adrenal cortex function, reducing aldosterone production. Endocrinology 143, 4358–4365.

Heinonen, K.M., Vanegas, J.R., Brochu, S., Shan, J., Vainio, S.J., Perreault, C., 2011. Wnt4 regulates thymic cellularity through the expansion of thymic epithelial cells and early thymic progenitors. Blood 118, 5163–5173.

Hetman, M., J.E. Cavanaugh, D. Kimelman, and Z. Xia. 2000. Role of glycogen synthase kinase-3beta in neuronal apoptosis induced by trophic withdrawal. J. Neurosci. 20:2567–2574

Hirabayashi, Y, Y Itoh, H Tabata, K Nakajima, T Akiyama, N Masuyama, and Y Gotoh. 2004. "The Wnt/Beta-Catenin Pathway Directs Neuronal Differentiation of Cortical Neural Precursor Cells." Development 131 (12): 2791–2801. https://doi.org/10.1242/dev.01165.

Huang, Liwei, Yongbing Pu, Wen Yang Hu, Lynn Birch, Douglas Luccio-Camelo, Terry Yamaguchi, and Gail S. Prins. 2009. "The Role of Wnt5a in Prostate Gland Development." Developmental Biology 328 (2): 188–99. https://doi.org/10.1016/j.ydbio.2009.01.003.

Ito K, Lim AC, Salto-Tellez M, Motoda L, Osato M, Chuang LS, Lee CW, Voon DC, Koo JK, Wang H, Fukamachi H, Ito Y. RUNX3 attenuates beta-catenin/T cell factors in intestinal tumorigenesis. Cancer Cell. 2008 Sep 9;14(3):226-37. doi: 10.1016/j.ccr.2008.08.004. PubMed PMID: 18772112.

Järvinen E, Salazar-Ciudad I, Birchmeier W, Taketo MM, Jernvall J, Thesleff I.Continuous tooth generation in mouse is induced by activated epithelial Wnt/beta-catenin signaling. Proc Natl Acad Sci U S A. 2006 Dec 5;103(49):18627-32. doi:

10.1073/pnas.0607289103. Epub 2006 Nov 22. PubMed PMID: 17121988; PubMed Central PMCID: PMC1693713.

Jernvall, Jukka, and Irma Thesleff. 2000. "Reiterative Signaling and Patterning during Mammalian Tooth Morphogenesis" 92: 19–29.

Jho, E h, T Zhang, C Domon, C K Joo, J N Freund, and F Costantini. 2002. "Wnt/ -Catenin/Tcf Signaling Induces the Transcription of Axin2, a Negative Regulator of the Signaling Pathway." Molecular and Cellular Biology 22 (4): 1172–83. https://doi.org/10.1128/mcb.22.4.1172-1183.2002.

Jho, Eek-hoon, Tong Zhang, Claire Domon, Choun-ki Joo, Jean-noel Freund, and Frank Costantini. 2002. "Wnt / β -Catenin / Tcf Signaling Induces the Transcription of Axin2 , a Negative Regulator of the Signaling Pathway Wnt / -Catenin / Tcf Signaling Induces the Transcription of Axin2 , a Negative Regulator of the Signaling Pathway." Molecular and Cellular Biology 22 (4): 1172–83. https://doi.org/10.1128/MCB.22.4.1172.

Jian, H., Shen, X., Liu, I., Semenov, M., He, X.,Wang, X.F., 2006. Smad3-dependent nuclear translocation of beta-catenin is required for TGF-beta1-induced proliferation of bone marrow-derived adult human mesenchymal stem cells. Genes. Dev. 20, 666–674.

Jiang, X., Iseki, S., Maxson, R. E., Sucov, H. M., and Morriss-Kay, G. M. (2002). Tissue origins and interactions in the mammalian skull vault. Dev. Biol. 241, 106–116. doi: 10.1006/dbio.2001.0487

Jin, X.H. Han, M.M. Taketo, J.K. Yoon, Wnt9β-dependent FGF signaling is crucial for outgrowth of the nasal and maxillary processes during upper jaw and lip development, Development 139 (2012) 1821–1830.

Karner, C M, R Chirumamilla, S Aoki, P Igarashi, J B Wallingford, and T J Carroll. 2009. "Wnt9b Signaling Regulates Planar Cell Polarity and Kidney Tubule Morphogenesis." Nat Genet 41 (7): 793–99. https://doi.org/10.1038/ng.400.

Kettunen, P, S Loes, T Furmanek, K Fjeld, I H Kvinnsland, O Behar, T Yagi, et al. 2005. "Coordination of Trigeminal Axon Navigation and Patterning with Tooth Organ

Formation: Epithelial-Mesenchymal Interactions, and Epithelial Wnt4 and Tgfbeta1 Regulate Semaphorin 3a Expression in the Dental Mesenchyme." Development 132 (2): 323–34. https://doi.org/10.1242/dev.01541.

Kim, K.A., Kakitani, M., Zhao, J., Oshima, T., Tang, T., Binnerts, M., Liu, Y., Boyle, B., Park, E., Emtage, P., et al. (2005). Mitogenic influ- ence of human R-spondin1 on the intestinal epithelium. Science 309, 1256–1259.

Kim, Y, A Kobayashi, R Sekido, L DiNapoli, J Brennan, M C Chaboissier, F Poulat, R R Behringer, R Lovell-Badge, and B Capel. 2006. "Fgf9 and Wnt4 Act as Antagonistic Signals to Regulate Mammalian Sex Determination." PLoS Biol 4 (6): e187. https://doi.org/10.1371/journal.pbio.0040187.

Kispert, A, S Vainio, L Shen, D H Rowitch, and A P McMahon. 1996. "Proteoglycans Are Required for Maintenance of Wnt-11 Expression in the Ureter Tips." Development 122 (11): 3627–37. http://dev.biologists.org/content/develop/122/11/3627.full.pdf.

Kohn, A.D., and Moon, R.T. (2005). Wnt and calcium signaling: β- Catenin-independent pathways. Cell Calcium 38, 439–446.

Komiya, Y, and R Habas. 2008. "Wnt Signal Transduction Pathways." Organogenesis 4 (2): 68–75. https://www.ncbi.nlm.nih.gov/pmc/articles/PMC2634250/pdf/org0402_0068.pdf.

Korinek, V., Barker, N., Moerer, P., van Donselaar, E., Huls, G., Peters, P.J., Clevers, H., 1998. Depletion of epithelial stem–cell compartments in the small intestine of mice lacking Tcf-4. Nat. Genet. 19, 379–383.

Korinek, V., Barker, N., Morin, P. J., van Wichen, D., de Weger, R., Kinzler, K. W., Vogelstein, B. and Clevers, H. (1997). Constitutive transcriptional activation by a beta-catenin-Tcf complex in APC–/– colon carcinoma. Science 275, 1784-1787.

Kratochwil, K., Dull, M., Farin˜as, I., Galceran, J., Grosschedl, R., 1996.Lef1 expression is activated by BMP-4 and regulates inductive tissueinteractions in tooth and hair development. Genes Dev. 10, 1382–1394

Krauss, S., Korzh, V., Fjose, A. & Johansen, T. Expression of four zebrafish wnt- related genes during embryogenesis. Development 116, 249–259 (1992).

Kretzschmar, K, and H Clevers. 2017. "Wnt/Beta-Catenin Signaling in Adult Mammalian Epithelial Stem Cells." Dev Biol 428 (2): 273–82. https://doi.org/10.1016/j.ydbio.2017.05.015.

Kretzschmar, Kai, and Fiona M Watt. 2012. "Lineage Tracing." Cell 148 (1–2): 33–45. https://doi.org/10.1016/j.cell.2012.01.002.

Krishnan, Venkatesh, Henry U Bryant, and Ormond A Macdougald. 2006. "Review Series Regulation of Bone Mass by Wnt Signaling" 116 (5). https://doi.org/10.1172/JCI28551.1202.

Kubo, F. 2003. "Wnt2b Controls Retinal Cell Differentiation at the Ciliary Marginal Zone." Development 130 (3): 587–98. https://doi.org/10.1242/dev.00244.

Kubo, F, M Takeichi, and S Nakagawa. 2005. "Wnt2b Inhibits Differentiation of Retinal Progenitor Cells in the Absence of Notch Activity by Downregulating the Expression of Proneural Genes." Development 132 (12): 2759–70. https://doi.org/10.1242/dev.01856.

Kyrylkova K, Kyryachenko S, Biehs B, Klein O, Kioussi C, Leid M. BCL11B regulates epithelial proliferation and asymmetric development of the mouse mandibular incisor. PLoS One 2012;7(5):e37670.

Lapthanasupkul, Puangwan, Jifan Feng, Andrea Mantesso, Yuki Takada-horisawa, Miguel Vidal, Haruhiko Koseki, Longlong Wang, Zhengwen An, Isabelle Miletich, and Paul T Sharpe. 2012. "Ring1a / b Polycomb Proteins Regulate the Mesenchymal Stem Cell Niche in Continuously Growing Incisors." Developmental Biology 367 (2): 140–53. https://doi.org/10.1016/j.ydbio.2012.04.029.

Lee JE, Wu SF, Goering LM, Dorsky RI. 2006. Canonical Wnt signaling through Lef1 is required for hypothalamic neu- rogenesis. Development 133:4451–4461.

Lee, S M, S Tole, E Grove, and A P McMahon. 2000. "A Local Wnt-3a Signal Is Required for Development of the Mammalian Hippocampus." Development 127 (3): 457–67. http://dev.biologists.org/content/develop/127/3/457.full.pdf.

Lerner, U H, and C Ohlsson. 2015. “The WNT System : Background and Its Role in Bone.” https://doi.org/10.1111/joim.12368.

LEEB, C., JURGA, M., MCGUCKIN, C., MORIGGL, R. & KENNER, L. 2010. Promising new sources for pluripotent stem cells. Stem Cell Reviews, 6, 15-26.

Li, Changgong, Jing Xiao, Khadija Hormi, Zea Borok, and Parviz Minoo. 2002. “Wnt5a Participates in Distal Lung Morphogenesis.” Developmental Biology 248 (1): 68–81. https://doi.org/10.1006/dbio.2002.0729.

Li, R, C Wang, J Tong, Y Su, Y Lin, X Zhou, and L Ye. 2014. “WNT6 Promotes the Migration and Differentiation of Human Dental Pulp Cells Partly through C-Jun N-Terminal Kinase Signaling Pathway.” J Endod 40 (7): 943–48. https://doi.org/10.1016/j.joen.2013.12.023.

Lim, W H, B Liu, D Cheng, D J Hunter, Z Zhong, D M Ramos, B O Williams, et al. 2014. “Wnt Signaling Regulates Pulp Volume and Dentine Thickness.” J Bone Miner Res 29 (4): 892–901. https://doi.org/10.1002/jbmr.2088.

Lim, X, S H Tan, K L Yu, S B Lim, and R Nusse. 2016. “Axin2 Marks Quiescent Hair Follicle Bulge Stem Cells That Are Maintained by Autocrine Wnt/Beta-Catenin Signaling.” Proc Natl Acad Sci U S A 113 (11): E1498-505. https://doi.org/10.1073/pnas.1601599113.

Lin, C.R., Kioussi, C., O’Connell, S., Briata, P., Szeto, D., Liu, F., Izpisua-Belmonte, J.C., Rosenfeld, M.G., 1999. Pitx2 regulates lung asymme-try, cardiac positioning and pituitary and tooth morphogenesis. Nature401, 279–282

Lin, M, L Li, C Liu, H Liu, F He, F Yan, Y Zhang, and Y Chen. 2011. “Wnt5a Regulates Growth, Patterning, and Odontoblast Differentiation of Developing Mouse Tooth.” Dev Dyn 240 (2): 432–40. https://doi.org/10.1002/dvdy.22550.

Ling, Ling, Victor Nurcombe, and Simon M. Cool. 2009. “Wnt Signaling Controls the Fate of Mesenchymal Stem Cells.” Gene 433 (1–2): 1–7. https://doi.org/10.1016/j.gene.2008.12.008.

Liu, F, and S E Millar. “Wnt/beta-catenin signaling in oral tissue development and disease.” Journal of dental research vol. 89,4 (2010): 318-30. doi:10.1177/0022034510363373

Liu, P, M Wakamiya, M J Shea, U Albrecht, R R Behringer, and A Bradley. 1999. "Requirement for Wnt3 in Vertebrate Axis Formation." Nat Genet 22 (4): 361–65. https://doi.org/10.1038/11932.

Liu, W., Dong, X., Mai, M., Seelan, R.S., Taniguchi, K., Krishnadath, K.K., Halling, K.C., Cunningham, J.M., Boardman, L.A., Qian, C., et al. (2000). Mutations in AXIN2 cause colorectal cancer with defective mismatch repair by activating beta-catenin/TCF signaling. Nat. Genet. 26, 146-147.

Liu, Y, D Han, L Wang, and H Feng. 2013. "Down-Regulation of Wnt10a Affects Odontogenesis and Proliferation in Mesenchymal Cells." Biochem Biophys Res Commun 434 (4): 717–21. https://doi.org/10.1016/j.bbrc.2013.03.088.

Lobe, C. G., Koop, K. E., Kreppner, W., Lomeli, H., Gertsenstein,M., and Nagy, A. (1999). Z/AP, a double reporter for cre-mediated recombination. Biol.208,281–292.

Lobov, I B, S Rao, T J Carroll, J E Vallance, M Ito, J K Ondr, S Kurup, et al. 2005. "WNT7b Mediates Macrophage-Induced Programmed Cell Death in Patterning of the Vasculature." Nature 437 (7057): 417–21. https://doi.org/10.1038/nature03928.

Logan, C Y, and R Nusse. 2004. "The Wnt Signaling Pathway in Development and Disease." Annu Rev Cell Dev Biol 20: 781–810. https://doi.org/10.1146/annurev.cellbio.20.010403.113126.

Lustig, B, B Jerchow, M Sachs, S Weiler, T Pietsch, U Karsten, M van de Wetering, et al. 2002. "Negative Feedback Loop of Wnt Signaling through Upregulation of Conductin/Axin2 in Colorectal and Liver Tumors." Molecular and Cellular Biology 22 (4): 1184–93. https://doi.org/10.1128/mcb.22.4.1184-1193.2002.

MacDonald, B.T., Tamai, K., and He, X. (2009). Wnt/beta-catenin signaling: components, mechanisms, and diseases. Dev Cell 17, 9-26.

Majumdar, A. 2003. "Wnt11 and Ret/Gdnf Pathways Cooperate in Regulating Ureteric Branching during Metanephric Kidney Development." Development 130 (>14): 3175–85. https://doi.org/10.1242/dev.00520.

Makoto, Ikeya, Scott M.K. Lee, Jane E. Johnson, Andrew P. Mc Mahon, and Shinji Takada. 1997. "Wnt Signaling Required for Expansion of Neural Crest and Cns Progenitors." Nature 389 (6654): 966–70. https://doi.org/10.1038/40146.

Maruyama, T, J Jeong, T J Sheu, and W Hsu. 2016. “Stem Cells of the Suture Mesenchyme in Craniofacial Bone Development, Repair and Regeneration.” Nat Commun 7: 10526. https://doi.org/10.1038/ncomms10526.

Matsuo, Koichi, and Naoko Irie. 2008. “Osteoclast – Osteoblast Communication” 473: 201–9. https://doi.org/10.1016/j.abb.2008.03.027.

Matsuzaki, Yumi, Yo Mabuchi, and Hideyuki Okano. 2014. “Leptin Receptor Makes Its Mark on MSCs.” Cell Stem Cell 15 (2): 112–14. https://doi.org/10.1016/j.stem.2014.07.001.

McCulley, D, M Wienhold, and X Sun. 2015. “The Pulmonary Mesenchyme Directs Lung Development.” Curr Opin Genet Dev 32: 98–105. https://doi.org/10.1016/j.gde.2015.01.011.

McMahon, A. P., A. L. Joyner, A. Bradley, and J. A. McMahon. 1992. “The Midbrain-Hindbrain Phenotype of Wnt-1-Wnt-1-Mice Results from Stepwise Deletion of Engrailed-Expressing Cells by 9.5 Days Postcoitum.” Cell 69 (4): 581–95. https://doi.org/10.1007/s00198-012-2016-8.

McMahon, Andrew P., and Allan Bradley. 1990. “The Wnt-1 (Int-1) Proto-Oncogene Is Required for Development of a Large Region of the Mouse Brain.” Cell 62 (6): 1073–85. https://doi.org/10.1016/0092-8674(90)90385-R.

McWhirter., J, S. Neuteboom., E. Wancewicz., B. Monia., J. Downing., and C. Murre. 1999. “Oncogenic Homeodomain Transcription Factor E2A-Pbx1 Activates a Novel WNT Gene in Pre-B Acute Lymphoblastoid Leukemia.” Proceedings of the National Academy of Sciences 96: 11464–69.

Mericskay, M, J Kitajewski, and D Sassoon. 2004. “Wnt5a Is Required for Proper Epithelial-Mesenchymal Interactions in the Uterus.” Development 131 (9): 2061–72. https://doi.org/10.1242/dev.01090.

Mendez-Ferrer, S, D T Scadden, and A Sanchez-Aguilera. 2015. “Bone Marrow Stem Cells: Current and Emerging Concepts.” Ann N Y Acad Sci 1335: 32–44. https://doi.org/10.1111/nyas.12641.

Mikels, A J, and R Nusse. 2006. "Purified Wnt5a Protein Activates or Inhibits Beta-Catenin-TCF Signaling Depending on Receptor Context." PLoS Biol 4 (4): e115. https://doi.org/10.1371/journal.pbio.0040115.

Millar, Sarah E., Karl Willert, Patricia C. Salinas, Henk Roelink, Roel Nusse, Daniel J. Sussman, and Gregory S. Barsh. 1999. "WNT Signaling in the Control of Hair Growth and Structure." Developmental Biology 207 (1): 133–49. https://doi.org/10.1006/dbio.1998.9140.

Miller, C, and D A Sassoon. 1998. "Wnt-7a Maintains Appropriate Uterine Patterning during the Development of the Mouse Female Reproductive Tract." Development 125 (16): 3201–11. http://dev.biologists.org/content/develop/125/16/3201.full.pdf.

Miller, J R. 2002. "The Wnts." Genome Biol 3 (1): Reviews3001. https://www.ncbi.nlm.nih.gov/pmc/articles/PMC150458/pdf/gb-2001-3-1-reviews3001.pdf.

Millar SE, Koyama E, Reddy ST, Andl T, Gaddapara T, Piddington R, Gibson CW. Over- and ectopic expression of Wnt3 causes progressive loss of ameloblasts in postnatal mouse incisor teeth. Connect Tissue Res. 2003;44 Suppl 1:124-9. PubMed PMID: 12952185.

MIURA, M., GRONTHOS, S., ZHAO, M., LU, B., FISHER, L. W., ROBEY, P. G. & SHI, S. 2003. SHED: stem cells from human exfoliated deciduous teeth. Proceedings of the National Academy of Sciences of the United States of America, 100, 5807-12.

Mlodzik, M. (2002). Planar cell polarization: do the same mechanisms regulate Drosophila tissue polarity and vertebrate gastrulation? Trends Genet 18, 564-571.

Monkley, S J, S J Delaney, D J Pennisi, J H Christiansen, and B J Wainwright. 1996. "Targeted Disruption of the Wnt2 Gene Results in Placentation Defects." Development 122 (11): 3343–53. http://dev.biologists.org/content/develop/122/11/3343.full.pdf.

MORSCZECK, C., GOTZ, W., SCHIERHOLZ, J., ZEILHOFER, F., KUHN, U., MOHL, C., SIPPEL, C. & HOFFMANN, K. H. 2005. Isolation of precursor cells (PCs) from human dental follicle of wisdom teeth. Matrix Biology, 24, 155-65.

Morris, R.J., Liu, Y., Marles, L., Yang, Z., Trempus, C., Li, S., Lin, J.S., Sawicki, J.A., and Cotsarelis, G. (2004). Capturing and profiling adult hair follicle stem cells. Nat. Biotechnol. 22, 411–417

Moverare-Skrtic, S, P Henning, X Liu, K Nagano, H Saito, A E Borjesson, K Sjogren, et al. 2014. "Osteoblast-Derived WNT16 Represses Osteoclastogenesis and Prevents Cortical Bone Fragility Fractures." Nat Med 20 (11): 1279–88. https://doi.org/10.1038/nm.3654.

Movérare-skrtic, Sofia, Petra Henning, Xianwen Liu, Kenichi Nagano, Hiroaki Saito, Anna E Börjesson, Klara Sjögren, et al. 2014. "Osteoblast-Derived WNT16 Represses Osteoclastogenesis and Prevents Cortical Bone Fragility Fractures" 20 (11). https://doi.org/10.1038/nm.3654.

Nakashima M, Iohara K, Murakami M, Nakamura H, Sato Y, Ariji Y, Matsushita K. Pulp regeneration by transplantation of dental pulp stem cells in pulpitis: a pilot clinical study. Stem Cell Res Ther. 2017 Mar 9;8(1):61. doi: 10.1186/s13287-017-0506-5. PubMed PMID: 28279187; PubMed Central PMCID: PMC5345141

Nakaya, M A, K Biris, T Tsukiyama, S Jaime, J A Rawls, and T P Yamaguchi. 2005. "Wnt3a Links Left-Right Determination with Segmentation and Anteroposterior Axis Elongation." Development 132 (24): 5425–36. https://doi.org/10.1242/dev.02149.

Nanci, A. (ed.) 2007. Ten Cate's Oral Histology: Development, Structure, and Function: St. Louis, Missouri, Mosby.

NAKAHARA, H., DENNIS, J. E., BRUDER, S. P., HAYNESWORTH, S. E., LENNON, D. P. & CAPLAN, A. I. 1991. In vitro differentiation of bone and hypertrophic cartilage from periosteal-derived cells. Experimental Cell Research, 195, 492-503.

Nemoto, E, Y Sakisaka, M Tsuchiya, M Tamura, T Nakamura, S Kanaya, M Shimonishi, and H Shimauchi. 2016. "Wnt3a Signaling Induces Murine Dental Follicle Cells

to Differentiate into Cementoblastic/Osteoblastic Cells via an Osterix-Dependent Pathway." J Periodontal Res 51 (2): 164–74. https://doi.org/10.1111/jre.12294.

Neves, Vitor C M, Rebecca Babb, Dhivya Chandrasekaran, and Paul T Sharpe. 2017. "Promotion of Natural Tooth Repair by Small Molecule GSK3 Antagonists." Nature Publishing Group, no. January: 1–7. https://doi.org/10.1038/srep39654.

Niederreither K, Vermot J, Schuhbaur B, Chambon P, Doll?eP. 2000. Retinoic acid synthesis and hindbrain patterning in the mouse embryo. Development 127:75–85.

Niwa, H., Yamamura, K., and Miyazaki, J. (1991). Efficient selection for high-expression transfectants with a novel eukaryoticvector. Gene108,193–199.

Nusse, R., and Varmus, H.E. (1982). Many tumors induced by the mouse mammary tumor virus contain a provirus integrated in the same region of the host genome. Cell 31, 99–109.

Park, J S, M T Valerius, and A P McMahon. 2007. "Wnt/Beta-Catenin Signaling Regulates Nephron Induction during Mouse Kidney Development." Development 134 (13): 2533–39. https://doi.org/10.1242/dev.006155.

Parr, Brian A., Valerie A. Cornish, Myron I. Cybulsky, and Andrew P. McMahon. 2001. "Wnt7b Regulates Placental Development in Mice." Developmental Biology 237 (2): 324–32. https://doi.org/10.1006/dbio.2001.0373.

Parr, Brian A., and Andrew P. McMahon. 1998. "Sexually Dimorphic Development of the Mammalian Reproductive Tract Requires Wnt-7a." Nature 395 (6703): 707–10. https://doi.org/10.1038/27221.

Parr, B. A. &McMahon, A. P. Dorsalizing signal Wnt-7a required for normal polarity of D-Vand A-P axes of mouse limb. Nature 374, 350–353 (1995)

Pećina-šlaus, Nives. 2010. "Wnt Signal Transduction Pathway and Apoptosis : A Review," 1–5.

Plaisanci, Julie, Isabelle Bailleul-Forestier, Vronique Gaston, Frderic Vaysse, Didier Lacombe, Muriel Holder-Espinasse, Marc Abramowicz, et al. 2013. "Mutations in WNT10A Are Frequently Involved in Oligodontia Associated with Minor Signs of Ectodermal Dysplasia." American Journal of Medical Genetics, Part A 161 (4): 671–78. https://doi.org/10.1002/ajmg.a.35747.

Qian, Dong, Chonnettia Jones, Agnieszka Rzadzinska, Sharayne Mark, Xiaohui Zhang, Karen P. Steel, Xing Dai, and Ping Chen. 2007. "Wnt5a Functions in Planar Cell Polarity Regulation in Mice." Developmental Biology 306 (1): 121–33. https://doi.org/10.1016/j.ydbio.2007.03.011.

Qian, J., Jiang, Z., Li, M., Heaphy, P., Liu, Y.H., and Shackleford, G.M. (2003). Mouse Wnt9b transforming activity, tissue-specific ex- pression, and evolution. Genomics 81, 34–46.

Rao, T P, and M Kuhl. 2010. "An Updated Overview on Wnt Signaling Pathways: A Prelude for More." Circ Res 106 (12): 1798–1806. https://doi.org/10.1161/CIRCRESAHA.110.219840.

Rattis FM, Voermans C, Reya T. Wnt signaling in the stem cell niche. Curr Opin Hematol. 2004;11:88e94.

Reya, T., Duncan, A. W., Ailles, L., Domen, J., Scherer, D. C., Willert, K., Hintz, L., Nusse, R. and Weissman, I. L. (2003). A role for Wnt signaling in self-renewal of haematopoietic stem cells. Nature 423, 409-414.

Richardson, Melville, Diane Redmond, Christine J. Watson, and John O. Mason. 1999. "Mouse Wnt8B Is Expressed in the Developing Forebrain and Maps to Chromosome 19." Mammalian Genome 10 (9): 923–25. https://doi.org/10.1007/s003359901115.

Roarty, K, and R Serra. 2007. "Wnt5a Is Required for Proper Mammary Gland Development and TGF-Beta-Mediated Inhibition of Ductal Growth." Development 134 (21): 3929–39. https://doi.org/10.1242/dev.008250.

Rodriguez-Niedenfu¨ hr M, Dathe V, Jacob HJ, Prols F, Christ B (2003) Spatial and temporal pattern of Wnt-6 expression during chick development. Anat Embryol (Berl) 206:447–451

Roelink, H., Wang, J., Black, D.M., Solomon, E. & Nusse, R. Molecular cloning and chromosomal localization to 17q21 of the human WNT3 gene. Genomics 17, 790–792 (1993).

Roelink, H., Wagenaar, E., Lopes da Silva, S., and Nusse, R. (1990). Wnt-3, a gene activated by proviral insertion in mouse mammary tumors, is homologous to int-1/Wnt-1

and is normally expressed in mouse embryos and adult brain. Proc. Natl. Acad. Sci. USA 87, 4519–4523

Ross, S.E., et al., 2000. Inhibition ofadipogenesis byWnt signaling. Science 289, 950–953.

Rosso, S. B., Sussman, D., Wynshaw-Boris, A. and Salinas, P. C. (2005). Wnt signaling through Dishevelled, Rac and JNK regulates dendritic development. Nat. Neurosci. 8, 34-42.

Salibian, A. A., Widgerow, A. D., Abrouk, M., & Evans, G. R. (2013). Stem cells in plastic surgery: a review of current clinical and translational applications. Archives of plastic surgery, 40(6), 666–675. doi:10.5999/aps.2013.40.6.666

Sarkar, L, and P T Sharpe. 1999. "Expression of Wnt Signaling Pathway Genes during Tooth Development." Mech Dev 85 (1–2): 197–200. SELL, S. (ed.) 2004. Stem Cell Handbook, Totowa, New Jersey: Humana Press.

Seidel, K, C P Ahn, D Lyons, A Nee, K Ting, I Brownell, T Cao, et al. 2010. "Hedgehog Signaling Regulates the Generation of Ameloblast Progenitors in the Continuously Growing Mouse Incisor." Development 137 (22): 3753–61. https://doi.org/10.1242/dev.056358.

Seifert, J.R., and Mlodzik, M. (2007). Frizzled/PCP signaling: a conserved mechanism regulating cell polarity and directed motility. Nat. Rev. Genet. 8, 126–138.

SEO, B.-M., MIURA, M., GRONTHOS, S., BARTOLD, P. M., BATOULI, S., BRAHIM, J., YOUNG, M., ROBEY, P. G., WANG, C.-Y. & SHI, S. 2004. Investigation of multipotent postnatal stem cells from human periodontal ligament. Lancet, 364, 149-55.

Sharma, R.P. and V. L. Chopra. 1976. Effect of the wingless (wg l) mutation on wing and haltere development in Drosophila melanogaster. Dev. Biol. 48: 461—465

Sharpe, Paul T. 2016. "Dental Mesenchymal Stem Cells," 2273–80. https://doi.org/10.1242/dev.134189.

Shu, Weiguo, Yue Qin Jiang, Min Min Lu, and Edward E Morrisey. 2002. "Wnt7b Regulates Mesenchymal Proliferation and Vascular Development in the Lung." Development (Cambridge, England) 129: 4831–42. https://doi.org/10.1101/gad.13.23.3149.

Slusarski DC, Pelegri F. Calcium signaling in vertebrate embryonic patterning and morphogenesis. Dev Biol. 2007 Jul 1;307(1):1-13. doi: 10.1016/j.ydbio.2007.04.043. Epub 2007 May 3. Review. PubMed PMID: 17531967; PubMed Central PMCID: PMC2729314.

Smith, M. M. (2003) Vertebrate dentitions at the origin of jaws: when and how pattern evolved. Evolution and Development. 5 (4), 394–413.

SONOYAMA, W., LIU, Y., FANG, D., YAMAZA, T., SEO, B.-M., ZHANG, C., LIU, H., GRONTHOS, S., WANG, C.-Y., WANG, S. & SHI, S. 2006. Mesenchymal stem cell-mediated functional tooth regeneration in swine. PLoS ONE [Electronic Resource], 1, e79.

Spater, D. 2006. "Wnt9a Signaling Is Required for Joint Integrity and Regulation of Ihh during Chondrogenesis." Development 133 (15): 3039–49. https://doi.org/10.1242/dev.02471.

Stamos, J L, and W I Weis. 2013. "The Beta-Catenin Destruction Complex." Cold Spring Harb Perspect Biol 5 (1): a007898. https://doi.org/10.1101/cshperspect.a007898.

Stark, Kevin, Seppo Vainio, Galya Vassileva, and Andrew P. McMahon. 1994. "Epithelial Transformation of Metanephric Mesenchyme in the Developing Kidney Regulated by Wnt-4." Nature. https://doi.org/10.1038/372679a0.

Stefater, J.A., 3rd, Lewkowich, I., Rao, S., Mariggi, G., Carpenter, A.C., Burr, A.R., Fan, J., Ajima, R., Molkentin, J.D., Williams, B.O., et al. (2011). Regulation of angiogenesis by a non-canonical Wnt-Flt1 pathway in myeloid cells. Nature 474, 511-515.

Stevens, Jennifer R., Gustavo A. Miranda-Carboni, Meredith A. Singer, Sean M. Brugger, Karen M. Lyons, and Timothy F. Lane. 2010. "Wnt10b Deficiency Results in Age-Dependent Loss of Bone Mass and Progressive Reduction of Mesenchymal Progenitor Cells." Journal of Bone and Mineral Research 25 (10): 2138–47. https://doi.org/10.1002/jbmr.118.

Strovel, E.T., and D.J. Sussman. 1999. Transient overexpression of murine di- shevelled genes results in apoptotic cell death. Exp. Cell Res. 253:637–648.

Sugimura, R., and Li, L. (2010) Noncanonical Wnt signaling in vertebrate development, stem cells, and diseases. Birth Defects Res. C Embryo Today 90,243–256

Sugimura, Xi C. He, Aparna Venkatraman, Fumio Arai, Andrew Box, Craig Semerad, Jeffrey S. Haug, Lai Peng, Xiao-bo Zhong, Toshio Suda, Linheng Li, Noncanonical Wnt Signaling Maintains Hematopoietic Stem Cells in the Niche, Cell, Volume 150, Issue 2, 2012, Pages 351-365, ISSN 0092-8674, https://doi.org/10.1016/j.cell.2012.05.041.

Summerhurst, Kristen, Margaret Stark, James Sharpe, Duncan Davidson, and Paula Murphy. 2008. "3D Representation of Wnt and Frizzled Gene Expression Patterns in the Mouse Embryo at Embryonic Day 11.5 (Ts19)." Gene Expression Patterns 8 (5): 331–48. https://doi.org/10.1016/j.gep.2008.01.007.

Suomalainen, Marika, and Irma Thesleff. 2010. "Patterns of Wnt Pathway Activity in the Mouse Incisor Indicate Absence of Wnt/Beta-Catenin Signaling in the Epithelial Stem Cells." Developmental Dynamics : An Official Publication of the American Association of Anatomists 239 (1): 364–72. https://doi.org/10.1002/dvdy.22106.

Takada, R., Satomi, Y., Kurata, T., Ueno, N., Norioka, S., Kondoh, H., Takao, T., and Takada, S. (2006). Monounsaturated fatty acid modification of Wnt protein: its role in Wnt secretion. Dev Cell 11, 791-801.

Takada, Shinji, Kevin L. Stark, Martin J. Shea, Galya Vassileva, Jill A. McMahon, and Andrew P. McMahon. 1994. "Wnt-3a Regulates Somite and Tailbud Formation in the Mouse Embryo." Genes and Development 8 (2): 174–89. https://doi.org/10.1101/gad.8.2.174.

Tanaka, K., Okabayashi, K., Asashima, M., Perrimon, N., and Kadowaki, T. (2000). The evolutionarily conserved porcupine gene family is involved in the processing of the Wnt family. European journal of biochemistry / FEBS 267, 4300-4311.

Tanaka, K., Kitagawa, Y., and Kadowaki, T. (2002). Drosophila segment polarity gene product porcupine stimulates the posttranslational N-glycosylation of wingless in the endoplasmic reticulum. J Biol Chem 277, 12816-12823.

Thesleff, I. 2003. “Epithelial-Mesenchymal Signaling Regulating Tooth Morphogenesis.” J Cell Sci 116 (Pt 9): 1647–48. http://jcs.biologists.org/content/joces/116/9/1647.full.pdf.

Thesleff, Irma, Xiu-Ping Wang, and Marika Suomalainen. 2007. “Regulation of Epithelial Stem Cells in Tooth Regeneration.” Comptes Rendus Biologies 330 (6–7): 561–64. https://doi.org/10.1016/j.crvi.2007.03.005.

Tournier C., P. Hess, D.D. Yang, J. Xu, T.K. Turner, A. Nimnual, D. Bar-Sagi, S.N. Jones, R.A. Flavell, and R.J. Davis. 2000. Requirement of JNK for stress-induced activation of the cytochrome c-mediated death pathway. Sci- ence. 288:870–874.

Tsukiyama, Tadasuke, and Terry P. Yamaguchi. 2012. “Mice Lacking Wnt2b Are Viable and Display a Postnatal Olfactory Bulb Phenotype.” Neuroscience Letters 512 (1): 48–52. https://doi.org/10.1016/j.neulet.2012.01.062.

Tu, Xiaolin, Kyu Sang Joeng, Keiichi I Nakayama, Keiko Nakayama, Jayaraj Rajagopal, Thomas J Carroll, Andrew P Mcmahon, and Fanxin Long. 2007. “Noncanonical Wnt Signaling through G Protein-Linked PKC d Activation Promotes Bone Formation,” no. January: 113–27. https://doi.org/10.1016/j.devcel.2006.11.003.

Tuli R, Tuli S, Nandi S, Huang X, Manner PA, Hozack WJ, Danielson KG, Hall DJ, Tuan RS. Transforming growth factor-beta-mediated chondrogenesis of human mesenchymal progenitor cells involves N-cadherin and mitogen-activated protein kinase and Wnt signaling cross-talk. J Biol Chem. 2003 Oct 17;278(42):41227-36. doi: 10.1074/jbc.M305312200. Epub 2003 Jul 31. PubMed PMID: 12893825.

Tummers, M. & Thesleff, I. (2008) Observations on continuously growing roots of the sloth and the K14-Eda transgenic mice indicate that epithelial stem cells can give rise to both the ameloblast and root epithelium cell lineage creating distinct tooth patterns. Evolution and Development

Tummers M, Thesleff I. Root or crown: a developmental choice orchestrated by the differential regulation of the epithelial stem cell niche in the tooth of two rodent species. Development 2003;130(6):1049–57.

Undi, R B, U Gutti, I Sahu, S Sarvothaman, S R Pasupuleti, R Kandi, and R K Gutti. 2016. "Wnt Signaling: Role in Regulation of Haematopoiesis." Indian J Hematol Blood Transfus 32 (2): 123–34. https://doi.org/10.1007/s12288-015-0585-3.

Vaahtokari, A.,ÅAberg, T., Thesleff, I., 1996b. Apoptosis in the devel-oping tooth: association with an embryonic signaling center and sup-pression by EGF and FGF-4. Development 122, 121–129

Vainio, Seppo, Minna Heikkilä, Andreas Kispert, Norman Chin, and Andrew P. McMahon. 1999. "Female Development in Mammals Is Regulated by Wnt-4 Signaling." Nature 397 (6718): 405–9. https://doi.org/10.1038/17068.

Van Amerongen, R., Berns, A., 2006. Knockout mouse models to study Wnt signal transduction. Trends in Genetics 22, 678–689.

Van Amerongen, R, A N Bowman, and R Nusse. 2012. "Developmental Stage and Time Dictate the Fate of Wnt/Beta-Catenin-Responsive Stem Cells in the Mammary Gland." Cell Stem Cell 11 (3): 387–400. https://doi.org/10.1016/j.stem.2012.05.023.

Van den Heuvel, M., Harryman-Samos, C., Klingensmith, J., Perrimon, N., and Nusse, R. (1993). Mutations in the segment polarity genes wingless and porcupine impair secretion of the wingless protein. Embo J 12, 5293-5302.

Van Es, J.H., van Gijn, M.E., Riccio, O., van den Born, M., Vooijs, M., Begthel, H., Cozijnsen, M., Robine, S., Winton, D.J., Radtke, F., and Clevers, H. (2005). Notch pathway/γ-secretase inhibition turns prolif- erative cells in intestinal crypts and neoplasia into Goblet cells. Nature 435, 959–963

Vasioukhin V, Degenstein L, Wise B, Fuchs E. The magical touch: genome targeting in epidermal stem cells induced by tamoxifen application to mouse skin. Proc Natl Acad Sci U S A. 1999 Jul 20;96(15):8551-6. doi: 10.1073/pnas.96.15.8551. PubMed PMID: 10411913; PubMed Central PMCID: PMC17554.

Vendrell, Victor, Citlali Vázquez-Echeverría, Iris López-Hernández, Beatriz Durán Alonso, Salvador Martinez, Cristina Pujades, and Thomas Schimmang. 2013. "Roles of Wnt8a during Formation and Patterning of the Mouse Inner Ear." Mechanisms of Development 130 (2–3): 160–68. https://doi.org/10.1016/j.mod.2012.09.009.

Wang, J., and G. M. Shackleford. 1996. Murine Wnt10a and Wnt10b: cloning and expression in developing limbs, face and skin of embryos and in adults. Oncogene 13:1537–1544.

Wang, X P, M Suomalainen, S Felszeghy, L C Zelarayan, M T Alonso, M V Plikus, R L Maas, C M Chuong, T Schimmang, and I Thesleff. 2007. "An Integrated Gene Regulatory Network Controls Stem Cell Proliferation in Teeth." PLoS Biol 5 (6): e159. https://doi.org/10.1371/journal.pbio.0050159.

Wang, X P, M Suomalainen, C J Jorgez, M M Matzuk, S Werner, and I Thesleff. 2004. "Follistatin Regulates Enamel Patterning in Mouse Incisors by Asymmetrically Inhibiting BMP Signaling and Ameloblast Differentiation." Dev Cell 7 (5): 719–30. https://doi.org/10.1016/j.devcel.2004.09.012.

Weissman, Irving L. 2000. "Stem Cells : Units of Development , Units of Regeneration , and Units in Evolution" 100: 157–68.

Westendorf, Jennifer J, Rachel A Kahler, and Tania M Schroeder. 2004. "Wnt Signaling in Osteoblasts and Bone Diseases" 341: 19–39. https://doi.org/10.1016/j.gene.2004.06.044.

Willert, K, J D Brown, E Danenberg, A W Duncan, I L Weissman, T Reya, J R Yates 3rd, and R Nusse. 2003. "Wnt Proteins Are Lipid-Modified and Can Act as Stem Cell Growth Factors." Nature 423 (6938): 448–52. https://doi.org/10.1038/nature01611.

Witte, Florian, Janine Dokas, Franziska Neuendorf, Stefan Mundlos, and Sigmar Stricker. 2009. "Comprehensive Expression Analysis of All Wnt Genes and Their Major Secreted Antagonists during Mouse Limb Development and Cartilage Differentiation." Gene Expression Patterns 9 (4): 215–23. https://doi.org/10.1016/j.gep.2008.12.009.

WOBUS, A. M. & BOHELER, K. R. 2005. Embryonic stem cells: prospects for developmental biology and cell therapy. Physiological Reviews, 85, 635-78.

Worthley, D L, M Churchill, J T Compton, Y Tailor, M Rao, Y Si, D Levin, et al. 2015. "Gremlin 1 Identifies a Skeletal Stem Cell with Bone, Cartilage, and Reticular

Stromal Potential." Cell 160 (1–2): 269–84. https://doi.org/10.1016/j.cell.2014.11.042.

Wu, B.-T., S.-H. Wen, S.-P. L. Hwang, C.-J. Huang, and Y.-S. Kuan. 2015. "Control of Wnt5b Secretion by Wntless Modulates Chondrogenic Cell Proliferation through Fine-Tuning Fgf3 Expression." Journal of Cell Science 128 (12): 2328–39. https://doi.org/10.1242/jcs.167403.

Wylie AD, Fleming JA, Whitener AE, Lekven AC. 2014. Post-tran- scriptional regulation of wnt8a is essential to zebrafish axis development. Dev Biol 386:53–63.

Xiang, Lusai, Mo Chen, Ling He, Bin Cai, Yu Du, Xinchun Zhang, Chen Zhou, Chenglin Wang, Jeremy J Mao, and Junqi Ling. 2014. "Wnt5a Regulates Dental Follicle Stem/Progenitor Cells of the Periodontium." Stem Cell Research & Therapy 5 (6): 135. https://doi.org/10.1186/scrt525.

Xiao, Qian, Zhengxi Chen, Xiaozhuang Jin, Runyi Mao, and Zhenqi Chen. 2017. "The Many Postures of Noncanonical Wnt Signaling in Development and Diseases." Biomedicine and Pharmacotherapy 93 (July): 359–69. https://doi.org/10.1016/j.biopha.2017.06.061.

Xing Y, Clemens WK, Kimmelman D, Xu W. 2003. Crystal structure of a β-catenin/Axin complex suggests a mech- anism for the β-catenin destruction complex. Genes Dev 17: 2753–2764

Xuan K, Li B, Guo H, Sun W, Kou X, He X, Zhang Y, Sun J, Liu A, Liao L, Liu S, Liu W, Hu C, Shi S, Jin Y. Deciduous autologous tooth stem cells regenerate dental pulp after implantation into injured teeth. Sci Transl Med. 2018 Aug 22;10(455). doi: 10.1126/scitranslmed.aaf3227. PubMed PMID: 30135248.

Yamaguchi, T P, A Bradley, A P McMahon, and S Jones. 1999. "A Wnt5a Pathway Underlies Outgrowth of Multiple Structures in the Vertebrate Embryo." Development 126 (6): 1211–23. http://dev.biologists.org/content/develop/126/6/1211.full.pdf.

Yamaguchi, Heads or tails: Wnts and anterior-posterior patterning, Curr. Biol. 11 (2001) R713–R724,

YAMANAKA, S., LI, J., KANIA, G., ELLIOTT, S., WERSTO, R. P., VAN EYK, J., WOBUS, A. M. & BOHELER, K. R. 2008. Pluripotency of embryonic stem cells. Cell & Tissue Research, 331, 5-22.

Yamashiro, T, L Zheng, Y Shitaku, M Saito, T Tsubakimoto, K Takada, T Takano-Yamamoto, and I Thesleff. 2007. "Wnt10a Regulates Dentine Sialophosphoprotein MRNA Expression and Possibly Links Odontoblast Differentiation and Tooth Morphogenesis." Differentiation 75 (5): 452–62. https://doi.org/10.1111/j.1432-0436.2006.00150.x.

Yamashiro, Takashi, Li Zheng, Yuko Shintaku, Masahiro Saito, Takanori Tsubakimoto, Kenji Takada, Teruko Takano-Yamamoto, and Irma Thesleff. 2007. "Wnt10a Regulates Dentine Sialophosphoprotein MRNA Expression and Possibly Links Odontoblast Differentiation and Tooth Morphogenesis." European Cells and Materials 14 (SUPPL.2): 140. https://doi.org/10.1111/j.1432-0436.2006.00150.x.

Yang, J, A Cusimano, J K Monga, M E Preziosi, F Pullara, G Calero, R Lang, T P Yamaguchi, K N Nejak-Bowen, and S P Monga. 2015. "WNT5A Inhibits Hepatocyte Proliferation and Concludes Beta-Catenin Signaling in Liver Regeneration." Am J Pathol 185 (8): 2194–2205. https://doi.org/10.1016/j.ajpath.2015.04.021.

Yang, Jie, Shih-Kai Wang, Murim Choi, Bryan M. Reid, Yuanyuan Hu, Yuan-Ling Lee, Curtis R. Herzog, et al. 2015. "Taurodontism, Variations in Tooth Number, and Misshapened Crowns in Wnt10a Null Mice and Human Kindreds." Molecular Genetics & Genomic Medicine 3 (1): 40–58. https://doi.org/10.1002/mgg3.111.

Yang, P.T., Lorenowicz, M.J., Silhankova, M., Coudreuse, D.Y., Betist, M.C., and Korswagen, H.C. (2008). Wnt signaling requires retromer-dependent recycling of MIG-14/Wntless in Wnt-producing cells. Dev Cell 14, 140-147.

Yang, Y. 2003. "Wnt5a and Wnt5b Exhibit Distinct Activities in Coordinating Chondrocyte Proliferation and Differentiation." Development 130 (5): 1003–15. https://doi.org/10.1242/dev.00324.

Yang Z, Balic A, Michon F, Juuri E, Thesleff I. Mesenchymal Wnt/β-Catenin Signaling Controls Epithelial Stem Cell Homeostasis in Teeth by Inhibiting the Antiapoptotic Effect of Fgf10. Stem Cells. 2015 May;33(5):1670-81. doi: 10.1002/stem.1972. PubMed PMID: 25693510.

Yoshikawa, Yoshiaki, Toshihiko Fujimori, Andrew P. McMahon, and Shinji Takada. 1997. "Evidence That Absence of Wnt-3a Signaling Promotes Neuralization Instead of Paraxial Mesoderm Development in the Mouse." Developmental Biology 183 (2): 234–42. https://doi.org/10.1006/dbio.1997.8502.

Yu, H M, B Jerchow, T J Sheu, B Liu, F Costantini, J E Puzas, W Birchmeier, and W Hsu. 2005. "The Role of Axin2 in Calvarial Morphogenesis and Craniosynostosis." Development 132 (8): 1995–2005. https://doi.org/10.1242/dev.01786.

Yu, H.M., Jin, Y., Fu, J., and Hsu, W. (2010). Expression of Gpr177, a Wnt trafficking regulator, in mouse embryogenesis. Developmental dynamics : an official publication of the American Association of Anatomists 239, 2102-2109.

Yu, J, T J Carroll, J Rajagopal, A Kobayashi, Q Ren, and A P McMahon. 2009. "A Wnt7b-Dependent Pathway Regulates the Orientation of Epithelial Cell Division and Establishes the Cortico-Medullary Axis of the Mammalian Kidney." Development 136 (1): 161–71. https://doi.org/10.1242/dev.022087.

Yu, T., Angelova Volponi, A., Babb, R., An, Z. and Sharpe, P. T. (2015). Stem cells in tooth development, growth, repair, and regeneration. Curr. Top. Dev. Biol. 115, 187-212.

Zakin, S. Mazan, M. Maury, N. Martin, J.L. Guenet, P. Brulet, Struc- ture and expression of Wnt13, a novel mouse Wnt2 related gene, Mech. Dev. 73 (1998) 107–116, http://www.sciencedirect.com/science/article/pii/ S0925477398000409.

Zeichner-David, M., Diekwisch, T., Fincham, A., Lau, E., MacDougall, M., Moradian-Oldak, J., Simmer, J., Snead, M., and Slavkin, H.C. (1995). Control of ameloblast differentiation. Int. J. Dev. Biol. 39, 69–92.

Zeng L, Fagotto F, Zhang T, Hsu W, Vasicek TJ, Perry WL, Lee JJ, Tilghman SM, Gumbiner BM, Costantini F (1997) The mouse fused locus encodes Axin, an

inhibitor of the Wnt signaling pathway that regulates embryonic axis formation. Cell 90:181–192

Zhang, P., Wu, Y., Belenkaya, T.Y., and Lin, X. (2011). SNX3 controls Wingless/Wnt secretion through regulating retromer-dependent recycling of Wntless. Cell Res.

Zhang, Z, Q Guo, H Tian, P Lv, C Zhou, and X Gao. 2014. "Effects of WNT10A on Proliferation and Differentiation of Human Dental Pulp Cells." J Endod 40 (10): 1593–99. https://doi.org/10.1016/j.joen.2014.07.009.

Zhao, H, J Feng, T V Ho, W Grimes, M Urata, and Y Chai. 2015. "The Suture Provides a Niche for Mesenchymal Stem Cells of Craniofacial Bones." Nat Cell Biol 17 (4): 386–96. https://doi.org/10.1038/ncb3139.

Zhao, H, J Feng, K Seidel, S Shi, O Klein, P Sharpe, and Y Chai. 2014. "Secretion of Shh by a Neurovascular Bundle Niche Supports Mesenchymal Stem Cell Homeostasis in the Adult Mouse Incisor." Cell Stem Cell 14 (2): 160–73. https://doi.org/10.1016/j.stem.2013.12.013.

Zhao X, Duester G. 2009. Effect of retinoic acid signaling on Wnt/ beta-catenin and FGF signaling during body axis extension. Gene Expr Patterns 9:430–435.

Zheng, Hou Feng, Jon H. Tobias, Emma Duncan, David M. Evans, Joel Eriksson, Lavinia Paternoster, Laura M. Yerges-Armstrong, et al. 2012. "WNT16 Influences Bone Mineral Density, Cortical Bone Thickness, Bone Strength, and Osteoporotic Fracture Risk." PLoS Genetics 8 (7). https://doi.org/10.1371/journal.pgen.1002745.

Zhong, Z, C R Zylstra-Diegel, C A Schumacher, J J Baker, A C Carpenter, S Rao, W Yao, et al. 2012. "Wntless Functions in Mature Osteoblasts to Regulate Bone Mass." Proc Natl Acad Sci U S A 109 (33): E2197-204. https://doi.org/10.1073/pnas.1120407109.

Appendix (Stock solutions)

- **LacZ staining**

Trizma	60.5g
H20	450ml
HCl	To adjust pH to 7.3
TRIS-HCl solution with P^h 7.3	

Sodium deoxycholate	0.25 g
Water	50ml
0.5% Sodium Deoxycholate	

IGEPAL	5ml
Water	Up to 50ml
10% IGEPAL	

Potassium ferricyanide ($K_3[Fe(CN)_6$)	2.05g
Water	25ml
Potassium Ferricyanide solution	

Potassium ferrocyanide ($K_4[Fe(CN)_6]$)	2.65g
Water	25ml
Potassium Ferrocyanide solution	

Magnesium chloride ($MgCl_2$)	10.1g
Water	Up to 50ml
Magnesium chloride solution	

X-Gal	80mg
Dimethylformamide	1ml
X-Gal solution	

- ***in situ* hybridisation**

H_2O	14ml
20X SSC	3.5ml
Formamide	17.5ml
HIS (High stringency wash)	

5M NaCl	20ml
1M Tris-HCL pH 8	2ml
0.5M EDTA	2ml
RNAse free water	176ml
RNAse buffer	

5M NaCl	700ul
1M Tris-HCL ph 8.5	3.5ml
1M $MgCl_2$	1.75ml
10% Tween-20	350ul
distalled water	28.7ml
NTMT	

10% Tween-20	0.5ml
1XPBS	49.5 ml
PBT	

NaCl	175.3g
Sodium Citrate	88.2g
Adjust Ph with citric acid	
20XSSC	

NaCl	292.2g
RNAse free water	Up to 1L
5M NaCL	

Tris Base	121.1g
RNAse free water	Upto 1L
concentrated HCL	Adjust pH to 9.5 and 8
1M Tris-HCL	

Publications

Article

Cell Reports

Regulation of Mesenchymal Stem to Transit-Amplifying Cell Transition in the Continuously Growing Mouse Incisor

Graphical Abstract

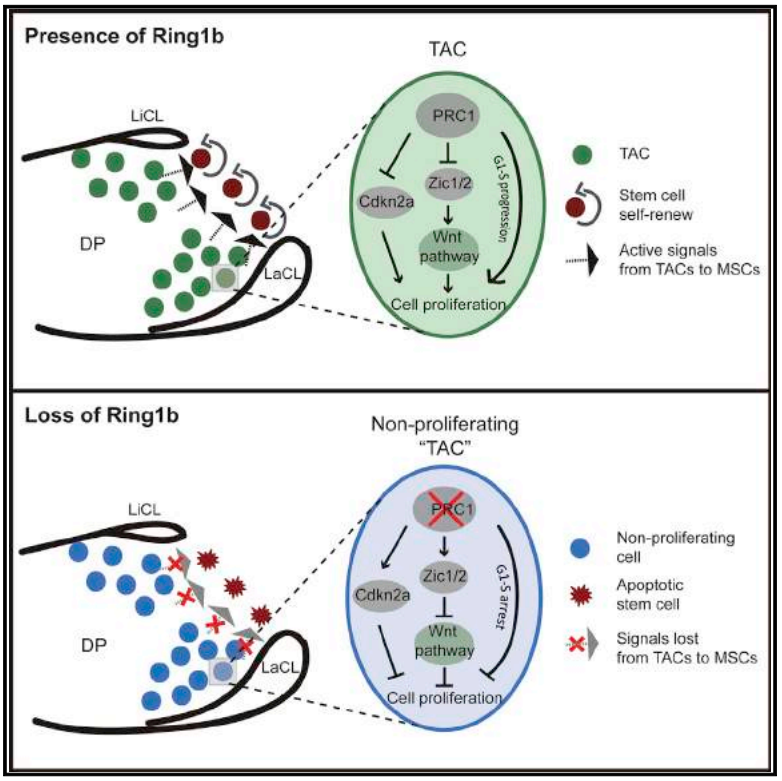

Authors

Zhengwen An, Basem Akily, Maja Sabalic, Guo Zong, Yang Chai, Paul T. Sharpe

Correspondence

paul.sharpe@kcl.ac.uk

In Brief

Using a combination of transcriptomic and epigenomic approaches, An et al. show that polycomb Ring1 in transit-amplifying cells acts as a global regulator by directly inhibiting Cdkn2a and regulating Wnt/β-catenin-signaling activity. Loss of proliferation of TACs results in MSC apoptosis, yielding positive feedback between TACs and mesenchymal stem cells.

Highlights

- Transcriptomic and epigenomic identification of PRC1 targets in TACs
- Control of proliferation by PRC1 via repressing Cdkn2a and activating G1-S genes
- Activation of Wnt signaling in TACs is a main pathway regulated by PRC1
- TACs are required to maintain stem cells

Data and Software Availability

GSE104893
GSE104891
GSE104892
GSE104934

An et al., 2018, Cell Reports *23*, 3102–3111
June 5, 2018
https://doi.org/10.1016/j.celrep.2018.05.001

CellPress

OPEN ACCESS
CellPress

Cell Reports
Article

Regulation of Mesenchymal Stem to Transit-Amplifying Cell Transition in the Continuously Growing Mouse Incisor

Zhengwen An,[1] Basem Akily,[1] Maja Sabalic,[1] Guo Zong,[1] Yang Chai,[2] and Paul T. Sharpe[1,3,*]
[1]Centre for Craniofacial and Regenerative Biology, Dental Institute, Kings College, London, UK
[2]Center for Craniofacial Molecular Biology, University of Southern California, Los Angeles, CA, USA
[3]Lead Contact
*Correspondence: paul.sharpe@kcl.ac.uk
https://doi.org/10.1016/j.celrep.2018.05.001

SUMMARY

In adult tissues and organs with high turnover rates, the generation of transit-amplifying cell (TAC) populations from self-renewing stem cells drives cell replacement. The role of stem cells is to provide a renewable source of cells that give rise to TACs to provide the cell numbers that are necessary for cell differentiation. Regulation of the formation of TACs is thus fundamental to controlling cell replacement. Here, we analyze the properties of a population of mesenchymal TACs in the continuously growing mouse incisor to identify key components of the molecular regulation that drives proliferation. We show that the polycomb repressive complex 1 acts as a global regulator of the TAC phenotype by its direct action on the expression of key cell-cycle regulatory genes and by regulating Wnt/β-catenin-signaling activity. We also identify an essential requirement for TACs in maintaining mesenchymal stem cells, which is indicative of a positive feedback mechanism.

INTRODUCTION

The continuously growing mouse incisor is increasingly studied as a model to investigate the organization of adult mesenchymal stem cell (MSC) niches (An et al., 2018; Sharpe, 2016; Yu et al., 2015). The self-sharpening action at the tips of opposing incisors resulting from their occlusion results in the continuous loss of cells (Pang et al., 2016). These cells are continuously replaced by the activity of stem cell populations located at the proximal end of the incisor. The directional growth of the incisor means that the stem cells and their progeny (transit-amplifying cells) have clearly defined positions along the proximodistal axis, and thus cell conversions and interactions can be studied easily. A population of slow-cycling, Shh-responsive mesenchymal stem cells occupies an area of dental pulp in the proximal core of the incisors between the epithelial cervical loops, which can be identified as $Gli1^{+}$ cells (Zhao et al., 2014). These MSCs give rise to a spatially distinct transit-amplifying cell (TAC) population of rapidly proliferating cells that differentiate into the main specialized tooth-specific cell type, odontoblasts, and the fibroblastic pulp cells. Odontoblasts are required for the formation of the main mineralized tissue of the tooth, the dentin.

The MSCs reside in a neurovascular bundle at the proximal end of the incisor from which they receive Shh signals required for their maintenance (Zhao et al., 2014). Genetic lineage tracing has established that both neuronal glial cells and pericytes act as sources of these MSCs (Feng et al., 2010, 2011; Kaukua et al., 2014). Distal to the MSCs, the TACs continuously form odontoblasts and pulp cells, although because TACs are pulp cells themselves, it is unclear whether this is an active or a passive differentiation process. Odontoblasts form around the periphery of the incisor and the spatial location of individual MSCs, and their TAC progeny determines the relative contributions to odontoblast and/or pulp cell differentiation (Kaukua et al., 2014). In addition to their high proliferation rate, TACs can be distinguished by the expression of the components of the polycomb repressive complex 1 (PRC1) that are required to maintain TAC proliferation (Lapthanasupkul et al., 2012).

In adulthood, a state of growth homeostasis is achieved by the rate of transition of MSCs to TACs and the subsequent rate of TAC proliferation and differentiation. The transition from a slow-cycling, self-renewing, non-differentiating stem cell into a fast-cycling, non-self-renewing, differentiating progenitor cell phenotype (TAC) must be a highly regulated process but one that is poorly understood. In addition, the extent to which there is feedback communication between TACs and MSCs to maintain the rate of MSC-TAC conversion is unknown.

Using a combination of transcriptomic and epigenomic approaches, we show here that expression of components of PRC1 in TACs regulates their proliferation by directly inhibiting the cell-cycle inhibitor Cdkn2a and activating the expression of positive cell-cycle regulators such as cyclin E2, Cdc6, and Cdc45. The transition from slow to fast cycling is enhanced further by the Wnt/β-catenin-signaling pathway, which is elevated in TACs by the action of members of the Zic family of transcription factors that also are regulated directly by PRC1. Finally, we show that loss of proliferation of the TAC population results in the rapid loss of MSCs as a result of apoptosis, identifying a positive feedback mechanism of communication between TACs and MSCs.

RESULTS

Ring1b Expression Co-localizes with TACs

Ring1b expression has been shown to be localized in the region of mesenchymal cells, with the highest rates of proliferation in the mouse incisor, and its targeted deletion resulted in the loss of TAC proliferation and arrest of incisor growth (Lapthanasupkul et al., 2012). To visualize different cell proliferation rates in the incisor, we used nucleoside analog (5-ethynyl-2′-deoxyuridine [EdU]) incorporation to identify the TACs (Figures 1A and S1) as being distal to the slow-cycling MSCs (Figure 1B). TACs were identified as EdU^+ cells chased for 16 to 24 hr, while slow-cycling cells were EdU labeled for 4 weeks followed by chasing for another 2 to 6 months. Fluorescence-activated cell sorting (FACS) analysis of EdU^+ cells identified approximately 16% of total pulp cells as TACs (Figure 1A) and 2.5% as slowcycling MSCs (Figure 1B). Using immunohistochemistry on sections of incisors from mice that had received EdU 24 hr previously, we established that rapidly proliferating cells (TACs) co-localize with Ring1b protein (Figures 1C–1G). Co-immunolocalization for slow-cycling label-retaining stem cells and Ring1b protein confirmed the location of Ring1b as being TACs and absent from the stem cells (Figures 1H–1K). Finally, to confirm the effect of the loss of Ring1 proteins on cell proliferation, we stained sections for Ki67 protein. In controls, Ki67 co-localized in the same region as Edu^+ cells, but in $Ring1a^{-/-};Ring1b^{cko/cko}$ incisors, $Ki67^+$ cells were barely detectable (Figure 1L), as shown previously (Lapthanasupkul et al., 2012). Ring1b protein is thus specifically localized in the rapidly proliferating MSCs of the incisor, just distal to the location of the slow-cycling MSCs.

Genome-wide Analysis of PRC1 in TACs

To gain a genome-wide view of PRC1 components in TACs, we used FACS-sorted TACs and carried out low-input chromatin immunoprecipitation sequencing (ChIP-seq) with Ring1b antibodies in addition to H3K4me3 and H3K27me3 histone codes to determine the active and repressive regions regulated by Ring1. Peak calling on H3K4me3, H3K27me3, and Ring1b ChIP-seq, identified 14,361, 11,341, and 3,938 gene loci, respectively (Figure 2A). A total of 2,624 gene loci were co-marked by H3K4me3 and Ring1b, whereas 1,591 loci were marked with H3K27me3 and Ring1b. Representative genome browser snapshots of repressed and active genes are shown in Figure 2B. Heatmaps were generated to determine active region distribution across targets on H3K4me3 and H3K27me3 ChIP-seq via bigWIG metrics and defined as five clusters, C1–C5 (Figure 2C). C1, C4, and C5 groups are gene loci bound by H3K4me3 at the transcription start site (TSS), 500 bp downstream and 1 kb upstream of the TSS, respectively. C2 is a group bound by H3K4me3 only, and group C3 shows no difference between H3K4me3 and H3K27me3.

Hox genes are known targets of PRC1 (Elderkin et al., 2007; Eskeland et al., 2010; Suzuki et al., 2002), and our ChIP-seq data identified a number of Hox genes occupying the same loci as Ring1b with H3K27me3 but no enrichment with H3K4me3 (Figure S2). Peak calling on H3K4me3 revealed PRC1 component genomic distribution in TACs. Genome browser snapshots showed enriched peaks of Ring1a, Ring1b, Cbx2, and Pcgf1/2 at gene promoter regions on H3K4me3 ChIP but no enrichment on H3K27me3 ChIP (Figure 2D). To identify the protein-protein co-localization, we collected flow-sorted EdU^+ cells (TACs) and carried out immunofluorescence with Ring1b and Cbx2. We found co-localization of Ring1b and Cbx2 in TACs (Figures 2E–2G and S3). Based on the role of PRC1 in chromatin modification, we performed co-immunoprecipitation and identified a Ring1b interaction with H3K27me3 but not with H2AK119ub (Figure 2H). Conditional knockout of Ring1b decreased trimethylation levels of H3K27 as revealed by western blots (Figure 2I). These results demonstrate that the PRC1 complex in TACs comprises Ring1b, Cbx2, and Pcgf1/2 and has a repressive role via trimethylation of H3K27 rather than monoubiquitination on H2AK119.

Linking Gene Expression to PRC Binding and Histone Codes Identifies Cell-Cycle Regulation

Given that knock out of Ring1 decreases cell proliferation (Figure 1D) (Lapthanasupkul et al., 2012), we used whole-genome microarrays to compare gene expression between $Ring1^+$ and $Ring1^-$ incisor pulp mesenchymal cells. Volcano plots revealed that 499 genes increased by >2-fold ($p < 0.05$) and 466 decreased (Figure 3A; Table S1). Principal component analysis (PCA) confirmed and grouped the samples by similarities and differences. As visualized in the PCA plot, the control samples clustered separately from the Ring1 deletion samples (Figure 3B). Hierarchical clustering of samples showed the genes differentially expressed upon Ring1 deletion and included a number of Hox genes and cell-cycle inhibitors as upregulated (Figures 3C and S4; Table S1). We carried out detailed Gene Ontology, *Kyoto Encyclopedia of Genes and Genomes* (KEGG), and WiKiPathways analyses of downregulated genes that revealed the top five pathways to be related to cell proliferation (Figure 3D). These results demonstrated that Ring1b likely acts as a cell-cycle regulator during homeostasis in the continuously growing mouse incisor.

Because the defining feature of TACs is their high rate of proliferation, we focused on the epigenomic status of key cell-cycle regulatory genes. We further validated four of the positive cell-cycle regulators, cyclin E2, Cdc45, Cdc6, and Cdc7, as genes involved in G1-S control and DNA replication and found to be downregulated upon Ring1 deletion (Figures 3E and 3I; Table S2). These gene loci also were recognized by Ring1b and H3K4me3 but not by H3K27me3 in ChIP-seq datasets (Figure 3F). We next analyzed the upregulated genes via heatmaps and dot plots and identified the elevated expression of Cdkn2a, a major negative cell-cycle regulator from the microarray analysis (Figure 3G). ChIP-seq identified Cdkn2a as a direct target of Ring1b marked by H3K27me3 bound across the entire gene locus (Figure 3H). This overall pattern was consistent for all positive and negative cell-cycle regulatory genes in microarrays and ChIP-seq data, because all of them were found bound by Ring1b. Real-time PCR confirmed the downregulated G1-S control genes and the upregulated cell-cycle inhibitor Cdkn2a following depletion of Ring1 (Figure 3J; Table S2). Loss of Ring1 function thus has major effects on gene expression in incisor mesenchymal cells. Genes that positively regulate the

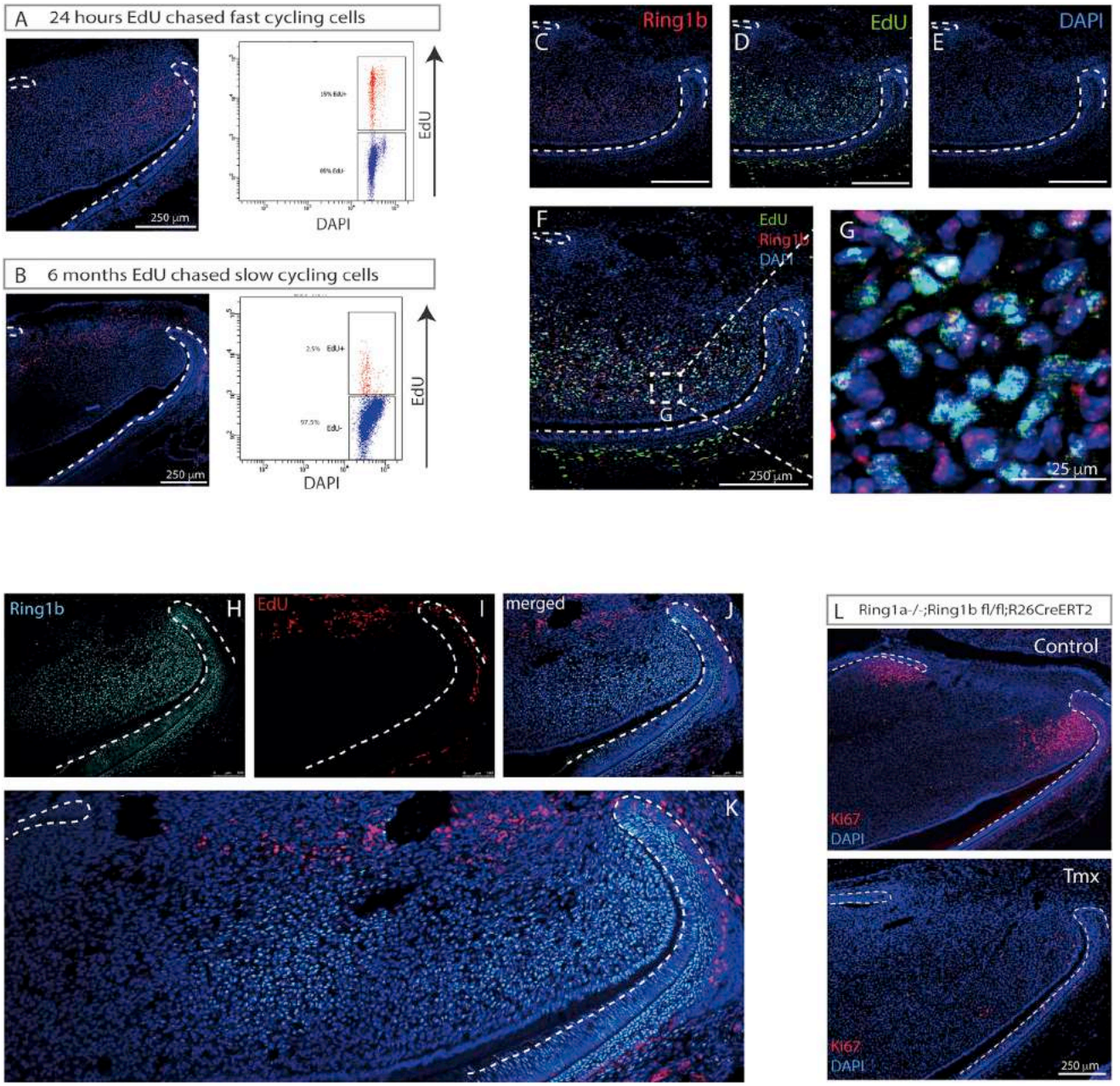

Figure 1. MSC Niche in the Mouse Incisor

(A and B) To label fast-cycling cells (TACs), postnatal day 5 pups were given a single EdU injection (3.3 μg/g BW) and sacrificed after 16–24 hr (A). To identify slow-cycling cells, postnatal day 5 pups were given daily EdU injections (3.3 μg/g BW) for 4 weeks and traced for 2–6 months before tissue collection (B). Click-it EdU image kit was used for EdU detection on sagittal sections of mouse incisors. EdU was labeled with Alexa Fluor 594 dye and DAPI was used for nuclear labeling.

(C–G) Immunofluorescence showed that Ring1b (C) co-localized with EdU-labeled TACs (D) in dental mesenchyme (82% EdU^+ are $Ring1b^+$, and 70% $Ring1b^+$ are EdU^+). DAPi staining (E), merged image (F), and (G) Enlarged field of (F) showing localization of Ring1b and EdU^+ in the TAC region.

(H–K) Immunolocalization of Ring1b (H) and slow-cycling (label-retaining) cells (I).

(J) Merged image.

(K) Tilescan image of (J).

(L) Loss of Ring1a/b showed decreased cell proliferation identified by Ki67 staining.

N ≥ 3 mice per group.

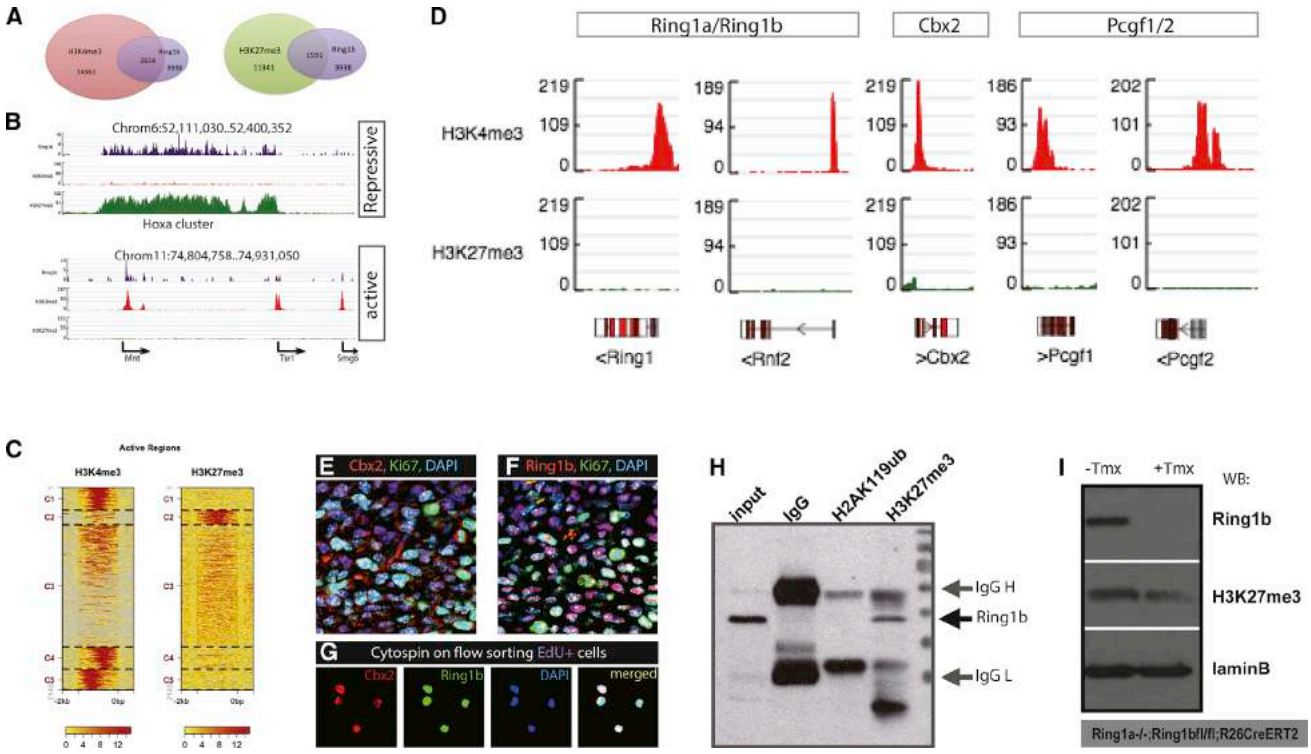

Figure 2. Genome-wide Landscapes of PRC1 in TACs

(A) ChIP-seq on Ring1b, H3K4me3, and H3K27me3 identified 3,939, 14,361, and 11,341 gene loci, respectively. There were 2,624 gene loci co-occupied by both H3K4me3 and Ring1b, whereas 1,591 loci were marked with H3K27me3 and Ring1b.

(B) Genome browser snapshots representing repressive and active gene loci regulated by Ring1b.

(C) BigWIG metrics identified five clusters across targets in H3K4me3 and H3K27me3 active regions.

(D) Snapshots of genome browser showed the enrichment of PRC1 components in TACs.

(E and F) Double immunolocalization of Ki67 (E) with Cbx2 and Ring1b (F), respectively, in the TAC region.

(G) Flow-sorted EdU$^+$ fast-cycling cells were collected by cytospin and immunofluorescence staining showed co-localization of Ring1b and Cbx2 on EdU$^+$ cells.

(H) Co-immunoprecipitation with H2AK119ub1 and H3K27me27 on primary dental pulp cells by Ring1b antibody identified interaction of Ring1b and H3K27m3 rather than H2AK119ub1.

(I) Conditional knock out of Ring1b caused decreased levels of H3K27me3 demonstrated by western blots. Lamin B antibody was used as an internal loading control.

N $\geq$ 5 mice per group.

cell cycle were downregulated, whereas a major negative regulator was upregulated.

Identification of the Wnt/β-Catenin Pathway in TACs

The microarray analysis revealed downregulation of Wnt/β-catenin pathway genes in TACs following the loss of Ring1 function (Figure 3D). To investigate this further, we mined the ChIP-seq datasets for cell-signaling pathways using Protein Analysis Through Evolutionary Relationships (PANTHER) (Mi et al., 2013). GO enrichment analysis showed that Wnt/β-catenin signaling emerged as the top pathway hit on both Ring1b (Figure 4A) and H3K4me3 datasets (Figure 4B). Wnt target genes such as Axin2, β-catenin, cyclin D1, cMyc, E2f1, and Twist1 showed peaks co-occupied by H3K4me3 and Ring1b but not by H3K27me3 in ChIP-seq (Figure 4C). qPCR confirmed the downregulation of Wnt targets by Ring1 deletion (Figure 4D). Zic genes code for transcriptional repressors of Wnt signaling activity and are repressed in cells where Wnt pathway genes are active (Chiacchiera et al., 2016). The H3K27me3 dataset identified Zic1/2 genes as bound loci that also were bound by Ring1b (Figure 4E), which is consistent with Wnt-signaling activity in TACs being regulated by Ring1. Further support for this role came from qPCR of Ring1b$^{-/-}$ pulp cells that showed dramatically increased expression of Zic1 and Zic2 (Figures 4F and S4; Table S2). Ring1 is thus bound at loci of both Wnt-signaling pathway active genes and Wnt-signaling pathway repressor genes in combination with either H3K4me3 or H3K27me3, respectively.

Wnt/β-Catenin Pathway *In Vivo*

To confirm the status of Wnt/β-catenin-signaling activity in TACs *in vivo*, we used Axin2^{LacZ} mice (van Amerongen et al., 2012). Maximum levels of Axin2 expression (Figure S5) were localized in the regions occupied by TACs (Figure S5) and was expressed in odontoblasts. Little Axin2 expression could be visualized in stem cells, as has been suggested from TOPGal staining (Yang et al., 2015). To confirm this location, we used genetic lineage tracing of Axin2-expressing cells with

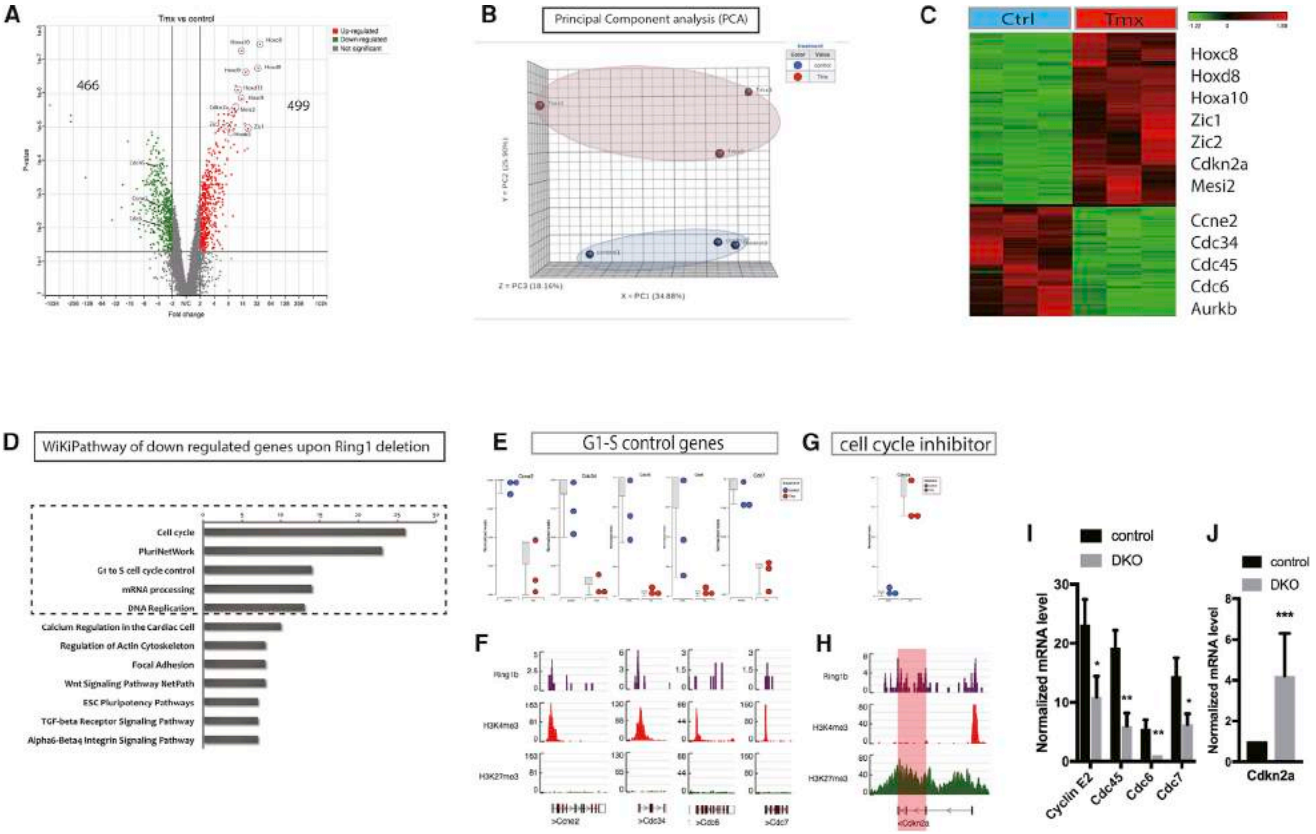

Figure 3. Gene Expression and ChIP-Seq Identify the Role of PRC1 on Cell-Cycle Regulation

(A) Whole-genome microarrays revealed that 499 genes were upregulated and 466 genes were downregulated with >2-fold change ($p < 0.05$) upon Ring1a/b deletion represented by volcano plots.

(B) PCA plots identified and grouped the samples by similarities and differences.

(C) Heatmaps representing hierarchical clustering of differentially expressed genes following loss of Ring1a/b (n = 3 biological replicates, minimum four mice per group).

(D) WiKiPathway revealed the top five pathways to be related to cell-cycle regulation.

(E) G1-S control and DNA replication genes were found downregulated upon Ring1 deletion on gene microarray datasets and (F) the enrichment loci also were co-marked by Ring1b and H3K4me3 but not with H3K27me3 on ChIP-seq datasets.

(G) Cell-cycle inhibitor Cdkn2a was found to be upregulated in Ring1b^{-} cells and (H) identified as a direct target of Ring1b marked by H3K27me3. A single peak of H3K4me3 is present upstream of the Cdkn2a start site in a region also bound by H3K27me3. Highlighted region shows the gene transcription region for Cdkn2a.

(I and J) Real-time PCR confirmed the (I) upregulated cell-cycle genes and downregulation (J) of Cdkn2a upon Ring1 deletion in mouse dental pulp cells.

N ≥ 3 mice per group. *$p < 0.05$, **$p < 0.01$, and ***$p < 0.001$ by Student's t test. Data presented as means ± SEMs.

Axin2^{ERT2cre};Rosa26R$^{mt/mg}$ reporter mice. Immediately following tamoxifen induction, GFP^{+} cells were seen in the odontoblast layer (odontoblasts express Axin2) and pulp cells in the proximal region (Figure 5). At later time points post-tamoxifen, GFP^{+} cells became progressively more distally located, and by 30 days, all GFP^{+} cells have disappeared. Thus, Axin2^{+} cells are located in the TAC zone and give rise to pulp cells that show a temporal proximal-distal progression. These labeled cells are removed at the tips during growth and are not continuously replaced by new labeled cells. Axin2^{+} cells, therefore, correspond to a population of rapid-cycling, non-self-renewing cells, consistent with a TAC identity (Figure 5).

TACs Are Required for Stem Cell Maintenance

We hypothesized that the loss of cell proliferation in the TAC zone as a result of the loss of Ring1 function also may indirectly affect the stem cells because TAC numbers and stem cell division must be interlinked in some way. Using the nucleoside retention to detect the slow-cycling stem cells (Figure 6A), we observed that EdU^{+} cells were barely detectable 96 hr post-tamoxifen induction of Ring1b deletion on a Ring1a$^{-/-}$ background compared with controls (Figure 6B). Tunel assays showed that whereas few apoptotic cells were present in the stem cell zone before tamoxifen administration, 96 hr after administration (Ring1b$^{cko/cko}$;Ring1a$^{-/-}$), a line of apoptotic cells corresponding to the location of slow-cycling stem cells was observed (Figure 6C). Significantly, no increase in apoptotic cells was observed in the TAC zone or elsewhere in the incisor (Figure 6C). Because Wnt signaling activity is localized to TACs, we investigated the impact of blocking Wnt activity in TACs. Gpr177 codes for the Wntless protein that is required for the secretion of Wnt ligands (Carpenter et al., 2010). We generated

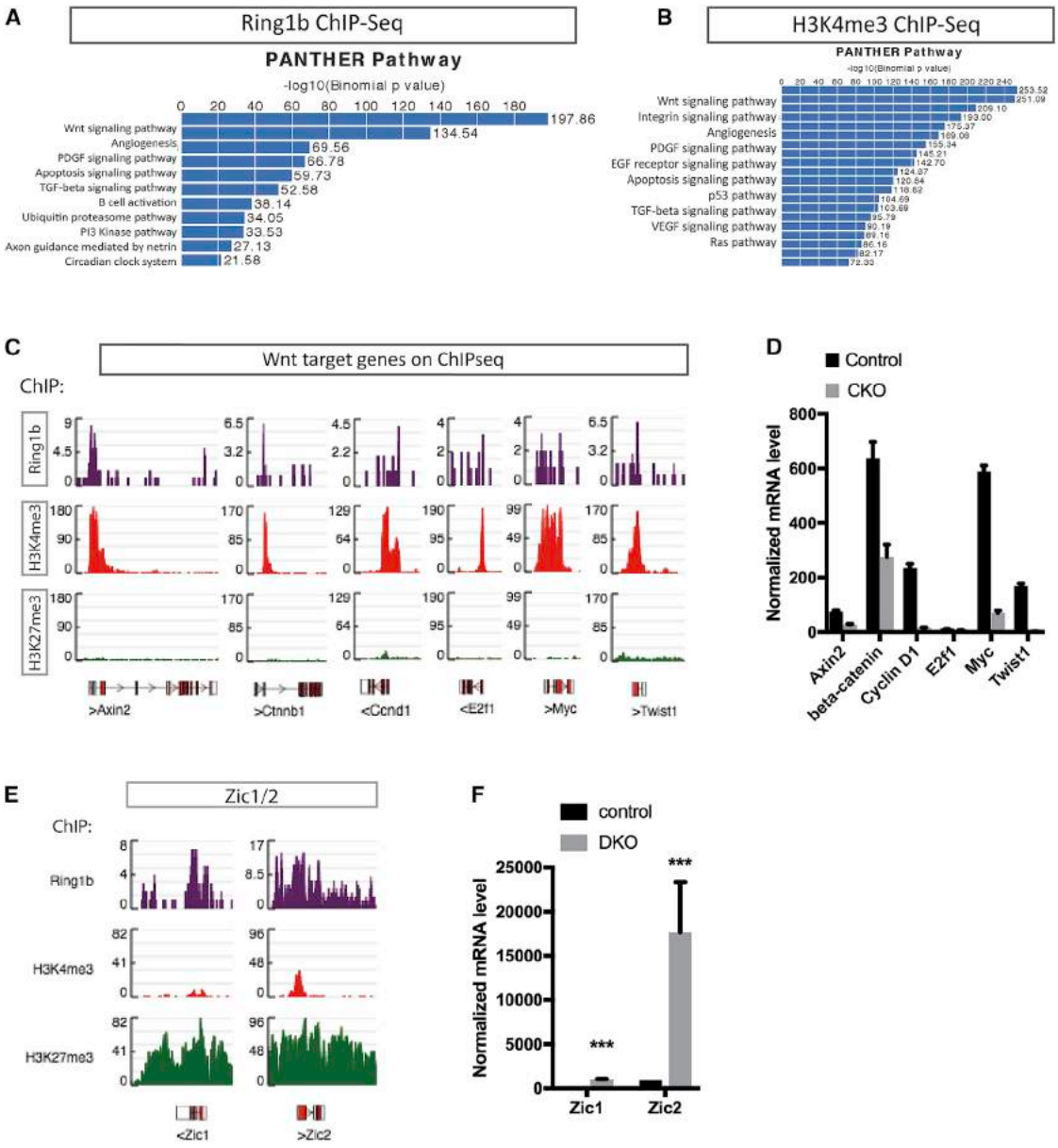

Figure 4. ChIP-Seq Analysis Reveals Ring1b Targets in the Wnt Pathway

(A and B) GO enrichment analysis using PANTHER pathway identified Wnt/β-catenin signaling as the top pathway in Ring1b (A) and H3K4me3 (B) ChIP-seq datasets.

(C) Peak calling showed the enrichment of Wnt target genes co-marked by Ring1b and H3K4me3 but no enrichment with H3K27me3.

(D) Validation of downregulated Wnt target genes by Ring1b using real-time PCR. N ≥ 3 mice per group. $p < 0.05$ by Student's t test. Data presented as means ± SEMs.

(E) Genomic view of Zic1/2 co-occupying the same loci as Ring1b and H3K27me3 rather than H3K4me3.

(F) Zic1/2 were upregulated following deletion of Ring1a/b identified by real-time PCR.

N ≥ 3 mice per group. ***$p < 0.001$ by Student's t test. Data presented as means ± SEMs.

Wntless conditional mutant mice using $Wls^{flox/flox}$ crossed with $Axin2^{ERT2cre}$ and administered tamoxifen to adult animals. Seven days post-tamoxifen, cell proliferation in TACs detected by nucleoside incorporation was substantially reduced, as was the rate of incisor growth (Figures 6D and S5C). Using the early apoptosis marker, annexin V, we identified apototic cells exclusively in the stem cell zone 2 days post-tamoxifen following Ring1-targeted deletion in TACs ($Axin2^{ERT2cre}$) (Figure 6E). Loss of Wnt activity in TACs thus phenocopies the loss of Ring1 function showing reduced proliferation and stem cell apoptosis.

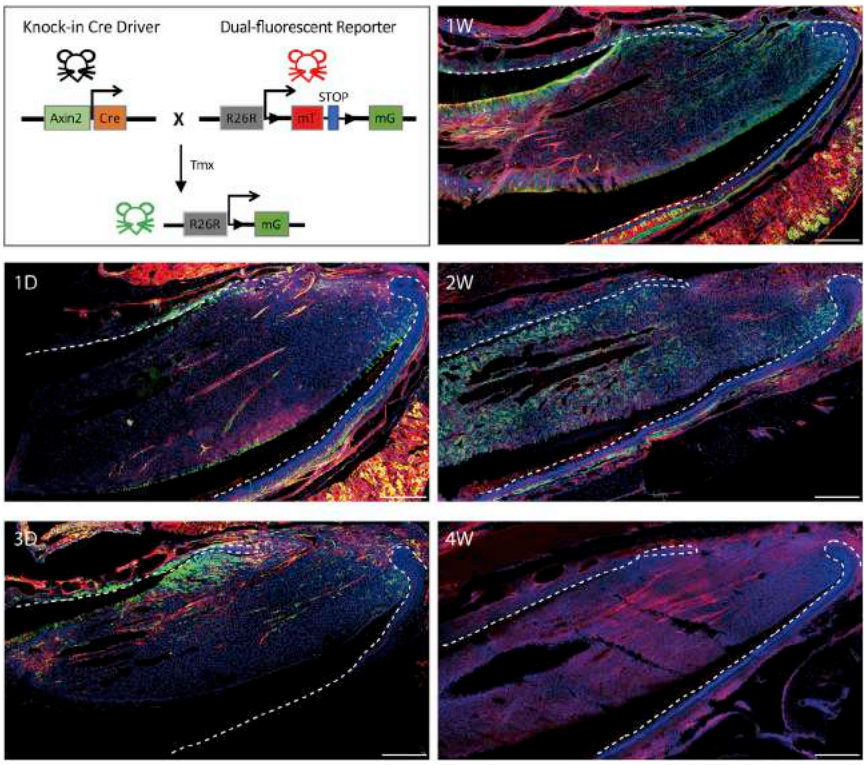

Figure 5. Wnt Signals in the MSC Niche

Lineage tracing of Axin2 progeny (GFP$^+$) at 1 day, 3 days, 1 week, 2 weeks, and 4 weeks post-tamoxifen injection of Axin2^{ERT2cre};mTmG mice on sagittal sections of mouse incisors. GFP$^+$ cells were detected in the TAC region of dental mesenchyme close to the epithelial cervical loop after 1 day and increased in number by 3 days post-tamoxifen. Axin2-derived cells (GFP$^+$) showed an increased contribution to dental pulp cells and odontoblasts toward the apical end by 1 week and progressively advanced toward the tip of the incisor by 2 weeks post-tamoxifen. There were no GFP$^+$ cells detected in the mouse incisor after 4 weeks post-tamoxifen. Green is GFP$^+$, red is Tomato$^+$, and blue is DAPI for nuclear staining. N $\geq$ 3 mice per group. Scale bar: 250 μm.

DISCUSSION

The continuously growing mouse incisor provides a model for studying stem cell functions in growth homeostasis. The extremely rapid growth (500–600 μm/day) (Smith and Warshawsky, 1975) and the distinct anatomical locations of the stem cell compartments enables cell interactions to be studied *in vivo* (An et al., 2018; Feng et al., 2011; Juuri et al., 2012; Kaukua et al., 2014; Lapthanasupkul et al., 2012; Seidel et al., 2010; Wang et al., 2007; Zhao et al., 2014). Nucleoside incorporation identifies spatially distinct populations of slow- and fast-cycling cells at the proximal end of the tooth. The slow-cycling cells are Shh responsive, and lineage tracing using Gli1Ert2cre confirms these cells to be stem cells (Zhao et al., 2014). A distally adjacent population of fast-cycling cells are progenitors (TACs) that differentiate into the specialized mesenchymal cells of the tooth, the odontoblasts that form dentin, and the fibroblastic pulp cells.

The transition from slow-cycling, self-renewing stem cells to fast-cycling, non-self-renewing TACs that differentiate into tooth mesenchymal cells is pivotal in controlling the growth rate of the incisor. Whereas genetic lineage tracing has identified the stem cells as Gli1$^+$ cells occupying a neurovascular niche, less is known about the TACs and how their proliferation is activated. We had identified components of the PRC1 complex as being expressed in the TACs and shown that deletion of the core complex component Ring1 resulted in a loss of TAC proliferation (Lapthanasupkul et al., 2012). Functional PRC1 is thus required for TAC proliferation and incisor growth, but its function in controlling proliferation was not understood. We describe here the application of gene expression comparisons and ChIP-seq analysis to identify PRC1 target loci in TACs and correlate these with changes in gene expression following the loss of Ring1. We find that Ring1 co-localizes with Cbx2 in TACs and with H3K27me3 but not H2AK119ub in immunoprecipitations, suggesting a repressive role for PRC1 via association with trimethylation on H3K27 rather than monoubiquitination on H2AK119. Cbx2 shows preference for H3K27me3, whereas Cbx4 and Cbx7 chromatin domains exhibit preference for H3K9me3 (Bernstein et al., 2006; Kaustov et al., 2011; Tardat et al., 2015), and almost no affinity for Cbx6 and Cbx8 for H3K27me3 (Bernstein et al., 2006; Kaustov et al., 2011). Previous ChIP-seq data revealed that PRC1 target domains are broadly or sharply localized with H3K27me3 (Ku et al., 2008), which also was identified by our ChIP-seq datasets. Likewise, our results further suggested that a repressive mechanism of PRC1 in TACs is via Cbx2 association with H3K27me3 independent of histone H2A modification.

There were 2,624 loci identified that bound both Ring1b and H3K4me3, a gene transcription activation mark. Among these Ring 1b/H3K4me3-bound loci were a number of positive regulators of the cell cycle, whereasloci bound by Ring1b and H3K27me3 included major cell-cycle inhibitors such as Cdkn2a, a known direct target of PRC1 (Biehs et al., 2013; Dietrich et al., 2007). Microarrays comparing gene expression between Ring1b$^+$ and Ring1b$^-$ pulp cells showed a decrease in positive cell-cycle-regulator expression following Ring1a/b deletion and a significant increase in Cdkn2a expression. These results suggest that the cell cycle is dually regulated by PRC1 through activating positive cell-cycle regulators and repressing negative regulators.

Identification of the range of expression levels at PRC1 targets by ChIP-seq suggests that PRC1 does not act as an absolute repressor, but it may regulate the extent of RNA polymerase II (RNAPII) transcriptional activity (Brookes et al., 2012; Enderle et al., 2011; Schwartz and Pirrotta, 2008). Studies have highlighted the opposite scenario of polycomb group (PcG) complexes as activators of gene transcription (Aranda et al., 2015;

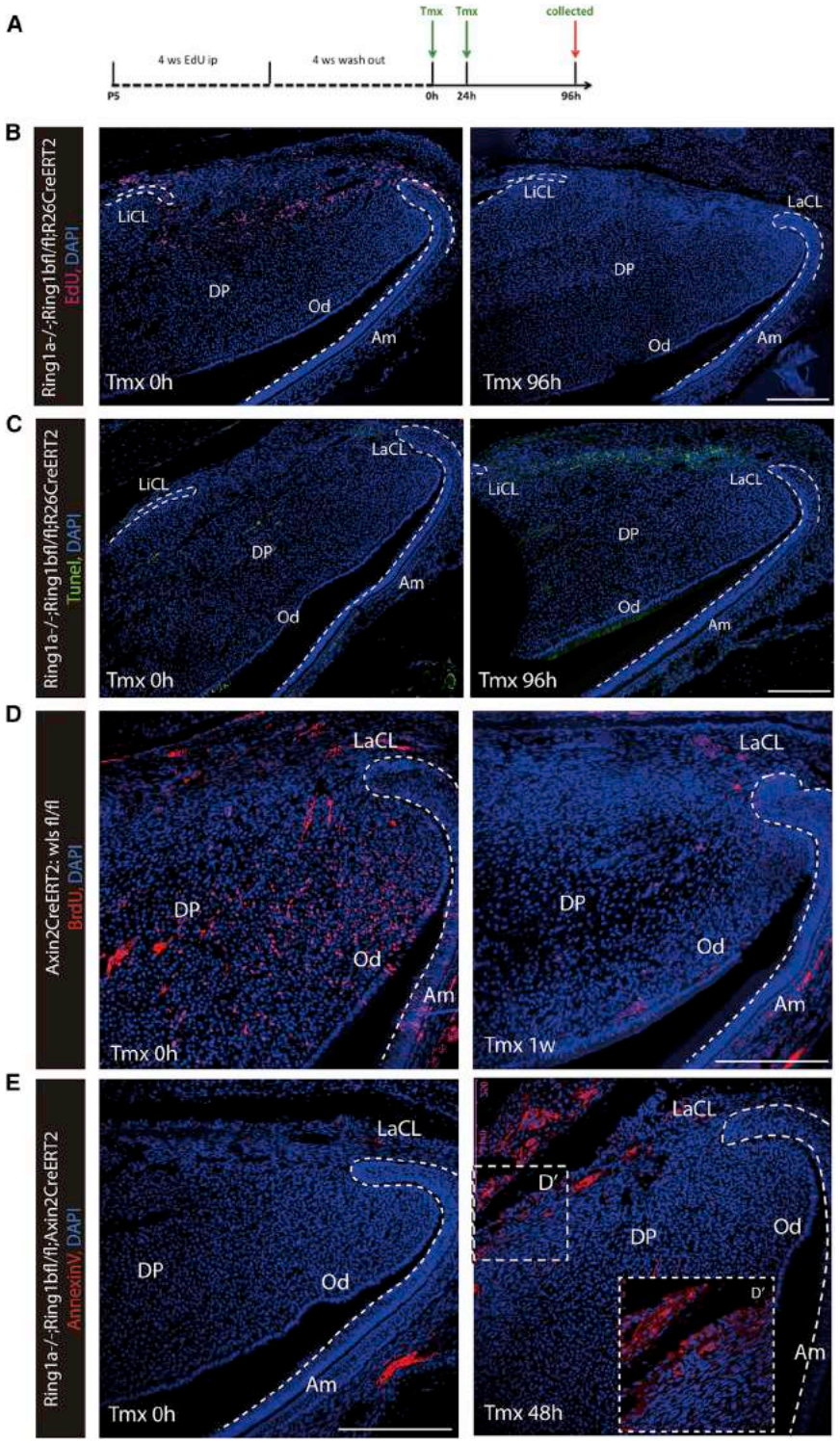

Figure 6. Maintenance of Stem Cell Stability by PRC1

(A) Schematic illustration demonstrated EdU retention assay to detect slow-cycling stem cells.

(B) EdU^{+} cells were distinctly localized between the labial and lingual aspects of the cervical loop, but they disappeared by 96 hr post-tamoxifen induction of Ring1 deletion.

(C) Tunel assays revealed apoptotic cells in the stem cell zone in Ring1^{-} cells, whereas no obvious apoptosis was detected in control incisors.

(D) Reduced cell proliferation was detected in Wls$^{flox/flox}$;Axin2^{CreERT2} marked by BrdU-labeled cells.

(E) Annexin V^{+} apoptotic cells were visible in the stem cell zone 2 days post-tamoxifen on Ring1a$^{-/-}$;Ring1b$^{flox/flox}$:Axin2^{CreERT2} mice compared to controls.

N $\geq$ 3 mice per group.

Frangini et al., 2013; Gao et al., 2014) under different cellular contexts. For example, PRC1 co-occupies active target genes with the Aurora B kinase (Frangini et al., 2013); CK2 protein phosphorylates Ring1B at serine 168 (Gao et al., 2014) and regulates the local topological interaction with Meis2, which binds to a tissue-specific enhancer involved in removing PRC1 from the promoter (Kondo et al., 2014). Aurora B kinase is present in mouse dental pulp mesenchyme and is localized to the TAC region (Figure S6; Table S3), which is the same expression region as Ring1b and may explain the role of PRC1 on transcriptional activation for controlling some positive cell-cycle regulators in TACs.

The main signaling pathway identified from the Ring1/H3K4me3 ChIP-seq datasets was Wnt/β-catenin. The Wnt/β-catenin pathway is involved in the control of cell proliferation, stem cell self-renewal, and cell fate specification, and is associated with several diseases (Clevers, 2006; Clevers and Nusse, 2012; Moon et al., 2004; Reya and Clevers, 2005) Wnt signaling can either stimulate or restrain the process of apoptosis, according to specific cellular environment contexts (Brocardo and Henderson, 2008; Pećina-Slaus, 2010; Yeo and Gautier, 2004). Through the inhibition of Zic transcription factors, PRC1 sustains Wnt/β-catenin activity and preserves adult stem cell identities (Chiacchiera et al., 2016). Our results identify the co-occupied binding loci of Zic1/2 and Wnt target genes by Ring1b. Loss of Ring1b causes the upregulation of Zic1/2 and the downregulation of Wnt signals, indicating that PRC1 regulates the Wnt signaling pathway by repressing Zic1/2 transcription factors.

Depletion of Ring1b decreased cell proliferation in TACs and, surprisingly, caused specific apoptosis of the stem cells. We assume that TACs act as a supportive environment for stem

cell maintenance and hypothesize that secreted signaling proteins produced by TACs act as positive regulators on the adjacent stem cell population. Loss of Wnt signaling also resulted in the apoptosis of stem cells, indicating that Wnt/β-catenin activity downstream of PRC1 is required for stem cell maintenance.

EXPERIMENTAL PROCEDURES

EdU/BrdU Incorporation and Staining

To label fast-cycling cells, mice were intraperitoneally (IP) injected with one dose of EdU (3.3 μg/g body weight) or 5-bromo-2′-deoxyuridine (BrdU) (100 mg/kg body weight) and sacrificed after 16–24 hr. For slow-cycling cell labeling, pups post-natal days 2–5 were IP injected with EdU daily for 4 weeks and chased for another 4 weeks to 6 months before tissue collection. See the Supplemental Experimental Procedures for details.

Flow Cytometry

Mouse incisor pulp tissue was freshly dissected and dissociated as a single cell suspension by TrypLE Express Enzyme (Thermo Fisher Scientific, catalog no. 12604013). Cells were then fixed and stained by Click-iT EdU Alexa Fluor 647 Flow Cytometry Assay kit (Invitrogen, catalog no. C10424), according to the protocol before being subjected to flow cytometry. FACS analysis was carried out on a BD Fortessa cell analyzer and data were analyzed by BD FACSDiva 6.1.3 (both BD Biosciences) or FlowJo software.

ChIP-Seq

See the Supplemental Experimental Procedures for details. Basically, 75-nucleotide sequence reads generated by Illumina sequencing (NextSeq500) were mapped to the mouse genome (mm10 assembly) using the Burrows-Wheeler Aligner (BWA) algorithm. The resulting BAM files were then analyzed, and peak calling used model-based analysis of ChIP-seq (MACS) (Zhang et al., 2008) to identify genomic regions enriched in the proteins in comparison to the total genomic input DNA. Histone ChIPs were analyzed with Spatial Clustering for Identification of ChIP-Enriched Regions (SICER) (Zang et al., 2009).

Gene Microarray

Biological triplicates were processed separately through the entire microarray procedure. Total RNA was extracted using miRNeasy Mini Kits (Qiagen, catalog no. 217004), and cDNA was synthesized using standard Affymetrix protocols. Samples were hybridized to Affymetrix GeneChip Mouse Genome 430 2.0 Arrays. CEL files were generated and then analyzed using Partek Flow pipelines. Reads were aligned with BWA and quantified to the annotation model (Partek E/M). Data were normalized, and genes were analyzed using differential gene expression (GSA) algorithm.

Mice Information

All of the animal work was carried out according to Home Office guidelines in the UK under project license number PPL70/7866. See the Supplemental Experimental Procedures for details.

Statistics

Statistical analysis was done using GraphPad Prism and the Microsoft Office 2016 program package. Paired Student's t test was used to calculate statistical significance. Values of $p < 0.05$ were considered statistically significant. A minimum of three to five animals were used for each experiment.

Microscopy and Imaging

Confocal microscopy used a Leica TCS SP5 system and imaging processing analysis used Leica LAS AF imaging software. For Ring1b and Tunel detection, argon laser 488 nm line excitation and emission maximum at 525 nm were used. For EdU, BrdU, and annexin V excitation, the argon laser 561 nm was used for excitation and, at 617 nm, used as maximum emission. DAPI/Hoechst 33342 was detected using violet (405 nm) laser line and emission maximum at 470 nm. LacZ sections images were obtained on a Zeiss microscope.

DATA AND SOFTWARE AVAILABILITY

The accession number for data reported in this paper is GEO: GSE104893. The SubSeries accession number for the histone ChIPs data reported in this paper is GEO: GSE104891. The accession number for the Ring1b ChIP data reported in this paper is GEO: GSE104892. The accession number for the microarray expression data reported in this paper is GEO: GSE104934.

SUPPLEMENTAL INFORMATION

Supplemental Information includes Supplemental Experimental Procedures, six figures, and three tables and can be found with this article online at https://doi.org/10.1016/j.celrep.2018.05.001.

ACKNOWLEDGMENTS

This study was funded by Medical Research Council grant number MRK018035/1 (to P.S.).

AUTHOR CONTRIBUTIONS

P.T.S. conceived the experiments. Z.A. carried out most of the experiments, analysed the data, and prepared all the figures. B.A. and Y.C. assisted with the Axin2 mice experiment. M.S. and G.Z. assisted with the *in situ* experiment. Z.A. and P.T.S. wrote the manuscript.

DECLARATION OF INTERESTS

The authors declare no competing interests.

Received: October 23, 2017
Revised: February 22, 2018
Accepted: April 25, 2018
Published: June 5, 2018

REFERENCES

An, Z., Sabalic, M., Bloomquist, R.F., Fowler, T.E., Streelman, T., and Sharpe, P.T. (2018). A quiescent cell population replenishes mesenchymal stem cells to drive accelerated growth in mouse incisor. Nat. Commun. *9*, 378.

Aranda, S., Mas, G., and Di Croce, L. (2015). Regulation of gene transcription by polycomb proteins. Sci. Adv. *1*, e1500737.

Bernstein, E., Duncan, E.M., Masui, O., Gil, J., Heard, E., and Allis, C.D. (2006). Mouse polycomb proteins bind differentially to methylated histone H3 and RNA and are enriched in facultative heterochromatin. Mol. Cell. Biol. *26*, 2560–2569.

Biehs, B., Hu, J.K.-H., Strauli, N.B., Sangiorgi, E., Jung, H., Heber, R.-P., Ho, S., Goodwin, A.F., Dasen, J.S., Capecchi, M.R., et al. (2013). BMI1 represses Ink4a/Arf and Hox genes to regulate stem cells in the rodent incisor. Nat. Cell Biol. *15*, 846–852.

Brocardo, M., and Henderson, B.R. (2008). APC shuttling to the membrane, nucleus and beyond. Trends Cell Biol. *18*, 587–596.

Brookes, E., de Santiago, I., Hebenstreit, D., Morris, K.J., Carroll, T., Xie, S.Q., Stock, J.K., Heidemann, M., Eick, D., Nozaki, N., et al. (2012). Polycomb associates genome-wide with a specific RNA polymerase II variant, and regulates metabolic genes in ESCs. Cell Stem Cell *10*, 157–170.

Carpenter, A.C., Rao, S., Wells, J.M., Campbell, K., and Lang, R.A. (2010). Generation of mice with a conditional null allele for Wntless. Genesis *48*, 554–558.

Chiacchiera, F., Rossi, A., Jammula, S., Piunti, A., Scelfo, A., Ordóñez-Morán, P., Huelsken, J., Koseki, H., and Pasini, D. (2016). Polycomb compex PRC1 preserves intestinal stem cell identity by sustaining Wnt/β- catenin transcriptional activity. Cell Stem Cell *18*, 91–103.

Clevers, H. (2006). Wnt/β-catenin signaling in development and disease. Cell *127*, 469–480.

Clevers, H., and Nusse, R. (2012). Wnt/β-catenin signaling and disease. Cell *149*, 1192–1205.

Dietrich, N., Bracken, A.P., Trinh, E., Schjerling, C.K., Koseki, H., Rappsilber, J., Helin, K., and Hansen, K.H. (2007). Bypass of senescence by the polycomb group protein CBX8 through direct binding to the INK4A-ARF locus. EMBO J. *26*, 1637–1648.

Elderkin, S., Maertens, G.N., Endoh, M., Mallery, D.L., Morrice, N., Koseki, H., Peters, G., Brockdorff, N., and Hiom, K. (2007). A phosphorylated form of Mel-18 targets the Ring1B histone H2A ubiquitin ligase to chromatin. Mol. Cell *28*, 107–120.

Enderle, D., Beisel, C., Stadler, M.B., Gerstung, M., Athri, P., and Paro, R. (2011). Polycomb preferentially targets stalled promoters of coding and non-coding transcripts. Genome Res. *21*, 216–226.

Eskeland, R., Leeb, M., Grimes, G.R., Kress, C., Boyle, S., Sproul, D., Gilbert, N., Fan, Y., Skoultchi, A.I., Wutz, A., and Bickmore, W.A. (2010). Ring1B compacts chromatin structure and represses gene expression independent of histone ubiquitination. Mol. Cell *38*, 452–464.

Feng, J., Mantesso, A., and Sharpe, P.T. (2010). Perivascular cells as mesenchymal stem cells. Expert Opin. Biol. Ther. *10*, 1441–1451.

Feng, J., Mantesso, A., De Bari, C., Nishiyama, A., and Sharpe, P.T. (2011). Dual origin of mesenchymal stem cells contributing to organ growth and repair. Proc. Natl. Acad. Sci. USA *108*, 6503–6508.

Frangini, A., Sjöberg, M., Roman-Trufero, M., Dharmalingam, G., Haberle, V., Bartke, T., Lenhard, B., Malumbres, M., Vidal, M., and Dillon, N. (2013). The aurora B kinase and the polycomb protein ring1B combine to regulate active promoters in quiescent lymphocytes. Mol. Cell *51*, 647–661.

Gao, Z., Lee, P., Stafford, J.M., von Schimmelmann, M., Schaefer, A., and Reinberg, D. (2014). An AUTS2-polycomb complex activates gene expression in the CNS. Nature *516*, 349–354.

Juuri, E., Saito, K., Ahtiainen, L., Seidel, K., Tummers, M., Hochedlinger, K., Klein, O.D., Thesleff, I., and Michon, F. (2012). Sox2+ stem cells contribute to all epithelial lineages of the tooth via Sfrp5+ progenitors. Dev. Cell *23*, 317–328.

Kaukua, N., Shahidi, M.K., Konstantinidou, C., Dyachuk, V., Kaucka, M., Furlan, A., An, Z., Wang, L., Hultman, I., Ährlund-Richter, L., et al. (2014). Glial origin of mesenchymal stem cells in a tooth model system. Nature *513*, 551–554.

Kaustov, L., Ouyang, H., Amaya, M., Lemak, A., Nady, N., Duan, S., Wasney, G.A., Li, Z., Vedadi, M., Schapira, M., et al. (2011). Recognition and specificity determinants of the human cbx chromodomains. J. Biol. Chem. *286*, 521–529.

Kondo, T., Isono, K., Kondo, K., Endo, T.A., Itohara, S., Vidal, M., and Koseki, H. (2014). Polycomb potentiates meis2 activation in midbrain by mediating interaction of the promoter with a tissue-specific enhancer. Dev. Cell *28*, 94–101.

Ku, M., Koche, R.P., Rheinbay, E., Mendenhall, E.M., Endoh, M., Mikkelsen, T.S., Presser, A., Nusbaum, C., Xie, X., Chi, A.S., et al. (2008). Genomewide analysis of PRC1 and PRC2 occupancy identifies two classes of bivalent domains. PLoS Genet. *4*, e1000242.

Lapthanasupkul, P., Feng, J., Mantesso, A., Takada-Horisawa, Y., Vidal, M., Koseki, H., Wang, L., An, Z., Miletich, I., and Sharpe, P.T. (2012). Ring1a/b polycomb proteins regulate the mesenchymal stem cell niche in continuously growing incisors. Dev. Biol. *367*, 140–153.

Mi, H., Muruganujan, A., Casagrande, J.T., and Thomas, P.D. (2013). Large-scale gene function analysis with the PANTHER classification system. Nat. Protoc. *8*, 1551–1566.

Moon, R.T., Kohn, A.D., De Ferrari, G.V., and Kaykas, A. (2004). WNT and β-catenin signalling: diseases and therapies. Nat. Rev. Genet. *5*, 691–701.

Pang, Y.W., Feng, J., Daltoe, F., Fatscher, R., Gentleman, E., Gentleman, M.M., and Sharpe, P.T. (2016). Perivascular stem cells at the tip of mouse incisors regulate tissue regeneration. J. Bone Miner. Res. *31*, 514–523.

Pećina-Slaus, N. (2010). Wnt signal transduction pathway and apoptosis: a review. Cancer Cell Int. *10*, 22.

Reya, T., and Clevers, H. (2005). Wnt signalling in stem cells and cancer. Nature *434*, 843–850.

Schwartz, Y.B., and Pirrotta, V. (2008). Polycomb complexes and epigenetic states. Curr. Opin. Cell Biol. *20*, 266–273.

Seidel, K., Ahn, C.P., Lyons, D., Nee, A., Ting, K., Brownell, I., Cao, T., Carano, R.A., Curran, T., Schober, M., et al. (2010). Hedgehog signaling regulates the generation of ameloblast progenitors in the continuously growing mouse incisor. Development *137*, 3753–3761.

Sharpe, P.T. (2016). Dental mesenchymal stem cells. Development *143*, 2273–2280.

Smith, C.E., and Warshawsky, H. (1975). Cellular renewal in the enamel organ and the odontoblast layer of the rat incisor as followed by radioautography using 3H-thymidine. Anat. Rec. *183*, 523–561.

Suzuki, M., Mizutani-Koseki, Y., Fujimura, Y., Miyagishima, H., Kaneko, T., Takada, Y., Akasaka, T., Tanzawa, H., Takihara, Y., Nakano, M., et al. (2002). Involvement of the polycomb-group gene Ring1B in the specification of the anterior-posterior axis in mice. Development *129*, 4171–4183.

Tardat, M., Albert, M., Kunzmann, R., Liu, Z., Kaustov, L., Thierry, R., Duan, S., Brykczynska, U., Arrowsmith, C.H.H., and Peters, A.H.F.M. (2015). Cbx2 targets PRC1 to constitutive heterochromatin in mouse zygotes in a parent-of-origin-dependent manner. Mol. Cell *58*, 157–171.

van Amerongen, R., Bowman, A.N., and Nusse, R. (2012). Developmental stage and time dictate the fate of Wnt/β-catenin-responsive stem cells in the mammary gland. Cell Stem Cell *11*, 387–400.

Wang, X.-P., Suomalainen, M., Felszeghy, S., Zelarayan, L.C., Alonso, M.T., Plikus, M.V., Maas, R.L., Chuong, C.-M., Schimmang, T., and Thesleff, I. (2007). An integrated gene regulatory network controls stem cell proliferation in teeth. PLoS Biol. *5*, e159.

Yang, Z., Balic, A., Michon, F., Juuri, E., and Thesleff, I. (2015). Mesenchymal Wnt/β-catenin signaling controls epithelial stem cell homeostasis in teeth by inhibiting the antiapoptotic effect of Fgf10. Stem Cells *33*, 1670–1681.

Yeo, W., and Gautier, J. (2004). Early neural cell death: dying to become neurons. Dev. Biol. *274*, 233–244.

Yu, T., Volponi, A.A., Babb, R., An, Z., and Sharpe, P.T. (2015). Stem cells in tooth development, growth, repair, and regeneration. Curr. Top. Dev. Biol. *115*, 187–212.

Zang, C., Schones, D.E., Zeng, C., Cui, K., Zhao, K., and Peng, W. (2009). A clustering approach for identification of enriched domains from histone modification ChIP-Seq data. Bioinformatics *25*, 1952–1958.

Zhang, Y., Liu, T., Meyer, C.A., Eeckhoute, J., Johnson, D.S., Bernstein, B.E., Nusbaum, C., Myers, R.M., Brown, M., Li, W., and Liu, X.S. (2008). Model-based analysis of ChIP-Seq (MACS). Genome Biol. *9*, R137.

Zhao, H., Feng, J., Seidel, K., Shi, S., Klein, O., Sharpe, P., and Chai, Y. (2014). Secretion of shh by a neurovascular bundle niche supports mesenchymal stem cell homeostasis in the adult mouse incisor. Cell Stem Cell *14*, 160–173.

Cell Reports, Volume *23*

Supplemental Information

Regulation of Mesenchymal Stem to Transit-Amplifying Cell Transition in the Continuously Growing Mouse Incisor

Zhengwen An, Basem Akily, Maja Sabalic, Guo Zong, Yang Chai, and Paul T. Sharpe

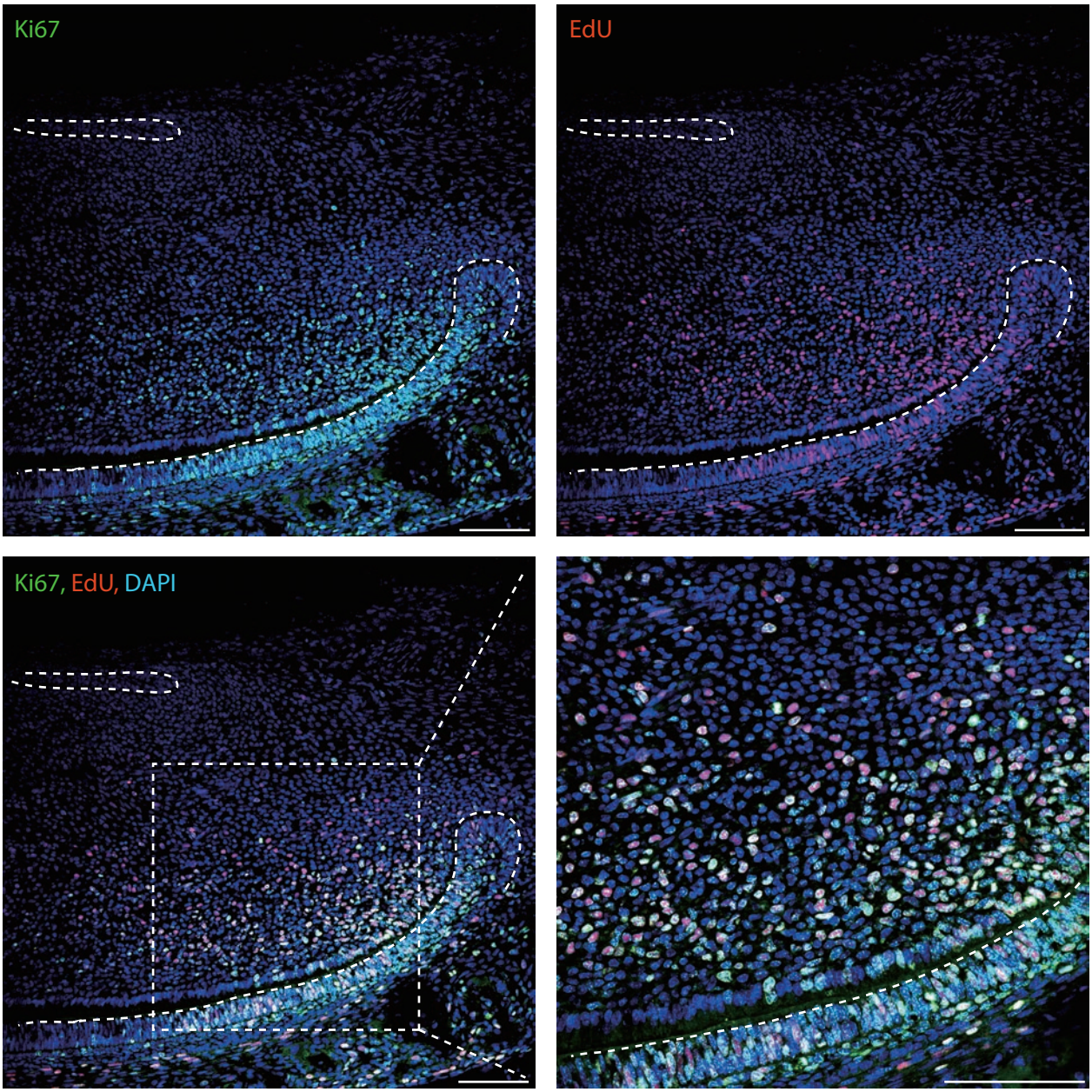

Figure S1. Identification of the TAC region by the cell proliferation marker Ki67 and EdU labelled cells. Related to Figure 1A. Double staining of mouse incisor sagittal sections showing co-localization of Ki67 with 16-24 hours chased EdU+ cells in the TAC region indicative of EdU+ fast cycling TACs. n>=5 mice. Bar is 100 μ m.

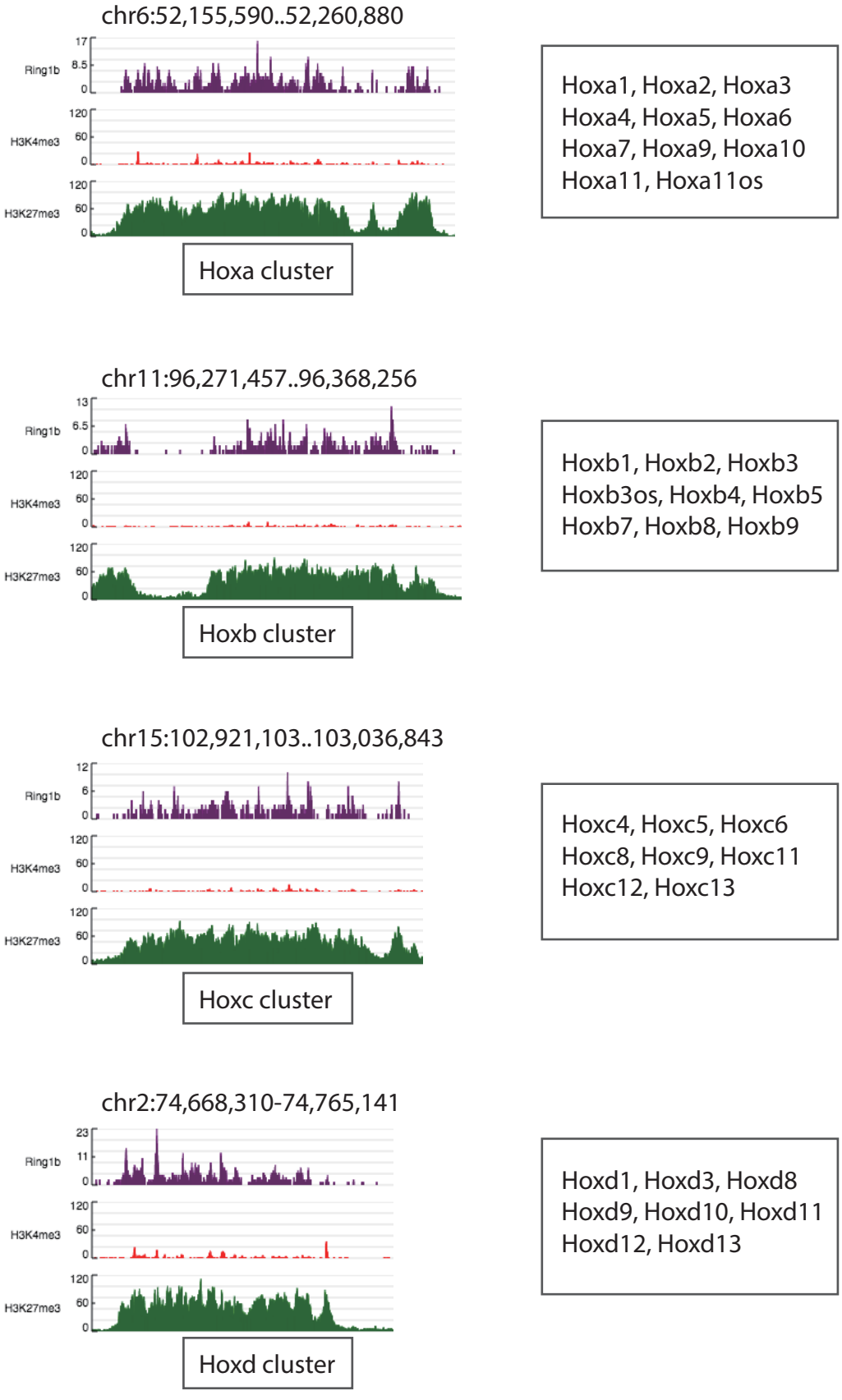

Figure S2. ChIP-seq identifies Hox gene clusters as Ring1b binding loci in TACs. Related to Figure 2A. Genomic views showing Hox clusters co-marked by Ring1b and H3K27me3 but no enrichment with H3K4me3 (left panel). List of Hox genes revealed on ChIP-seq datasets in TACs.

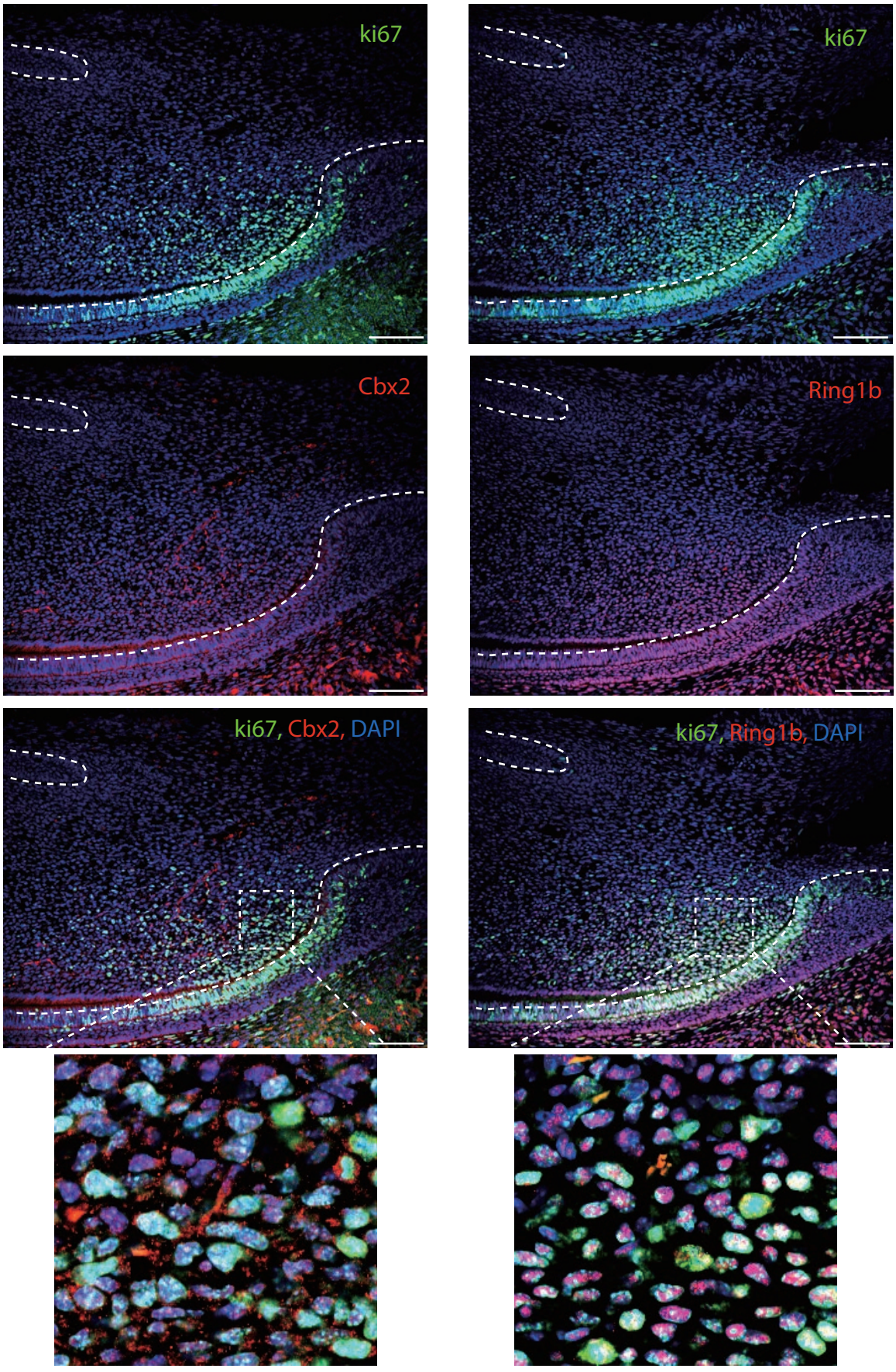

Figure S3. Co-localization of Cbx2 and Ring1b in the mouse dental pulp. Related to Figure 2E-G. Double immuno-staining of Cbx2 and Ring1b both showed co-localization with Ki67 in the TAC region on sequential sections of mouse incisors indicating co-localization of Cbx2 and Ring1b. n>=5 mice per group. Bar is 100 μ m.

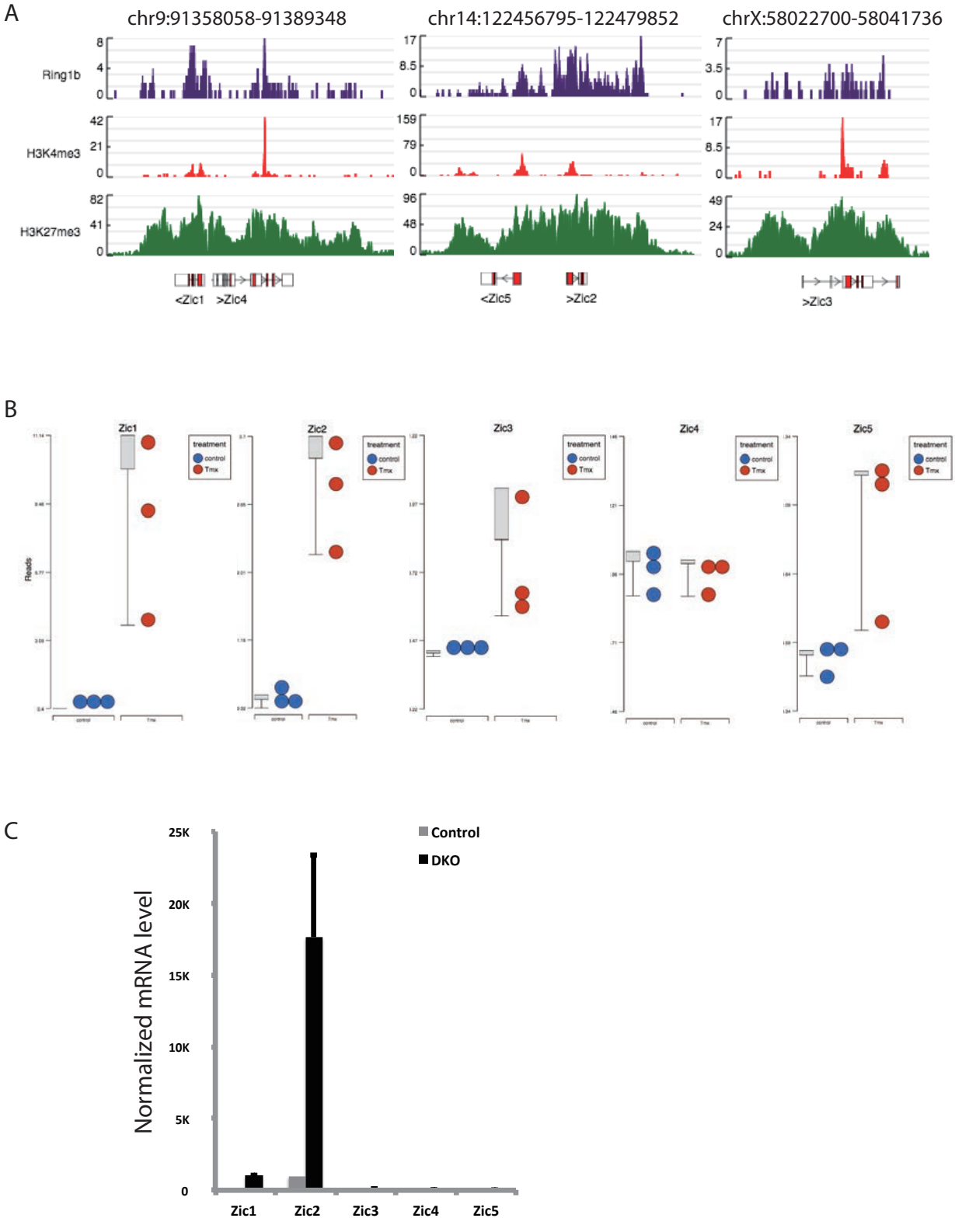

Figure S4. Genomic profiles of Zic family members in TACs. Related to Figure 4E. (A) Genome browser snapshots of Zic1-5 binding profiles. Zic1/2 shows co-occupation with Ring1b and H3K27me3, while other Zic family members also showed binding with H3K4me3. (B) Dot plots showed only Zic1/2 significantly up-regulated following deletion of Ring1b (n=3, $P<0.05$), whereas Zic3, Zic4 and Zic5 showed no significant difference (n=3, $P>0.05$) on microarray datasets. (C) Validation of Zic expression following loss of Ring1b by qPCR confirmed that Zic1/2 were significantly up-regulated compared with other Zic family members (n>=3, $P<0.001$ by Student's t-test). Data presented as mean ± S.E.M.

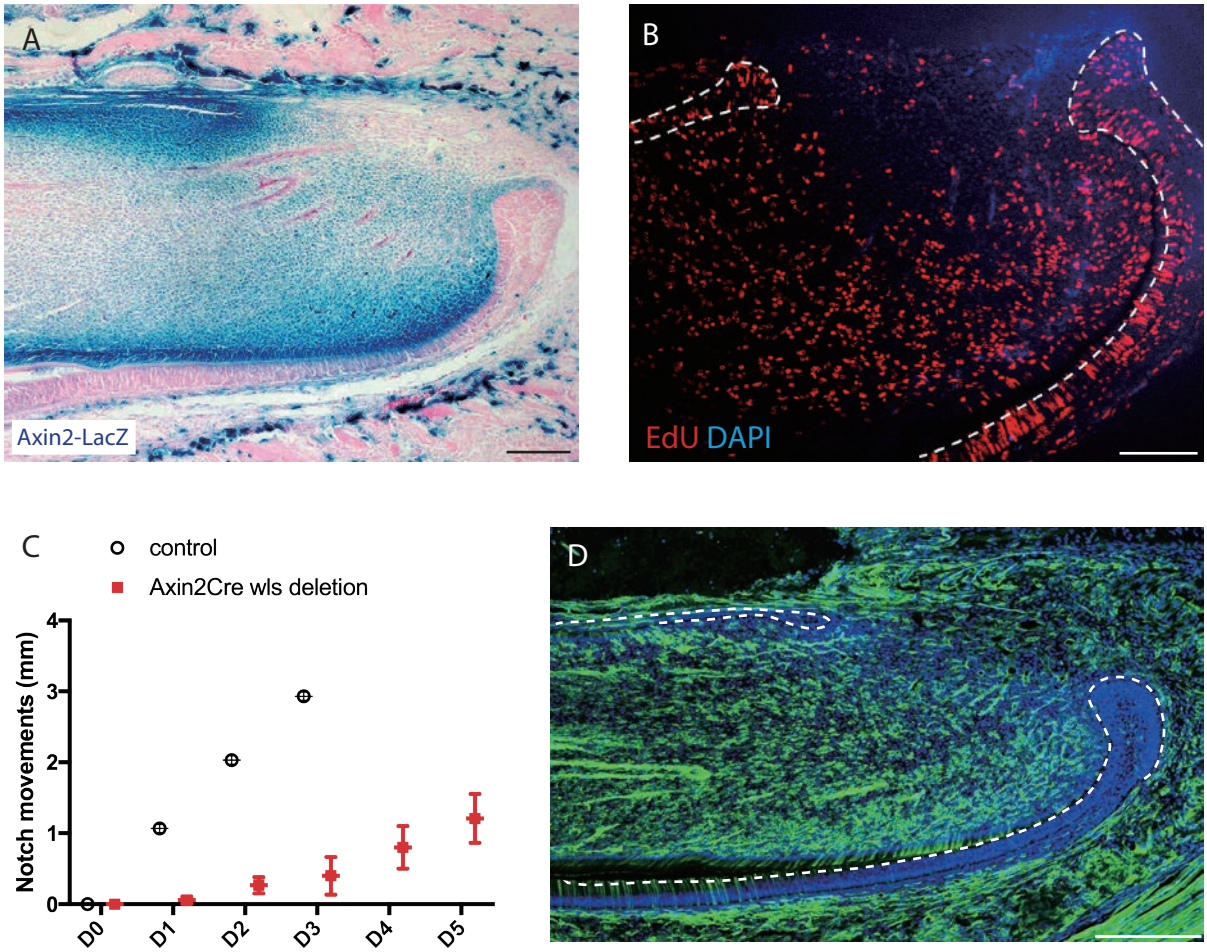

Figure S5. Axin2 expressed in TACs in the mouse incisor. Related to Figure 5 and Figure 6D.
(A) Sagittal section of Axin2LacZ mouse incisor stained for beta-galactosidase (LacZ) activity using X-gal showing Axin2 expression in the TAC region. (B) EdU+ cells detected in the TAC region after 16-24 hours chasing. n>=5 mice. (C) Comparison of growth rates. After one week of three doses of tamoxifen, notches were made 0.8-0.9 mm above the incisor gingiva at day 0 (D0) in Axin2cre;wls cko/cko and control mice. Notch movements were measured every day for five days. Notches in control incisors reach the tip after 3 days, while the notches in Axin2cre;wls cko/cko incisors only reach about 1/3 of full length incisor by day 5. n=3 and P<0.01 by Student's t-test. (D) Efficiency of Cre recombinase in the mouse incisor. PcagCreERT2 mice crossed with the mTmG reporter mouse line. Mouse incisors were harvested after two doses of tamoxifen (5 mg/30 g body weight) showed widespread location of GFP+ cells in mesenchyme. n=4 mice. Bar is 250 μ m.

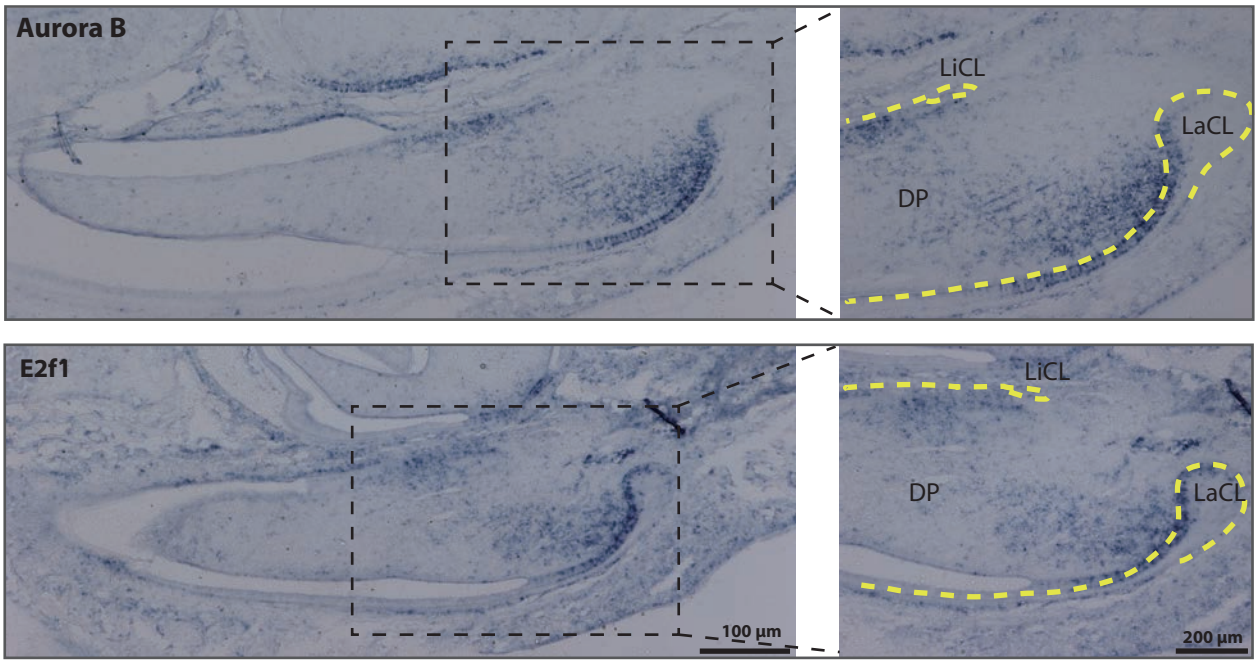

Figure S6. In situ hybridisation identifies Aurora B and E2f1 in TACs. Related to Figure 3E.
Aurora B and a positive cell cycle regulator E2f1 are detected mainly in the incisor mesenchyme between the labial and lingual aspects of the cervical loop where TACs are located. n>=3 mice per group. DP is for Dental Pulp, LiCL is for Lingual Cervical Loop and LaCL is for Labial Cervical Loop.

Table S2. List of real-time PCR primers. Related to Figure 3I, 3J and Figure 4D, 4F.

Primer name	Primer sequencing
Axin2-Forward	gagagtgagcggcagagc
Axin2-Reverse	cggctgactcgttctcct
Beta-actin-Forward	ctaaggccaaccgtgaaaag
Beta-actin-Reverse	accagaggcatacagggaca
Beta-catenin-Forward	ttcctatgggaacagtcgaag
Beta-catenin-Reverse	ttgtattgttactcctcgaccaaa
Cdc6-Forward	ctgtttcaggagacatccgtaa
Cdc6-Reverse	tcctgacatccgactccac
Cdc7-Forward	gcggacgtcctaacttctgt
Cdc7-Reverse	gcttccactacgcacgact
Cdc45-Forward	ggcaagaacttgaaactgcat
Cdc45-Reverse	cactggcctgtgggtatca
Cdkn2a-Forward	cgtaccccgattcaggtg
Cdkn2a-Reverse	accagcgtgtccaggaag
CyclinD1-Forward	tttctttccagagtcatcaagtgt
CyclinD1-Reverse	tgactccagaagggcttcaa
CyclinE2-Forward	cgagctgtggagggtctg
CyclinE2-Reverse	aaacggctactgcgtcttga
E2f1-Forward	tgccaagaagtccaagaatca
E2f1-Reverse	cttcaagccgcttaccaatc
Myc-Forward	cctagtgctgcatgaggaga
Myc-Reverse	tccacagacaccacatcaattt
Twist1-Forward	agctacgccttctccgtct
Twist1-Reverse	tccttctctggaaacaatgaca
Zic1-Forward	aacctcaagatccacaaaagga
Zic1-Reverse	cctcgaactcgcacttgaa
Zic2-Forward	gatccacaaaagaactcatacagg
Zic2-Reverse	cttcttcctgtcgctgctgt
Zic3-Forward	cctgcgcaaacacatgaa
Zic3-Reverse	ctatagcgggtggagtggaa
Zic4-Forward	gtggagcagggctcaaac
Zic4-Reverse	tggtgtccacagctgctact
Zic5-Forward	cactgccaccaacagtgg
Zic5-Reverse	aggacgaagtccctgctgt

Table S3. Plasmids used for Digoxigenin-labelled RNA probes. Related to Figure S6.

Name	Vector	5' clone site	3' clone site	Anti-sense probe	Sense probe	IMAG ID
Aurora B	pT7T3D-PacI	EcoRI	NotI	T3	T7	1226941
E2f1	pSPORT1	SalI	NotI	Sp6	T7	934181

Supplemental Experimental Procedures:

EdU / BrdU incorporation and staining

EdU was detected by Click-iT EdU Alexa Fluor 647 Imaging kit (Invitrogen C10340) according to the protocol. BrdU was detected by anti-BrdU antibody (ab6326, Abcam) 1:100 followed by secondary antibody donkey anti-Rat IgG (H+L) Alexa Fluor 594 (Invitrogen) 1:400 prior to DAPI staining for nuclei and cover-slipped for microscopy.

Immunofluorescence

Immunofluorescence staining used standard protocols on 12 µm sagittal cryosections of mouse incisors. Anti-mouse Ring1b antibody (Active motif #39663, 1:100), anti-Rabbit Ring1b (ab101273, Abcam, 1:500), anti-Rabbit Ki67 antibody (Abcam ab15580, 1:100) and anti-Rabbit CBX2 antibody (Abcam ab184968, 1:100) were used as primary antibodies. Goat anti-mouse IgG (H+L) Alexa Fluor 488, Donkey anti-rabbit IgG (H+L) Alexa Fluor 488, Alexa Fluor 594 and Alexa Fluor 647 (invitrogen, 1:400) were used as secondary antibodies. Hoechst 33342 (Invitrogen 62249, 1:500) used for DNA staining. Slides were then mounted using glycerol based antifade Citifluor™ AF1 (Citifluor Ltd., AF1-100) and cover slips added.

Cytospin

Flow sorted EdU+ cells were collected and re-suspended as 100 µl aliquots in 2% BSA in PBS before loading into a Shandon Single Cytofunnel. Cells were then forced to separate and deposited as a monolayer on slides to preserve the cellular integrity using Shandon Cytospin 3 Centrifuge at 1350 rpm for 5 minutes. Slides were then post-fixated, permeablized and immunostained with primary and secondary antibodies followed by DNA staining with Hoechst33342 prior to coverslips being added according to the standard protocol.

ChIP seq

Primary incisor pulp cells were isolated from 80 incisors for each set of ChIP-Seq. Cells were cross-linked with 1% formaldeyde at room temperature for 12 minutes and then quenched with 0.125 M glycine for another 5 minutes. Cells were suspended in 100 µl saponin-based permeablization buffer and labelled EdU by Click-iT® EdU Alexa Fluor® 647 Flow Cytometry Assay Kit (Thermo Fisher Scientific, C10424). FACS sorted EdU+ cells were collected and sonicated to yield chromatin at 100-500bp. Low-input ChIP was performed by

standard procedures using antibodies from Active motif (Ring1b antibody, 39663; H3K4me3, 39915; H3K27me3, 39155).

Two replicate ChIPseq experiments for Ring1b were pooled for the input sample. Total number of reads were over 40 million for each ChIPseq. The unique alignments without duplicate reads (final tags) were less than 1 million for Ring1b ChIPseq. Peaks were determined using the MACS peak finding algorithm. Using a cutoff of p-value = 1e-6, 3938 peaks were identified. A total of 6.2 million final tags were obtained for H3K4me3 and 13.6 million for H3K27me3. Peaks were determined using the SICER algorithm at a cutoff of E-value = 1 and a Gap parameter of 600 bp. 14,361 H3K4me3 enriched regions and 11,341 H3K27me3 enriched regions were identified respectively.

Western blots

Mouse incisor pulp tissues were disrupted by a hand rotor homogenizer and protein was extracted using cell lysis buffer (CLB) (10 mM Tris pH8.0, 10 mM NaCl, 0.2%NP40) followed by nuclear lysis buffer (NLB) (50 mM Tris pH8.1, 10 mM EDTA, 1%SDS). Equal volume of 2x SDS loading buffer (100 mM TrisHCL PH6.8, 4% SDS, 12% Glycerol, 2% β-mercapitalethanol, 0.008% bromophenol blue) was added to 30µg protein followed by incubation at 95° C for 3 minutes before loading onto SDS-PAGE gels and wet transfer to nitrocellulose membranes. Anti-Ring1b (Active motif 39663, 1:500) and anti-H3K27me3 antibodies (Diagenode pAb-069-050, 1:500) were used to detect protein expression levels and anti-Lamin B1 antibody (Abcam, Ab16048, 1:1000) used as an internal loading control. Peroxidase-conjugated Affinipure Goat-anti Rabbit IgG (H+L) (Jackson immunoResearch, 111-035-003, 1:3000) and Peroxidase-conjugated Affinipure Goat-anti mouse IgG (H+L) (Jackson immunoResearch 111-035-003, 1:3000) were used as secondary antibodies against primary antibodies prior to ECL (GE Healthcare Life Science, RPN2232) detection.

Co-immunoprecipitation

Protein was extracted from mouse incisor pulp tissue using RIPA buffer (150 mM NaCl, 1.0% NP-40, 0.5% sodium deoxycholate, 0.1% SDS and 50 mM Tris, pH 8.0) supplemented with protease inhibitor cocktail (Roche). The protein extract was precleared with 35 µl protein A/G Plus-Agarose beads (Santa Cruz, sc-2003) and immunoprecipitated with 3µg antibody of anti-H3K27me3 (Diagenode, pAb-069-050), anti-H2AK119ub (Cell signalling, #8240), anti-Ring1b (Active motif, 39663), 3µg anti-mouse IgG (PEPROTECH, 500-M00) was used as a

control, together with 35 µl protein A/G Plus-Agarose beads incubated at 4° C for 2 hours on a rotator. Beads were pelleted by centrifuge at 13000 rpm for 1minute. Equal volume of 2x SDS loading buffer (100 mM TrisHCL PH6.8, 4% SDS, 12% Glycerol, 2% β-mercaptoethanol, 0.008% bromophenol blue) was added to the bead pellets and protein complexes were eluted by incubation at 95° C for 3 minutes before loading onto SDS-PAGE gels and wet transfered to nitrocellulose membranes. Primary antibody anti-Ring1b and secondary antibody Peroxidase-conjugated Affinipure Goat-anti mouse IgG (H+L) were used to detect the interaction proteins in the precipitated protein complex followed by ECL detection.

Quantitative Real-time PCR

Total RNA was extracted from mouse dental pulp tissue using RNeasy Mini Kit (Qigen 74104), and purified by Ambion DNA-free DNA Removal Kit (Invitrogen, AM1906). cDNA was then synthesised using MMLV Reverse Transcriptase (Promega, 9PIM170). Both cDNA without MMLV reverse transcriptase and RNase-free water with MMLV reverse transcriptase were used as negative controls. For each sample, 1 µg cDNA was used for qPCR reaction with the LightCycler 480 SYBR Green I Master (Roche, 04707516001) using LightCycler 480 system qPCR platform (Roche, 05015278001). All primers used in the experiments are listed in Table S2. Data were analysed with $2^{-\Delta\Delta ct}$ methods. All ct values were normalized with β-actin levels as internal controls. Standard deviations were calculated from biological triplicate samples and were represented as error bars.

Cryosection preparation

Moue incisor samples were fixed in 4% PFA in PBS for 24-48 hours at 4° C and decalcified in 10-19% EDTA for 4 weeks. Samples were then sucrose cryoprotected by incubation with 30% sucrose until samples sunk to the bottom followed by incubation with half of 30% sucrose and half of OCT compound (VWR, 361603E) before embedding in OCT. Cryosectioning of samples at 10-12 um thickness was carried by Cryostat Microtome (Bright, OTF5000). Sections were stored at -80 ° C prior to staining.

LacZ staining

Frozen sections were post-fixed in 0.2% glutaraldehyde and permeabilized in 0.05% Tween20 (Sigma Aldrich) in PBS and then incubated in X-gal solution (Thermo scientific) overnight at 37° C for LacZ staining. Fast red was used for counterstaining.

Tunel assay

Frozen incisor sections were post-fixed in 4% PFA then permeabilized in 0.1M Sodium Citrate buffer with PH 6.0 (11.5% 0.1M citric acid monohydrate and 88.5% 0.1M Trisodium Citrate dihydrate) on ice. The sections were incubated in Tunnel reaction mixture at 37° C for 60 minutes according to the protocol (In Situ Cell Death Detection Kit, Fluorescein 11684795910 Roche) and counterstained with Hoechest33342 prior to coverslip. Fluorescein was detected by Confocoal microscopy (Leica TCS SP5) with an argon laser at 488nm excitation.

Digoxigenin-labelled section in situ hybridization

In situ hybridization (ISH) for detection of mouse Aurora B and E2f1 mRNA expression was performed on 12 μm cryo-sections of mouse incisors following the standard procedures. Briefly, 10 μg plasmid (Table S3) was linearized by 5' and 3' clone site restriction enzymes for sense and anti-sense probes. 1μg linearized DNA was used for DIG-labelling (Roche) and RNA probes were synthesised at 37° C for 2 hours followed by 2 μl DNase I incubation for 15 minutes at 37° C. Probes were then purified by SigmaSpin post-Reaction Clean-up Colums (S0185-70EA). Sections were fixed in 4% paraformaldehyde and hybridized with 1μl digoxigenin-labelled sense and antisense probes. Sections were treated with RNase-A or treated with the sense probe are used as negative controls. Images were taken on a Zeiss Axioskop 2 microscope equipped with a Zeiss AxioCam camera (Carl Zeiss).

Mice information

Wild type CD1 mice were obtained from CRL (Charles River Laboratory, UK). Mutant Ring1a and Ring1b floxed alleles were generated as described previously (Lapthanasupkul et al., 2012; Cales et al., 2008; and del Mar Lorente et al., 2000). $Ring1a^{-/-}$;$Ring1b^{fl/fl}$ compound mice were crossed with $pCAG^{CreERT2}$ transgenic mice to generate Ring1a-/-;Ring1bfl/fl ;Rosa26::CreERT2 mice. Ring1a-/-;Ring1bcko/cko mice were obtained by injecting 4-hydroxy tamoxifen (OHT) (40mg/kg body weight) and corn oil as control for 2 days before being scarified.

Axin2CreERT2/+ mouse line was described previously (Van Amerongen et al, 2012). A total of 14 mice were divided into 4 groups and Cre recombination was activated by 3 doses of Tamoxifen (Sigma Aldrich) injections (5 mg/30 g body weight) and corn oil as control. Mice then collected at 1, 3, 7, 14 and 28 days following the last injection of tamoxifen.

Ubiquitous $Pcag^{CreERT2}$ mouse line was crossed with $Wls^{fl/fl}$ mouse line (Carpenter et al, 2010). A total of 6 mice were divided in to 2 groups. The first group were treated with 3 doses of tamoxifen injections to activate cre recombination. The other groups were treated with 3 doses of corn oil injections as control. Both groups were collected 7 days post injection. Cre activity was analysed by crossing $Pcag^{CreERT2}$ with the R26R-mTmG reporter mice (Figure S5).